E-7059

NASA Reference Publication 1310

July 1993

Solar Dynamic Power System Development for Space Station *Freedom*

Staff of Solar Dynamic Power System Branch

NASA

NASA Technical Paper 1310

1993

Solar Dynamic Power System Development for Space Station *Freedom*

Staff of Solar Dynamic Power System Branch
Lewis Research Center
Cleveland, Ohio

NASA
National Aeronautics and Space Administration
Office of Management
Scientific and Technical Information Program

Preface

This report documents the development of a solar dynamic electric power generation system as part of the Space Station *Freedom* Program. Solar dynamic development was stopped in March 1991 as a result of the restructuring of that program. The report covers solar dynamic development managed by the NASA Lewis Research Center from 1986 to February 1991. It serves as a summary of technology and hardware development, a description of "lessons learned," and, through an extensive bibliography, a source list of documents that provide details of the design and analytic results achieved. It was prepared by the staff of the Solar Dynamic Power System Branch at NASA Lewis Research Center in Cleveland, Ohio. Contributors were Linda J. Bartos, Edward P. Braunscheidel, Robert D. Corrigan, Clinton B. Ensworth III, Kent S. Jefferies, Thomas W. Kerslake, Laura K. Lathem, Kerry L. McLallin, Jennifer L. Rhatigan, Daniel S. Rylicki, Richard R. Secunde, and Rodger R. Slutz. Organization, coordination, and editorial aspects of this report were performed by Kent S. Jefferies, Thomas W. Kerslake, Richard R. Secunde, Clinton B. Ensworth III, and Robert D. Corrigan.

The Solar Dynamic Power Module (SD) Program was part of the Space Station *Freedom* Program. As a compilation of information from the SD program, this report includes results from the prime contractor as well as from in-house efforts, university grants, and other contracts. A primary goal of this report is to summarize and reference all of the important work that was done as part of the SD program. As much as possible, readers are directed to more detailed sources of information. References are listed at the ends of each chapter. In addition, a comprehensive bibliography lists additional documents related to solar dynamic power. Most reference and bibliography entries are not available in the open literature but are available from the Space Station *Freedom* library at NASA Lewis Research Center in Cleveland, Ohio 44135 (tel. 216–433–5367 and fax 216–433–8050).

Because the SD program was terminated before the prime contractor had completed a preliminary module design, a complete, consistent solar dynamic module design is not described in this report. Inconsistencies among the various sections of this report are due to the status of the program at its termination. Nevertheless, the information contained herein should provide the reader with a reasonable idea of how a solar dynamic module would look and operate on Space Station *Freedom*. Also included are the writers' opinions on the best way to proceed technically and programmatically with solar dynamic efforts in the future, on the basis of their experiences in the SD program.

Page intentionally left blank

Contents

Chapter 1
Introduction

In the design that existed at the beginning of the flight hardware phase of the Space Station *Freedom* Program (phase C/D), electric power for *Freedom*'s manned base was to be supplied from two solar power modules (SPM's). One SPM would be located on the port side of the transverse boom of the manned base and the other on the starboard side; each would be joined to the central part of the transverse boom by a single-degree-of-freedom rotating joint (alpha gimbal). Initially, the SPM's would supply a total of 75 kW of electric power by using photovoltaic power modules as shown in figure 1.1. As *Freedom* evolved to greater capabilities, increased power needs would be satisfied by the addition of 25-kW solar dynamic power modules at the outboard ends of the initial SPM's, as shown also in figure 1.1. For the first growth increment, which was expected to be 50 kW, one solar dynamic power module was to be added on each side. The evolution of *Freedom* was expected to require total power capability growth to about 300 kW.

There are two primary reasons for the interest in the solar dynamic system as the source of growth power. A photovoltaic/solar dynamic hybrid system offers the flexibility of a power system with two types of sources, thus ensuring an uninterrupted power supply in the unlikely event of a major or systematic problem in either type of source. But even more compelling is the potential cost saving that can be realized with solar dynamics. Solar dynamic power generating and storage components have longer lifetimes than photovoltaic arrays and batteries. Long lifetimes result in substantial savings in hardware replacement, launch, and on-orbit installation costs. Because of the significantly higher solar-to-electric power efficiency of a solar dynamic system, its solar collection area is only about 25 percent of that for a photovoltaic system for a given power output. Therefore, it will have lower aerodynamic drag and lower reboost requirements. For constant-drag operation, solar dynamic systems would allow operation at lower altitudes. This would permit the National Space Transportation System (NSTS) orbiter to rendezvous with *Freedom* at lower altitudes, significantly increasing the orbiter's payload capacity and lowering the launch cost per pound to orbit.

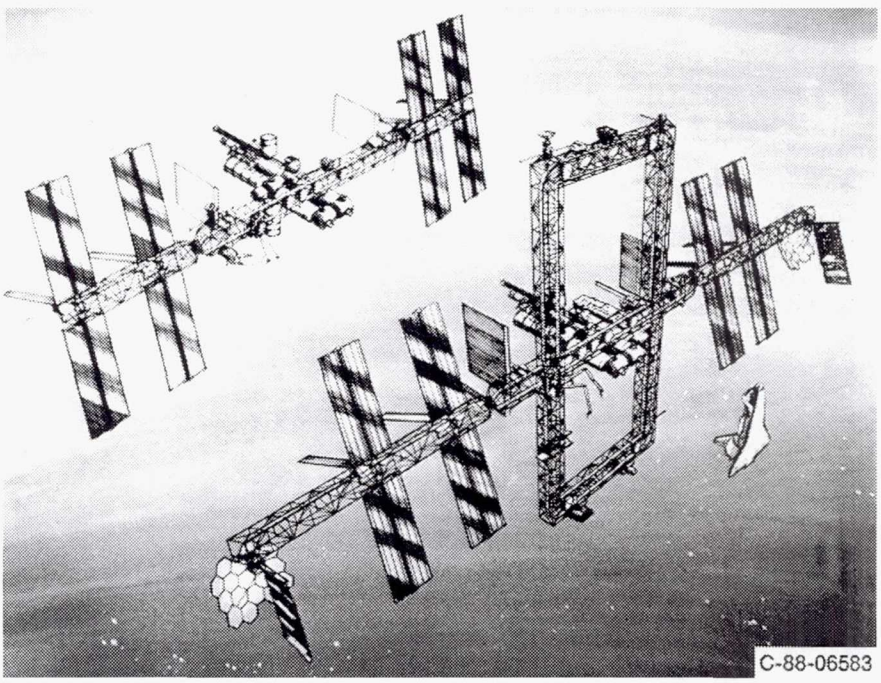

Figure 1.1.—Space Station *Freedom*.

Studies have shown that the various operations and hardware cost savings resulting from the use of solar dynamic power rather than photovoltaic power for growth would amount to a reduction in life-cycle costs of several billion dollars over the 30-year life of *Freedom* station.

Advanced development of critical solar dynamic technology began as part of the Space Station Program in 1984 and contributed to the later studies of the concept development phase (phase B). This advanced development effort built upon, and extended, the technology base established in the 1960's and early 1970's.

The preliminary design and hardware development for a 25-kW solar dynamic power module were included as part of the flight hardware development phase (phase C/D) of the Space Station *Freedom* Program, which began in 1987. Program constraints limited the solar dynamic efforts to preliminary design, development of critical component technology, and identification of the hardware and software design features (also called "hooks and scars") that must be included to allow the addition of solar dynamic power in a timely and cost-effective manner when needed.

The Space Station *Freedom* organization is a three-tiered NASA management structure consisting of level I, the Office of Space Flight at NASA Headquarters in Washington, DC; level II, the Space Station *Freedom* Program and Operations Office in Reston, Virginia; and level III, the NASA centers charged with direct implementation responsibilities. Each of the level III centers is designated as a work package (WP) center. The NASA Lewis Research Center together with its prime contractor is known as WP–04. WP–04 is responsible for the total, end-to-end, electric power system (EPS) for *Freedom*.

The WP–04 prime contractor is the Rocketdyne Division of Rockwell International. In addition to their own effort, Rocketdyne had three subcontractors for solar dynamic development. The Harris Corporation was responsible for the solar concentrator. AiResearch and Garrett Divisions of Allied-Signal Aerospace Company were responsible for the heat receiver with thermal energy storage and for the thermodynamic power conversion hardware (also called the power conversion unit, or PCU). And, finally, LTV was responsible for the radiator. Rocketdyne's internal solar dynamic efforts were aimed at overall module integration and system design along with design and development of integration hardware, system controls, and other hardware that was not part of the concentrator, receiver, PCU, or radiator.

Separate from the prime contract, NASA pursued a supporting development program to serve several major purposes. These were to complete critical developments that were started in the advanced development program; to develop and provide the contractor and subcontractors with design data that were needed but otherwise not available; to provide use of NASA test facilities for critical tests; and to conduct independent analyses and tests to ensure that NASA would remain a "smart buyer." This supporting development work was accomplished through NASA in-house effort, contracts with industry, and university grants.

In late 1990 the Space Station *Freedom* Program was restructured to accommodate significant budget restraints. As part of this restructuring, the station's design was simplified and the anticipation of evolutionary power needs greater than 75 kW was removed from the program planning. Development of solar dynamic power for *Freedom* was stopped.

It is the purpose of this report to help ensure that information on the significant progress in solar dynamic hardware and system design that was achieved during this program will be available for future solar dynamic, or related, programs. To achieve this purpose, this report describes the constraints and performance requirements imposed on the solar dynamic power module by the Space Station *Freedom* Program, explains the principles of solar dynamic operation, describes the design and development status of the module and its components as they existed at the time of restructuring, and summarizes the top-level tradeoff studies and system analyses. The lessons learned, provisions needed on *Freedom* for power growth, and recommendations for needed development are included. Finally, to aid solar dynamic progress in the future, references (both published and unpublished) and a comprehensive bibliography of documents that contain detailed information on the results of design, test, and analytical work by NASA, contractors, and universities are also included.

Chapter 2
Solar Dynamic Requirements Documents and Drawings

2.1 Introduction

A baseline design can be defined as a design at a specific time that is tied to specific documentation. At different stages in a program the baseline will be represented by different documentation. At the end of the definition phase (phase B) the Rocketdyne solar dynamic module baseline was the design at a conceptual level as described in the Rocketdyne final phase B summary report. As a program matures, the baseline becomes more formally represented by released (authorized) drawings and specifications, along with descriptive documents, such as Rocketdyne's engineering design document (EDD) (ref. 2.1). Also as the program matures, the requirements become more detailed, evolving from top-level design-to requirements to detailed design-solution specifications.

Within the span of a development/production program phase (phase C/D) there are specific times, such as the preliminary design review (PDR) and critical design review (CDR), when the design is reviewed, evaluated, and approved, resulting in major updates to the baseline. These major program milestones aid in ensuring that all elements of the system are integrated and consistent with each other.

Even before the phase C/D Solar Dynamic Power Module (SD) Program was cancelled, it was intended to be a limited effort with no formal program review milestones. At the closeout of the progam some work remained to arrive at a fully integrated and consistent baseline design. The final Rocketdyne documentation can be used, however, to define a solar dynamic system and allow for discussion of the design as it evolved. The documentation includes drawings and requirements documents and a design description in an engineering information document (EID)[1] (ref. 2.2). The discussion that follows covers the requirements documents and drawings that have been produced for the phase C/D SD program.

[1]The information in this EID is identical to the type of information in Rocketdyne's EDD. Because the EDD dropped the inclusion of solar dynamics before the last solar dynamic information was available, this EID was created especially to document the latest solar dynamic design.

2.2 Requirements Documents

Requirements for Space Station *Freedom*, the electric power system, and the solar dynamic module are contained in requirements documents that exist within a hierarchy. Top-level program requirements are contained in the program requirements document (ref. 2.3), a level I document. The next level of requirements are in the program definition and requirements document (ref. 2.4), which invokes the baseline configuration document (ref. 2.5) (for program elements), architectural control documents (for distributed systems), and various interface documents. These are all level-II-controlled documents that further define the elements and systems through requirements which are more specific than the level I requirements.

The WP–04 contract's technical content is governed by a Lewis-controlled document, WP–04 Technical Requirements Document (ref. 2.6) (formerly known as the EPS Requirements Document). All applicable level II requirements are "flowed down" to the electric power system in this document, sometimes being modified or tailored to make the higher level requirements apply more specifically. Below this document in the requirements hierarchy are the three contract end item (CEI) specifications for the photovoltaic power module (ref. 2.7), the solar dynamic power module (ref. 2.8), and the power management and distribution (PMAD) system (ref. 2.9). The CEI specifications are intended to contain all of the requirements that are applicable to the CEI's, including requirements that flowed down from all higher level documents and callout of all other applicable documents. As part of the prime contract, Rocketdyne was required to develop and maintain new versions of the CEI specifications.

An important function of the CEI specifications is their use in the verification process, where hardware and software items are methodically verified with respect to every requirement. Verification occurs in all of the program phases from development to the final on-orbit checkout. Included within the CEI specifications are verification crossreference indices that link the requirements with the verification phase and the verification method. Key solar dynamic CEI requirements are summarized in chapter 5, section 5.1. Key requirements for

TABLE 2.1.—SOLAR DYNAMIC SPECIFICATION AND REQUIREMENTS DOCUMENTS

Document number	Revision	Title	Release date
LERC–SS–0003	A	Solar Dynamic (SD) Power Module System, Part 1, Contract End Item Specification	18 Oct. 1988
DRD E–02 CP409R0006	B	SD Power Module System CEI Specification, Part 1	1 May 1990 (draft)
RC1800	D	Procured Items, General Specification for	22 May 1990
RC1811	D	Power Generation Subsystem, CBC[a]	18 May 1990
RC1812	C	Reflector/Structure and Launch Cradle Set	28 Mar. 1990
RC1814	B	Frequency Changer, ORU, SS EPS	27 Oct. 1989
RC1815	E	Panel Assembly, Radiator, Deployable—CBC	5 Mar. 1990
RC1819		Actuator, Linear	9 Nov. 1989
RC1820		Meter, Insolation	9 Nov. 1989
RC1821		Sensor, Sun	9 Nov. 1989
RC1860		Simulator, Power, Solar Dynamic	22 June 1989
RJ000107		Controller, SD	Not released
RJ00122	C	Designed Items, General Specification for	4 June 1990
RJ00130	A	Beta Gimbal Assembly	2 May 1990
RJ00163		Structure Assembly, Interface	24 May 1989
RJ00164		Gimbal Assembly, Two-Axis	22 Sept. 1989
RJ00176	A	Plate, Utility, SD	11 Sept. 1990
RJ00177		Management Unit, Fluid	Not released
RJ00198		Fine Pointing and Tracking Subsystem, SD	1 June 1990 (draft)
RJ00231		SD Power Module, Specification for	23 Aug. 1990 (draft)
RJ00235		Launch Element, Power Generation and Control Subassembly, Solar Dynamic	25 July 1990
RJ00255		Power Generation and Control Subassembly	24 Oct. 1990
RB0110–17		*n*-Heptane, Coolant	15 Aug. 1989

[a] Closed Brayton cycle.

particular assemblies are discussed in chapter 6 in the appropriate component design sections.

Rocketdyne established its own system of requirements documents that augment and tie into the CEI specifications. These documents pertain to the assembly or orbital replacement unit (ORU) hardware level and in some cases lower levels. All of the Rocketdyne requirements documents include verification crossreference indices, just as do the CEI specifications.

For items that are to be built by Rocketdyne, design requirement specifications are used to establish and document the technical requirements that the item must meet. For items that are to be procured, a source control drawing serves as the top-level instrument for their purchase. Because specifications are typically too long to be included directly on the drawing face, a procurement specification document is invoked by the source control drawing. Rocketdyne designates its design requirement specifications with the prefix RJ and its procurement specifications with the prefix RC. A third type of document, a material procurement specification, is used only for basic materials and is designated with the prefix RB.

Among the most important specifications are those that were written for each of the major parts that are being built by subcontractors: reflective surface (Harris Corp.), radiator (LTV), and receiver/PCU (Allied-Signal). Each of these major parts had a source control drawing and a corresponding procurement specification.

All existing solar dynamic specification and requirements documents are listed in table 2.1.

2.3 Drawings

The first drawings that were developed for the solar dynamic module in phase C/D were preliminary layouts and source control drawings. The preliminary layouts were used to document the phase B concept baseline. The source control drawings were used to establish the baseline for purchased items. As the designs progressed at Rocketdyne and their subcontractors, detailed layouts were made to define interfaces and to fill in lower levels of detail. All released Rocketdyne and subcontractor solar dynamic drawings are listed in table 2.2.

References

2.1 Marshall, M.; and Papac, T.: Engineering Design Document—WP–04 Power System. Rockwell International, Rocketdyne Division, EID–00259[a], rev. G, Jan. 24, 1991.

2.2 Solar Dynamic Design Description. Rockwell International, Rocketdyne Division, EID–00787[a], Apr. 2, 1991.

[a]Space Station *Freedom* library at the NASA Lewis Research Center in Cleveland, OH 44135 (tel. 216–433–5367 and fax 216–433–8050).

TABLE 2.2. – RELEASED DRAWINGS

Drawing number	Revision	Sheet number	Title	Release date
Rocketdyne drawings				
R077000L	A	1	Layout – Solar Dynamic Module, Electric Power System, Space Station	26 July 1990
R077030L	A	1–4	Layout – NSTS[a] Packaging, Solar Dynamic Module, Space Station	14 May 1990 (draft)
R077100L	A	1–2	Layout – PGCS[b], Solar Dynamic Module, Space Station	28 June 1990
R077110L	A	1	Layout, – Two-Axis Gimbal, Solar Dynamic Module, Space Station	24 Sept 1990
R077150L	A	1–2	Layout – Interface Structure, Solar Dynamic Module, Space Station	20 June 1990
R077200L		1	Layout – EEA[c], Solar Dynamic Module, Space Station	28 Feb. 1989
R077210L		1–7	Layout – Utility Plate Assembly Solar Dynamic Module, Space Station	12 Apr. 1989
R077250L		1–5	Layout – Fluid Management Unit EEA, Solar Dynamic Module, Space Station	17 May 1989
RE1811	F B	1 2	Power Generation Subsystem, CBC[d]	27 Nov. 1990 30 June 1989
RE1812	C A	1 2	Reflector/Structure and Launch Cradle Set, Solar Dynamic Module	27 Nov. 1990 28 Mar. 1990
RE1815	D B	1 2	Panel Assembly, Radiator, Deployable – CBC[d], Solar Dynamic Module	28 Nov. 1990 29 Jan. 1990
RE1819	B	1	Actuator, Linear, Solar Dynamic Module	27 Nov. 1990
RE1820	B	1	Meter Subassembly, Insolation, Solar Dynamic Module	27 Nov. 1990
RE1821	B	1	Sensor, Sun	21 Nov. 1990

[a] National Space Transportation System.
[b] Power generation and control system.
[c] Electrical equipment assembly.
[d] Closed Brayton cycle.

TABLE 2.2. – Concluded.

Drawing number	Revision	Sheet number	Title	Release date
Allied-Signal drawings				
L145953		1	Cooler Layout, Space Station, FSD[c]/Rocketdyne/NASA	27 Nov. 1989
L145954		1	Recuperator/Cooler Package, Space Station, FSD/ Rocketdyne/NASA	27 Nov. 1989
L196854	D	1–2	Receiver Layout, Solar, Space Station, Brayton Cycle	27 Nov. 1989
L3793141	B	1	Accumulator, Space Station CBC–PGS[f]	31 Aug. 1989
L3793262		1–2	Turbo Alternator Compressor (TAC) 38 kW	31 Jan 1989
L3793263		1	Rotor and Wheel Assembly, TAC, 38 kW	26 Feb. 1989
L3793265		1	Scroll Sections, Generic	30 Jan. 1989
L3793266		1	Scroll, Turbine Manufacturing Method	30 Jan. 1989
L3793520		1	Valve, Inventory Control	30 July 1989
L3793560		1	Parasitic Load Radiator	13 Apr. 1989

[c]Fluid Systems Division.
[f]Power-generating system

2.3 Space Station *Freedom* Program – Program Requirements Document (PRD). NASA, SSP 3000[a], rev. E, Feb. 11, 1992.

2.4 Space Station Program Definition and Requirements: Space Station Systems Requirements. NASA SSP 30000[a], section 3, rev. G, Oct. 31, 1988.

2.5 Space Station *Freedom* Program – Baseline Configuration Document. NASA SSP 30255[a], rev. C1, Nov. 15, 1988.

2.6 WP–04 Technical Requirements Document. LeRC–SS–0001[a], June 30, 1992.

2.7 Photovoltaic (PV) Power Module Systems – Part 1 Contract End Item Specification. Space Station *Freedom* Directorate, Work Package 04 (WP–04), LeRC–SS–0002[a], Oct. 31, 1988.

2.8 Solar Dynamic (SD) Power Module System – Part 1 Contract End Item Specification. Space Station *Freedom* Directorate, Work Package 04 (WP–04), LeRC–SS–0003[a], Oct. 18, 1988.

2.9 Power Management and Distribution (PMAD) Systems – Part 1 Contract End Item Specification. Space Station *Freedom* Directorate, Work Package 04 (WP–04), LeRC–SS–0004[a], Oct. 24, 1988.

[a]Space Station *Freedom* library at the NASA Lewis Research Center in Cleveland, OH 44135 (tel. 216–433–5367 and fax 216–433–8050).

Chapter 3
Freedom Station's Constraints on Solar Dynamic Design

3.1 Introduction

This chapter describes the various interfaces and constraints that affect the design of the solar dynamic power module. These interfaces and constraints are defined in detail in reference 3.1 and include those caused by the natural environment, the induced environment, and the induced contamination environment. The solar dynamic system is required to function without operational constraints in any of these environmental conditions during assembly, checkout, storage, launch, and orbital operations.

3.2 Natural and Induced Environments

The natural environmental conditions are defined for Space Station *Freedom* in reference 3.2. This environment includes orbital state points, plasma, radiation, meteoroids and space debris, magnetic and gravitational fields, and ground conditions. The induced environmental conditions included radiation, electrostatic environments, and induced structural loads. Radiation and electrostatic environments are discussed in references 3.3 and 3.4. The induced contamination environment includes all contamination induced by *Freedom*'s elements, experiments, and payloads.

During the preliminary design phase of the Solar Dynamic Power Module Program, four environmental areas were addressed in detail: atomic oxygen, micrometeoroids and space debris, NSTS orbiter docking, and the plume impingement from orbiter reaction control jets. For both the concentrator and the radiator the atomic oxygen effects were evaluated through analysis and testing (refs. 3.5 and 3.6). The major method for protecting components against atomic oxygen was proper surface fabrication and the addition of protective coating layers. For the concentrator and the radiator micrometeoroid and space debris effects were also evaluated by both analysis and testing (refs. 3.7 to 3.9). Dynamic structural analysis of the solar dynamic module during orbiter docking has been performed by the prime contractor (ref. 3.10). At the current time orbiter docking structural loads are believed to be the most critical loads for the solar dynamic module. This analysis addressed system natural frequencies and displacement, acceleration, element force, and element stress-time histories for selected modes. This information was used for quasi-static load determination and structural integrity studies. Plume impingement structural impacts and radiator and concentrator contamination were analyzed by the prime contractor. The study found that plume loads on the radiator were not a problem. However, plume contamination of the concentrator from the orbiter primary reaction control system (PRCS) during emergency braking operations was found to be significant; it exceeded the current NASA contamination limit of 0.4 $\mu g/cm^2$-yr. There is also expected to be some mechanical degradation by hypervelocity particles from the PRCS plume.

3.3 Structural Loads

Additional analysis of solar dynamic module environmental loads was conducted by the NASA Lewis Engineering Directorate. These studies (ref. 3.11) were performed to determine the loading on the solar dynamic module during on-orbit operations and were part of the pointing control design system efforts. Environmental forces and torques due to atmospheric drag and the gravity gradient were calculated. Structural loading of the solar dynamic module due to plume impingement from the firing of the orbiter PRCS engines that is associated with an approach to docking was also investigated. From these analyses a set of worst-case loads and torques were determined.

3.4 Station Hardware

Another document that defines the interfaces and constraints for the solar dynamic power module is reference 3.12. This document defines the hardware and software features that must be incorporated into the assembly-complete phase of Space Station *Freedom* so that solar dynamic power

modules can be added as part of station growth. Once incorporated, these features become interfaces and constraints to which the solar dynamic power module must be designed. The document covers system-level interfaces, element-level interfaces, and functional interfaces.

References

3.1 WP–04 Technical Requirements Document. LeRC–SS–0001[a], June 30, 1992.

3.2 Space Station Program Natural Environment Definition for Design. SSP 30425,[a] rev. A, June 1991.

3.3 Space Station Electromagnetic, Ionizing Radiation, and Plasma Environment Definition and Design Requirements. SSP 30420[a], rev. A, Aug. 30, 1991.

3.4 Electrical, Electronic, and Electromechanical Parts Management and Implementation Plan for Space Station Program. SSP 30312[a], rev. D, July 1992.

3.5 de Groh, K.; Terlep, J.A.; and Dever, T.M.: Atomic Oxygen Durability of Solar Concentrator Materials for Space Station Freedom. NASA TM–105378, 1990.

3.6 Dever, J.A.; Rodriquez, E.; and Slemp, W.S,: Evaluation of Thermal Control Coatings for Use on Solar Dynamic Radiators in Low Earth Orbit. NASA TM–104335. (Also AIAA Paper 91–1327, 1991.)

3.7 Peterson, T.: Solar Concentrator Reflective Surface Damage Caused by Meteoroid and Space Debris Impacts. Cleveland State University MSME Project, key 23610[a], March 11, 1991.

3.8 Rhatigan, J.; Christiansen, E.; and Fleming, M.: On Protection of *Freedom*'s Solar Dynamic Radiator From the Orbital Debris Environment, Part 1: Preliminary Analysis and Testing. NASA TM–102458, 1990. (ASME Journal of Solar Energy Engineering, vol. 114, Aug., 1992, pp. 135–141.)

3.9 Rhatigan, J.; Christiansen, E.; and Fleming, M.: On Protection of *Freedom*'s Solar Dynamic Radiator From the Orbital Debris Environment. NASA TM–104514, 1991. Part 2: Further Testing and Analysis. (ASME Journal of Solar Energy Engineering, vol. 114, Aug. 1992, pp. 142–149.).

3.10 Dynamic Analysis of Option 1, Solar Dynamic Module Under Shuttle Docking Load. Rockwell International, Internal Letter No. 90–EPS–8E–81, key 36481[a], Dec. 20, 1990.

3.11 Porada, T.W.: SD Module Environmental Loads. ED87012, key 24276[a], Nov. 28, 1990.

3.12 O'Brien, D.L.: Solar Dynamic Hooks and Scars. Rockwell International, Rocketdyne Division. EID–00365, key 33955[a], rev. D, July 9, 1990.

---

[a]Space Station *Freedom* library at the NASA Lewis Research Center in Cleveland, OH 44135 (tel. 216–433–5367 and fax 216–433–8050).

Chapter 4
Overall Description of Solar Dynamic Power System

4.1 Principles of Operation

The solar dynamic electric power system for Space Station *Freedom* is based on the closed-loop form of the Brayton thermodynamic cycle, which is shown in simplified form in figure 4.1. Heat is supplied to the cycle by means of a reflecting concentrator that focuses incident solar energy into a cavity type of heat receiver. The receiver includes heat-exchanging tubes through which the gaseous working fluid for the closed-loop Brayton cycle (CBC) heat engine passes. Also a quantity of a eutectic mixture of lithium fluoride–calcium fluoride ($LiF\text{-}CaF_2$) salts is contained in capsules around the receiver tubes for storage of thermal energy by the salt mixture's heat of fusion. The phase change (freeze-melt) temperature of the salt mixture is near 1042 K (1416 °F). During the sunlit portion of *Freedom*'s orbit, sufficient thermal energy is stored so that the gaseous working fluid exiting the receiver remains within a range of about 990 to 1030 K (1330 to 1400 °F) throughout the orbit.

The Brayton thermodynamic cycle is a single-phase gas cycle. In the closed-loop form of this cycle a compressor raises the pressure of the gaseous working fluid that then flows to a recuperator. There its temperature increases by transfer of heat from another part of the cycle. From the recuperator the gas passes to the receiver, where collected heat is added, and the gas temperature rises to the maximum level in the cycle. The high-temperature, high-pressure gas then flows to the turbine, where it expands to a lower temperature and pressure to produce mechanical work. A portion of the turbine work drives the compressor and the remainder drives the alternator, producing electric energy. After leaving the turbine the gas passes through the low-pressure side of the recuperator, where it transfers a large part of its remaining heat energy to the high-pressure gas from the compressor. From the recuperator the gas passes through the heat rejection system, where it gives up more heat, which is radiated to space. The cold gas then returns to the compressor, completing the loop.

The temperatures of the state points in the closed Brayton cycle have been selected so that refractory materials are not needed anywhere in the system. The gaseous working fluid is a mixture of helium and xenon with an equivalent molecular weight of 40, which results in the best combination of heat transfer and thermodynamic performance. Because the Brayton cycle is all gas, it is essentially insensitive to gravitational forces. Therefore, components and the system can be designed for space operation, and the performance can be proven with confidence in test facilities on Earth.

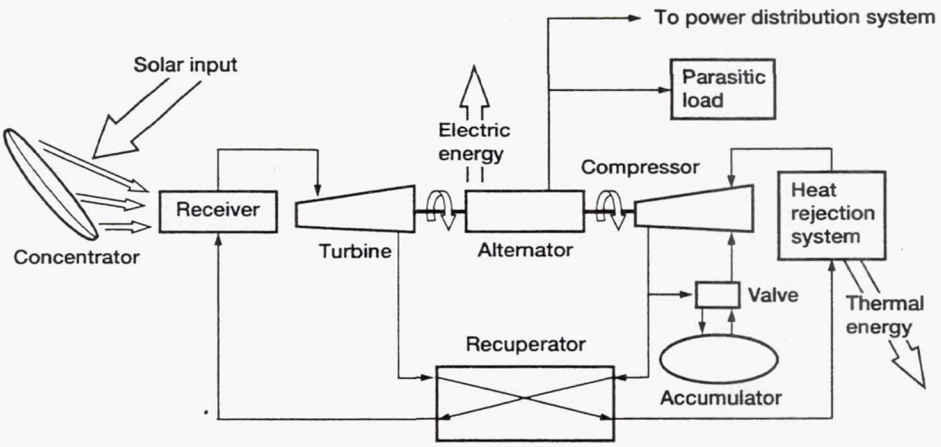

Figure 4.1.—Solar dynamic Brayton power system.

A solid-rotor, Lundell type of three-phase alternator that is mounted on the common shaft with the turbine and compressor converts mechanical energy to electrical energy as three-phase power. Power-conditioning equipment converts the three-phase electric power from the alternator to distribution-quality direct-current power.

The solar dynamic system must convert all of the energy collected by the concentrator because it is not practical to modulate, or control, energy collection. Therefore, variations in solar input energy (insolation) and in electric load demand are accommodated by combining control of the total amount of gas in the closed loop with a controllable parasitic electric load. The gas inventory in the loop is increased or decreased by valves connecting a gas-storing accumulator to the compressor inlet or outlet, respectively.

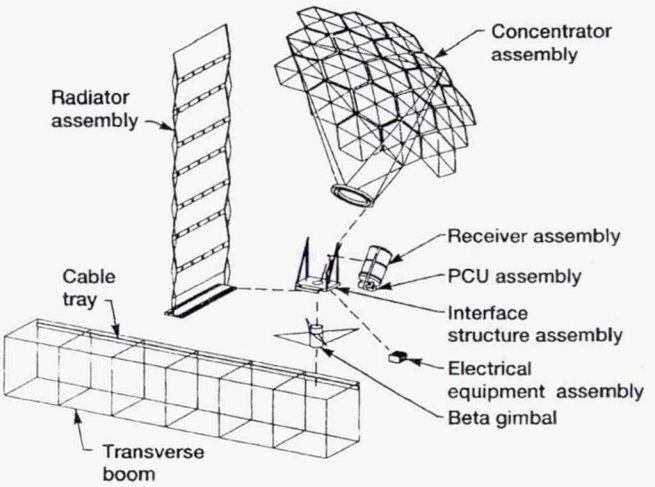

Figure 4.3.—Solar dynamic power module components.

4.2 Major Solar Dynamic Assemblies

Figure 4.2 shows a model of the solar dynamic power module as it existed in design documents at the beginning of the phase C/D Space Station *Freedom* Program. The main assemblies of the module are shown and identified in figure 4.3. Design progress has modified the details of the module, but these figures serve to orient the reader to the scale and nomenclature of the hardware. The designs as they existed just before the restructuring of the Space Station *Freedom* Program are treated later in this report.

The module includes six bays of the common 5-m truss structure that was to be used on *Freedom*. The solar dynamic functional equipment is attached to the outermost bay by a single-degree-of-freedom rotating joint (beta gimbal). The inner five bays ensure adequate clearance for equipment rotation and prevention of concentrator shadowing by other power modules. The rotation axis of this beta gimbal is at 90° to the axis of the alpha gimbal. The combined operation of the alpha and beta gimbals provides the coarse pointing of the concentrator. The alpha gimbal rotates once per orbit for orbit-by-orbit Sun tracking. The beta gimbal oscillates very slowly within a range of about ±52° to track the Sun through its periodic variation in position relative to the plane of *Freedom*'s orbit. Pointing the concentrator on the true line to the Sun to within the required accuracy is accomplished by a fine-pointing subsystem.

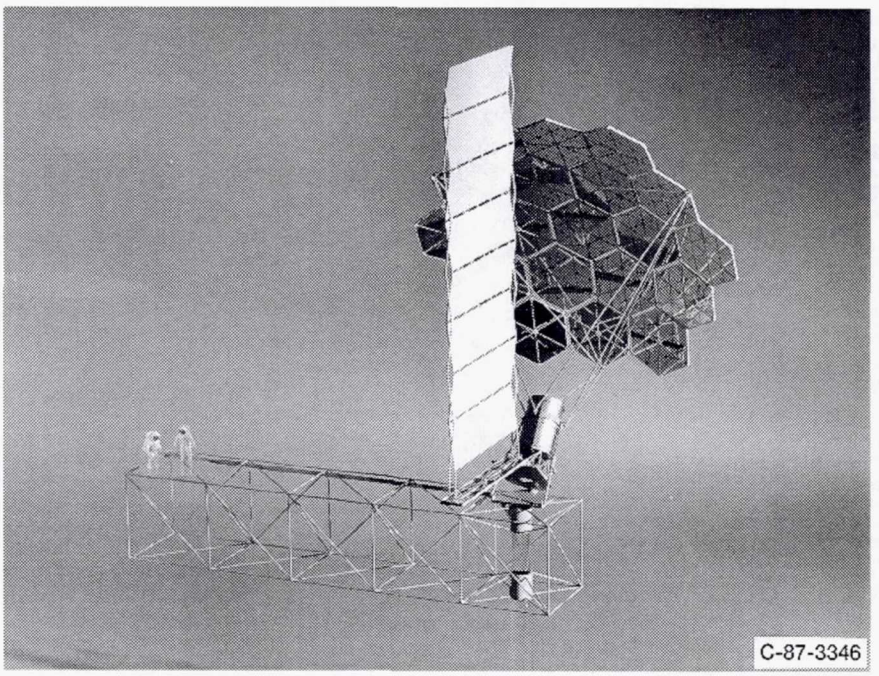

Figure 4.2.—Model of solar dynamic power module.

The major assemblies in the solar dynamic power module are the concentrator with its support structure and fine-pointing subsystem, the receiver, the power conversion unit, the heat rejection assembly, the electrical equipment assembly (EEA), and the beta gimbal. These assemblies are all mounted to, and tied together by, the interface structure, the seventh major assembly. These seven assemblies make up the functional set of hardware in the solar dynamic module. The truss was to be supplied by another program participant (NASA Johnson Space Center) and will not be treated in detail in this report. Electronics for control, power conditioning, and data handling are in the electrical equipment assembly.

The receiver, power conversion unit, and radiator combination is completely assembled and charged with gaseous working fluid (helium-xenon) and cooling liquid on Earth before launch to orbit. The concentrator panels and facets will be prealigned. The panels, with facets installed, are stowed in the NSTS orbiter bay before launch.

For growth in power capability, additional sets of functional solar dynamic hardware will be added to the manned base. Each set will increase the power capability by 25 kW. These hardware sets may or may not include truss bays, depending on the power increment added. Solar dynamic equipment sets are designed to be located on opposite faces of the outermost truss bay to provide 50 kW on each six-bay truss set. Solar dynamic module operation and provision of power will be continued for the required 30 years by periodic maintenance and replacement of assemblies or parts as orbital replacement units.

4.3 Solar Dynamic Interface With Remainder of Electric Power System

The physical interface between the solar dynamic module and the other electric power system components and elements was to be at the point where the solar dynamic module would be attached to the outermost photovoltaic module. The functional interface (i.e., where power is delivered or received and where commands and/or data are transmitted) was to be at the electrical connection points inside the outermost photovoltaic module.

Page intentionally left blank

Chapter 5
Solar Dynamic Module System Design

5.1 Key Requirements

Initial requirements for the solar dynamic module were formulated during phase B for use in the request for proposals. Since that time the key requirements have changed little. These requirements are contained in module-level contract end item (CEI) specifications, both a Government version and an expanded contractor-written version. See chapter 2 for a discussion of requirements documents.

The most fundamental requirement is the one that governs the energy conversion process. It requires the use of the closed Brayton cycle to convert solar thermal energy to mechanical energy and an alternator to convert mechanical energy to electrical energy. The solar dynamic power module is also required to provide electrical energy during the eclipse portion of the orbit by using stored thermal energy.

The CEI specifications also dictate the general characteristics of the assemblies that make up the solar dynamic power module. In most cases these requirements are actually design solutions and may not represent essential characteristics. For example, the hexagonal panel concentrator configuration and the pumped-fluid-loop radiator are currently specified, but if attractive alternatives are developed, the requirements could be modified and changes could be adopted.

The overall design of the solar dynamic power module is constrained by requirements for power output and for mass and volume limits. These requirements are discussed in this section.

5.1.1 Power Output

The specification of solar dynamic power includes not only the output power level but also requirements for the power characteristics and quality, the performance of the system over time (degradation), and the power availability.

The nominal power output level for one solar dynamic module was initially intended to provide 25 kW, measured at the user interface. Taking into consideration a particular electric power system architecture and expected losses and inefficiencies, a value could be calculated for the output of a solar dynamic module measured at the photovoltaic–solar dynamic interface. With the original 20-kHz EPS architecture this value was 28 kW (solar dynamic output power minus auxiliary power supplied to the solar dynamic module). The nominal power level is to be maintained throughout the orbit.

Between the solar dynamic alternator output and the photovoltaic–solar dynamic interface, there are electrical devices that make the alternator output compatible with the primary distribution (in voltage, frequency, and power quality). Because of the uncertainty in the power distribution architecture (and distribution efficiencies), it is convenient to refer to the solar dynamic module power in terms of alternator output. An alternator output specification of 30 kW corresponds to the original specification at the photovoltaic–solar dynamic interface and ensures that the sizing of all major solar dynamic components remains unaffected by changes in distribution architecture.

The solar dynamic module is required to provide peaking power at a level that is 15 percent higher than the nominal value for as long as 7.5 min during the sunlit portion of the orbit and 7.5 min during the eclipse. During orbits in which peaking occurs, the total energy that is requested from the solar dynamic module is limited to the total amount of energy that is provided during a nominal orbit. When designed to meet the specific solar dynamic peaking requirements, the solar dynamic module will inherently have the capacity to meet many other peaking scenarios (with various peaking levels and multiple peaks within an orbit). The exact implementation of a solar dynamic peaking orbit has not yet been defined. (It is probably necessary to use a peaking warning signal to notify the solar dynamic module that peak power is required.) See section 5.11.2 for more discussion of peaking operations.

Power degradation has not yet been specified for the solar dynamic module although the original CEI specification limited the rate of degradation of the concentrator reflective surface. It is expected that the degradation rate of the solar dynamic system will be less than that of the photovoltaic system, which is driven by solar array and battery degradation. A complete power specification must specify power availability, a measure of the probable output power level for a given period of time. Availability is difficult to predict because it depends not only on the reliability of a system and the hands-on repair time, but also on the time between a failure and the start of the repair (including, possibly, the time to get the replacement parts from the ground). For

design and requirements purposes an electric power system design availability has been defined. For design availability the replacement parts are assumed to be available after a uniform, specified administrative delay. Design availability is specified for the entire EPS; the translation to subsystems and the effect on reliability requirements has not been defined. Some initial lifetime requirements were defined at the start of the SD program to guide the designs of particular assemblies. See section 5.8 for a complete discussion on reliability, availability, and maintainability.

5.1.2 Mass and Volume

Two other important constraints on the solar dynamic module are the mass and volume requirements. These requirements call for the launch of two solar dynamic modules on one NSTS flight (with the exclusion, perhaps, of integration hardware). See section 5.9 for more discussion of launch packaging.

Some of the other important requirements that influence the design of the solar dynamic module are summarized here. Several key requirements have not yet been explicitly defined in formal documentation. Some of the requirements are addressed in other sections of this report. Most requirements are from reference 5.1.

The key solar dynamic requirements are as follows:

(1) Characteristics
- (a) Provide 30-kW continuous power output at the alternator (see sections 5.1 and 5.11).
- (b) Provide peak power output of 115 percent of nominal for 7.5 min during eclipse and 7.5 min during sunlit period (see section 5.1.1).
- (c) Limit power rating degradation to a value to be determined (as stated in section 5.1.1).
- (d) Limit power required for auxiliaries to 1 kW (except during startup).
- (e) Limit power required for the alternator spinup to self-starting speed to 6 kW for 30 sec (ref. 5.2).
- (f) Use closed Brayton cycle (see section 4.1).
- (g) Store thermal energy for use during eclipse (see section 6.2).
- (h) Accommodate coarse pointing (alpha/beta) performance of ±3° (see section 5.7).
- (i) Withstand solar walkoffs (movement of concentrated solar energy) and module detracking.
- (j) Accommodate on-orbit cold soaks, cold starts, and hot restarts (see section 5.11).
- (k) Allow safe planned and unplanned shutdowns (see section 5.11).
- (l) Allow automated startup and shutdown (see section 5.11).
- (m) Have control capability to monitor, evaluate, and control performance and to detect, isolate, and control faults.
- (n) Provide power protection against overloads and faults in the distribution system.
- (o) Provide thermal control through a local, autonomous system (see section 6.4).
- (p) Provide a fluid leak detection method.
- (q) Maintain power source design availability as to be determined (see sections 5.1.1 and 5.8).
- (r) Incorporate single-point grounding.
- (s) Provide software control functions.

(2) Physical characteristics
- (a) Limit on-orbit module mass to 15 673 lb, excluding the Government-furnished truss (see section 5.4).
- (b) Limit launch mass as to be determined (see sections 5.1.2, 5.4, and 5.9).
- (c) Keep launch volume sufficiently low to permit two modules per NSTS launch (see sections 5.1.2 and 5.9).
- (d) Maintain inertia and center-of-mass constraints as given in figure 5.3.
- (e) Be protected from natural and induced environments (see chapter 3).

(3) Reliability
- (a) Fail in safe mode and be on-orbit restorable.
- (b) Provide automatic redundancy management and redundancy status to PMAD.
- (c) Remain operational for 30 years through inspection, maintenance, and ORU restoration (see section 5.8).

(4) Maintainability — Limit maintenance to amount of extra- and intravehicular activity (EVA/IVA in person-hours per year) as to be determined (see section 5.8).

(5) Environmental conditions
- (a) Accommodate natural environment prescribed in reference 5.3.
- (b) Although orbit is circular with 28.5° inclination and an altitude range of 180 to 240 n mi, be capable of operating in degraded mode from as low as 150 n mi to as high as 270 n mi.
- (c) Accommodate a solar insolation range from 1326 to 1418 W/m^2.
- (d) Accommodate specified induced environments (see chapter 3).
- (e) Accommodate NSTS and on-orbit design loads (see chapter 3).

(6) Transportability
- (a) Be delivered to orbit within the NSTS orbiter (see section 5.9).
- (b) Satisfy ground transportation requirements.

(7) Design and construction standards — Conform to specified standards.

(8) Safety
- (a) Follow safety design order of precedence — eliminate hazards by design, use safety devices,

use warning devices, and minimize hazards through maintenance.

(b) Provide precautions against concentrated solar flux (see chapter 6).

(9) Logistics

(a) Use initial assembly resource allocations as to be determined (see section 5.10).

(b) Limit yearly resupply mass and volume as to be determined (see section 5.8).

(10) Characteristics of solar dynamic assemblies (see chapters 6 to 10).

(11) Flight support equipment, orbital support equipment, and ground support equipment—Follow physical characteristic and construction standards.

(12) Verification—Use verification methods and phases given in reference 5.4.

5.2 Design Evolution

5.2.1 Phase B Design Evolution

From April 1985 to January 1987 the Space Station Program conducted studies and analyses in a period called phase B. WP–04 had contracts with TRW and Rocketdyne for the space station[2] electric power system. Each contractor investigated systems that included both photovoltaic and solar dynamic power sources. Both organic Rankine cycle (ORC) and recuperated closed Brayton cycle (CBC) solar dynamic systems were studied in phase B. The objective during phase B was to define the electric power system in sufficient detail so that its performance and physical characteristics could be evaluated and cost estimates could be formulated.

Throughout phase B the selection of photovoltaic or solar dynamics as the power source for the space station remained an issue. The photovoltaic systems were judged to have lower development costs and risk and good inherent peak and contingency power characteristics, but probably higher life-cycle costs and a limited growth power level. The solar dynamic systems were expected to have higher development costs and risks but lower life-cycle costs and higher growth power potential. By the end of phase B the recommendation was for a hybrid power system with 37.5 kW photovoltaic and 50 kW solar dynamic.

An iterative design process was used during the phase B development of the solar dynamic modules (ORC and CBC). First, the initial reference concepts were defined and then promising options and updates of reference concepts were identified and developed. Next, the preferred options were selected and the final reference concepts were defined and characterized.

The solar dynamic modules evolved during phase B largely by means of tradeoff studies. Tradeoff studies were used to investigate many of the assembly- and component-level design options including, for example, concentrator deployment options, radiator type, and alternator selection. System-level studies looked at thermodynamic state-point selection, module power level (from 18.75 to 37.5 kW), and methods and configurations for solar pointing.

A number of significant solar dynamic design decisions were made during the Rocketdyne phase B effort. Among these was the selection of the parabolic offset concentrator concept. This concept solved a potential problem of a high module mass moment of inertia about the alpha axis, which could lead to controls and structures interaction problems. The erectable hexagonal panel concentrator concept was selected over deployable concepts. The two-axis gimbal mechanism for concentrator pointing was developed as the preferred fine-pointing method. A deployable, planar, single-phase, pumped-loop radiator was identified as the best concept for heat rejection, winning out over constructible heat pipe concepts. Most of these design decisions were based on expected cost savings plus other factors, such as technical risk.

The CBC module size was set at 25 kW largely on the basis of EPS redundancy requirements (in particular the power level requirement after the failure of one solar dynamic module). See the appropriate sections for more discussion of the evolution of the assembly designs.

About three-fourths of the way through phase B, TRW withdrew from the program. Their efforts are reported in a number of data submittals. Probably the most helpful document, containing TRW's most advanced solar dynamic concepts, is reference 5.5. Rocketdyne summarized their phase B efforts in reference 5.6, from which all of their other phase B documents can be identified.

By the time of the phase C/D proposal evaluation the decision had been made to develop *Freedom*'s electric power system (EPS) in a two-phase approach with a 75-kW photovoltaic source in phase 1 followed by a 50-kW solar dynamic source in phase 2. During the proposal evaluation process the closed Brayton cycle was selected over the organic Rankine cycle for the solar dynamic source.

Rocketdyne was awarded the phase C/D contract in 1987. The solar dynamic team included subcontractors that had been associated with Rocketdyne in phase B: Rocketdyne as prime contractor, AiResearch Division of Allied-Signal for the receiver and PCU, Harris Corporation for the concentrator, and LTV for the radiator.

5.2.2 Phase C/D Design Evolution

Because of the two-phase approach for the development of space station power, the SD program was a limited effort during phase 1 while the rest of the EPS entered a true,

[2]The space station was named Space Station *Freedom* in 1988.

classical phase C/D of the project cycle. Full-scale solar dynamic development and production of the solar dynamic power system was to begin with the start of phase 2.

The design of the solar dynamic module was refined, however, during phase 1. Most of the design refinements occurred within the individual assemblies and are discussed in chapters 6 to 10. With the exception of the fine-pointing method, which was being rebaselined at the close of the SD program, the overall solar dynamic module configuration changed little during the phase 1 design effort, although several other areas were investigated.

Some of the module investigations were of a highly interdependent nature, involving many systems and assemblies. For example, solar dynamic state-point selection directly affects the receiver, the PCU turbomachinery and heat exchangers, and the radiator. It also affects the concentrator sizing as tradeoffs are made between cycle efficiency and the ratio of concentrator to radiator area. The state-point analysis results are discussed in section 5.5.

Another example of a highly interdependent area is solar dynamic pointing system design, where pointing characteristics (controller bandwidth, pointing accuracy, slew rates, configuration, etc.) are traded off against receiver aperture plate capabilities, launch mass and volume considerations, and structural modal frequency requirements for the solar dynamic module assembly. As a result of the pointing system study, a new concept was developed, called the beta-fine pointing concept. This concept was developed too recently to be baselined in Rocketdyne documentation. See section 5.7 for a description of the solar dynamic pointing configurations.

The radiator location was part of another module-level study during phase 1, as it had been briefly in phase B. The original, "collocated" concept had the radiator placed in front of the concentrator, on the same side of the truss as the other solar dynamic assemblies. An alternative had the radiator located on the opposite side of the truss, for the primary purpose of balancing the solar dynamic module mass and drag about the centerline of the truss (alpha axis). This "underslung" configuration could minimize the impact of solar dynamic modules on the space station guidance, navigation, and control (GN&C) system. The study concluded that the original configuration did not place excessive burdens on the GN&C system and the collocated configuration was retained. The underslung configuration also had the practical problems of running the fluid lines to the radiator and supporting the radiator and difficulties in adding solar dynamic modules for power growth. (The growth plan calls for solar dynamic modules to be paired up on opposite sides of the truss.)

The specification of solar dynamic module power output characteristics (ac or dc and voltage levels) affects the design of the module to the extent that the alternator output and electrical equipment are different for different distribution architectures. As the station architecture changed from 20 kHz to dc, the function (and efficiencies) of the electrical equipment changed, the PMAD efficiency changed and the solar-dynamic-generated power available to the user changed. Had the original solar dynamic power to the user been fixed (it was not), the entire module would have needed resizing.

Electrical equipment efficiency is also affected by the fact that the solar dynamic heat rejection system must actively cool the electrical equipment. This load on the heat rejection system is in addition to the cycle waste heat load. For a fixed radiator area, increases in electrical equipment thermal losses (reduced efficiencies) result in higher gas temperatures at the compressor inlet, increasing the work required of the compressor and decreasing useful work output at the alternator.

Future development of a solar dynamic power module will require the reevaluation of these and other module-level design issues.

5.3 Module Configuration and Hardware Tree

5.3.1 Baseline Definition

The baseline configuration of the solar dynamic module is documented in a Rocketdyne engineering design document (EDD) (ref. 5.7), which was updated periodically. The solar dynamic configuration in the EDD is intended to be consistent with released versions of Rocketdyne specifications and drawings (see chapter 2). For information purposes only, Rocketdyne included some preliminary (nonbaseline) solar dynamic information in the EDD, along with a note of its preliminary nature. The EDD was officially submitted to NASA Lewis at regular intervals as power system description documents (e.g., ref. 5.8).

Changes to the EDD are made through a formal change procedure. Since the release of the last official update of the EDD that included solar dynamics, some changes have been developed and proposed for the solar dynamic module, resulting in several different configurations. The EDD baseline is the module configuration as it appears in the EDD, revision G. The revised baseline is a minor departure from the EDD baseline, primarily in an update of assembly masses. The module configuration with beta fine pointing represents a third configuration, called the beta fine-pointing concept. This concept also includes a change in the receiver tilt angle and the aperture offset. (See section 5.7 for more discussion of the beta fine-pointing concept.)

5.3.2 Hardware Tree

The solar dynamic module (all configurations) is composed of eight assemblies that were originally defined in the CEI specification. Most of these eight assemblies can be

further divided into smaller components. Components that are designed to be replaceable on orbit are called orbital replacement units (ORU's). There are 42 different kinds of ORU's in a solar dynamic module for the EDD and revised baselines (the beta fine-pointing concept has fewer). The selection and designation of ORU's depend on the particular function and design of the components as well as maintainability considerations. See section 5.8 for more discussion on solar dynamic ORU selection and designation.

The solar dynamic hardware tree identifies all of the solar dynamic assemblies and ORU's and some lower level parts. It is shown in figure 5.1 (EDD and revised baselines).

A corresponding hardware tree has not been developed for the beta fine-pointing concept.

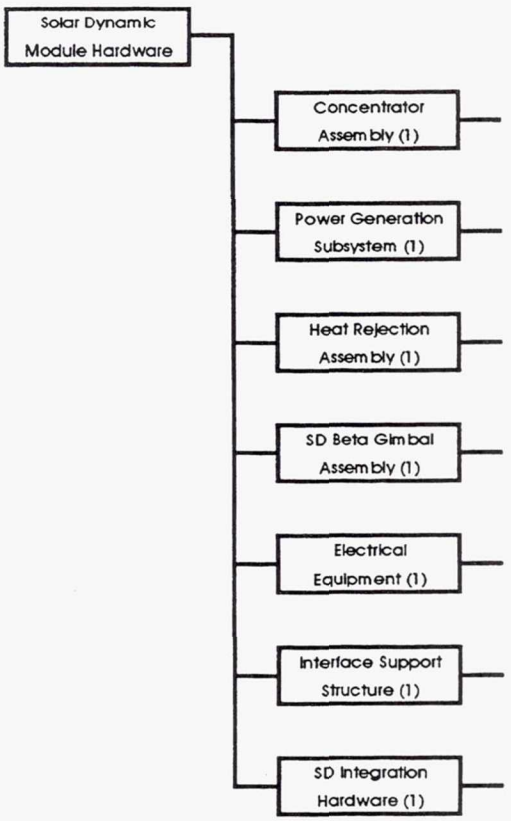

Figure 5.1.—Solar dynamic hardware tree. (See following figures for lower hardware levels.)

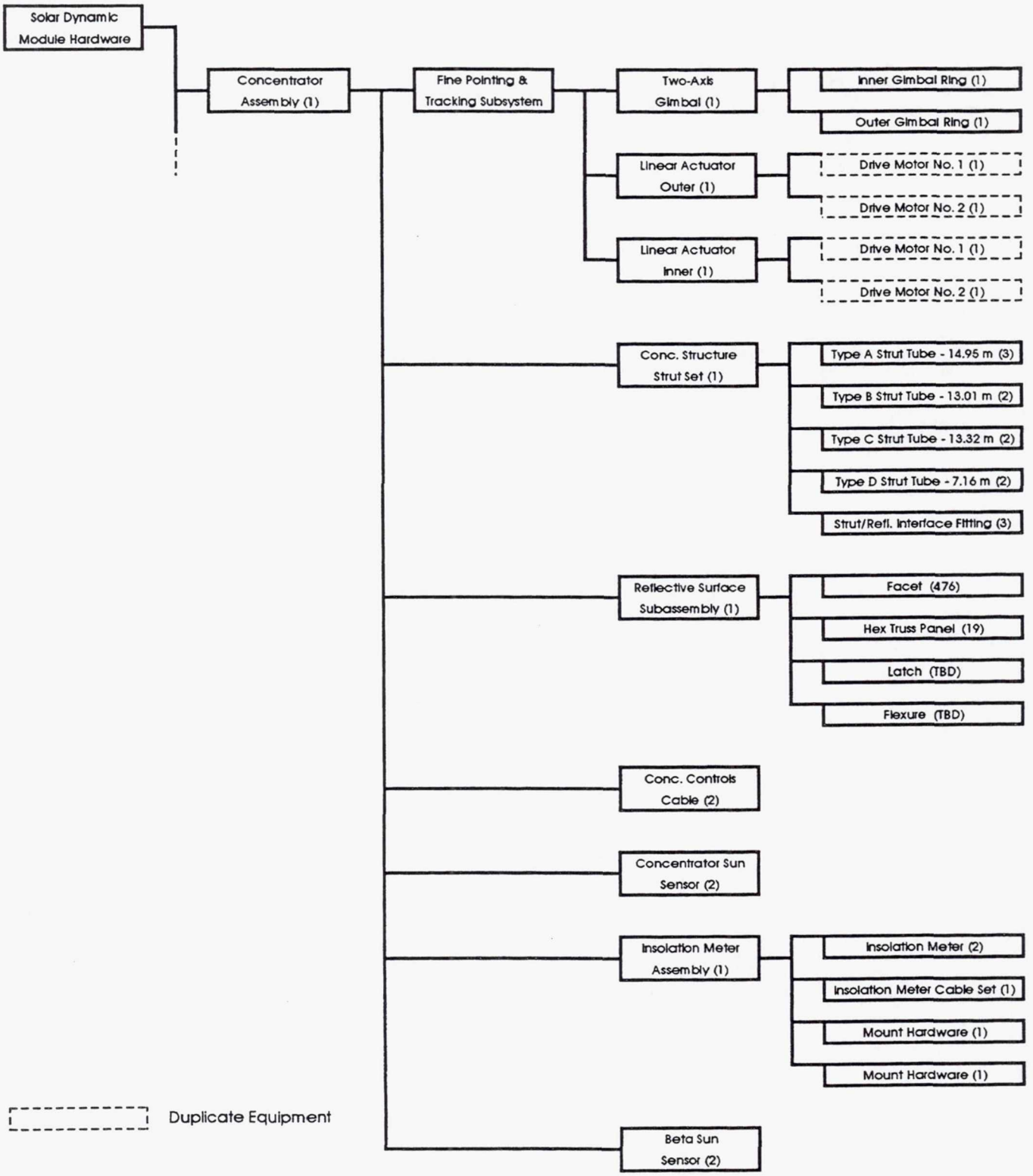

Figure 5.1.—Continued.

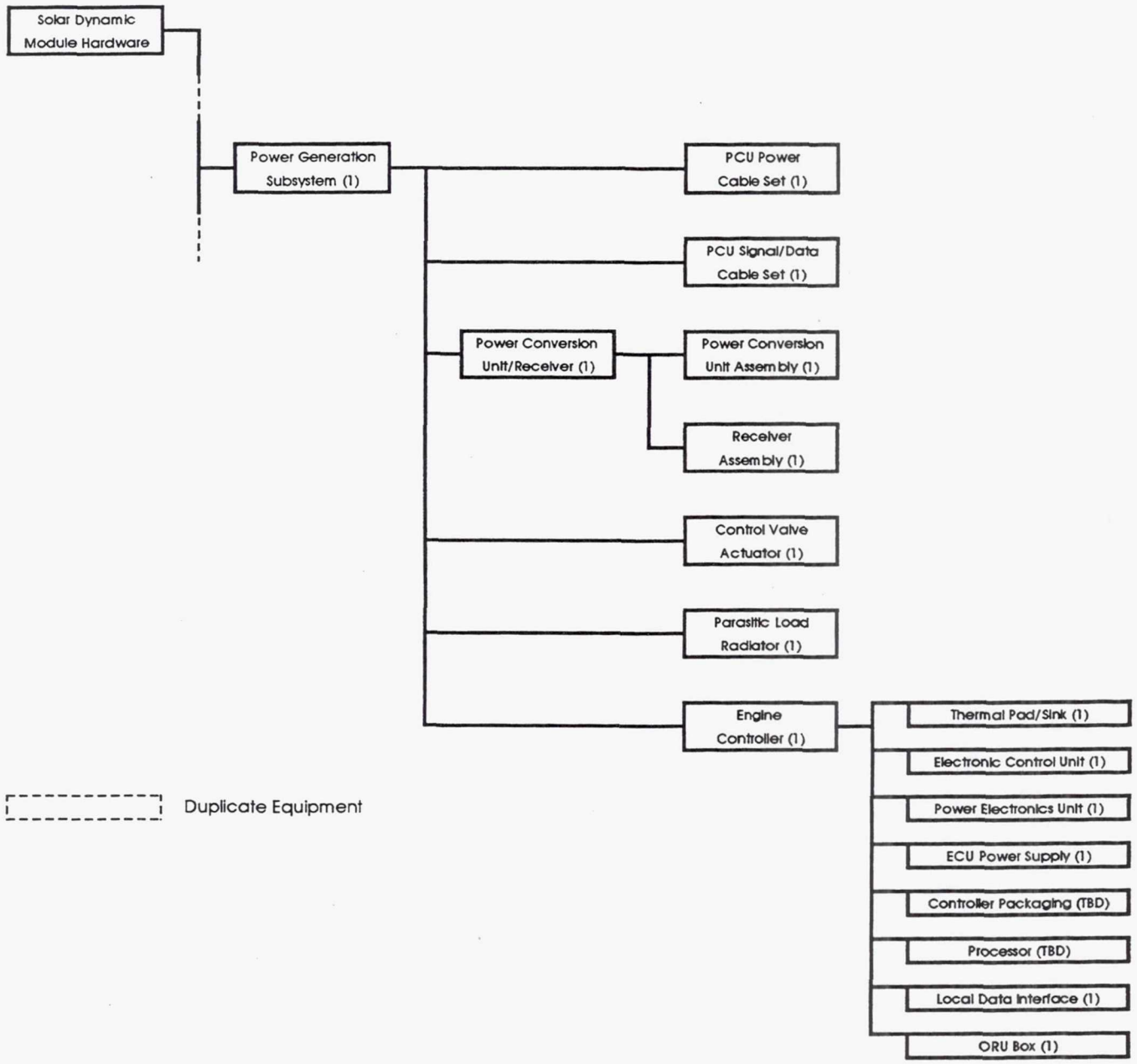

Figure 5.1.—Continued.

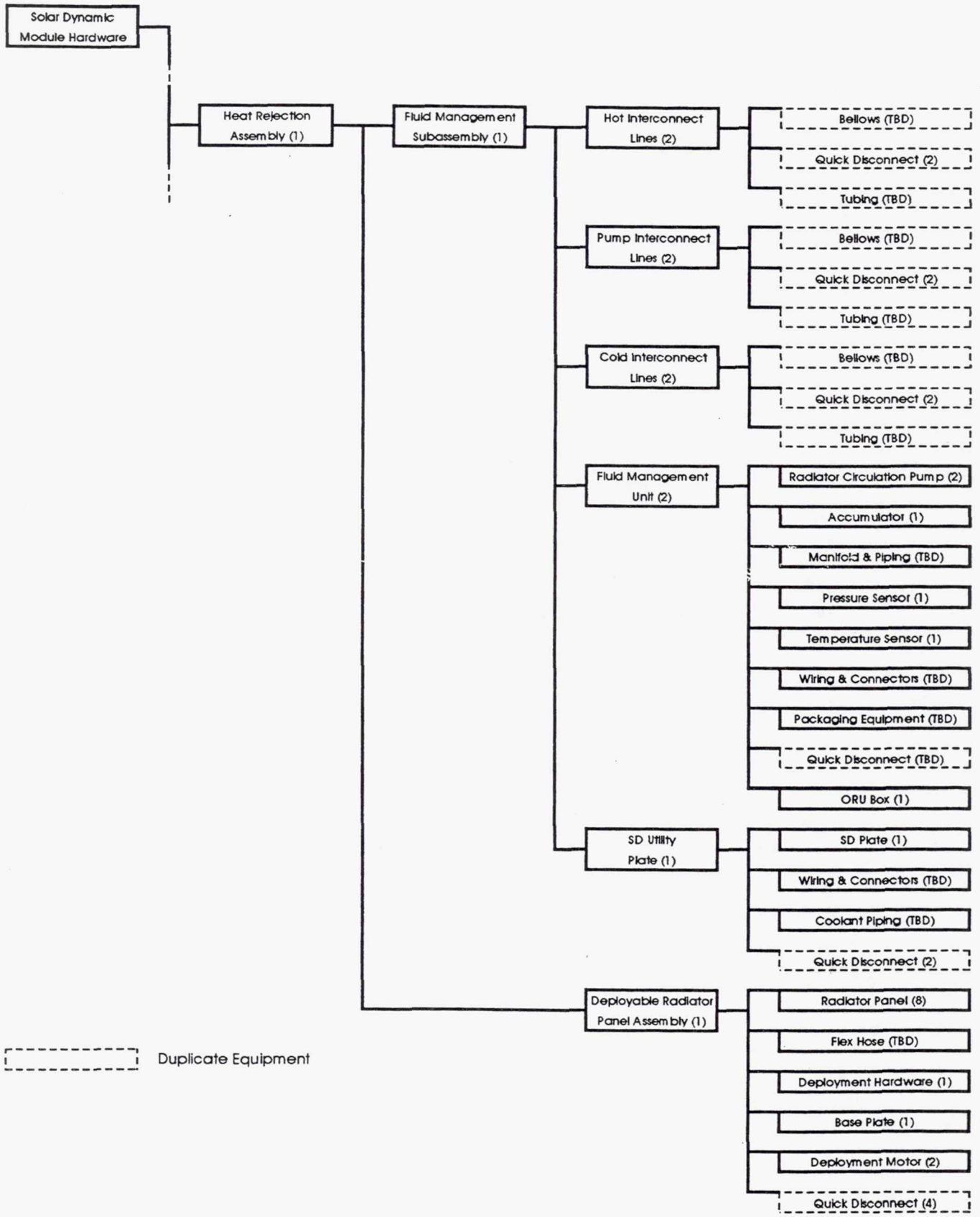

Figure 5.1.—Continued.

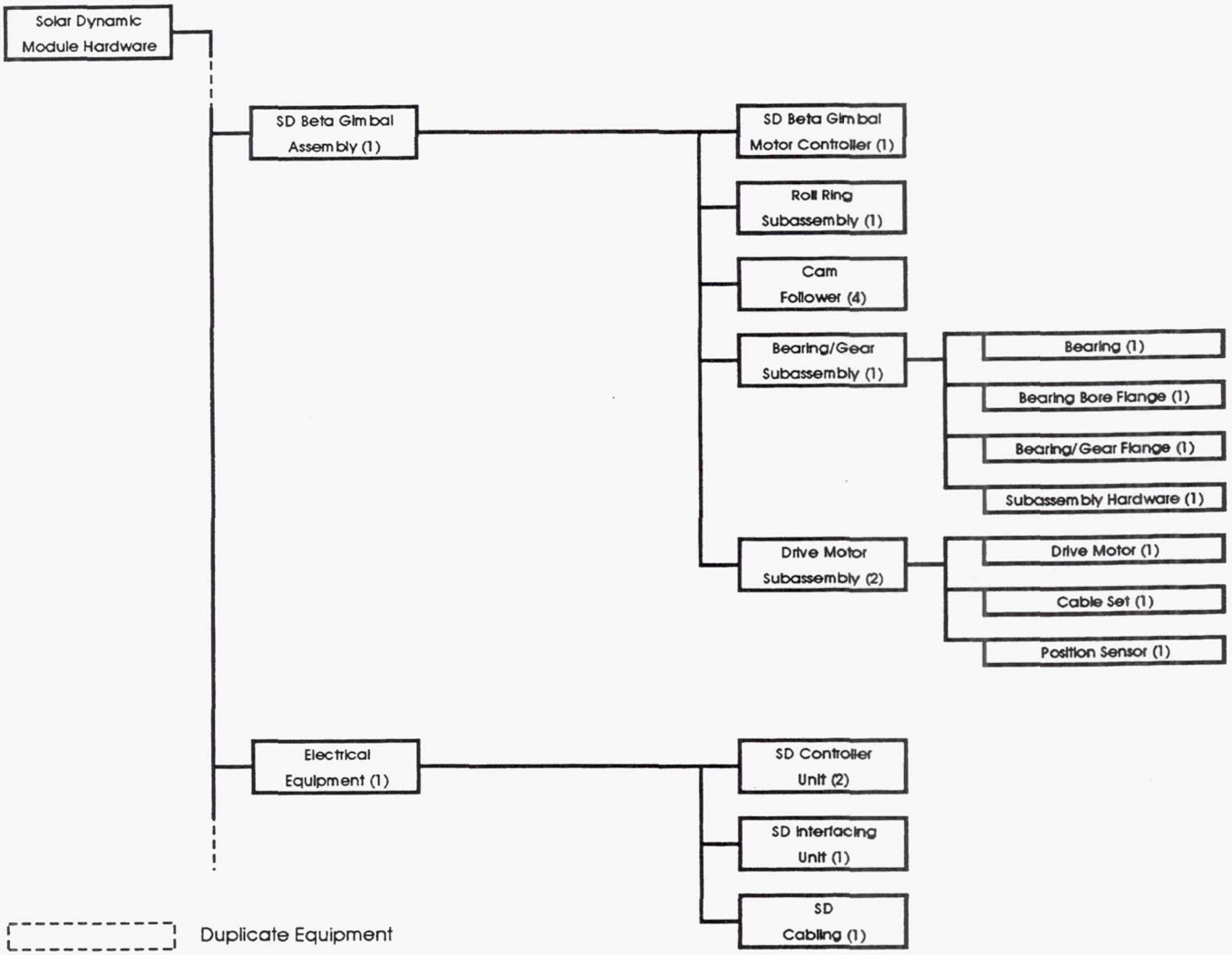

Figure 5.1.—Continued.

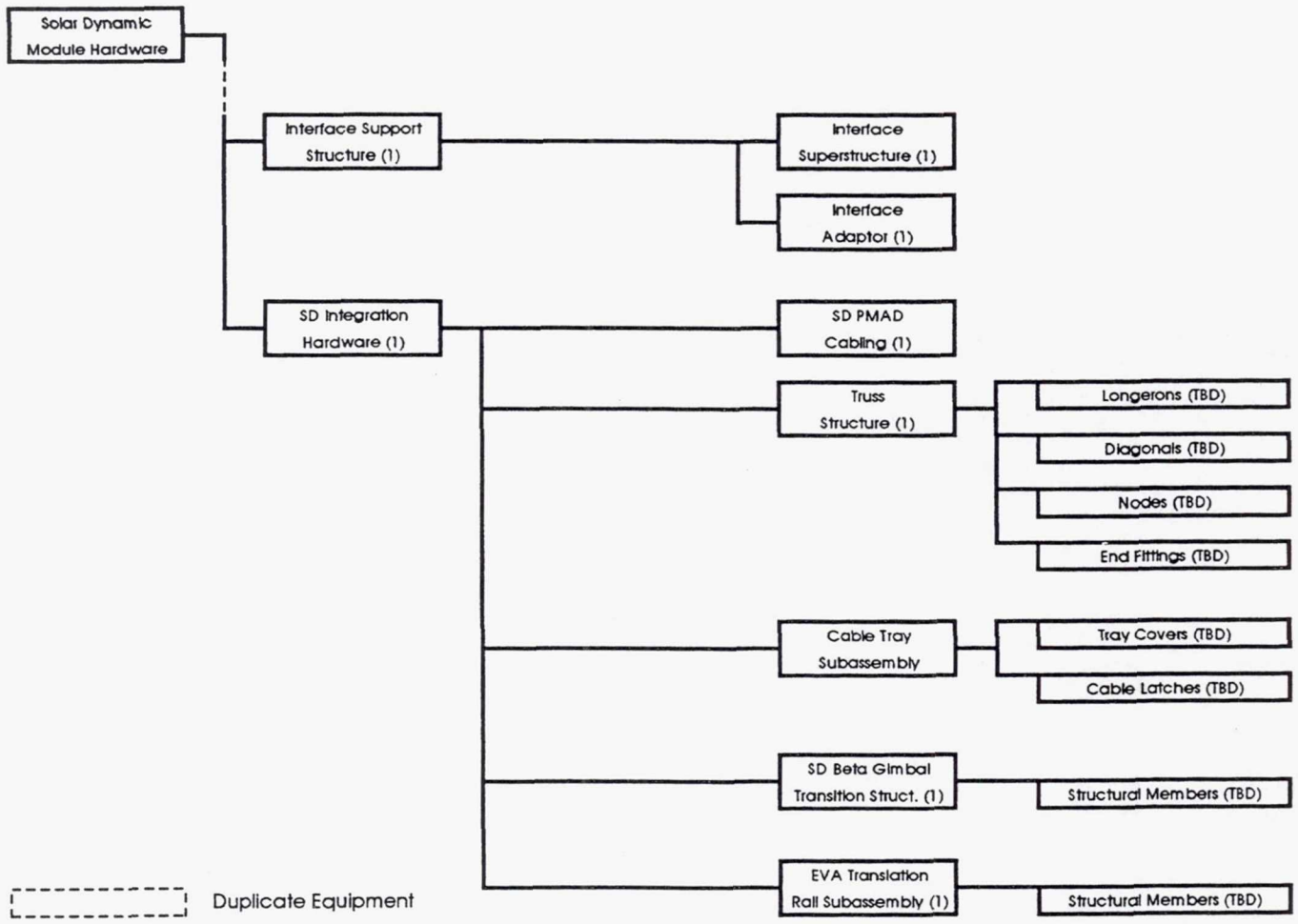

Figure 5.1.—Concluded.

5.4 On-Orbit Physical Characteristics

On-orbit module physical characteristics include mass and mass distribution, mass moment of inertias, drag areas, and deployed envelopes.

Figure 5.2 shows a layout of the solar dynamic module for the EDD baseline. For the revised baseline and the beta fine-pointing concept the relative locations of the radiator, the concentrator, and the receiver are almost the same as for the EDD baseline (see section 5.3.1 for baseline definition).

Table 5.1 presents the solar dynamic assembly masses for the EDD baseline, the revised baseline, and the beta fine-pointing concept. Also shown for comparison are the proposed assembly masses at the start of phase 1. Individual assembly masses are discussed in chapter 6.

Each module configuration has its own mass distribution and corresponding inertia matrix. For rough calculation purposes the centers of mass and the mass moments of inertia are given for the EDD baseline in figure 5.3. More information on solar dynamic mass properties is given in references 5.2 and 5.9.

Aerodynamic drag is difficult to quantify because it depends on the orientation of the solar dynamic module with respect to *Freedom*'s direction of flight. The orientation varies not only continuously throughout the orbit but also as the beta angle changes to accommodate orbit precession. The drag areas of most of the solar dynamic module components can be found in reference 5.10. Drag forces are based on the drag area, the drag coefficient, and the atmospheric density. Solar dynamic module drag forces are calculated for various beta angles in reference 5.9.

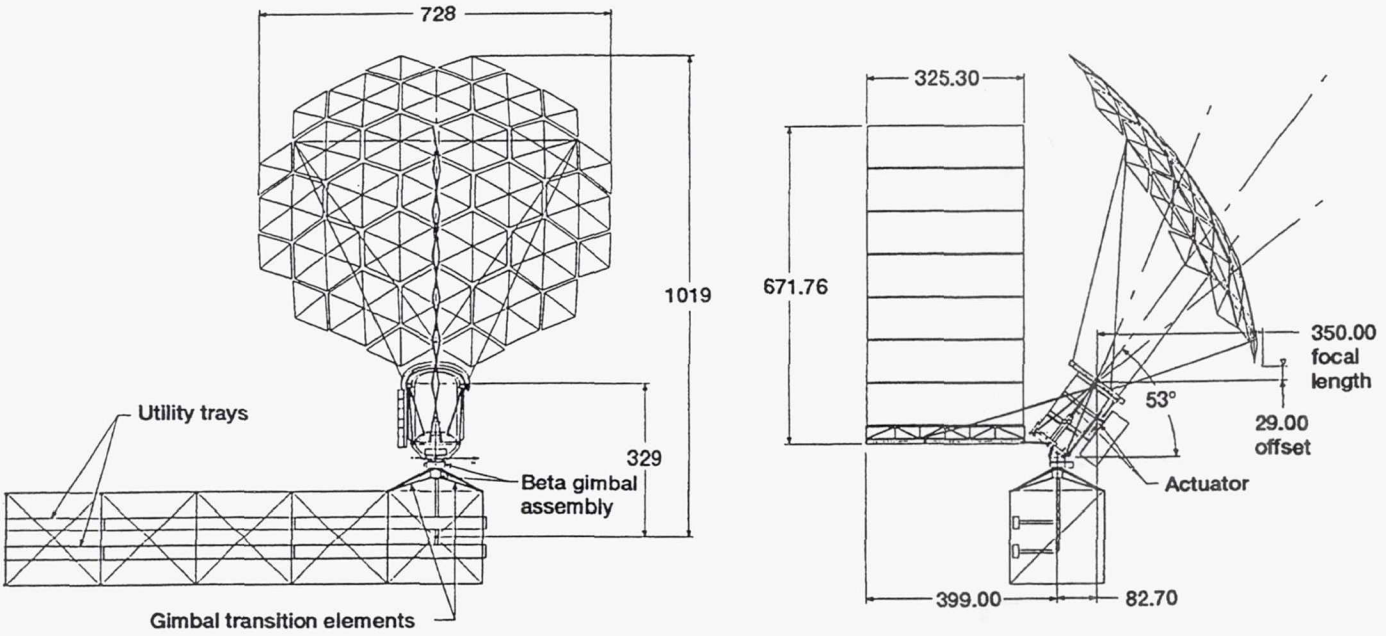

Figure 5.2.—Solar dynamic module layout. (Linear dimensions are in inches.)

TABLE 5.1.—SOLAR DYNAMIC MODULE MASS HISTORY

Assembly	Configuration			
	Proposed[a]	EDD baseline[b]	Revised baseline[c]	Beta fine pointing[d]
	Mass, lb			
Concentrator	3 275	3 345	3 468	2 205
Receiver	3 862	3 862	3 862	3 862
PCU	1 742	1 742	1 742	1 742
Heat rejection	3 371	2 990	2 990	2 990
Interface structure	828	828	1 328	437
Beta gimbal	605	420	420	420
Electrical equipment	564	634	634	634
WP–04 total	14 247	13 821	14 444	12 290
Integration hardware	1 500	2 110	2 974	2 974
Solar dynamic module total	15 747	15 931	17 418	15 264

[a] From Rocketdyne technical proposal, July 1987 (ref. 5.11).
[b] From Rocketdyne solar dynamic design description, April 1991 (ref. 5.10).
[c] Private communication from Rocketdyne, February 1991 (ref. 5.12).
[d] From module design change documentation, December 1990 (ref. 5.13).

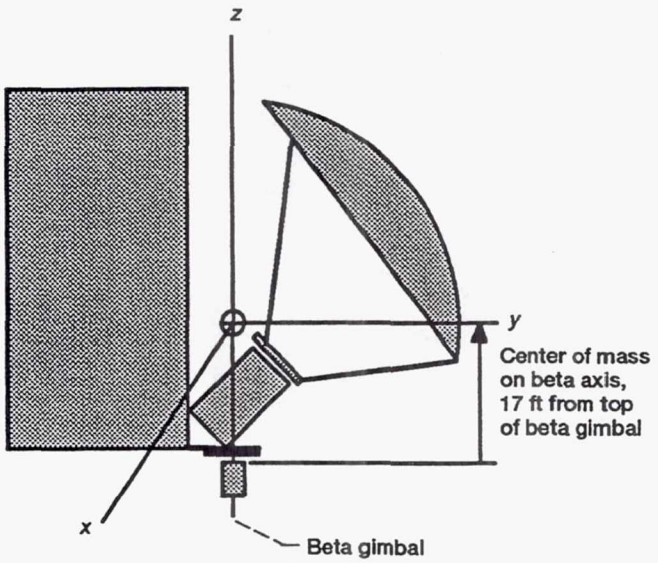

Figure 5.3.—Module mass properties. Module mass, 13 821 lb (excluding integration hardware). I_{xx} = 6.4 x 10^6 lbm-ft^2; I_{yy} = 4.5 x 10^6 lbm-ft^2; I_{zz} = 2.9 x 10^6 lbm-ft^2. (Not to scale.)

5.5 Performance Analysis Results

The power flow diagram for the solar dynamic module is shown in figure 5.4 for the design conditions (i.e., 180-n mi altitude, minimum insolation, 3-year degradation, at sunrise). The module power output at the photovoltaic–solar dynamic interface corresponds to a user power level of 25 kW with a margin associated with the excess power on the parasitic load radiator (PLR). The PCU produces more power than is required for the 25-kW demand, and the excess power is dissipated in the PLR. The CBC state points for the design conditions are shown in figure 5.5.

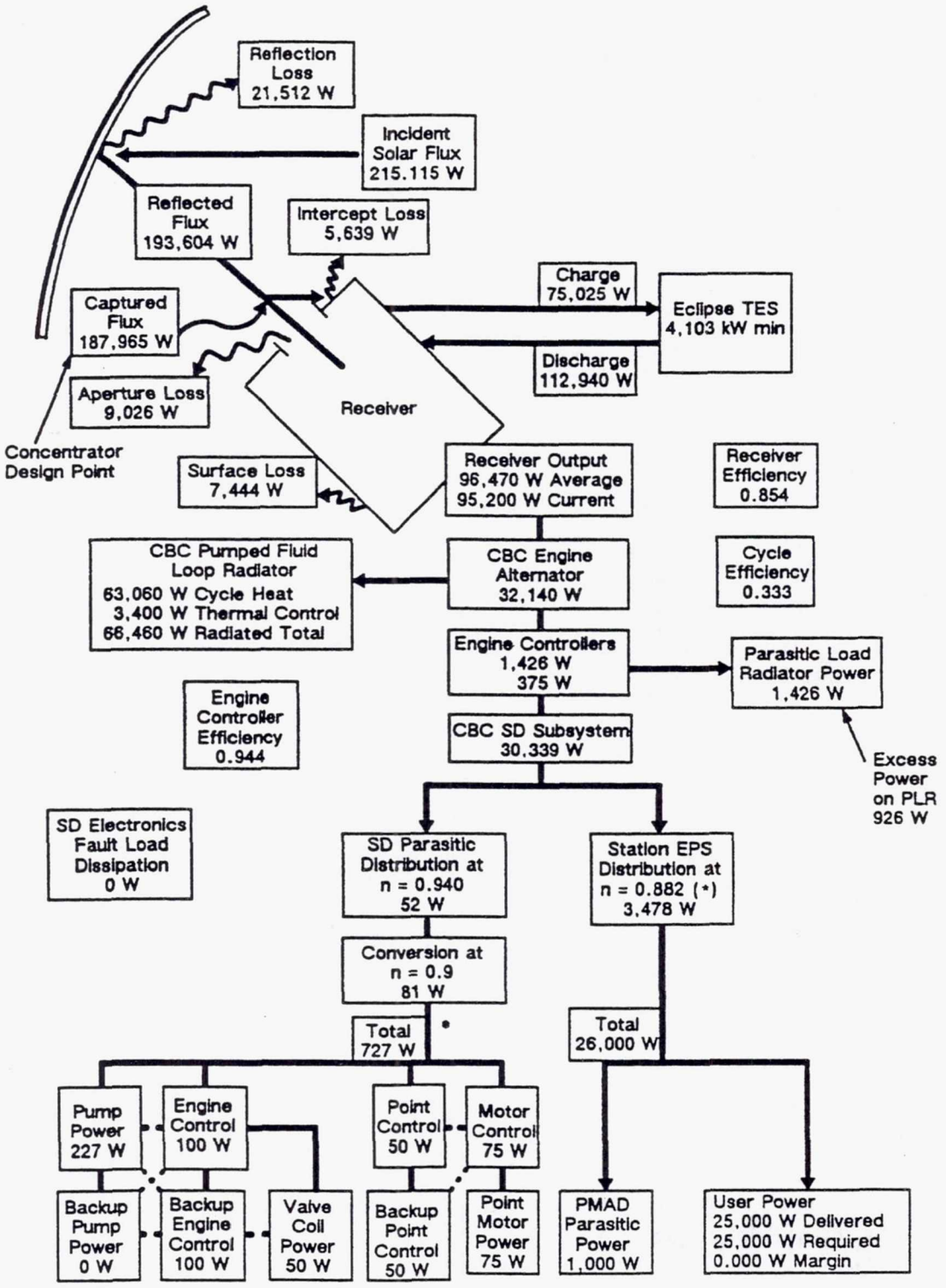

*Based on phase B 20-kHz efficiency.

Figure 5.4.—Power flow diagram—minimum insolation orbit (sunrise) and nominal demand. Period, 91.02 min; sunlight, 54.69 min; insolation, 1323 W/m ^{2}; reflectivity, 0.9; required concentrator net effective area, 162.6 m ^{2}

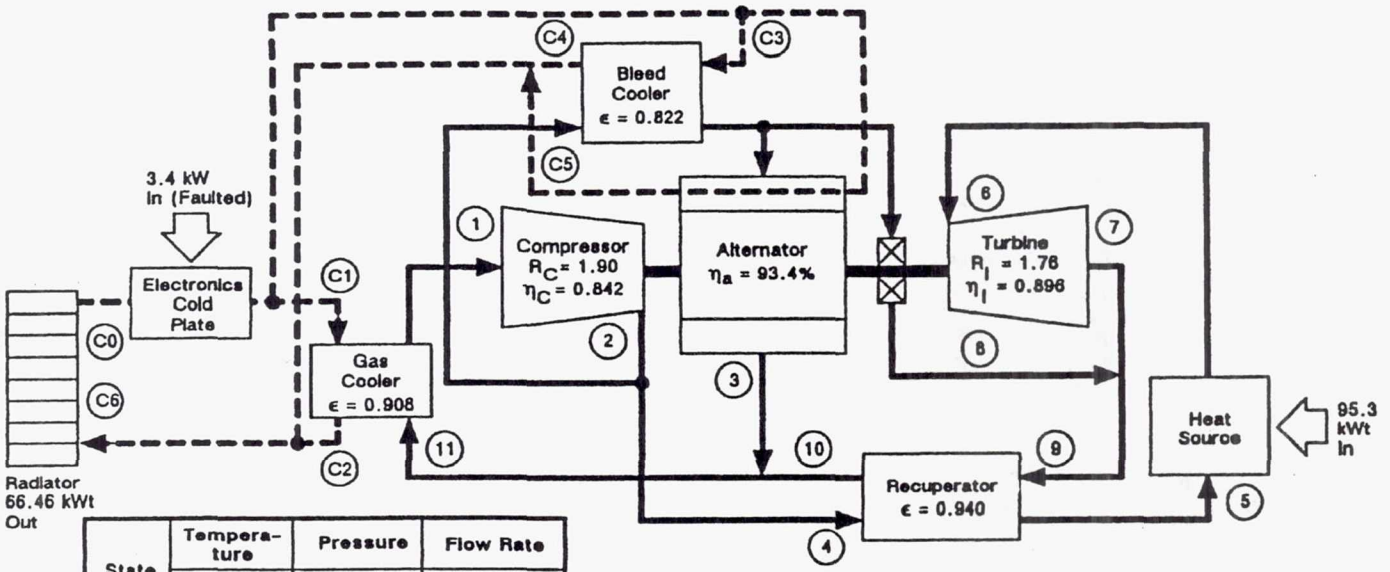

State Point	Temperature (°F)	Pressure (psia)	Flow Rate (lbm/s)
1	58.02	26.97	1.9276
2	238.67	51.35	1.9276
3	440.69	27.25	0.0386
4	239.04	51.28	1.8794
5	974.67	50.90	1.8794
6	1361.49	49.17	1.8794
7	1025.90	27.66	1.8794
8	133.66	27.66	0.0096
9	1021.29	27.62	1.8890
10	289.39	27.25	1.8890
11	292.42	27.25	1.9276
C0	15.99	-	0.5405
C1	27.54	-	0.4534
C2	244.87	-	0.4534
C3	27.54	-	(a)
C4	145.55	-	(a)
C5	98.47	-	(a)
C6	224.19	-	0.5405

[a]To be determined.

Figure 5.5.—CBC subsystem state-point diagram for design-point conditions and nominal demand. Electrical output, 32.15 kWe; beta, 0.934; bearing loss, 0.822 kW; windage loss, 1.745 W; net cycle efficiency, 33.75%; rotor speed, 32 000 rpm; sink temperature = 186 K (–125 °F); emissivity, 0.9; coolant, *n*-heptane; minimum insolation orbit at sunrise.

The power flow diagram for the solar dynamic module for the maximum-insolation case (250-n mi altitude, maximum insolation, beginning of life, at sunset) is shown in figure 5.6. For these conditions the module power output meets the 25-kW requirement with a margin associated with the excess power on the PLR. The CBC state points for these conditions are shown in figure 5.7.

Power flow diagrams for the solar dynamic module during peak power demand at the design conditions are shown in figure 5.8. The peak power demand from the solar dynamic module at the users is 28.75 kW (15 percent peaking). During off-peak periods the solar dynamic power module output is reduced so that the orbital average power output at the users is 25 kW. CBC system state-point parameters during peak conditions are shown in figure 5.9.

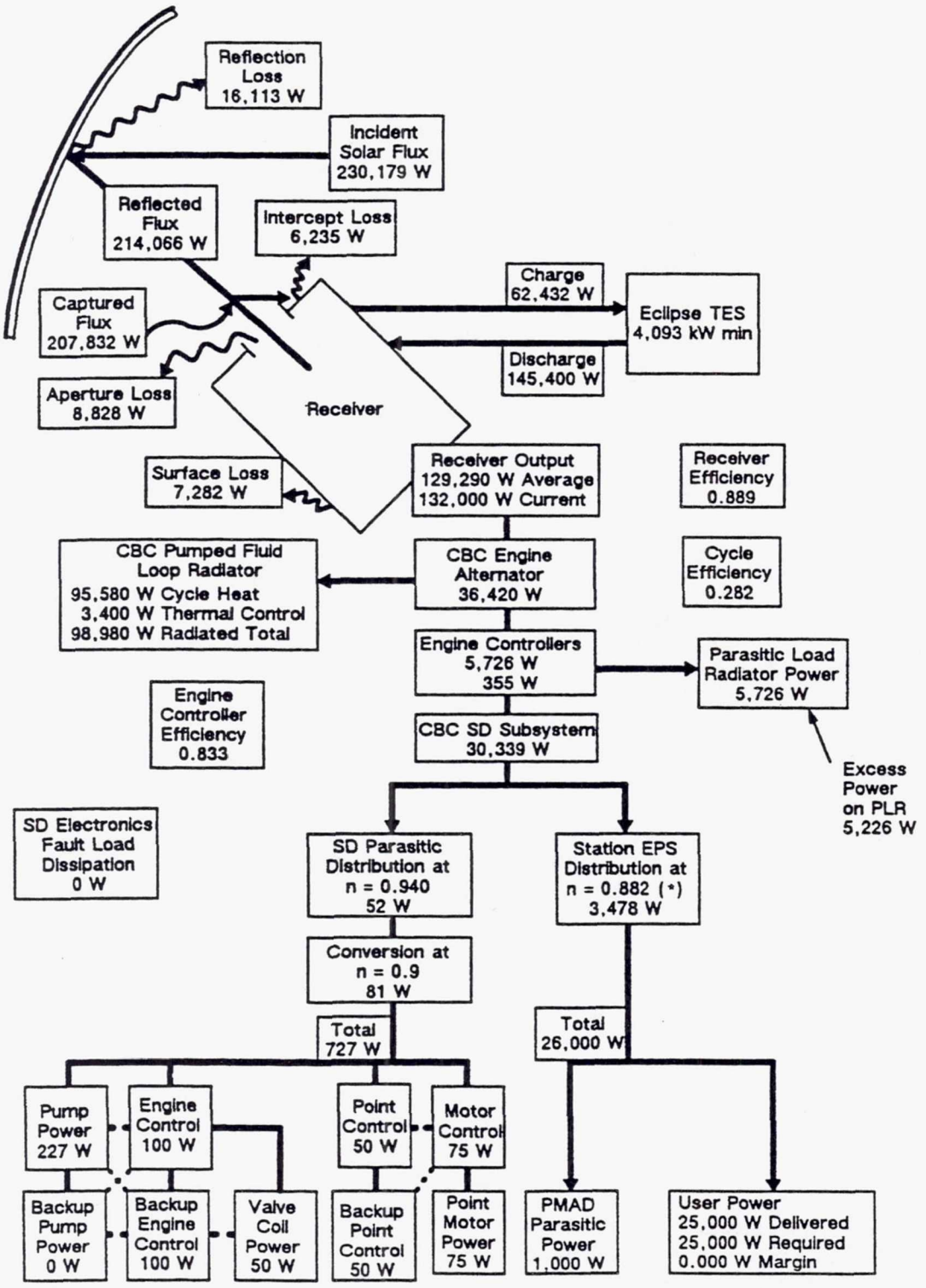

*Based on phase B 20-kHz efficiency.

Figure 5.6.—Power flow diagram—minimum insolation orbit (sunrise) and nominal demand. Period, 93.71 min; sunlight, 65.56 min; insolation, 1419 W/m ^{2}; reflectivity, 0.93; required concentrator net effective area, 162.6 m ^{2}.

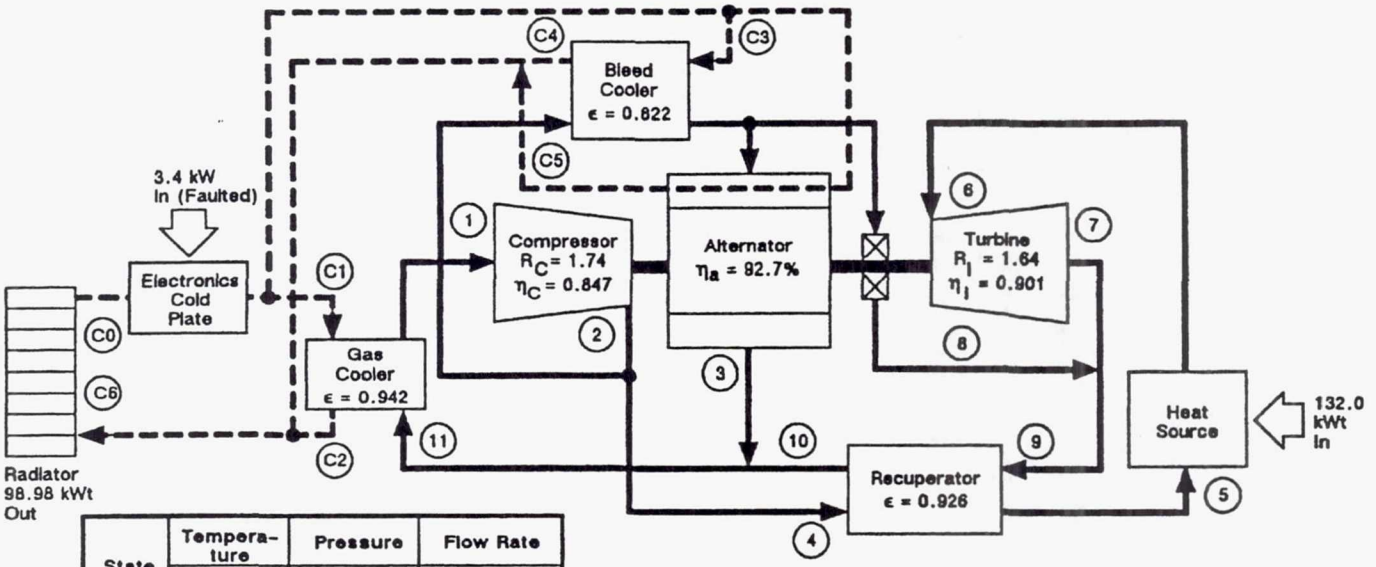

State Point	Temperature (°F)	Pressure (psia)	Flow Rate (lbm/s)
1	149.31	46.58	2.8408
2	328.05	81.16	2.8408
3	465.39	46.96	0.0568
4	328.29	81.05	2.7698
5	1037.95	80.58	2.7698
6	1401.58	78.35	2.7698
7	1099.15	47.66	2.7698
8	181.54	47.66	0.0142
9	1094.43	47.60	2.7640
10	388.41	46.96	2.7840
11	389.95	46.96	2.8408
C0	46.52	-	0.5261
C1	58.13	-	0.4392
C2	370.41	-	0.4392
C3	58.13	-	(a)
C4	268.39	-	(a)
C5	152.68	-	(a)
C6	341.19	-	0.5261

[a]To be determined.

Figure 5.7.—CBC subsystem state-point diagram for maximum insolation conditions. Electrical output, 36.42 kWe; beta, 0.944; bearing loss, 1.38 kW; windage loss, 2.52 W; net cycle efficiency, 27.60%; rotor speed, 32 000 rpm; sink temperature, 191 K (-116 °F); emissivity, 0.9; coolant, *n*-heptane; maximum insolation orbit at sunset.

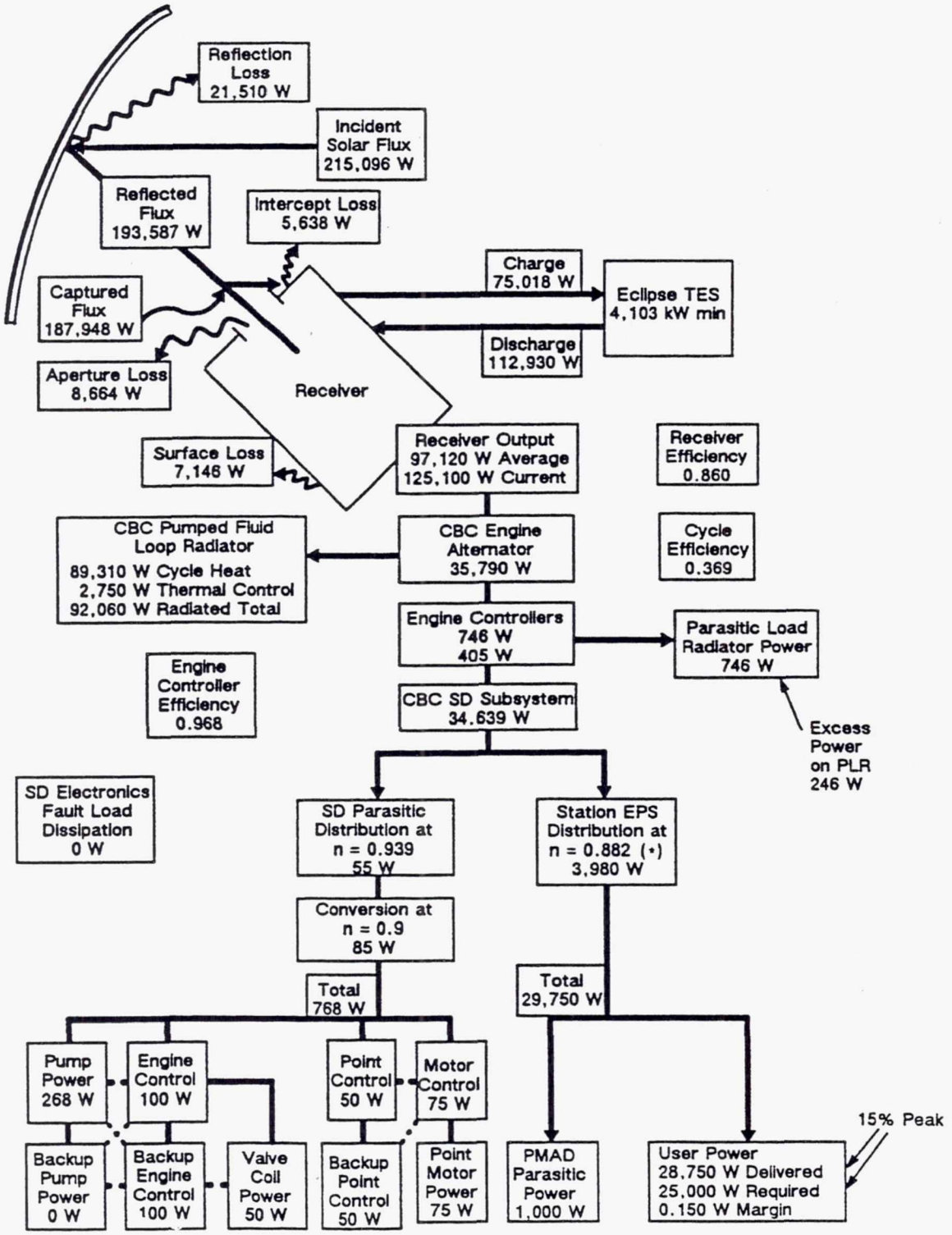

*Based on phase B 20-kHz efficiency.

Figure 5.8.—Power flow diagram—minimum insolation orbit (sunrise) and peaking demand. Period, 91.02 min; sunlight, 54.69 min; insolation, 1323 W/m ^{2}; reflectivity, 0.9; required concentrator net effective area, 162.6 m ^{2}.

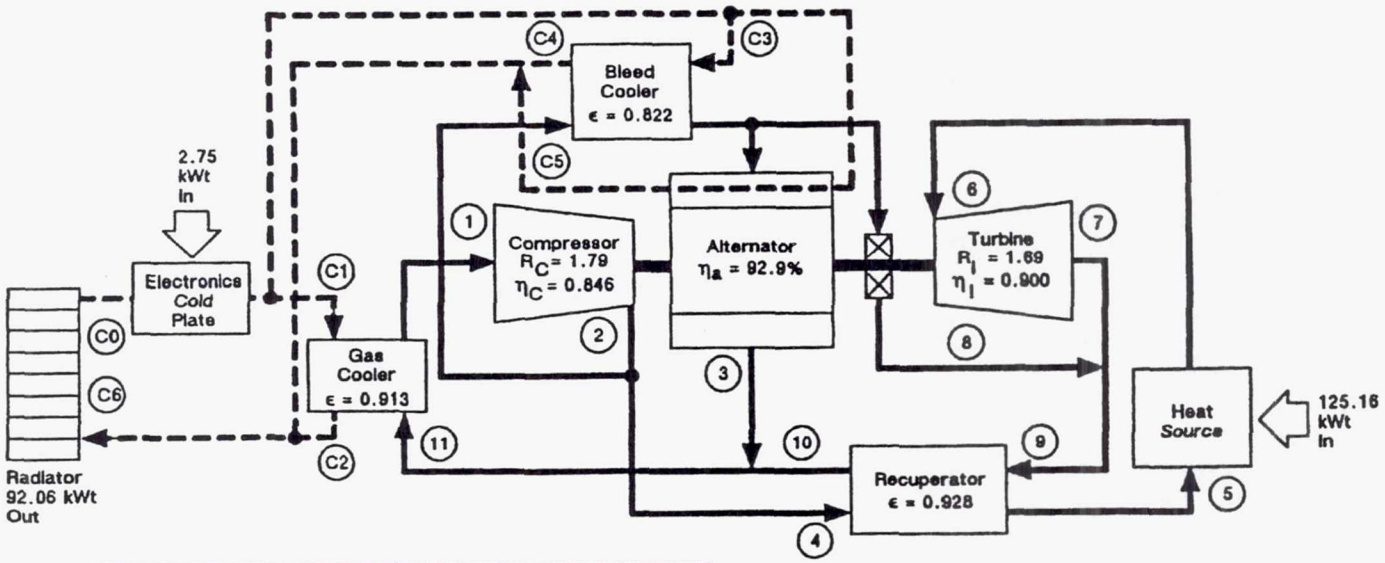

State Point	Temperature (°F)	Pressure (psia)	Flow Rate (lbm/s)
1	116.35	41.49	2.6884
2	295.34	74.35	2.6884
3	448.50	41.86	0.0538
4	295.58	74.24	2.6212
5	980.11	73.79	2.6212
6	1344.27	71.63	2.6212
7	1037.95	42.48	2.6212
8	165.75	42.48	0.0134
9	1033.46	42.42	2.6346
10	352.44	41.86	2.6346
11	354.36	41.86	2.6884
C0	36.71	-	0.5607
C1	45.89	-	0.4703
C2	327.53	-	0.4703
C3	45.89	-	(a)
C4	223.95	-	(a)
C5	131.30	-	(a)
C6	300.96	-	0.5607

[a]To be determined.

Figure 5.9.—CBC subsystem state-point diagram for design-point conditions and peaking demand. Electrical output, 35.79 kWe; beta, 0.941; bearing loss, 1.24 kW; windage loss, 2.33 W; net cycle efficiency, 28.62%; rotor speed, 32 000 rpm; sink temperature, 186 K (–125 °F); emissivity, 0.9; coolant, *n*-heptane; minimum insolation peaking orbit at sunrise.

5.6 Structural Considerations and Module Design

Structural considerations in the design of the solar dynamic module include the module and station responses to loads and the potential for controls/structures interaction. One key concern is that the solar dynamic module maintain a specified alignment with the Sun while mounted on a large, relatively flexible structure. The module will have active pointing devices to accommodate base motion due to disturbances to the station, station maneuvers, and module disturbances. Flexibilities within the structures of the module itself must also be considered when determining the pointing accuracy capability.

A second concern is that when the module is actively pointing, it should not induce excessive loads on the station, unstable station controller (GN&C, alpha gimbal) interactions, or unstable solar dynamic controller interactions.

Several studies have been conducted to determine the feasibility of solar dynamic pointing that is based on the station truss stiffness characteristics. Some of the original concerns were with the truss torsional stiffness and the solar dynamic module mass moment of inertia about the truss (alpha) axis (ref. 5.14). These concerns were partly assuaged when the stiffer, 5-m truss was baselined instead of the 9-ft-truss concept. The truss torsional stiffness concern did influence the configuration of the solar dynamic module, leading to the development of the offset concentrator (see sections 6.1 and 5.7), which had a lower mass moment of inertia than other concepts under consideration.

During the course of solar dynamic development in phase 1, a reduction in station truss stiffness was contemplated, prompting an investigation into the effects of truss stiffness on solar dynamic pointing capability (ref. 5.15). This study concluded that the solar dynamic controllability characteristics of both a high-truss-stiffness and a low-truss-stiffness station were similar and acceptable.

See section 5.7 for further discussion of solar dynamic module controls/structures interaction considerations. See also the descriptions of the individual solar dynamic assemblies, especially the concentrator and the radiator, for discussion of assembly structural considerations.

5.7 Pointing System

The solar dynamic pointing and tracking system orients the concentrator to focus the Sun's rays into the receiver. Many different methods and designs have been investigated to achieve the solar dynamic pointing functions. In the final stages of the phase 1 SD program, prime contractor and supporting development efforts were under way to completely evaluate the solar dynamic pointing system, including a review of the pointing requirements. These efforts remain incomplete and some areas were left unresolved. This section documents the requirements and some of the concepts for the solar dynamic pointing system.

5.7.1 Pointing Performance Requirements

The solar dynamic pointing requirements that are discussed here are from reference 5.16, which was created as a draft document late in the phase 1 effort. A few requirements originate from higher level requirements documents as noted. Early pointing requirements were developed before and during phase B.

The fundamental requirement for the pointing system is that it align the concentrator optical axis with the Sun line while the solar dynamic module orbits the Earth and is subjected to loads and disturbances. The loads and disturbances include gravity-gradient and gyroscopic torques, aerodynamic drag, thermally induced displacements and misalignments, NSTS orbiter reaction control system (RCS) plume impingement and docking, and various Space Station *Freedom*-based disturbances, such as astronaut treadmill and extravehicular activities (see chapter 3). Within specified tolerances the module must act to maintain alignment of the concentrator while subjected to these loads and disturbances. The pointing system also actuates commanded movements of the solar dynamic module (or concentrator) for various operational modes, such as startup and shutdown (see section 5.11).

Alignment of the concentrator optical axis requires rotation of the concentrator about two axes (neither of which can be collinear with the optical axis). Maximum effectiveness (minimum actuator output) is attained if the axes are perpendicular to the optical axis and also perpendicular to each other. More than two axes are used in some pointing system configurations, providing some degree of redundancy.

The alpha axis is along the center of the truss boom, perpendicular to the direction of *Freedom*'s flight and parallel to the surface of the Earth. The alpha gimbal rotates once every orbit, approximately 90 min, to keep the solar power module (SPM) fixed relative to the Sun while the station core retains its attitude with respect to the Earth's surface. (The SPM is composed of both the photovoltaic and the solar dynamic modules that are outboard of the alpha gimbal.) The alpha gimbal accuracy as derived from the program design and requirements document (PDRD) is about ±2°.[3]

[3]The PDRD actually defines a composite alpha and beta accuracy of ±3.0° within which the individual alpha and beta gimbal accuracies must be allocated. If alpha and beta are to be equally accurate, they would each need accuracies within ±2.12° ($2.12^2 + 2.12^2 < 3.0^2$). The situation is complicated by the fact that consideration must also be given to other sources of pointing error, besides the gimbals themselves, such as truss misalignments and twists and pointing knowledge uncertainty.

The beta axis intersects and is perpendicular to the alpha axis. The photovoltaic and solar dynamic modules include beta gimbals that rotate the modules to accommodate an angle that results when the Sun line is not coplanar with *Freedom*'s orbital plane. The beta angle varies between extremes of ±52° throughout a year. The beta gimbal coarse-pointing accuracy has been specified as ±2° in the WP–04 technical requirements document. Because of the relatively slow rate at which the beta angle changes, no more than about 4 deg per day, the beta gimbal does not need to be continuously operated for Sun tracking.

The ±2° alignments about the alpha and beta axes provide the coarse pointing of the photovoltaic and solar dynamic modules. For the solar dynamic power system more accurate alignment is needed to point the Sun's concentrated energy into the receiver aperture. Limited studies during phase B showed that the solar dynamic pointing system should align the concentrator optical axis with the Sun line within 0.1° with a confidence of 99.7 percent (three standard deviations, or 3σ; ref. 5.17).

The fine-pointing accuracy requirement is dependent on many interrelated factors. For example, receiver thermal performance can be increased by decreasing the aperture size (to reduce reradiation losses), by decreasing pointing error, by decreasing concentrator slope error (to reduce flux spillage on the aperture plate), or by increasing concentrator area. In order to meet a particular receiver thermal performance requirement, one or more of those factors can be varied. Improvements in any particular quality are limited by cost, technical considerations, or both. The optimum design solution requires simultaneous consideration of all relevant factors.

Throughout most of phase 1 the fine-pointing accuracy requirement remained at ±0.1°, 3σ. In conjunction with investigations of alternative fine-pointing concepts, all of the pointing requirements were reevaluated. The fine-pointing accuracy was studied by D. O'Brien (ref. 5.18) and K. Jefferies and C. Gallo (ref. 5.19). As a result of these studies the fine-pointing accuracy requirement was changed to ±0.3° per axis, 3σ, within every orbit (equivalent to ±0.1°, 1σ).[4] This change eases the job of designing the fine-pointing system, with slight loss of solar input into the receiver. The flux spillage will hit the lip of the aperture, which must be designed to handle the increased energy.

It has been suggested that the pointing requirements may be further altered to allow greater pointing errors during short periods of time when disturbances are especially large, such as during NSTS orbiter docking. This would ease the demands on the pointing system, with an insignificant loss of energy input, but it does present a more severe case for the aperture plate. The tentative requirement for pointing accuracy during large, infrequent disturbances is 1.0°, 1σ, during any 6-min time period. The necessity of this tentative pointing requirement has not been proven; it may eventually be adjusted or eliminated.

When discussing fine pointing for solar dynamics it is convenient to name the fine-pointing axes. It is common to designate a fine-pointing axis that is parallel to the alpha axis (when the beta angle equals zero) as the pitch axis or the elevation axis. A fine-pointing axis that is parallel to the beta axis can be called a yaw or azimuth axis.[5] In some configurations the fine-pointing axes may not necessarily be aligned with a pure elevation or azimuth axis; however, a fine-pointing mechanism may be named for the primary axis about which it is intended to make corrections.

Another important characteristic of the fine-pointing system is its control frequency bandwidth. It is the major determining factor in the system transient response. The bandwidth is defined from the closed-loop frequency response (at the −3-dB cutoff) between command position and actual position. The original selection of the bandwidth requirement was largely based on a desire to avoid interactions with the alpha and beta controllers (at 0.04 Hz) at the lower end and with solar dynamic module structural interactions (at 1 Hz and above) at the higher end. The fine-pointing controller bandwidth requirement was 0.5 Hz during most of phase 1.

Because the fine-pointing bandwidth requirement was based primarily on structural interaction concerns, the actual performance-based bandwidth requirements were not much considered at first. Just as the fine-pointing accuracy requirement was relaxed, it was found that the fine-pointing bandwidth requirement could be relaxed with little loss of energy input. Besides energy input, another key consideration is receiver aperture plate thermal loading, which is highly dependent on the fine-pointing system bandwidth. This relationship was investigated by R. Quinn and T. Kerslake (ref. 5.20).

The reevaluation was partially due to the difficulties that arose for the assembly designers with their structural frequency requirements. In particular, the radiator fundamental frequency was less than 0.1 Hz for a design based on strength considerations, instead of 1 Hz as desired. The concern with this low frequency was that there could be interactions between the fine-pointing controller and the radiator structural modes. Raising the lowest radiator frequencies to at least 1 Hz proved to be difficult (see section 6.4.1). Questions were raised about the structural frequency requirement and

[4]The original fine-pointing requirement was formulated to specify the fine-pointing accuracy in terms of cone angle, which is a two-axis specification. A ±0.3° per axis fine-pointing requirement is equivalent to a 0.42° half-cone-angle requirement.

[5]Some authors make a distinction between a fine-pointing, local-body pitch axis and the elevation axis, which they use only in reference to the space station fixed body. A similar distinction is made for a local body yaw and a station fixed azimuth axis.

the selection of the controller bandwidth. After study by R. Quinn (ref. 5.21) and M. Kim (ref. 5.22), it was concluded that the radiator frequency did not need to be raised in order to have a stable system.

A new value of the controller bandwidth has yet to be defined. It is dependent on a number of different factors, including the pointing configuration and the aperture plate capabilities. There is general agreement that bandwidth can be lowered from 0.5 Hz for overall benefit to the module design. Fine-pointing bandwidth values from 0.05 Hz (ref. 5.21) to 0.24 Hz (ref. 5.23) have been investigated. The alpha and beta controller frequencies have remained at 0.04 Hz. Note that the fine controller bandwidth of 0.24 Hz in reference 5.24 is still higher than the fundamental radiator mode of less than 0.1 Hz; however, the radiator frequency did not cause problems in this particular analysis. The change from a fine-pointing frequency of 0.5 Hz to 0.24 Hz was driven by the desire to avoid interactions between the elevation fine-pointing controller and the alpha controller.

Other pointing system requirements include slew rates and accelerations for the various pointing gimbals. The beta gimbal slew rate is the rate at which the beta gimbal rotates the solar dynamic module about the beta axis. A fine-pointing slew rate, achieved by a fine-pointing mechanism, may be defined about a fine-pointing axis. Slew rates are important for Sun tracking during nominal operations, as well as for other solar dynamic operations, such as startup and normal and emergency shutdowns (see section 5.11).

The nominal alpha gimbal slew rate is about 4 deg/min (one orbit per 90 min), which keeps the solar power module tracking with the Sun. The beta gimbal slew rate has been tentatively set at about 1 deg/min, which was the value specified for the common-design beta gimbals of the photovoltaic arrays. The slew rate requirement for the fine-pointing mechanism is tentatively specified as 3 deg/min. This relatively low value was selected to simplify the design of the fine-pointing mechanism although other considerations (such as aperture plate capabilities) could force a change in the slew rate requirement.

In addition to slew rate requirements there are angular acceleration requirements for the solar dynamic pointing mechanisms. The pointing system's capability to respond to disturbances is related to the angular acceleration capabilities of the pointing mechanisms. The larger the amplitude and frequency of the disturbance, the higher the accelerations must be. The angular acceleration capability for any particular mechanism is directly proportional to the torque that its actuator produces.

The acceleration requirements are linked to the controller bandwidth requirements; a higher bandwidth requires higher actuator accelerations, which require higher actuator torques. Achievement of high accelerations and transmission of high torques place greater stiffness requirements on the pointing mechanisms and the structures they react against. Conversely, a reduction in the bandwidth frequency relaxes torque and stiffness requirements.

Like the controller bandwidth requirements, the pointing system acceleration requirements have not been fully evaluated. The requirements will need to be iteratively determined along with other module considerations.

The required range of the alpha and beta gimbal rotations is 360°, continuous. Note that for Sun pointing the beta gimbal needs only a range of ±52°, but for maintenance and contingency considerations a continuous rotation capability is specified. The fine-pointing gimbals were originally required to accommodate a range of ±15°. This range was specified to permit the fine-pointing system to move the concentrated solar flux completely off of the receiver aperture plate and any other equipment near the receiver.

5.7.2 Pointing Concepts

Many different pointing concepts have been considered during the development of the solar dynamic power module. Each concept has its advantages and disadvantages. Along with the development of the gimbaling configurations that characterize the pointing concepts, various optical configurations have been considered. The gimbaling configuration deals with the location of the gimbals; the optical configuration deals with the solar collector characteristics. The gimbaling and optical configurations are not necessarily independent; the selection of a particular gimbaling configuration may preclude the selection of a particular optical configuration. This section deals primarily with the gimbaling configurations.

The optical configurations include reflector concepts with the simple Newtonian, offset Newtonian, and Cassagrainian arrangements. Another optical configuration used a transparent, refractive Fresnel lens.

5.7.3 General Considerations

5.7.3.1 Gimbal axis location. — Several of the gimbaling configurations place the solar dynamic module center of gravity (CG) on the gimbal axes. This eliminates the inducement of torques on the module due to accelerations of the station structure. In the idealized case with no friction in the gimbals, rotational disturbances from the station are completely isolated from the module, which retains its pointing orientation while the base structure rotates. In the actual case the fine-pointing actuators need only compensate for the gimbal friction torques. Translational disturbances would translate the module but would not cause it to rotate because of the forces applied at the module CG. (Pure translation of the module does not cause noticeable pointing errors.)

Even if a gimbal axis does pass through the CG, the disturbances are not isolated if the gimbal acts as a rigid

coupler (e.g., if the gimbal is locked or if the disturbance has higher frequency components than the controller bandwidth). Also, depending on the disturbance, there may be conflicting requirements on the gimbal controllers: For isolation from disturbances transmitted through the truss, the gimbal should be "soft"; for disturbances applied directly to the module (e.g., plume loads), the gimbal should be stiff to minimize pointing error (but not loads).

Another factor favoring the use of a CG-gimbaled concept is its potential advantage during ground verification because it should be easier to minimize gravitational effects. There would be no movable overhanging masses that would need to be supported or balanced to simulate zero gravity.

Most of the gimbaling configurations have the beta axis aligned with the module center of gravity because it is convenient to do so. This gains the potential benefits for that axis only.

Gimbal axis location also needs to be considered when accounting for loads and disturbances that are applied directly to the solar dynamic module, such as aerodynamic drag or plume and gavity-gradient loads. Judicious placement of the axes, the arrangement of the solar dynamic assemblies, or both may reduce both the disturbance effect on fine pointing and the pointing actuator loads.

5.7.3.2 Effect on optics. —Another factor in evaluating gimbaling concepts is the effect that gimbaling has on the optical performance of the concentrator-receiver system. The receiver is very sensitive to the flux distributions produced by the concentrator (see sections 6.1 and 6.2). If in the gimbal system design the concentrator moves independently of the receiver, the flux distribution in the receiver may not be as desirable as when the concentrator and the receiver are fixed together and move as a pair (ref. 5.24).

A second optical consideration applies to those configurations where the radiator is located so that it casts a shadow on the concentrator. If only the concentrator is fine pointed while the rest of the module, including the radiator, is coarse pointed about the beta axis, the radiator shadow can be relatively large because the radiator could be misaligned up to 2° with respect to the Sun line. This shadow not only decreases the effective concentrator area but also can cause severe flux distortions within the receiver cavity. (One method of reducing the receiver flux impact is to slant the radiator so that the shadow that appears in the receiver cavity falls across parts of several tubes rather than just one.) On the other hand, if the configuration is such that the radiator is fine pointed along with the concentrator, the radiator shadow is small and is not expected to be a problem; see chapter 6 for references to work in this area.

5.7.3.3 Sensor location. — Some investigations have been done to determine the effect of the location of pointing system sensors on control stability. A potential problem exists when the position and velocity sensors are mounted on a flexible structure away from the actuators that are responding to those sensors. Instabilities can result if, because of structural deflection, the sensed motion is out of phase with actuator response. This situation could occur, for example, if the Sun sensors are mounted on the concentrator and the pointing actuators are far away at the ends of the concentrator struts. One solution to this problem is to collocate the sensors (or effectively collocate them through rigid structural connection) with the actuators.

Whether there is an instability problem depends not only on the sensor location and the module structural dynamic characteristics but also on the control laws and the controller bandwidth. Reducing the bandwidth requirement lessens the chance that the actuator will cause stability problems. Also, the controllers can be designed with filters to prevent the actuators from interacting with particular structural modes.

The importance of sensor location is discussed in references 5.21 and 5.25.

5.7.3.4 Module mass distribution. — During the development of the solar dynamic module configuration, there has been some concern about the module's mass moment of inertia and its effect on the station. In particular there was a desire to minimize the mass moment of inertia about the alpha axis, possibly to avoid interactions between the alpha controller and the truss structure. This concern has influenced the evolution of the gimbaling and module configuration, tending to weigh against concepts that had the module center of mass far from the alpha axis. Most concepts have placed the relatively heavy receiver near the truss, rather than away from the truss.

5.7.4 Other Considerations

The design of the pointing system involves tradeoffs. Many different concepts could meet the nominal pointing performance requirements. The "best" concept must not only provide the desired performance characteristics but must also score well in all major discriminating categories, which include performance characteristics; weight; cost; launch packaging; assembly, maintenance and reliability; and design risk. Except for a few concepts, detailed analysis for each of the six categories was not done. Within the selection process the gimbaling concepts were evaluated and traded off against each other on a mostly qualitative basis.

5.7.5 Gimbal Configuration Classification

The gimbaling configurations can be classified into three general categories on the basis of the required alpha and beta gimbal accuracies and further subdivided on the basis of the fine-pointing configuration. The gimbaling configurations listed here do not represent all possible configurations:

(1) High-accuracy alpha gimbal; high-accuracy beta gimbal
   (a) Teetered
   (b) Conventional

(2) Low-accuracy alpha gimbal; high-accuracy beta gimbal
  (a) Elevation fine pointing of module at module CG
  (b) Elevation fine pointing of module at module base
  (c) Elevation fine pointing of concentrator only
  (d) Exocentric gimbaling of module at module CG
(3) Low-accuracy alpha gimbal; low-accuracy beta gimbal
  (a) Two-axis fine pointing of concentrator with linear actuators
  (b) Two-axis fine pointing of concentrator with gimbal rings
  (c) Two-axis fine pointing of module at module CG

Further breakdowns could be made among the listed configurations, but unless a particular configuration was studied to some minimal degree in the SD progam, it is not listed distinctly. Table 5.2 lists some of the references where information may be found for the configurations.

The following are brief descriptions of some of the gimbaling configurations that have been developed in the SD program:

(1) Configuration 1-a: High-accuracy alpha gimbal; high-accuracy beta gimbal; teetered

The high-accuracy, alpha/beta gimbal, teetered concept was considered during phase B. In this concept, shown in figure 5.10, the major solar dynamic assemblies are rigidly connected and arranged to pass through the space station boom with the radiator on one side, the concentrator on the other, and the receiver and PCU in the middle. The entire assemblage is pivoted, or teetered, near the receiver/PCU about the beta axis, which is orthogonal to the truss centerline alpha axis. This concept relies on high-accuracy alpha and beta gimbals to accomplish fine pointing of the system.

This concept provides inherent stiffness and structural savings due to the lack of interface structures between the module and the beta and alpha gimbals. It presents a low mass moment of inertia about the alpha axis and makes it relatively easy to locate the module center of mass on the alpha and beta axes.

Potential disadvantages include the risk of relying on the alpha gimbal for fine pointing with more stringent pointing

TABLE 5.2.– REFERENCES FOR SOLAR DYNAMIC GIMBALING CONFIGURATIONS

Configuration	Minor references	Major references
1-a	5.26, 5.27, 5.28	----------
1-b	5.26, 5.27, 5.28	----------
2-a	5.29	----------
2-b	5.29, 5.31	5.23, 5.32, 5.33
2-c	----------	----------
2-d	5.26, 5.27, 5.28	----------
3-a	5.26, 5.27, 5.28	----------
	5.30, 5.31	----------
3-b	5.30, 5.31	5.10, 5.22
3-c	5.31, 5.34	----------

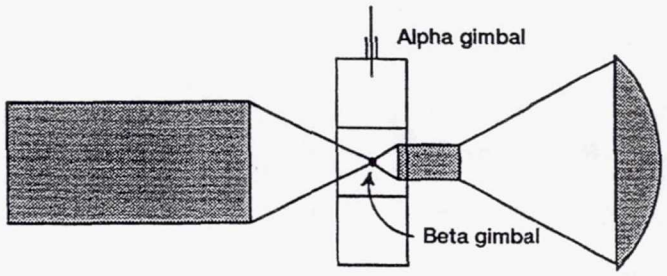

Figure 5.10.—High-accuracy alpha gimbal, high-accuracy beta gimbal, teetered concept.

accuracy requirements (by about a factor of 10) than currently planned. In addition, this concept may need increased truss torsional stiffness to minimize angular displacements between the alpha gimbal and the solar dynamic module and to prevent possible interaction between the alpha controller and the structure. This concept also reduces flexiblity for growth by preventing the placing of two solar dynamic modules at one longitudinal location along the truss (unless the modules are mounted on stub truss sections, taking them off the alpha axis). The physical arrangement and kinematics of the teetered concept restrict the ratio of focal length to concentrator diameter.

Another disadvantage of the teetered concept is that the reflector is partially blocked by the truss and the receiver, so that a larger reflective surface is required. An alternative optical concept with a refractive domed Fresnel lens was considered because it would not be blocked by the truss. The Fresnel concept was eliminated from consideration because of the technical risks associated with the Fresnel lens.

(2) Configuration 1-b: High-accuracy alpha gimbal; high-accuracy beta gimbal; conventional

One version of the conventional configuration places the beta axis behind the concentrator vertex, as shown in figure 5.11(a), and puts the entire module off the alpha axis. A Cassegrainian version of this concept was also considered.

Except possibly for reduced blockage and greater growth flexibility, this option has the same disadvantages as the teetered concept (primarily the stringent alpha and beta accuracy requirements) plus others so that it was eliminated from further consideration.

Another version of this configuration has the beta axis near the module CG, as shown in figure 5.11(b).

(3) Configuration 2-a: Low-accuracy alpha gimbal; high-accuracy beta gimbal; elevation fine pointing of module at module CG

This configuration, shown in figure 5.12, uses a structure between the beta gimbal and the module CG to locate a fine-pointing elevation axis that is orthogonal to the beta axis (and parallel to the alpha axis when the beta angle is zero). The beta gimbal provides the fine pointing about the beta axis. This concept has the advantages of the CG-gimbaled concepts (insensitivity to transmitted disturbances) and the advantages of the fixed concentrator-receiver.

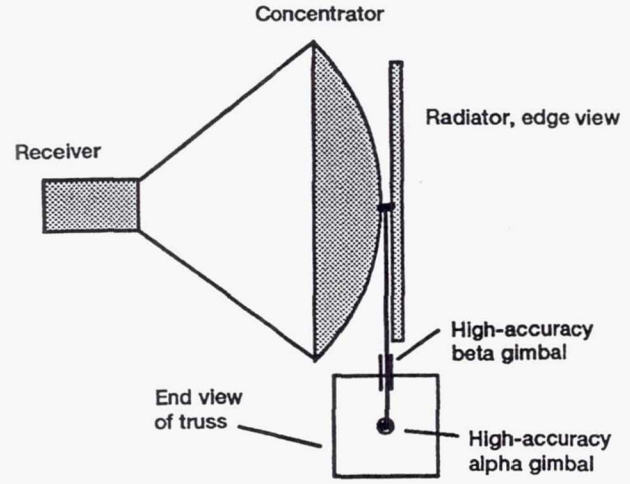

(a) Beta axis behind concentrator vertex.

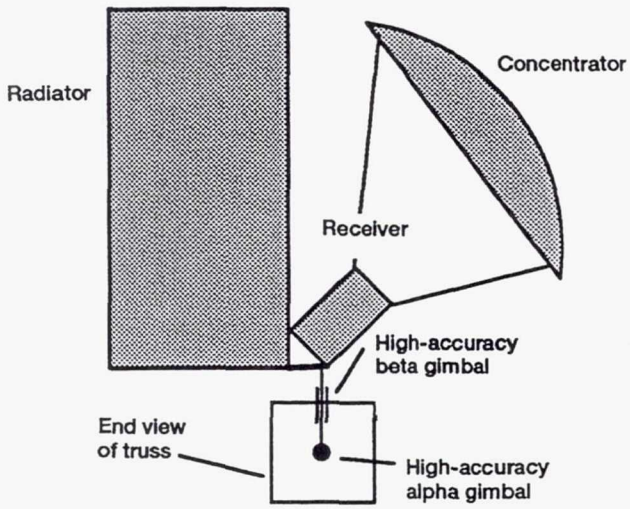

(b) Beta axis near module center of gravity.

Figure 5.11.— Two versions of high-accuracy alpha gimbal, high-accuracy beta gimbal, conventional concept.

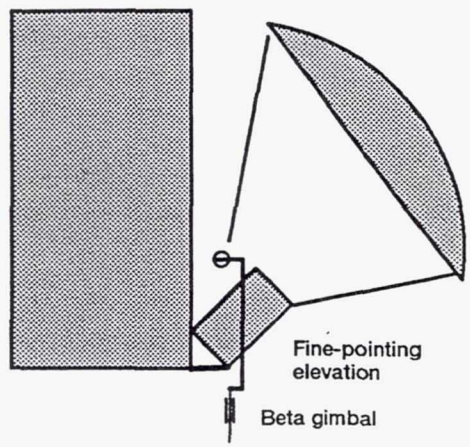

Figure 5.12.—Low-accuracy alpha gimbal; high-accuracy beta gimbal; elevation fine pointing at module center of gravity.

Its disadvantages include the mass, volume, and assembly complexity of the support structure, although preliminary estimates show that the mass penalty is not too great (ref. 5.34)[6]. Another consideration is the support structure stiffness requirements, noting that the beta fine-pointing torque must be transmitted through the structure and the elevation fine-pointing torques must react against the structure. Depending on the beta and elevation controller bandwidth selection, there could be the potential for controls/structures interaction.

Like all of the beta fine-pointing concepts, this concept has no beta axis pointing redundancy, although the beta gimbal drive and its control would probably be redundant. This factor would be important if the beta gimbal bearing or the overall command somehow failed because there would be no alternative means of pointing about the beta axis.

(4) Configuration 2-b: Low-accuracy alpha gimbal; high-accuracy beta gimbal; elevation fine-pointing of module at module base

This concept, shown in figure 5.13, is the most recent configuration advocated by Rocketdyne and is referred to elsewhere in this report as "the beta fine-pointing concept." It is similar to configuration 2-a except that the support structure is eliminated and the elevation axis is at the base of the module rather than at the CG.

Significant mass savings and launch packaging advantages are attained by this concept, relative to the baseline concept, 3-b, which it is intended to replace. A mass summary is shown in section 5.4, and launch packaging is discussed in section 5.9.

The references listed in table 5.2 for this configuration detail studies that were done to investigate the controls performance and stability. The studies concluded that this concept is feasible.

(5) Configuration 2-c: Low-accuracy alpha gimbal; high-accuracy beta gimbal; elevation fine pointing of concentrator only

Figure 5.14 shows a concept that is derived from the baseline with two-axis fine pointing of the concentrator. Making the beta gimbal capable of fine pointing allows the azimuth fine-pointing mechanism to be eliminated while retaining the elevation fine-pointing capability. The elevation fine pointing could be achieved by using a single gimbal ring at the concentrator focal plane or by adjusting the concentrator strut lengths with linear actuators.

The advantage of this concept is the elimination of the azimuth fine-pointing mechanism and thus the elimination of the potential problem of interaction between this mechanism and the beta gimbal controller. A disadvantage is the potential for flux distortion that is caused by movement of the concentrator relative to the receiver.

[6]Reference 5.34 was written for another configuration, 3-c, but the support structures are almost identical for 3-c and 2-a.

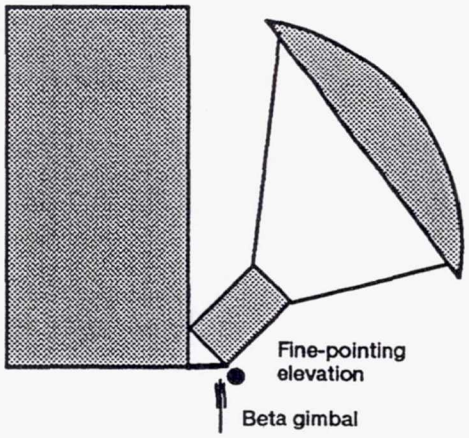

Figure 5.13.—Low-accuracy alpha gimbal; high-accuracy beta gimbal; elevation fine pointing at module base.

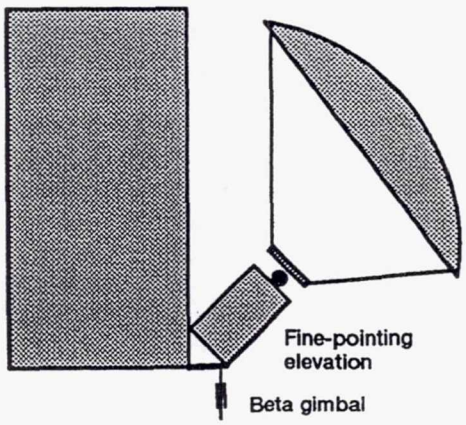

Figure 5.14.—Low-accuracy alpha gimbal; high-accuracy beta gimbal; elevation fine pointing of concentrator only.

(6) Configuration 2-d: Low-accuracy alpha gimbal; high-accuracy beta gimbal; exocentric gimbaling of module at module CG

The exocentric gimbal concept, shown in figure 5.15, was used in Rocketdyne's phase B proposal. The concept has three gimbals: alpha, beta, and gamma. The beta gimbal axis is orthogonal to the alpha axis. The gamma gimbal serves as the interface between the solar dynamic module and the beta gimbal. It is positioned by a rigid structure such that its axis is inclined 50° with respect to the beta axis to provide alpha and beta rotational components. Therefore, the gamma gimbal can accommodate misalignment in either the alpha or beta axis. This provides redundancy should either the alpha or beta gimbal become inoperable. In normal operation the gamma gimbal provides fine adjustment about the alpha axis and the beta gimbal provides fine adjustment for the beta axis (including compensation for the beta component induced by the gamma gimbal). As originally proposed, the exocentric gimbal concept had the beta and gamma axes pass through the module center of mass.

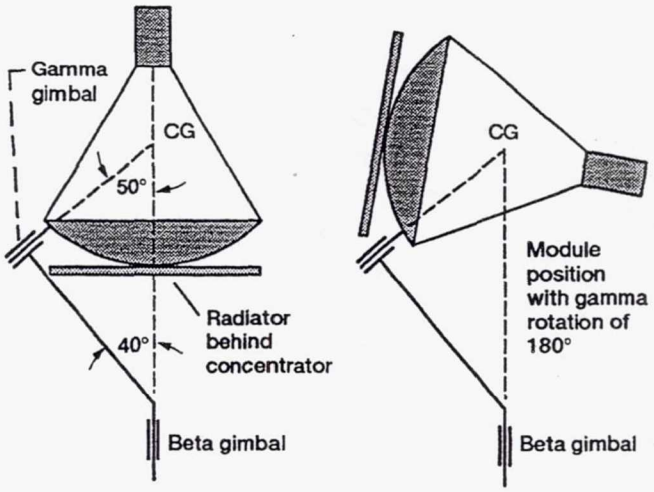

Figure 5.15.—Low-accuracy alpha gimbal; high-accuracy beta gimbal; exocentric gimbaling of module at module center of gravity.

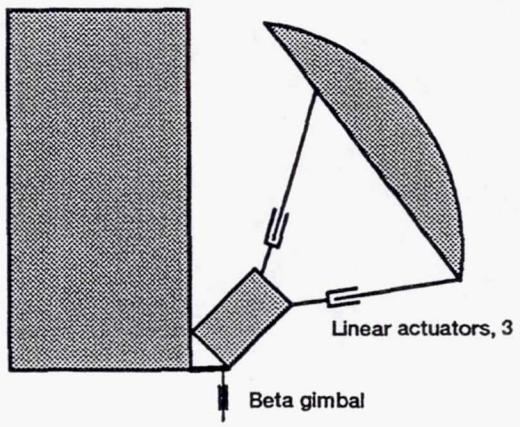

Figure 5.16.—Low-accuracy alpha gimbal; low-accuracy beta gimbal; two-axis fine pointing at concentrator with linear actuators.

(7) Configuration 3-a: Low-accuracy alpha gimbal; low-accuracy beta gimbal; two-axis fine pointing of concentrator with linear actuators

This concept is a particular application of the generic concept where the alpha and beta gimbals provide coarse pointing of the solar dynamic module while only the concentrator is fine pointed. Figure 5.16 shows a proposed option where the concentrator is rotated with respect to the receiver by linear actuators that are incorporated in the concentrator struts.

A particular application of this concept was developed as the parabolic offset linear actuated reflector (POLAR). The reflector consists of a paraboloid mounted offset from the parental parabolic axis (see chapter 6 for a full explanation of offset parabolic optics). Two primary reasons leading to the selection of an offset reflector were (1) that the offset configuration allows the CG of the whole solar dynamic system to be closer to the truss centerline and (2) that reflector

shadowing caused by other parts of the station would be reduced.

POLAR employs two length-positioning actuators that are contained on two struts; a third, fixed strut is attached at the reflector vertex. Equal movement of the two struts produces concentrator rotations about the elevation axis; differential movement produces azimuth rotations. One problem with this concept is that the focus is smeared and distorted as the struts are adjusted, leading to reduced interception and undesirable flux distributions within the receiver. In order to relieve these problems, a concept was developed where an adjustable strut replaced the fixed strut. With all three struts now adjustable, the concentrator can be actively focused, partially but not completely eliminating the flux distribution problem.

Like all of the concepts with two-axis fine pointing, this concept provides some degree of redundancy in the event of alpha or beta gimbal failure. Care must be taken to ensure that there is no interaction between the fine-pointing actuators and the alpha and beta gimbals.

This concept was originally developed during phase B, and later in phase 1 it was briefly explored as a concept with potential launch packaging advantages.

(8) Configuration 3-b: Low-accuracy alpha gimbal; low-accuracy beta gimbal; two-axis fine pointing of concentrator with gimbal rings

This concept, shown in figure 5.17, was the baseline gimbal concept for the entire phase 1 effort. It is a derivation from concept 3-a in which the adjustable concentrator struts are replaced with fixed struts and gimbal rings in the aperture plane. Struts are connected between the concentrator and the outer of the two gimbal rings, each of which has a linear actuator that is connected to the interface structure. The advantage of this concept over the strut linear actuators is that the focal plane remains at the desired location, at the intersection of the gimbal axes, as the concentrator is rotated. It also allows the addition of three more concentrator struts for a total of six and fixed strut end connections, raising the concentrator torsional mode structural frequency.

A disadvantage of this concept is the relatively heavy gimbal mechanism, estimated at 1200 lb. The gimbal rings also make launch packaging difficult. A modification of this concept was considered to meet the launch packaging requirements.

One complication of this concept is the fact that because the fine-pointing axes lie in the inclined aperture plane, one of these axes, the yaw axis, has a beta-axis component and a Sun-axis component. The sensors that feed information to the fine-pointing controller can only measure beta-axis misalignment (in fact, rotations about the Sun axis cause no pointing error). This could lead to problems with sensor observability and control stability as suggested in reference 5.21.

Others have suggested another problem with this configuration: Because the azimuth fine-pointing axis has a beta component, there can be interactions and stability problems with the beta controller. Some found this configuration to be stable only if the beta gimbal was locked to prevent any coupling between the azimuth and the beta controllers.

(9) Configuration 3-c: Low-accuracy alpha gimbal; low-accuracy beta gimbal; two-axis fine pointing of module at module CG

Two variations of this concept were investigated during phase 1. The first variation was one of the four concepts developed by Rocketdyne for a launch packaging study (see section 5.9). The receiver and concentrator are fixed to each other (along with the PCU) and mounted to a base plate with hinges and actuators in such a way that, as the concentrator and receiver rotate for fine pointing, the center of mass of the assemblage does not translate. This provides the advantage of the mass-centered concepts (i.e., insensitivity to transmitted disturbances).[7] In addition, the base plate in this concept doubles as an NSTS launch fixture. This concept was not carried along far enough to develop design details. Figure 5.18(a) shows a layout of the hinges and actuators for this concept.

The second variation is very similar to concept 2-a, where a structure extends from the beta gimbal to the module center of mass. In this concept, shown in figure 5.18(b), there are two fine-pointing axes at the module CG: elevation and azimuth. This concept was originally proposed to isolate the module from transmitted disturbances. In order to prevent interactions between the beta and azimuth controllers, the beta gimbal may have to be locked most of the time, operating open loop. This concept has all of the advantages and disadvantages of concept 2-a, with the additional benefit of beta axis redundancy at the expense of extra mass and complexity.

5.7.6 Summary

At this stage in the development of the solar dynamic pointing system, much work remains to investigate and verify the pointing requirements and proposed gimbaling concepts. Rocketdyne design activity has been converging on the beta fine-pointing concept with elevation control at the module base (concept 2-b) because it appears to satisfy a number of solar dynamic module issues: mass, launch packaging, and pointing performance. As more is learned about the pointing requirements (including design loads and disturbances) and as other concepts are further developed, better solutions may be adopted.

[7]Note, as initially presented, this concept did not fix the radiator with the other, CG-mounted assemblies. Thus, it is not really a module CG-mounted concept, although it retains most of the advantages for such concepts. The radiator was fixed to the base plate, requiring the use of flexible hoses between the PCU and the radiator.

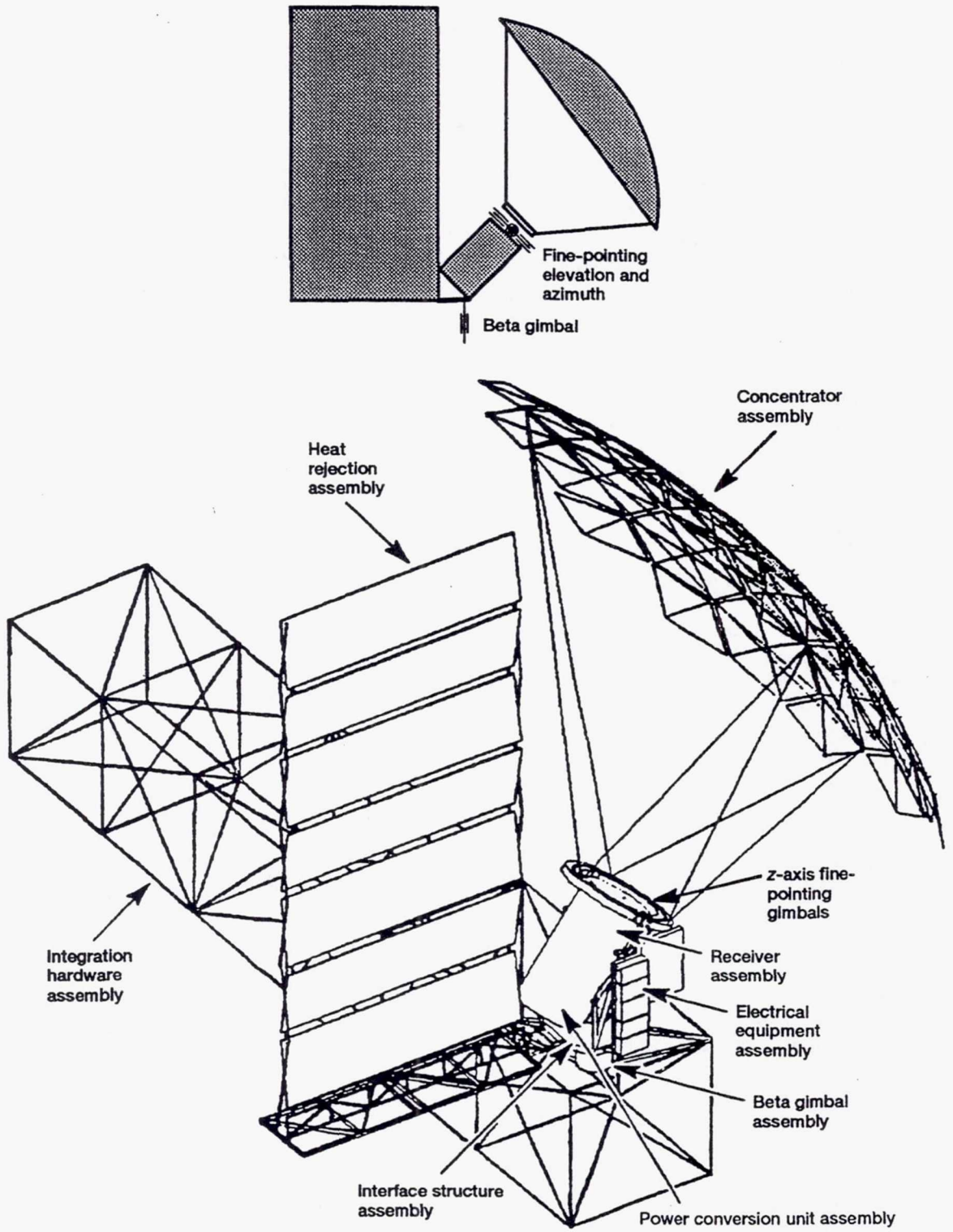

Figure 5.17.—Low-accuracy alpha gimbal; low-accuracy beta gimbal; two-axis fine pointing at concentrator with gimbal rings.

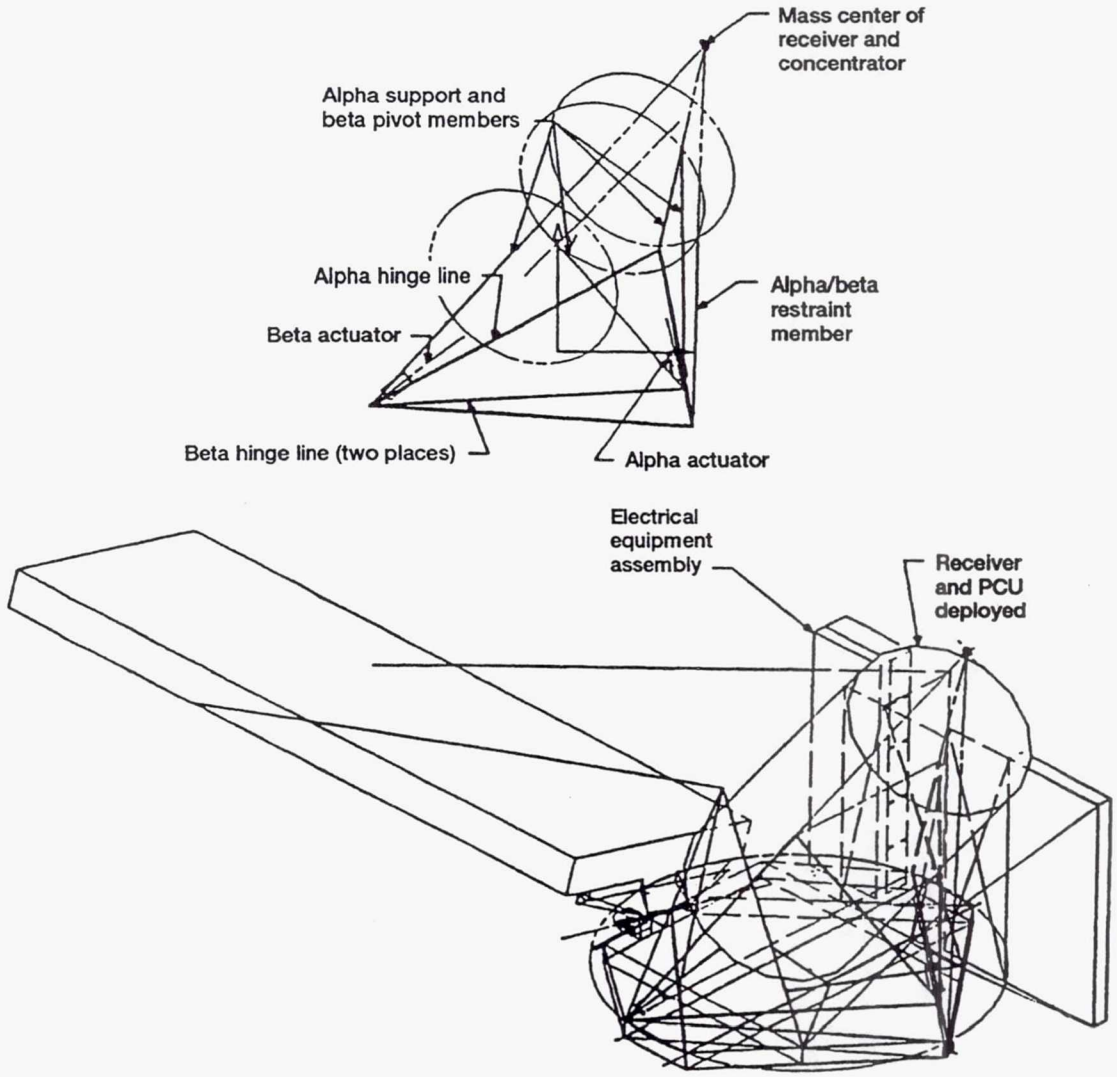

(a) Pointing mechanism need not be at CG.

Figure 5.18.—Low-accuracy alpha gimbal; low-accuracy beta gimbal; two-axis fine pointing at module center of gravity.

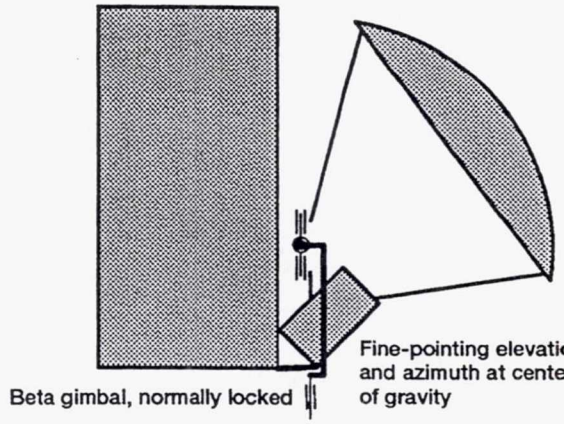

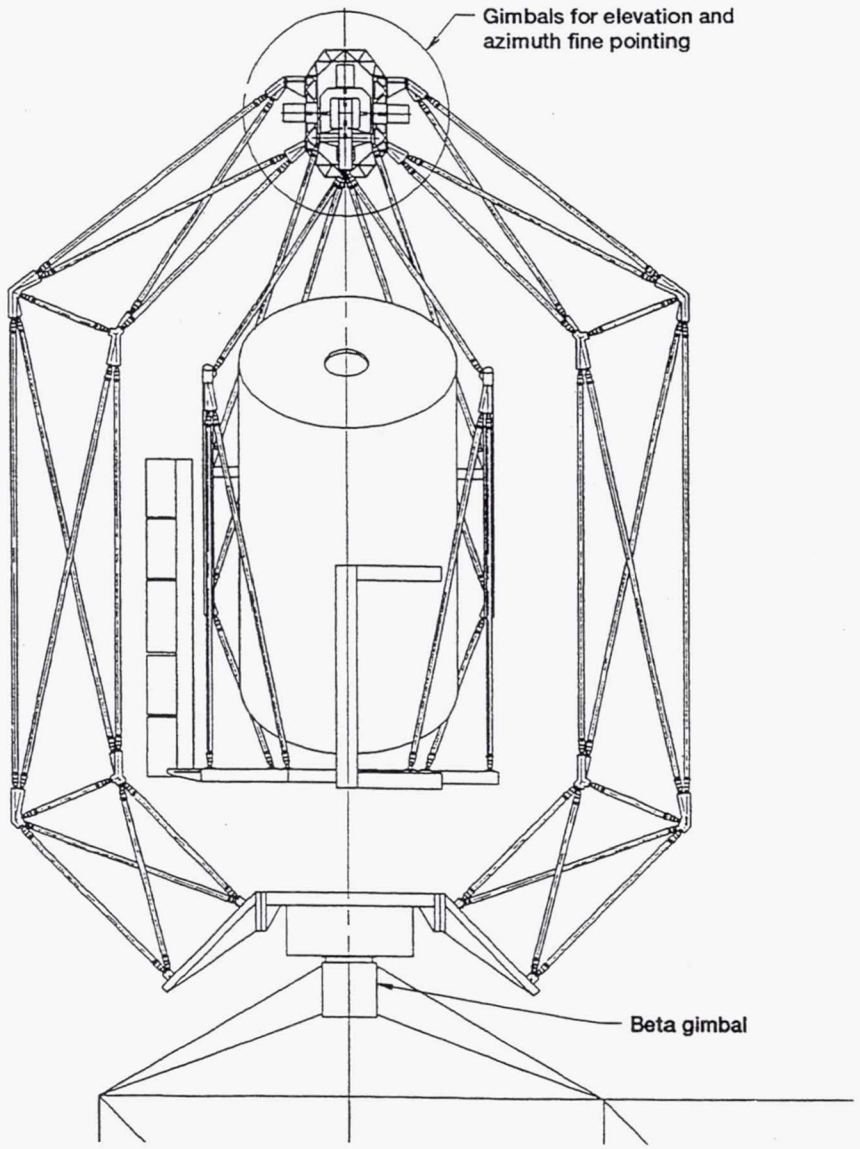

View of module support structure

(b) Pointing mechanism must be at CG.

Figure 5.18.—Concluded.

5.8 Reliability, Availability, and Maintainability

Reliability, availability, and maintainability (RAM) are three interrelated operational characteristics of a system. Defined briefly, reliability is a measure of the probability that a system will successfully operate in a given environment for a given period of time. Availability is a measure of the probable power output level for a given period of time. Lastly, maintainability is a measure of the annual extravehicular and intravehicular and resupply mass resources needed for replacing and or repairing the components of a system should they fail.

RAM characteristics are important because they define the dependability of the EPS (through quantification of availability) and also provide insight into its operating costs (maintainability and reliability). RAM analyses are particularly useful during the development phase in making comparative evaluations of design alternatives.

Another purpose of incorporating RAM methodology during development is to determine which components of the solar dynamic power system are most critical with respect to reliability and maintenance resources. Such components, when identified, can receive extra attention to minimize their unfavorable RAM qualities.

Many RAM properties and characteristics are tabulated at the orbital replacement unit hardware level. ORU's are the components that make up the EPS and are defined as the lowest level of equipment that can be replaced on orbit. ORU's are made up of smaller electrical, mechanical, and structural parts. When combined, the parts assist the ORU in performing its function. Preliminary quantitative reliability and maintainability analyses have been completed on the approximately 40 ORU's that form the solar dynamic system.

5.8.1 Requirements

5.8.1.1 Availability. — Availability requirements are part of the system power output specification. Several different measures of system availability are in use for the EPS. One, called operational availability, is based on the reliability of the system (time to failure), on the hands-on repair time, and also on the time between a failure and the start of the repair (including the time to get the replacement parts from the ground if necessary). Operational availability is supposed to give a realistic indication of how the system will operate. It is difficult to quantify at this time because of the uncertainty in the logistics scenario.

For design and requirements purposes an EPS design availability has been defined. For design availability the replacement parts are assumed to be available after a uniform, specified administrative delay (4.5 days). Design availability is specified as a requirement for the entire EPS in the WP–04 Technical Requirements Document (ref. 5.35). The availability requirement is formulated as a steady-state design availability (percent of time) as a function of power rating (also in percent). There are separate requirements for the permanently-manned-capability (PMC) configuration and the assembly-complete (AC) configuration.

It is not known what the design availability requirements will be for growth configurations (with solar dynamics), nor is it clear that EPS-level design availability will be applied to EPS subsystems including the solar dynamic module.

5.8.1.2 Reliability. — Some of the lower level solar dynamic specifications include lifetime requirements for particular assemblies and ORU's from which reliability requirements (in terms of mean time between failure (MTBF) values) can be derived. Most of these lifetime requirements were defined at the start of the SD program to guide the designs of particular assemblies and have not been evaluated from a system standpoint. Until solar dynamic system-level availability requirements are derived, it is impossible to evaluate the adequacy of existing individual assembly and ORU reliability (lifetime) requirements.

Solar dynamic module reliability requirements also include general failure tolerance and redundancy requirements that flow down from the program description and requirements document (PDRD) (ref. 5.36). In accordance with one of these requirements Rocketdyne has performed a preliminary failure modes and effects analysis (FMEA) and compiled a critical items list (CIL) (ref. 5.37).

A fundamental requirement that applies to all Space Station *Freedom* hardware is that all ORU's must have the ability to remain operational for 30 years through inspection, maintenance, restoration, and replacement. This requirement is a prime driver in the design of ORU's for reliability and maintainability.

5.8.1.3 Maintainability. — Maintainability requirements include general maintenance requirements that flow down from the PDRD along with annual EVA/IVA and resupply mass allocations. The maintenance resource allocations are in section 6 of the PDRD and are provided as total values for the WP–04 parts of various *Freedom* configurations (but not for growth). As in the case of availability, EPS level allocations will need to be broken down and allocated among the photovoltaic, PMAD, and solar dynamic systems (when growth allocations are developed).

5.8.1.4 General discussion of RAM requirements. — Since the start of the phase C/D effort there have been some trends in the evolution of RAM requirements. One predominant factor affecting the maintainance allocations has been the desire to minimize astronaut EVA for assembly and maintenance of *Freedom*. IVA and robotic IVA are favored as an alternative to EVA. This philosophy has not yet been reflected in the design and maintenance procedures for the solar dynamic module.

Note that the trend to reduce EVA is not necessarily consistent with the strong pressure to reduce program costs and in particular initial costs (sometimes at the expense of operations costs).

5.8.2 RAM Analyses

RAM analyses that have been conducted to date for the EPS are based on very preliminary information, especially for the solar dynamic module. Little effort has been expended to arrive at the initial values of ORU RAM properties. The analyses should be considered primarily in qualitative terms. The general approach to RAM analyses is to start at the lowest level components, combining their RAM characteristics in specific ways to form systems with system-level RAM properties.

The system can be broken down into smaller subsystems that consist of components which perform some operation within the system. The three interrelated parameters were used to study the solar dynamic power system. Various RAM analyses and studies are being conducted in greater detail on the EPS design. The solar dynamic results would then be integrated into the EPS to obtain overall RAM performance measures.

Preliminary reliability and maintainability results are contained in section 4 of reference 5.38. To date little effort has been devoted to availability analyses of the solar dynamic power module. However, a solar dynamic EPS model is documented in reference 5.39, upon which some availability analyses have been performed.

5.8.2.1 Methods.—The reliability parameters of a component are determined by using previously recorded test data and engineering estimates concerning the failure rates of the smaller electrical, mechanical, and structural parts of an ORU. Each part has an associated failure rate, and when these are combined, the reliability parameters can be calculated.

Maintainability parameters are also analytically determined but are based more on simulation than on actual test data, as few data are recorded for in-space removal and replacement of hardware. The differing degrees of uncertainty when analyzing the reliability and maintainability of each ORU are discussed elsewhere.

5.8.2.2 Results.—The quantitative reliability and maintainability predictions for the solar dynamic power module are listed in table 4.2.2–2 of reference 5.38. Listed in the table are the reliability and maintainability parameters including lifetime, maintenance intervals, replacement times, and rates for the ORU's that make up the solar dynamic module. Data in the table indicate that the following ORU's do not meet allocated design life: the solar dynamic engine controller, the radiator panel and deployment subassembly, the utility plate, the beta gimbal drive motor subassembly, the beta gimbal electronics control unit, the solar dynamic controller, and the PCU/receiver. In addition, the average maintenance person-hours per year for one solar dynamic module, based on a 30-year system life, are 11 hr/yr of EVA and 6 hr/yr of IVA or robotics. This is strictly hands-on time (i.e., it does not include any overhead time for preparation and cleanup, which is estimated to be 30 and 40 min per EVA, respectively).

The solar dynamic system design is predominately serial in that many of the individual components must operate successfully for the system to provide power. The availablity analysis (ref. 5.39) showed that as a result of the serial design it could be expected that the solar dynamic availability would be lower than that of the photovoltaic system with its highly parallel design. With preliminary predictions the solar dynamic module can be analyzed by studying parameters in hopes of optimizing the design and more accurately predicting performance.

5.8.3 Conclusions

Preliminary reliability studies indicate that some ORU's are unable to meet initial allocations and design goals established during the development phase of the solar dynamic design. Also of concern are the high resource allocations needed for servicing the solar dynamic module so that it will meet its 30-year operational life. Some of the problems can be attributed to conservative assumptions that were made on the basis of limited historical failure rate and repair data. Uncertainties in calculating the reliability and maintainability parameters also exist because there is little consistent correlation between use environments and failure rates.

Useful information can be observed, however, by comparing estimated RAM measures in the design options. This provides valuable qualitative insight on what improvements and tradeoffs should be considered early in the design process, when changes are most easily and economically implemented.

5.8.4 Recommendations

Future efforts should be aimed at a reassessment of the solar dynamic ORU definitions to optimize the allocation of system functions to be consistent with the RAM properties of the ORU's. This would be done by performing parametric sensitivity studies and further evaluations with the aim of increasing overall reliability and availability and reducing resupply requirements, EVA and IVA maintenance, and assembly time. These efforts should identify critical ORU's that consume the greatest resources. These candidate ORU's can then receive greater attention for possible ORU redefinition or redesign.

5.9 Launch Packaging

5.9.1 Background

In the phase C/D proposal (ref. 5.11) Rocketdyne conceived a two-solar-dynamic-module launch that included all of the "integration hardware" to be provided by the NASA Johnson Space Center (WP–02). At the time this integration hardware consisted of 12 truss bays and had a mass of 750 lb per module (1500 lb total for the launch). The launch package dimensions were 47.5 ft in length by 14.5 ft in diameter, fitting easily within the NSTS orbiter maximum dimensions of 60 ft in length by 15 ft in diameter. The cradles to carry the hardware were estimated to have a mass equal to 15 percent of the mass of the hardware that they contained. For a further mass breakdown and manifest of the cradles, refer to figure 5.19.

This launch package was designed to conform to an NSTS orbiter with a docking module, a remote manipulator system (RMS), and a full complement of EVA equipment to support assembly operations. This launch package design's cradle envelope also provides for an EVA corridor clearance and meets the NSTS orbiter center-of-gravity requirements with its mass distribution.

5.9.2 Launch Packaging/Interface Structure Tradeoff Study

In 1989 the NASA level I/II management investigated a change in the baseline power system from photovoltaic to primarily solar dynamic. It became clear that one of the main concerns was whether or not it was possible to launch two solar dynamic modules with their associated integration hardware in one launch. A quick look during the study of this option indicated that it was probably no longer possible. To determine whether or not it was, Rocketdyne began a launch packaging/interface structure tradeoff study.

Several changes since the phase C/D proposal tended to make a two-module launch highly improbable. The most significant change was the requirement to carry a 21-percent margin on the actual hardware mass as a reserve against future mass increases. Level II (the program office) required 5 percent, level III (the work package) required 7 percent, and level IV (the contractor) was required to carry 9 percent on the current hardware mass. Additional mass was added owing to a better definition of NSTS orbiter configuration and EVA requirements (e.g., docking module mass and additional EVA suits or extravehicular mobility units (EMU's)). Another significant change was the growth in mass of the integration hardware from 750 lb/module to 2106 lb/module (4212 lb for the launch). Not only did the mass increase by adding a 21-percent margin, but the integration hardware now included not only the original 12 truss bays, but an additional 12 bays worth of EVA handrails and cable trays with their associated extra volume. The overall launch package length was also becoming a constraint. The docking module requirements were now better defined as were the EVA corridor clearance requirements. Combined with a better understanding of the NSTS orbiter interface requirements (e.g., 18-in. cradle spacing required for RMS runaway and aft closed-circuit television (CCTV) clearance requirements), it had become clear that the two-solar-dynamic-module launch package because of these additional requirements was now too long.

It was clear at the outset of the launch packaging/interface structure tradeoff study that it was going to be necessary to reduce the mass and length of the launch package to maintain a two-module launch with the associated integration hardware. It was decided that the most effective way of accomplishing this objective was to examine three different fine-pointing and tracking options, all of which would eliminate the two-axis gimbal rings. Elimination of these gimbal rings had the potential of saving 1200 lb per module in mass (2400 lb for the launch).

While this tradeoff study was being conducted, a presentation on the status of the launch packaging effort was made to the Space Station *Freedom* director. As a result of that presentation this tradeoff study was redirected and became the alternative launch manifest tradeoff study.

The result of the launch packaging/interface structure tradeoff study (ref. 5.31) was that Rocketdyne recommended option 3, the beta fine-pointing option, which utilized the beta gimbal to fine point around the azimuth axis. The interface structure and the beta gimbal platform were hinged in front and an actuator was attached to the back of the interface structure to provide fine pointing around the elevation axis (see fig. 5.20). NASA Lewis personnel, however, felt that not enough quantitative analysis had been accomplished to support this conclusion, and Rocketdyne was directed to retain option 1 (fig. 5.21), the "baseline" option with the two-axis gimbal rings, for use in the alternative launch manifest tradeoff study. Quantitative analysis, however, would continue on option 3 because it provided many important advantages and improvements over the current baseline design.

5.9.3 Alternative Launch Manifest Tradeoff Study

During the redirection of the tradeoff study it became clear that the growth in the integration hardware mass and volume required that it be packaged in a cradle by itself. By this time

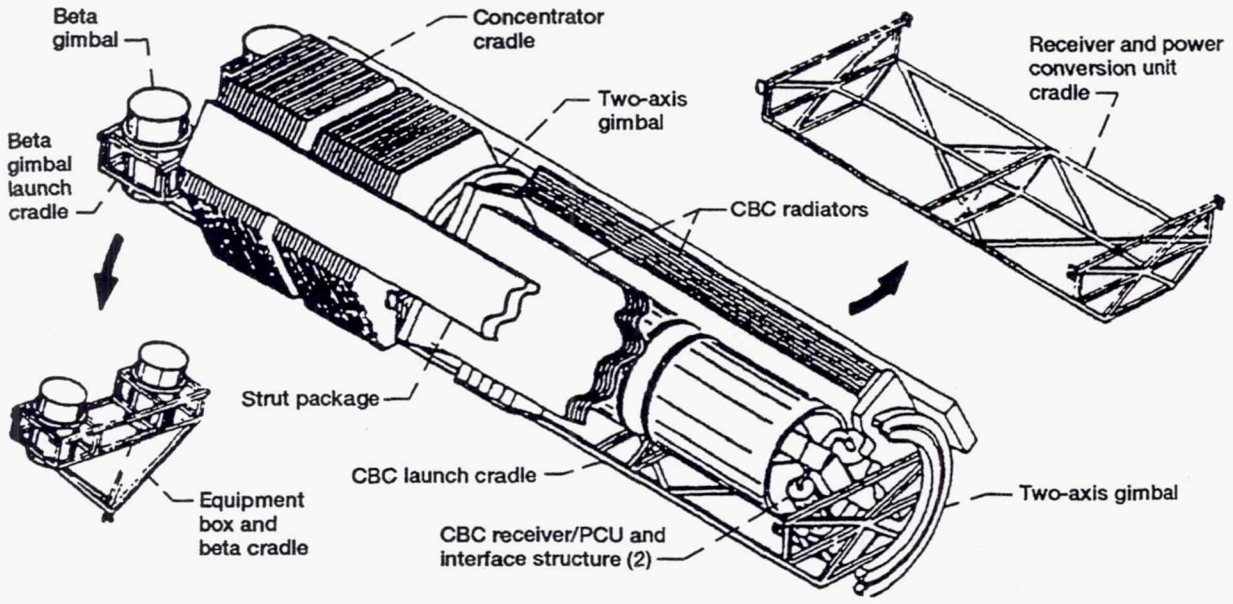

CBC configuration

Mass		Launch Volume
SD Module (2)	28 500 lb	14.5 ft diameter
Truss Bays (12)	1 500 lb	47.5 ft Long
Cradles	4 500 lb	
Total	34 500 lb	

Launch packages

Number	Launch Cradle Manifest	Launch Dimensions (ft)	Package Mass (lbm)
2	Reflective surface (set)	8 x 14.5 dia	2 010
1	Beta gimbal (2)	4 x 14.5 dia	1 290
1	CBC Receiver/PCU (2) Heat rejection assembly (2) Interface structure (2) Electrical equipment (2) Balance of concentrator (2)	29 x 14.5 dia	26 770
2	Struts[a] for: • Concentrator • Truss bay (6) • Beta gimbal	1 x 2 x 47.5	1 210

[a]Packaged separately and attached to above cradles.

Figure 5.19.—Two closed Brayton cycle solar dynamic modules configured for launch in single NSTS payload.

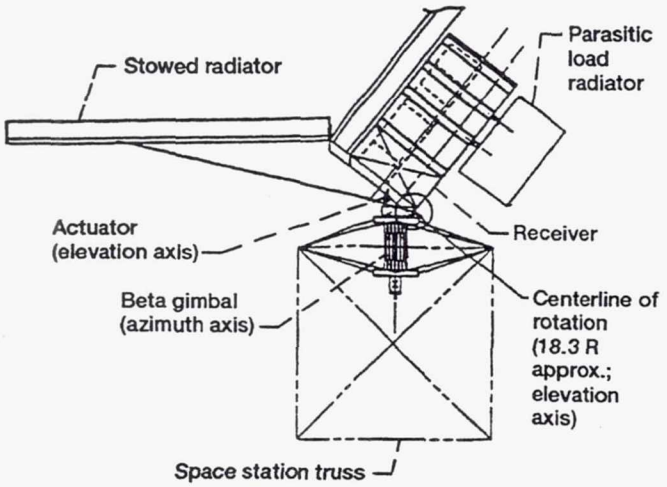

Figure 5.20.—Beta gimbal fine-pointing option.

the integration hardware consisted of 12 truss bays and their associated crew and equipment translation aid (CETA) rails and utility trays and had a mass of 8030 lb (4015 lb/module). This cradle, along with the concentrator cradle and the power generation and control system (PGCS) cradle are shown in figure 5.22 and represent the cradles used in the alternative launch manifest tradeoff study.

The alternative launch manifest tradeoff study (ref. 5.40) analyzed various combinations of cradles, with some minor hardware changes in the manifests of the PGCS and integration hardware cradles, using two- and three-flight launch scenarios. Various discriminators were used, with the most important three being EVA assembly time required versus time available, launch package overall mass, and overall length. Rocketdyne's conclusion was that it would require three launches, one for each cradle, to orbit two

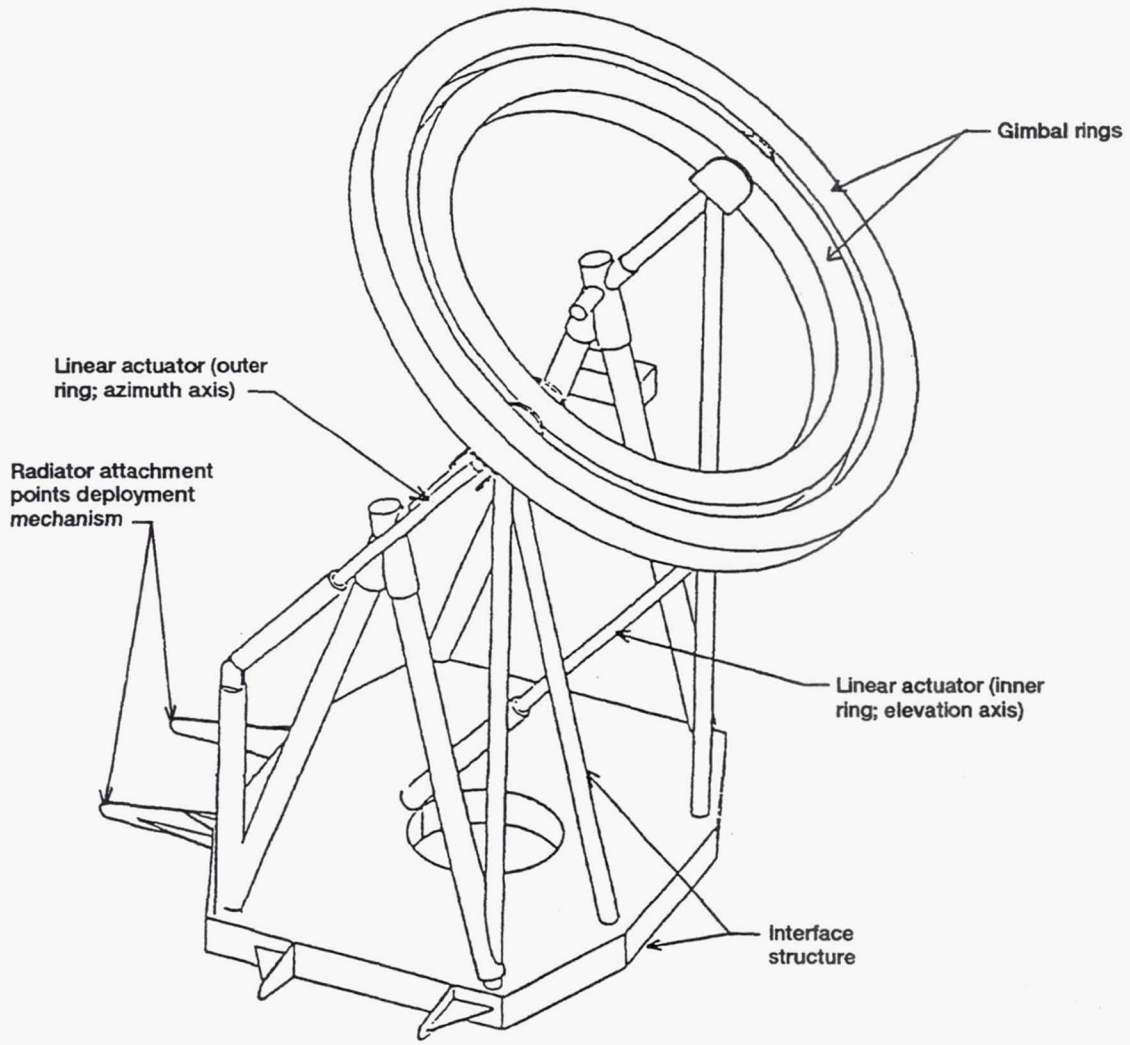

Figure 5.21.—Interface structure and gimbal rings.

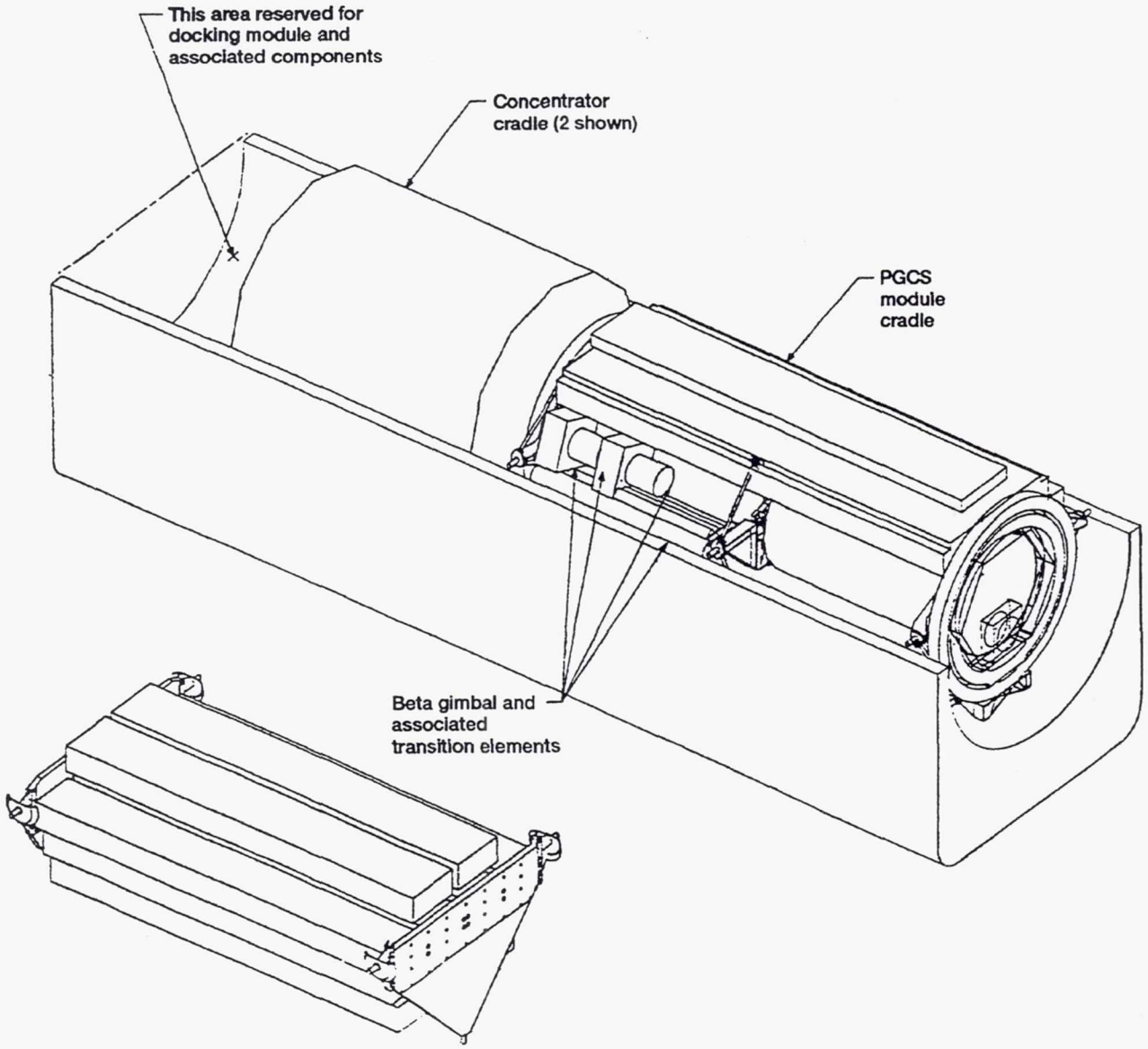

Figure 5.22.—Cradles used in alternative launch manifest tradeoff study.

complete solar dynamic modules and their associated integration hardware. Even though NASA Lewis personnel agreed with the conclusion, on the basis of the assumptions and ground rules, a decision was made to continue to pursue a two-launch scenario. This two-launch scenario would consist of the integration hardware cradle flying first, followed by the concentrator cradle and the PGCS cradle (the WP–04 hardware) on a subsequent flight.

Three options should permit the WP–04 hardware to be launched on the same flight. Using the beta fine-pointing option identified in the launch package/interface structure tradeoff study would permit the elimination of the two-axis gimbal rings and save up to 2400 lb of mass on this launch. If the overall launch package length were a problem, one option for reducing the cradle spacing would be to use the stabilized payload deployment system (SPDS) (ref. 5.41). A second option for reducing overall launch package length would be to apply for a waiver to remove the aft CCTV cameras in the orbiter bay. This could only be done, of course, if they were not needed for payload deployment operations.

5.9.4 Preliminary Launch Loads Analysis

Rocketdyne also performed a preliminary launch loads analysis, which is discussed in the loads section of reference 5.42.

5.10 On-Orbit Assembly of Solar Dynamic Module

This section of the report covers the developmental work that has been accomplished for the solar dynamic module on-orbit assembly during the phase C/D effort. The solar dynamic modules were slated for incorporation onto *Freedom* during the growth phase of the program. To date, work has been performed to ensure design compatibility with assembly equipment and astronaut capabilities for assembling the module in space. The paragraphs that follow provide a brief overview of the on-orbit assembly concept for the solar dynamic module as it existed prior to the restructuring of the Space Station *Freedom* Program.

5.10.1 On-Orbit Assembly

On-orbit assembly of the solar dynamic modules is based on the assembly equipment developed for the baseline phase (phase 1) of the Space Station *Freedom* Program. In addition, assembly of the solar dynamic modules will employ many of the techniques developed and performed on orbit during phase 1, such as those required for photovoltaic module assembly. The solar dynamic module assembly is based on EVA assembly and not on deployable systems, except for the heat rejection assembly. The assembly concepts for either phase, however, will require extensive testing and evaluation as the hardware matures.

The solar dynamic modules will be added outboard of the photovoltaic modules after the assembly-complete configuration of the phase 1 *Freedom* station. *Freedom* must have the capability to support the assembly of solar dynamic modules from orbiter unloading to module startup. The assembly process requires equipment to unload the launch package containing two solar dynamic module cargo elements from the orbiter cargo bay, equipment to move the solar dynamic module assemblies and hardware down the transverse boom, storage area for the hardware not being assembled, and standard equipment to assemble the module on orbit.

The major assemblies in the solar dynamic power module are the concentrator with its support structure and fine-pointing system, the receiver, the power conversion unit, the heat rejection assembly, the electrical equipment assembly, and the beta gimbal. These assemblies are all mounted to, and tied together by, the interface structure, which is the seventh major assembly. These seven assemblies make up the functional set of hardware in the solar dynamic module. The truss was to be supplied by another program participant (NASA Johnson Space Center (WP–02)) and will not be treated in detail in this report. Electronics for control, power conditioning, and data handling are in the electrical equipment assembly.

The receiver, power conversion unit, and radiator combination is completely assembled and charged with gas and cooling liquid on Earth before launch to orbit. Therefore, there will be no need to make on-orbit gas or liquid connections. The concentrator panels and facets will be prealigned on the ground, and the panels, with facets installed, will be stowed in the NSTS orbiter bay before launch.

Assembly of the solar dynamic modules will rely on the availability of the mobile servicing center (MSC) for transporting equipment to the assembly area outboard of the alpha gimbal and for positioning components for installation. The MSC will also serve as a work platform for the EVA required for solar dynamic module assembly. The astronaut positioning system (APS), which is attached to the mobile transporter on the MSC will position the EVA crew to make structural and utility connections after solar dynamic module components have been positioned by the space station's remote manipulator system (SSRMS). Figure 5.23 depicts the necessary assembly equipment and the solar dynamic module components as they would be located on the MSC.

Transferring solar dynamic module components from the orbiter payload bay to the MSC and transporting those components to the assembly site will be controlled by the IVA crew using the NSTS orbiter's remote manipulator system (RMS), the SSRMS, and a telerobotic system (such as the special-purpose dexterous manipulator or the flight telerobotic servicer) operating from the end of the SSRMS.

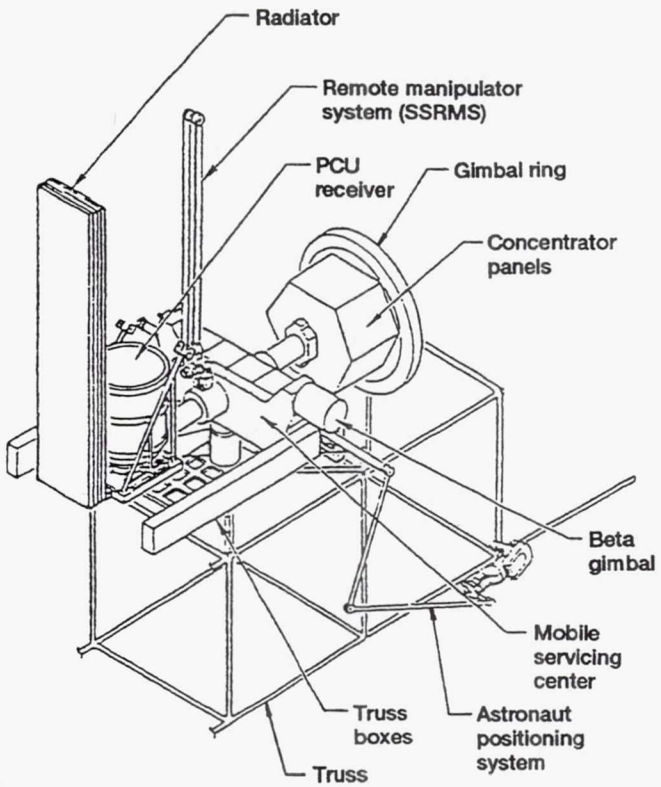

Figure 5.23.—Solar dynamic module components stowed in mobile servicing center for transport to assembly site.

The EVA crew (two crewmembers) will translate to the MSC by using the CETA and ingress the foot restraints on the APS. The EVA crew will erect six truss bays and install utility trays. The truss assembly method is based on NASA Langley Research Center's mobile transporter concept, which has been tested under neutral buoyancy conditions (see ref. 5.43).

The SSRMS will be used to retrieve each main component from the MSC and position it for installation. The beta gimbal will be installed first, followed by the receiver and radiator assembly, and then the gimbal ring (fig. 5.24). The structural and utility connections for each component will be performed by the EVA crew. The next step in the assembly process is to assemble the concentrator support structure and deploy the radiator assembly. For this procedure one crewmember will be positioned by the SSRMS using a manipulator foot restraint while the other will remain on the APS. The crewmembers will assemble strut segments into support members and attach these members to the gimbal rings. The radiator will then be deployed manually by the EVA crew using an EVA torque tool.

Once the support structure is in place, the concentrator will be assembled (fig. 5.25) on-orbit by two EVA crewmembers positioned on the APS, which is attached to the mobile transporter on the MSC. Crewmembers will release and raise the central hexagonal panel (panel one) for grappling by the SSRMS. This is accomplished by using the grapple fixture mounted on the back side (nonreflective surface) of the panel. Each additional panel will be raised from the concentrator cradle by the EVA crew and latched to the panel above. The wrist joint of the SSRMS will rotate a specified amount after the latching of each panel to provide clearance and to prepare for the latching of the next panel. This process will continue until the assembly of the concentrator is complete. The current concentrator assembly process is simple and repetitive. All actions were structured to minimize EVA. The process is expected to change slightly as phase 1 equipment becomes better defined.

The final step in the concentrator assembly process is to install (transport, align, position, and latch) the completed concentrator onto the concentrator support structure by using the SSRMS (see fig. 5.25). The operations will be planned to avoid positioning the concentrator on-Sun until the initiation of startup procedures. The on-orbit assembly of the solar dynamic module is described completely in reference 5.44.

A summary of preliminary concentrator on-orbit assembly activities was written by Harris Corporation (ref. 5.45). See chapter 6 for a more detailed description of the capabilities of the current EVA systems against the requirements for the assembly of the solar concentrator.

5.10.2 Disassembly

Freedom must be able to support the disassembly and maintenance of solar dynamic modules. Although the structure was designed to have a life expectancy of 30 years, the life expectancy of the concentrator is 15 years. This life expectancy and the possibility of damage to the concentrator while on orbit dictate the requirement for it to have the ability to be removed and disassembled so that a replacement can be installed.

The basic approach used for the disassembly of the solar dynamic concentrator is the reverse of the on-orbit assembly process. The EVA, IVA, and MSC operations that supported the concentrator assembly will also support disassembly. No additional tooling or modifications to the phase 1 equipment are needed to support the disassembly process.

5.10.3 Assembly EVA Times

Originally, the EVA time target was not a concern because of the *Freedom* EVA suit. However, the EVA suit is no longer in the Space Station *Freedom* Program. Therefore, the most recent EVA time target for assembly of the solar dynamic module is 24 person-hours, which is the maximum allowable from the *Freedom* EVA budget. The number of persons in an EVA crew is two.

The most current EVA time requirements for assembling one solar dynamic module are shown in table 5.3. Estimates have ranged between 1.5 and 2.0 EVA's (18 and 24 EVA person-hours). At this time 1.75 EVA's (21 EVA person-hours) is considered a reasonable estimate.

A more detailed description of EVA times, from unstowing the solar dynamic module from the orbiter cargo bay and assembling it through return of the MSC to its storage area, can be found in reference 5.44.

5.10.4 Assembly Tests

The only tests performed to date that relate to on-orbit assembly were the neutral buoyancy simulation (NBS) tests on the concentrator. The NBS tests are outlined in the following paragraphs, but a more complete description of these tests, including detailed results of the concentrator panel assembly tests (COPAT), can be found in chapter 6 of this report. These tests were conducted at the NASA Marshall Space Flight Center as part of the supporting development work at WP–04. NASA Lewis' neutral buoyancy COPAT's were a critical part of the early design evaluation process that allowed for reduced technical and schedule risks for the latch mechanism and guide effort, the development effort for the baseline concentrator configuration, and the anticipated flight operations and procedures.

The objectives of the NBS tests were to evaluate the feasibility of concentrator latch mechanisms and guides designed for on-orbit assembly, to evaluate anticipated flight operations and assembly procedures for the concentrator, to evaluate anticipated astronaut positions for on-orbit assembly, and to assess handhold locations and positions that would give the required leverage and line of sight for assembly.

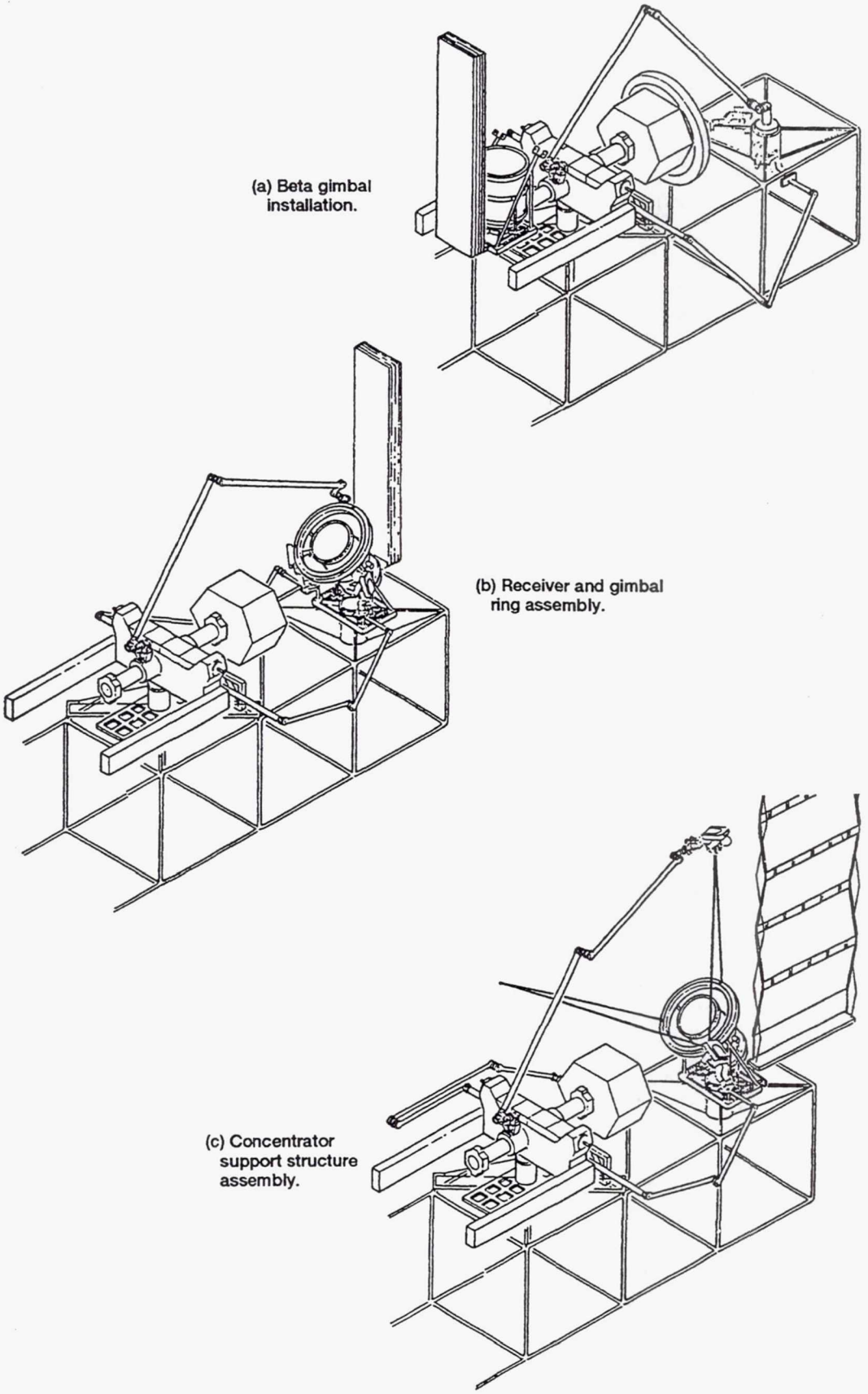

Figure 5.24.—Assembly of beta gimbal, receiver, gimbal ring, and concentrator support structure.

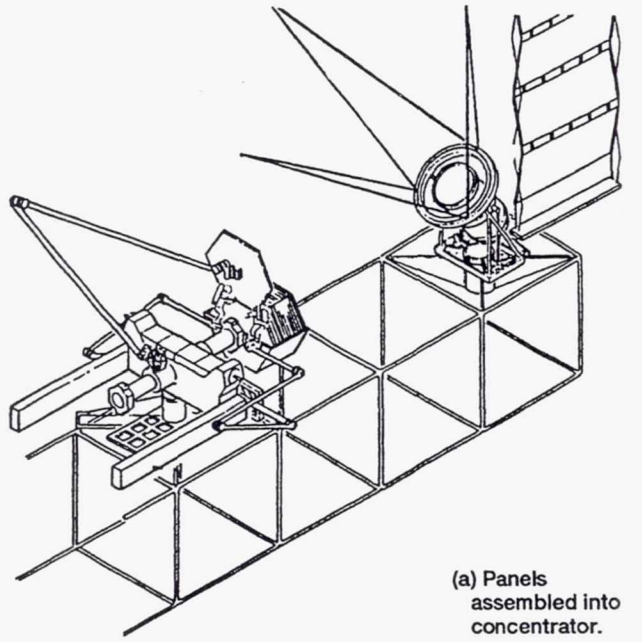

(a) Panels assembled into concentrator.

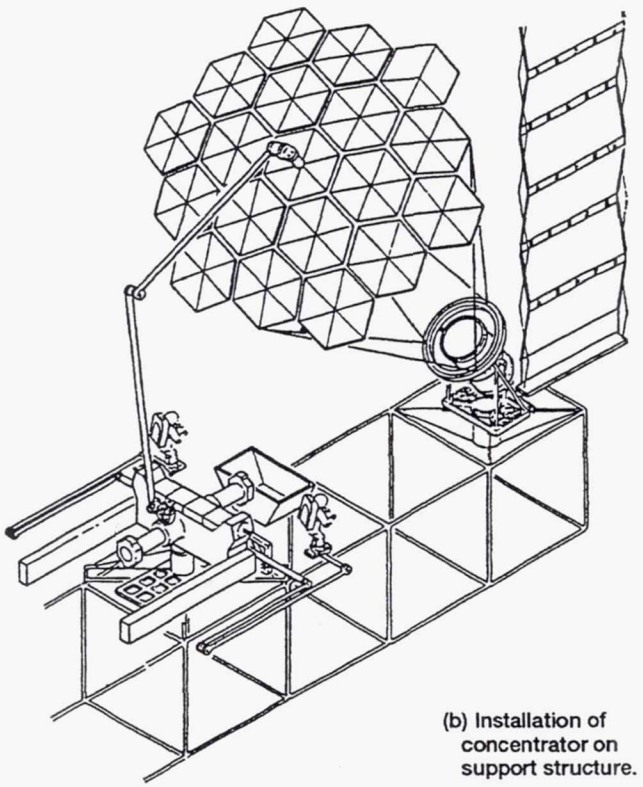

(b) Installation of concentrator on support structure.

Figure 5.25.—Concentrator assembly.

TABLE 5.3—EVA TIME

Step	Description	EVA time, min
1	Stow and transport equipment on the MSC	30
2	Install beta gimbal	17
3	Install receiver and radiator assembly	35
4	Install gimbal rings	45
5	Assemble concentrator support structure and deploy radiator	85
6	Assemble concentrator	180
7	Install concentrator	60
8	Clean up	40
	Subtotal (elapsed time)	[a]492
	Preparation and cleanup for second EVA	70
	Total elapsed time for one solar dynamic module	[b]562

[a]8.2 clock hours.
[b]9.4 clock hours.

Three different test configurations were evaluated: Astronauts and panels perpendicular to each other (configuration 1), astronauts and panels parallel to each other (configuration 2), and a combination of one astronaut perpendicular and one astronaut parallel to the panels (configuration 3). These three test configurations were rated for visibility, maneuverability, and latch reliability. Assessments were also made of latch guides, handrails, RMS capabilities, and assembly timelines.

The COPAT developmental hardware test addressed a major level I/II concern about the assembly of the solar concentrator. The primary accomplishment from the COPAT test series was that the precision latch and guide concept and associated assembly procedures and orientations were demonstrated and will enable successful on-orbit assembly of large space structures.

Latches functioned repeatedly without failure. Tolerances for slight misalignment and nonsimultaneous latchup were demonstrated. Gross guides functioned as intended without failure and aided in determining and attaining the correct panel angle for latching.

5.10.5 Summary

Details of the solar dynamic module on-orbit assembly sequence's evolution and current status can be found in reference 5.45. This reference summarizes the work done to date, the requirements of the assembly sequence, analysis assumptions and requirements, assembly sequence analysis, and maintenance considerations, as well as conclusions and recommendations for future work.

The solar dynamic module assembly analyses section in reference 5.45 includes a discussion of analysis methods, current assembly sequence and timelines, module assembly test results, and concerns and issues related to assembly.

Concerns and issues that need to be considered in the on-orbit assembly of the solar dynamic module include launch integration, disassembly of the cradles, transportation of the cradle to the assembly site, the orientation and location of astronauts during concentrator assembly, and the possible use of a removable grapple fixture on the back of the first panel because of the assembly and launch packaging volume constraints.

Some conclusions and recommendations mentioned in reference 5.44 include a study and selection of ORU's, a launch packaging study, and robotics/deployability tradeoffs if EVA is critical. Robotic assembly capability needs to be evaluated in order to define robotic-assembled ORU's and assemblies.

5.11 On-Orbit Operations

The solar dynamic module has several different on-orbit operating modes, which include startup, normal operations, detracking, shutdown, and maintenance modes. These modes cover all the expected on-orbit scenarios for solar dynamic module operation. The requirements for these modes are contained within the various solar dynamic requirements and specification documents. A brief description of these modes follows.

5.11.1 Startup Mode

The requirements call for the solar dynamic module to be capable of both cold starts and hot restarts. A cold start occurs after the module has been nonoperating for a time sufficiently long that the module reaches some low, nearly constant temperature, the cold-soak temperature. (Relatively small periodic temperature variations will occur because of solar insolation and sink temperature variations throughout the orbit.) A hot restart happens when the module is restarting with residual thermal energy within the module. The startup procedure is largely the same for the two cases; it differs primarily in the time to heat up the receiver.

The complete startup scenario has not yet been finalized, but it would involve these basic steps (estimated times in parentheses): initialization and health confirmation (30 min); Sun acquisition, at start of Sun period; warmup of the receiver (about 100 min from initialization for cold start); motoring of the turbine, alternator, and compressor unit (TAC) in the PCU (for less than 1 min) thereby circulating working fluid throughout the loop; and TAC output power generation, gradually increasing to full rated power (about 140 min). The total time for a cold start from initialization to rated power is thus about 270 min. Normal operations then follow.

5.11.2 Normal Operations Mode

Normal operations include the generation of nominal rated power and peak power. During normal operations all systems, such as the pointing system, the heat rejection system, and the power control systems respond to changing conditions (pointing disturbances, heat loads, power demand, etc.) to maintain desired setpoints.

During nominal power operation the actual module output will typically be greater than required. The reason is that the module is designed to produce rated power for the worst of a variety of conditions including minimum solar insolation, minimum orbital altitudes (eclipse/sunlit periods), and expected performance degradation. Except during the worst conditions, solar dynamic module electric power will exceed the rated output. Whenever the power demanded from the solar dynamic module falls below what is being generated, the excess electrical energy is dissipated on the parasitic load radiator.

When peak power (power exceeding rated value) is desired from the solar dynamic module, it may be all or partly available from the inherent generation at that time. If it is not, the module output is increased by increasing the mass flow rate of the working fluid through the release of stored gas from the accumulator (see section 6.3 for a full description of the operation of the PCU inventory control). There is a delay between the command for peak power and its delivery if the mass flow rate must be increased. Because of this, the solar dynamic module will require a peaking warning signal some time before the peak power is required.

5.11.3 Detracking Mode

Detracking actions of the pointing system cause the concentrated solar flux to move off the receiver aperture. Detracking would be commanded as part of a shutdown procedure, either an emergency shutdown or a normal shutdown. It could also be necessary during normal operations to limit the energy input into the receiver during a maximum-insolation period (although there is a design preference to avoid the need for this operation).

Detracking may be accomplished with the fine-pointing system (two-axis gimbal concept or beta fine-pointing concept) alone, or it could involve the coarse-pointing system (beta gimbal and alpha gimbal) depending on the reason for the action. The alpha gimbal would only be used if the solar dynamic pointing system failed.

Special provisions must be made to ensure that the concentrated solar flux does not damage solar dynamic and other hardware when detracking. However, for small tracking errors the concentrated flux can remain on the aperture plate for at least a short time, and possibly continuously, without causing damage.

5.11.4 Shutdown Modes

The shutdown modes include both emergency shutdowns and normal shutdowns. All shutdowns begin with the cutoff of input energy to the system through a detracking operation. In an emergency situation, if desired, load can be applied on the parasitic load radiator so as to rapidly decelerate the PCU's turbine, alternator, and compressor unit. Otherwise, in a normal shutdown the TAC will be held at constant speed as the alternator power drops along with receiver temperatures. When the power drops to zero, the TAC will be stopped. All other systems will be turned off or be set for standby mode.

5.11.5 Maintenance Mode

The maintenance mode is used to perform maintenance actions on the solar dynamic module. Maintenance will occur only while the module is shut down but may require the operation of specific systems in order to facilitate maintenance. For example, the pointing system may be commanded to point the concentrator away from the Sun in order to prevent high levels of reflected solar flux near the solar dynamic module.

References

5.1 SD Power Module System CEI Specification, Part 1. Rockwell International, Rocketdyne Division, DR–E–02[a], rev. B, May 1, 1990.

5.2 O'Brien, D.L.: Solar Dynamic Hooks and Scars. Rockwell International, Rocketdyne Division, EID–00365, key 33955[a], rev. D, July 9, 1990.

5.3 Space Station Program Natural Environment Definition for Design, SSP 30425[a], rev. A, June 1991.

5.4 Work Package 4 — Master Verification Plan. Rockwell International, Rocketdyne Division, DRD SE–06[a], Sept. 4, 1989.

5.5 Time-Phased SE&I Study Products. TRW, Data Requirement DR–19[a], Data Package DP 4.4, 45300.101–003, Nov. 19, 1985.

5.6 Space Station WP–04 Power System Final Study Report. Rockwell International, Rocketdyne Division, Data Requirement DR–15[a], RI/RD86–306. (Also NASA CR–179587, 1987.)

5.7 Marshall, M.; and Papac, T.: Engineering Design Document — WP–04 Power System. Rockwell International, Rocketdyne Division, EID–00259[a], rev. G, Jan. 24, 1991.

5.8 Power System Description Document. Rockwell International, Rocketdyne Division, SE–02[a], June 1, 1990.

5.9 Porada, T.: SD Module Environmental Loads. NASA Lewis Engineering Directorate, ED87012, key 24276[a], Nov. 28, 1990.

5.10 Solar Dynamic Design Description. Rockwell International, Rocketdyne Division, EID–00787[a], Apr. 2, 1991.

5.11 Space Station Electric Power System Design, Development, and Production, Vol. II, Technical Proposal.[a] Rockwell International, Rocketdyne Division, July 28, 1987.

5.12 Electronic Mail Communication to Clint Ensworth, NASA Lewis, From David O'Brien, Rocketdyne; Subject: EDD/Current Weights. key 24277[a], Feb. 22, 1991.

5.13 Thorgusen, R.L.; Receiver Tilt and Aperture Offset. Rockwell International, Rocketdyne Division, EID–00805[a], Dec. 11, 1990.

5.14 Nall, M.; and Irvine, T.: Transverse Boom Normal Modes Analyses for a Solar Dynamic Powered Space Station. PIR 147[a], May 7, 1986.

5.15 Lalonde, R.: Effects of Truss Stiffness on Solar Dynamic Fine Pointing. rev. A, Analex Corp., Prepared under NASA Contract NAS3–25776, key 24283[a], June 19, 1990.

5.16 Design Specification for Pointing and Tracking Subsystem. Rockwell International, Rocketdyne Division, RJ00198, key 24282[a], Draft (Unreleased), June 1, 1990.

5.17 Preliminary Analysis and Design Document. DR–02[a], vol. 1, Rockwell International, Rocketdyne Division, RI/RD85–320–1, June 30, 1986.

5.18 O'Brien, D.L.: Concentrator Mispointing Effects on Net Flux Input. Rockwell International, Rocketdyne Division, Internal Letter No. 659–314–IL–90–035, key 24281[a], Mar. 15, 1990.

5.19 Jefferies, K.; and Gallo, C.: OFFSET Runs To Verify Rocketdyne Analysis of Concentrator Mispointing Effects on Net Flux Input. Internal Branch Report SE–247[a], Apr. 4, 1990.

5.20 Quinn, R.D.; and Kerslake, T.W.: Solar Dynamic Modules for Space Station *Freedom*: The Relationship Between Fine-Pointing Control and Thermal Loading of the Aperture Plate. NASA TM–104498, 1992.

5.21 Quinn, R.D.: Control/Structure Interaction for Solar Dynamic Modules. Case Western Reserve University, key 24275[a], Aug. 25, 1989.

5.22 Kim, M.: Preliminary Design and Analysis of Fine Pointing and Tracking (FP&T) Control System for Solar Dynamic (SD) Power Module of Space Station. Rockwell International (RICA R–2528), IL 283–200–RGEE–90–036, key 24279[a], Sept. 28, 1990.

5.23 Cheng, J.K.: Preliminary Feasibility Study for Space Station Solar Dynamic Power Module Option 3 Configuration. Rockwell International, IL 585–142–42–IL–90–032, key 24274[a], Nov. 16, 1990.

5.24 Cassel, S.D.: Receiver Flux Distribution Sensitivity to Beta Gimbal Mispoint. Harris Corp., DR–55–E–601, SDP–0071[a], June 4, 1990.

5.25 Quinn, R.D.; and Yunis, I.: Control/Structure Interaction of *Freedom*'s Solar Dynamic Modules. Presented at the AIAA Guidance Navigation and Control Conference in Portland, Oregon, Aug. 1990.

5.26 Time-Phased SE&I Study Products. DR–19, vol. 1, Rockwell International, Rocketdyne Division, RI/RD85–194–1, (DP) 4.2[a], July 19, 1985.

5.27 Time-Phased SE&I Study Products. DR–19, vol. 2, Rockwell International, Rocketdyne Division, RI/RD85–194–2, (DP) 4.3[a], Oct. 3, 1985.

5.28 Time-Phased SE&I Study Products. DR–19, vol. 3, Rockwell International, Rocketdyne Division, RI/RD85–194–3, (DP) 4.4[a], Nov. 19, 1985.

5.29 Lawrence, C.; and Morris, R.: Space Station *Freedom* Solar Dynamic Modules Structural Modeling and Analysis. NASA TM–104506, 1991.

5.30 Preliminary Analysis and Design Document. DR–02, vol. 2, Rockwell International, Rocketdyne Division, RI/RD85–320–2[a], Dec. 19, 1986.

5.31 O'Brien, D.L.: Launch Packaging/Interface Structure Trade Study Interim Results. Rockwell International, Rocketdyne Division, EID–00648[a], May 2, 1990.

5.32 Ghosh, T.K.: Space Station *Freedom* On-Orbit Growth Configuration Normal Mode Math Model With Option 3 SD Module. Rockwell International, Rocketdyne Division, Internal Letter IL–90–EPS–8E–71, key 24280[a], Nov. 12, 1990.

5.33 Bednarczyk, R.G.; and Ghosh, T.K.: Space Station Freedom On-Orbit Growth Configuration Normal Mode Math Model With Option 3. SD Module Notebook, Rockwell International, Rocketdyne Division, Document EPS–D–SS–05–00–010, key 24278[a], Nov. 12, 1990.

[a]Space Station *Freedom* library at the NASA Lewis Research Center in Cleveland, OH 44135 (tel. 216–433–5367 and fax 216–433–8050).

5.34 Solar Dynamic Module Fine Pointing System. Aerospace Design and Fabrication, Inc., Memorandum Report – Task Order 67, NASA Contract NAS3–25767, key 34072[a], July 30, 1990.

5.35 WP–04 Technical Requirements Document. NASA LeRC–SS–0001[a], rev. D, Jan. 26, 1989. (Other revisions were applicable at different times in the program.)

5.36 Space Station Program Description and Requirements: Space Station *Systems Requirements*. NASA SSP–30000[a], *section 3, rev. G*, Oct. 31, 1988. (Other revisions were applicable at different times in the program.)

5.37 Failure Modes and Effects Analysis (FMEA) and Critical Items List (CIL) Report. Rockwell International, Rocketdyne Division, DR–PA–02[a], May 25, 1990.

5.38 Supporting Engineering Analysis and Data. System Assessment Report, Rockwell International, Rocketdyne Division, DR–SE–03[a], June 19, 1990.

5.39 Turnquist, S.R.: Space Station *Freedom* Electric Power Availability Study. NASA CR–185181, 1990.

5.40 O'Brien, D.L.: SD Alternative Launch Manifest Study. Rockwell International, Rocketdyne Division, EID–00760[a], Oct. 31, 1990.

5.41 Stabilized Payload Deployment System, Payload Integration Hardware (PIH). MV0790A, Design Requirements Document, STS86–0342A, NASA Contract NAS9–14000, 1988.

5.42 O'Brien, D.L.: Baseline PGCS Cargo Element Launch Loads Preliminary Analysis. Rockwell International, Rocketdyne Division, EID–00767[a], Nov. 28, 1990.

5.43 Labus, T.L.; Secunde, R.R.; and Lovely, R.G.: Solar Dynamic Power for Space Station *Freedom*. NASA TM–102016, 1989.

5.44 Marlatt, W.; Lovely, R.; Young, G.: Solar Dynamic Module On-Orbit Assembly Sequence. Rockwell International, Rocketdyne Division, EID–00890[a], Feb. 25, 1991.

5.45 Preliminary On-Orbit Assembly Plan for Space Station Work Package 04. Harris Corp., SD–2000, key 23654[a], July 31, 1989.

---

[a]Space Station *Freedom* library at the NASA Lewis Research Center in Cleveland, OH 44135 (tel. 216–433–5367 and fax 216–433–8050).

Page intentionally left blank

Chapter 6
Concentrator

6.1 Concentrator Description

6.1.1 Introduction

The solar concentrator (fig. 6.1) is one of four major assemblies of the solar dynamic power module. Solar insolation is intercepted by the concentrator's reflective surface and focused to the receiver assembly aperture. The current design will deliver from 188 to 209 kW of solar flux through the receiver aperture.

The solar dynamic concentrator is a large erectable structure designed to be assembled by astronauts on orbit. The concentrator consists of 19 hexagonal panels and up to 12 partial panels called edge wedges. Each panel has self-locking ball-and-socket latches located at the panel corners. The concentrator panels are raised from the concentrator container by the EVA crew and latched together to form the complete reflector. See section 5.10 for a description of on-orbit assembly of the solar dynamic module including the concentrator.

The concentrator assembly consists of 10 orbital replacement units. These ORU's are a reflective surface, a strut set, a two-axis gimbal, two linear actuators, two concentrator Sun sensors, two beta Sun sensors, and an insolation meter.

The reflective surface reflects the incoming solar radiation and focuses it into the receiver cavity. The strut set supports the reflective surface and provides a fixed reference system between the reflector vertex and the receiver aperture.

The two-axis gimbal, the linear actuators, the concentrator Sun sensors, and the beta Sun sensors combine to form the fine-pointing control loop. The purpose of this loop is to coordinate with the coarse-pointing control system and to maximize the amount of solar energy intercepted by the receiver by aligning the reflective surface's focal line parallel to the Sun's rays. See section 5.7 for a complete description of the pointing and tracking system.

An insolation meter provides overall health-monitoring data for the power generation system to the PMAD health-monitoring function.

6.1.2 Design Requirements and Specifications

The concentrator design was driven by a series of requirements stated in reference 6.1. The CEI specifications defined the performance, design, and verification requirements of the solar dynamic power module system. In particular for the concentrator the specifications stated that the assembly shall consist of the reflective surface components, the fine-pointing mechanism, the structure subassembly, the controls, and miscellaneous hardware. Component weights, packaging dimensions, the on-orbit assembly method, and environmental protection were also specified. The concentrator assembly was required to deliver concentrated solar insolation to the receiver assembly within prescribed flux distributions. Functional characteristics required a fine-pointing and tracking system with a control system and software and a pointing accuracy of 0.1°. These specifications were translated in level IV specifications by the prime contractor and are found in references 6.2 to 6.4. Reference 6.3 specifically addresses the reflector/structure and launch cradle set. This specification states concentrator assembly requirements covering item definition, characteristics, design and construction, documentation, logistics, personnel and training, major component characteristics, qualification, software, and instrumentation.

The most current update of the reflector design requirements is contained in reference 6.5. This requirements document was generated by the Harris Corporation and supplements the specifications for the reflector/structure and launch cradle set for the solar dynamic module (ref. 6.3). The requirements specified in reference 6.5 are design-specific goals that are necessary for detailing the current baseline design.

6.1.3 Assembly Components

The concentrator is an offset Newtonian parabolic reflector. Offset means that the concentrator surface is positioned in a quadrant of the paraboloid instead of being symmetrical about the vertex (fig. 6.2). Details of the concentrator are contained in references 6.6 to 6.8. The concentrator measures 59 ft in diameter and is composed of 19 hexagonally shaped panels and up to 12 partial panel sections called edge wedges, connected together with latch assemblies. Reflective triangular facets are mounted to the hexagonal panels and to the edge wedges.

The major structural element of the concentrator is the hexagonal panel (fig. 6.3). The design incorporates hardware for mounting the facets within the panels and latch assemblies for attaching the panels together as shown in figure 6.4. The panel,

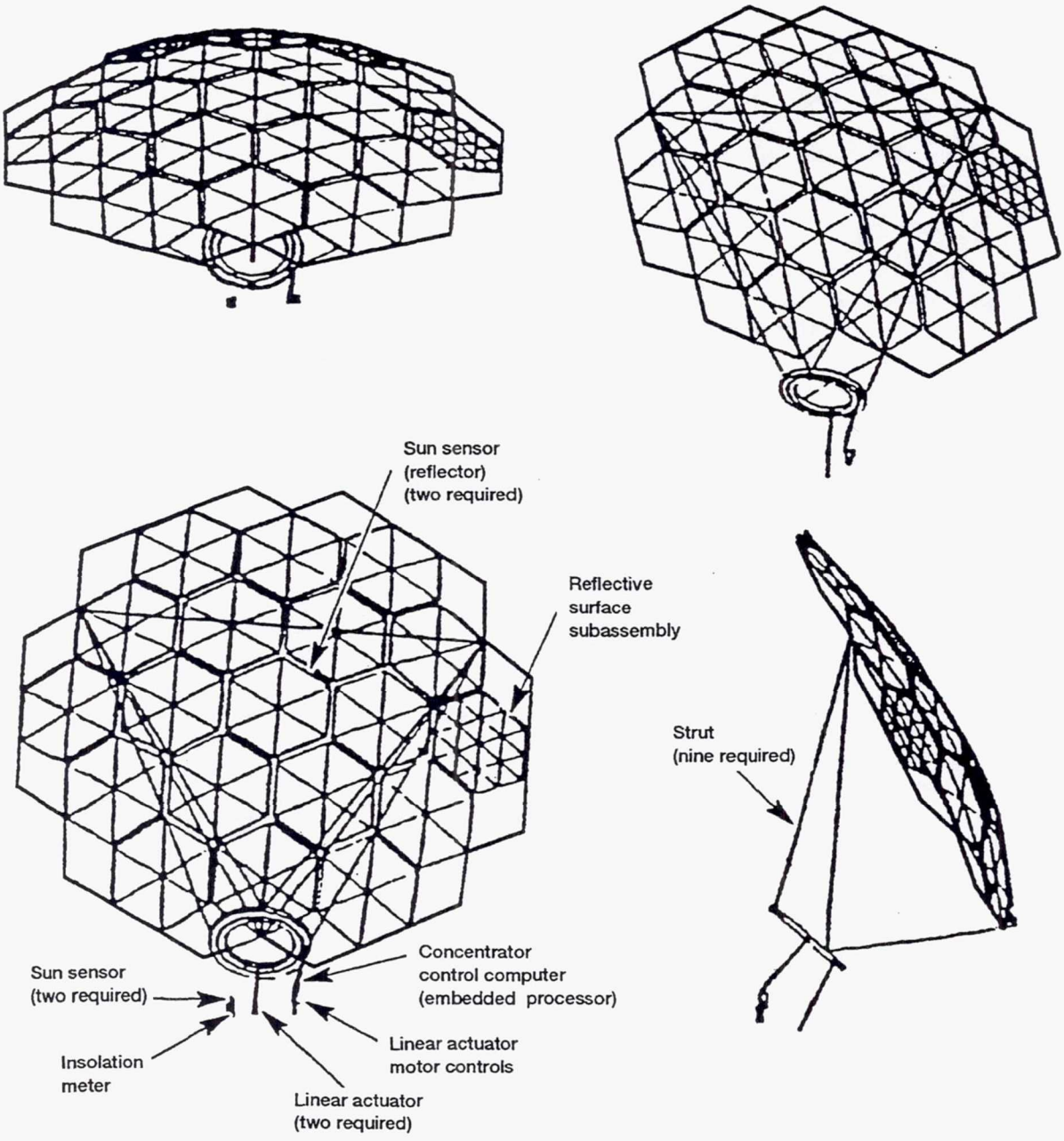

Figure 6.1.—Solar dynamic power module concentrator assembly. (Interface structure and wiring harness not shown.)

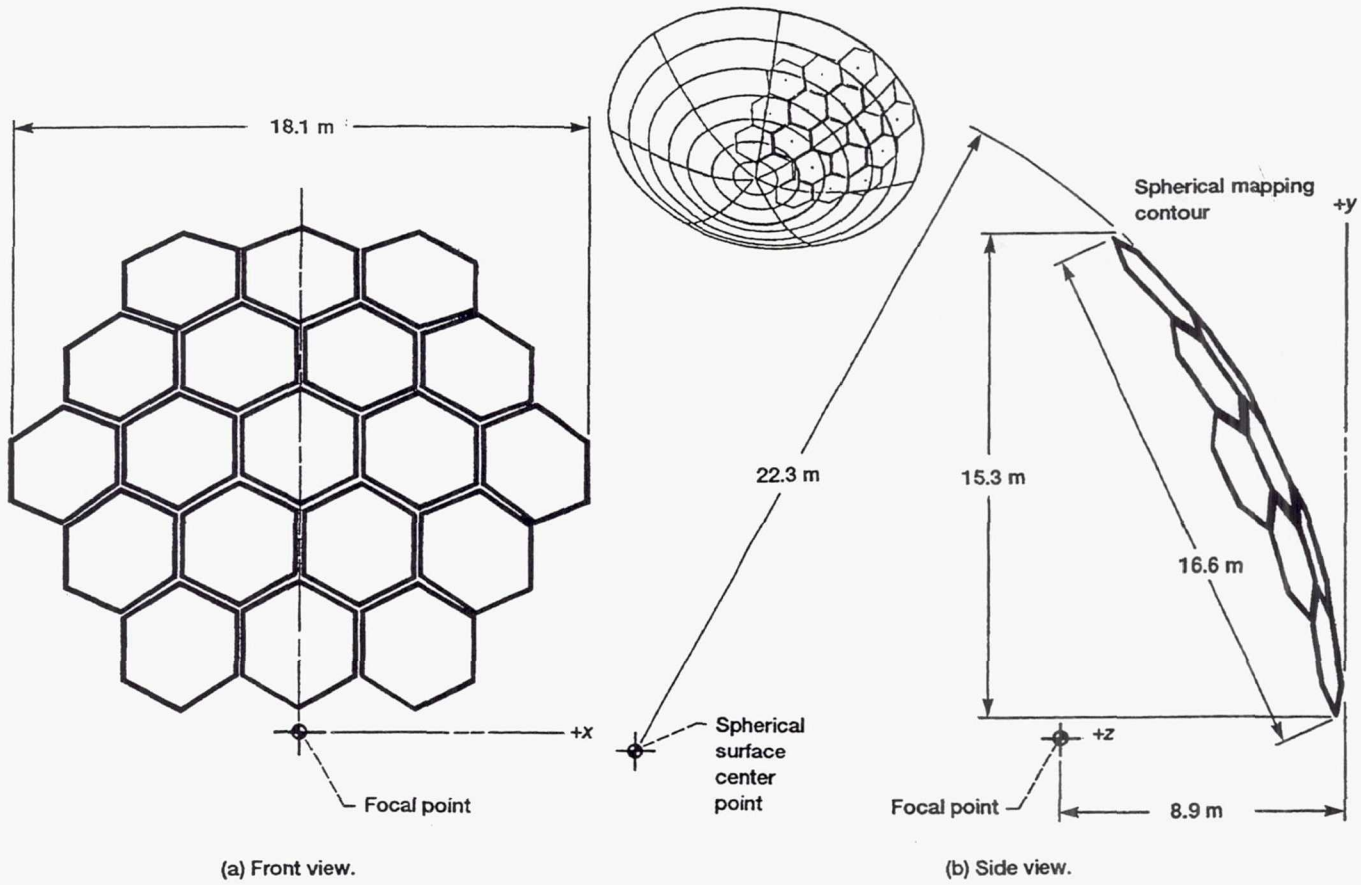

(a) Front view.

(b) Side view.

Figure 6.2.— Concentrator layout.

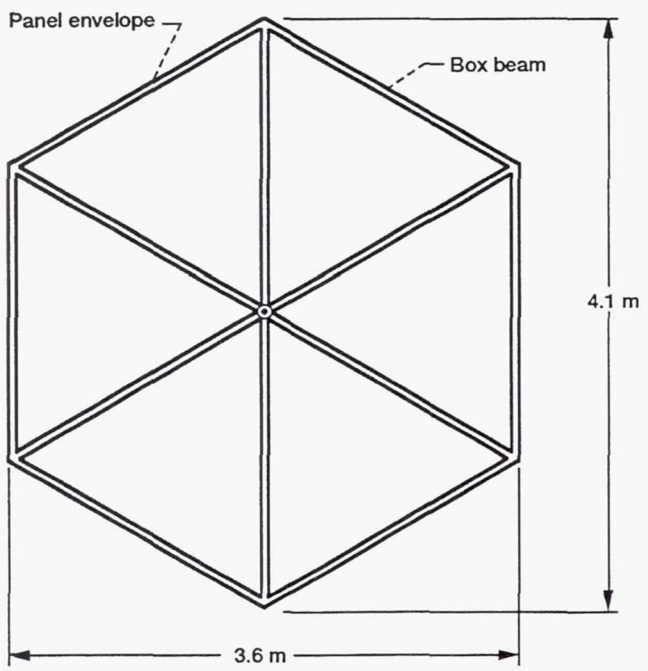

Figure 6.3.—Hexagonal panel structure.

described in references 6.7 and 6.8, consists of a framework constructed of 12 box beams, 6 as radial members and 6 as the outer periphery (fig. 6.3). The panel has a cup shape for correct pointing of the reflective facets while allowing for minimum beam depth and consequent minimum launch volume. This cupping of the panels is determined in conjunction with the depth of the beams that make up the panel and the canting of the facet within the panel that is needed to align the facets to achieve the parabolic optics required.

Dimensions of the panel are driven by NSTS orbiter bay compatibility, structural stiffness, ground testing loads, depth to accommodate canted facets, and the need to minimize the distortion that is introduced by mounting a regular polygon onto a curved surface. The hexagonal panels that make up the concentrator structure measure 164.2 in. point to point and 142.2 in. flat to flat. The panels have a depth of 3.5 in., and the framework has a cupped shape such that the hub is translated 4.25 in. from the panel perimeter.

Each edge wedge has a rhombus shape 82.1 in. on a side and is basically a 1/3 section of a panel (fig. 6.5). The 19 panels and edge wedges are mapped to a spherical surface to form the concentrator.

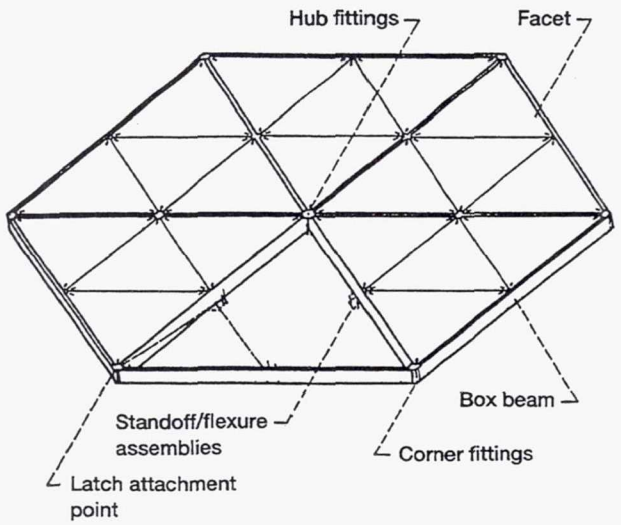

Figure 6.4.—Hexagonal panel nomenclature.

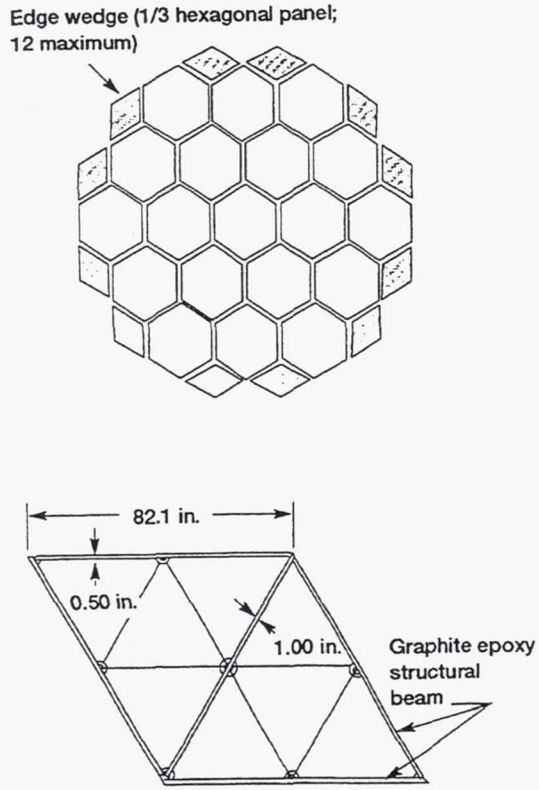

Figure 6.5.—Edge wedge panels constructed with same components as hexagonal panels.

The box beams that are used in the panel framework are rectangular-cross-section tubes made of graphite-fiber-reinforced epoxy (GFRE) with ultra-high-modulus graphite fibers. The material gives the box beam a high stiffness-to-weight ratio and a low coefficient of thermal expansion. The hexagonal panel framework is constructed with the box beam sections joined at the hub and corner points with shear plates and machined fittings. The top and bottom shear plates, also made of GFRE, provide the load path between the beams at the panel hub and the six corners. The gusset plate is the primary load path for loads entering into the corner fittings, from the latches, to be transmitted into the box beams and throughout the structure.

Mounted within each hexagonal panel framework are 24 triangular reflective facets (fig. 6.6). The facets are toroidally or spherically contoured equilateral triangles that measure 39.52 in. on a side. They have a sandwich construction of GFRE facesheets and an aluminum honeycomb core. The current baseline facet design uses a symmetric facet layup to minimize stresses and distortions due to thermal and moisture conditions. The reflective surfaces are fabricated by using a replication process. Basically a release agent and the protective and reflective layers are vapor deposited on a smooth caul plate; then a coating of epoxy and a skin of cured prepreg are applied and cured. Once curing is completed, the faceskin is pulled away from the caul plate. The faceskin and the backskin are then bonded to the honeycomb core on a contoured mold to complete the facet.

Each facet is attached to the panel framework through three standoff/flexure assemblies (fig. 6.7), one positioned at each of the facet corners. The stainless steel standoff is a threaded rod with a ball pressed on one end. The ball fits into a socket that is located in the facet corner. The standoff is threaded into a flexure fitting that is bolted to the panel framework. The flexure fitting is basically a thin aluminum web that will allow for angular displacement about its longitudinal axis and

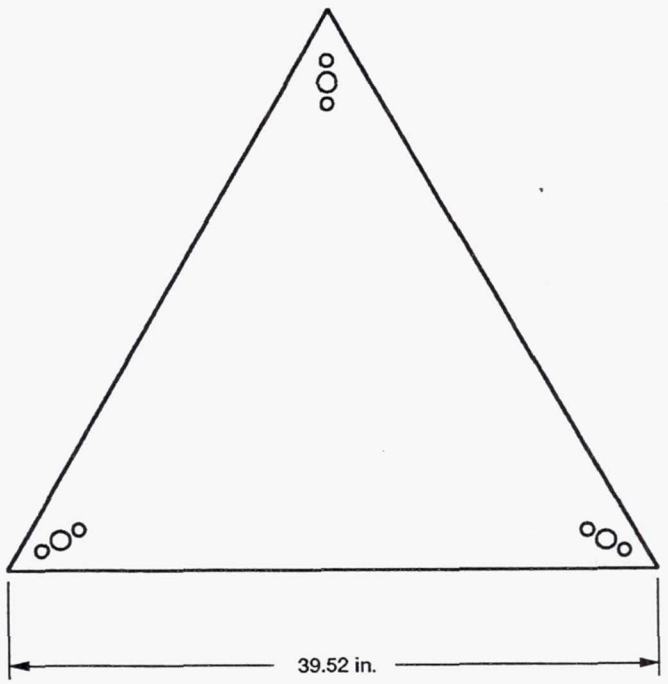

Figure 6.6.—Basic facet dimensions. (Dimension shown is point to point; 0.866 in. removed from each corner (1 in. on a side).)

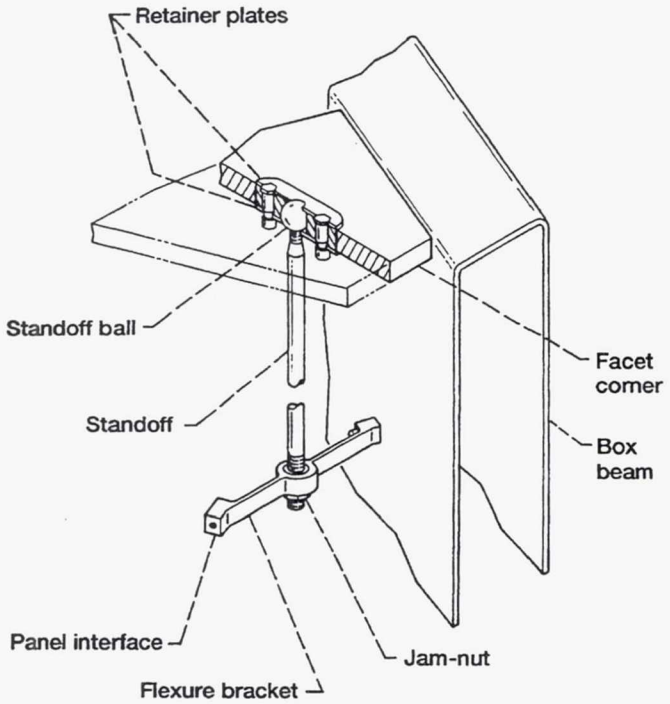

Figure 6.7.—Standoff/flexure assembly for joining facet to panel.

restrain all other motions. This design provides two important features: It allows for alignment of individual facets so that the concentrator assembly optically approximates the characteristics of a parabolic reflector, and it isolates the facets from loads imposed by panel framework distortions. Updated facet capture concepts are detailed in reference 6.9.

The panels are connected by latch assemblies (fig. 6.8), which also position the panels to the reflector geometry. The latches are attached to the panels at the panel corner fittings. The latch assemblies are self-locking ball-and-socket mechanisms that provide for zero translational displacement in three axes. The latch assemblies utilize a striker ball that fits into

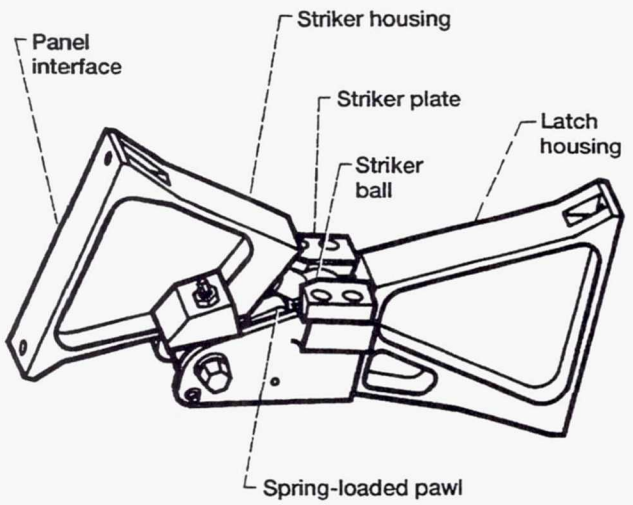

Figure 6.8.—Typical latch assembly.

a receptacle formed by the striker plates and the latch housing. Four versions or types of the latch concept are used in the assembly of the concentrator. The four types are required so that the panels can be assembled with a single radial motion toward the panel center (fig. 6.9). The all-latch feature is structurally efficient because it minimizes load eccentricities into the panel structure and component complexity during the design and fabrication of the concentrator. It also provides for efficient packaging of the panels and a minimal deployment envelope.

The hexagonal panel concentrator is an extremely stiff yet lightweight structure. Each panel weighs approximately 70 lb; 31 lb per panel for framework and fittings, and 39 lb for the 24 facets.

A strut set and delta frame (fig. 6.10) attach to the reflective surface and the fine-pointing system. The strut set is a prismatic truss space frame reinforced by a triangular frame. It is located between, and transmits the loads between, the reflective surface and the two-axis gimbal. The strut set consists of nine support struts, with each support strut containing two or more strut tubes connected by EVA end fittings. The EVA end fittings have common technology with *Freedom*'s truss end fittings. The strut set provides stiffness so that the fundamental frequency of the reflector struts and gimbal is 1 Hz or greater to separate the natural frequency of the structure from the controller bandwidth frequency of 0.5 Hz. The strut set also accommodates the wiring for the Sun sensors.

The pointing system (see section 5.7 for a detailed discussion) for the solar dynamic power module concentrator consists of coarse pointing of ±2.0° by the alpha and beta gimbals and fine pointing of ±0.1° by a gimbal ring mechanism. The fine-pointing mechanism consists of a two-axis gimbal and linear actuators that attach the struts to the interface structure. Gimbal rings (fig. 5.21) are described in reference 6.4. The two linear actuators couple to the two-axis gimbal, rotating it and the attached reflective surface. The linear actuators used in conjunction with the gimbal rings are described in reference 6.10. The two-axis gimbal system provides fine-pointing capability of 0.3° (3σ) and detracking capability of 15° per axis. This allows the focused image to be moved off the receiver structure in an emergency.

The concentrator and beta Sun sensors measure the reflector and interface structure pointing errors with respect to the Sun. The sensors are part of the fine-pointing control loop and provide data to the solar dynamic controller unit. They have pointing accuracy of 0.01° (3σ). The insolation meter measures and transmits direct normal insolation data. The meter will have a field of view greater than the combined inaccuracies of the alpha and beta angle but less than 10°.

Significant design changes that affect the two-axis gimbal were in process late in the program. An engineering change to do fine pointing with the beta gimbal would have eliminated the two-axis gimbal and achieved a large mass reduction with a simpler fine-pointing and tracking arrangement. Details of

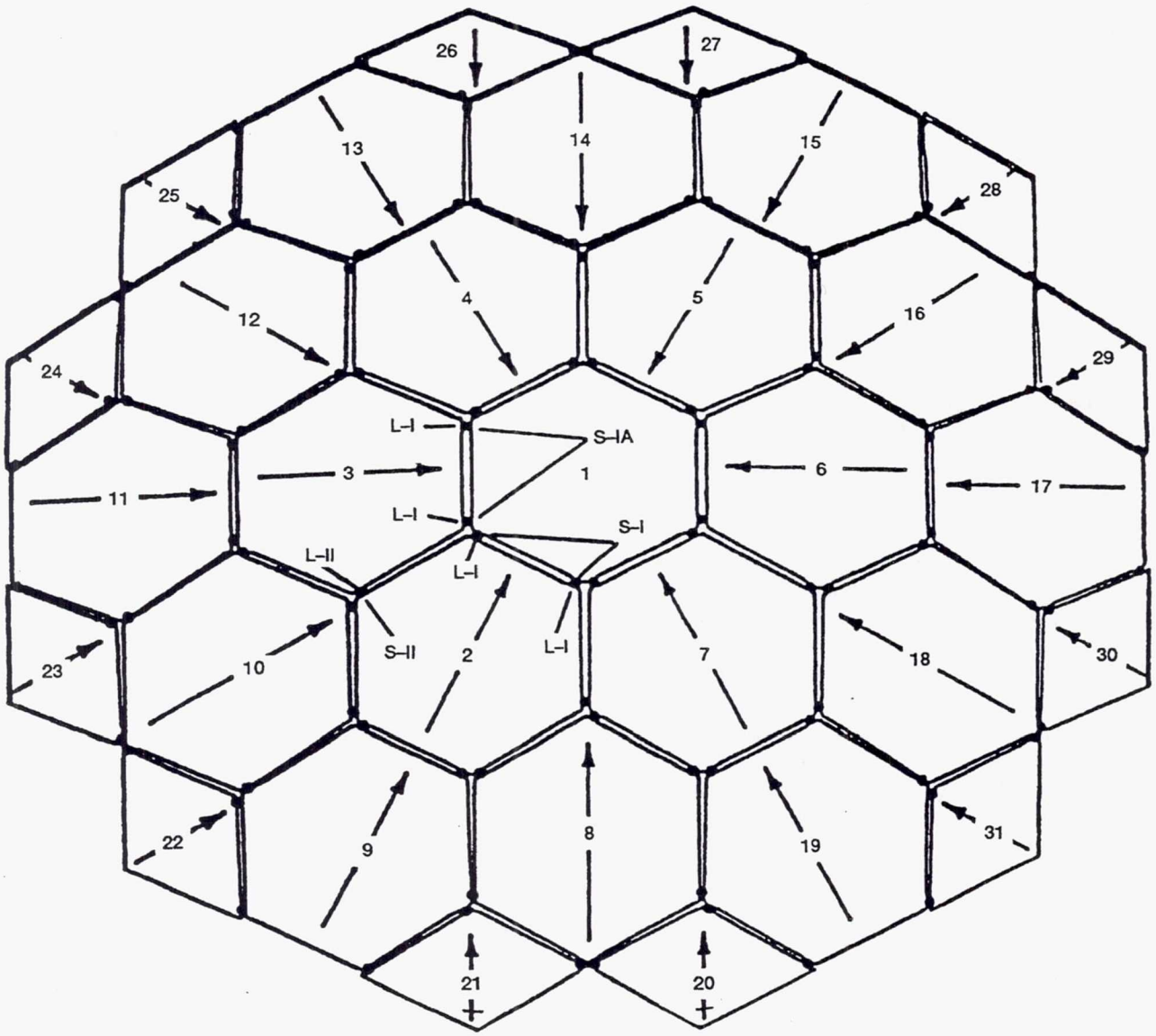

Figure 6.9.—Solar dynamic concentrator latching sequence (Sun view).

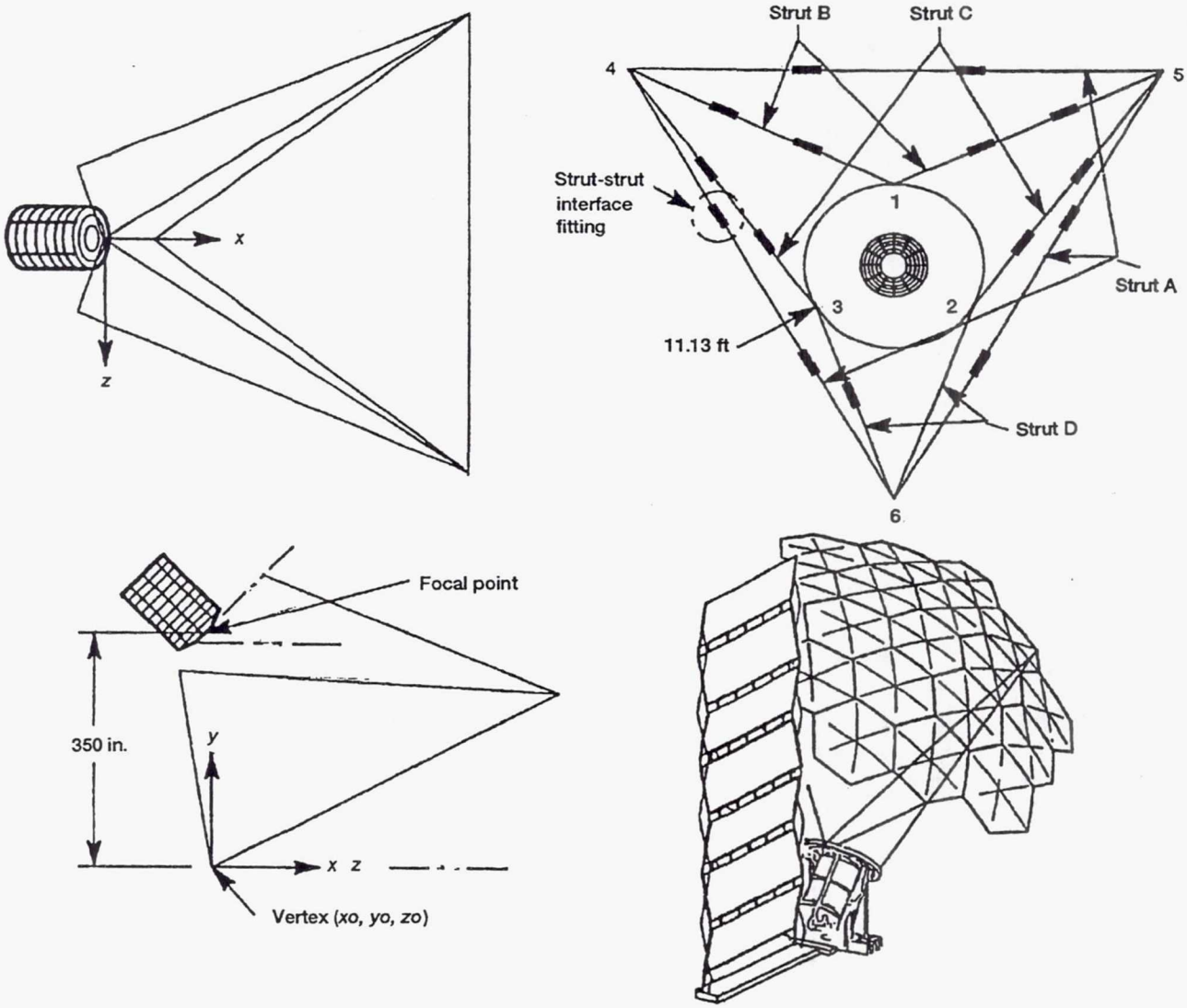

Figure 6.10.—Strut set and delta frame.

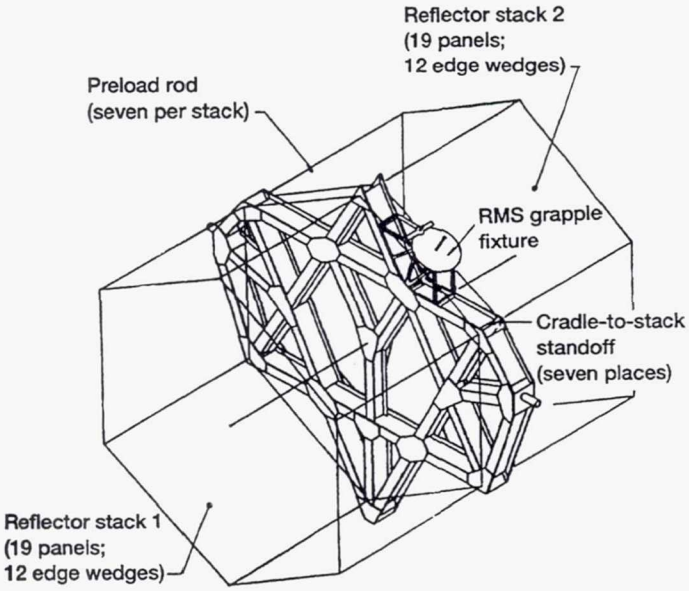

Figure 6.11.— Baseline design of launch cradle.

the change request are contained in reference 6.11, which includes a copy of the proposed change request as an appendix.

The launch cradle (fig. 6.11) is described in reference 6.3. The fabrication process for the prototype truss hexagonal concentrator is detailed in reference 6.8. This would be the starting point of the fabrication process for the flight concentrator.

6.1.4 Dimensions

The concentrator reflective surface forms a disk measuring 715 in. by 712 in. with a depth of 84 in. when installed on orbit. The reflective surface has a frontal planform of 2584 ft^2 and a profile planform of 274 ft^2. The launch configuration is contained in reference 6.3. The ORU stowed volumes are listed in table 6.1.

TABLE 6.1 – CONCENTRATOR ASSEMBLY ORU STOWED VOLUMES

ORU	Quantity	Length, in.	Diameter, in.	Volume, ft^3
Reflective surface	1	180	170	2364
Strut set	1	4442	3	18
Two-axis gimbal	1	---	---	(a)
Linear actuators	2	---	---	(a)
Sun sensors	3	12	7	.36
Cables	2	---	---	(a)
Insolation meter	1	---	---	(a)

[a]To be determined.

6.1.5 Weights

The weights for the reflector structure and the launch cradle evolved throughout the program. Table 6.2 lists the weights of the concentrator assembly ORU's as they are defined in reference 6.12.

A more recent weight evaluation was conducted on a post-baseline design and is reported in reference 6.7. This recent weight estimate took into consideration the following items:

(1) Increased stiffness in the hexagonal panel beams closest to the cradle to satisfy the specification requirement of 10-Hz stowed frequency
(2) Thermal control and atomic oxygen protection on the panel structure and the struts
(3) Delatching mechanism and latch indicator
(4) Two grapple fixtures on the cradle
(5) NSTS integration hardware
(6) Airborne (flight) support equipment
(7) Reflector consisting of 19 full panels and 4 full edge wedges

These weight changes are summarized in table 6.3 for the current weight estimates along with values reported at the systems requirements review and the first interim design review for the various concentrator components.

TABLE 6.2 – CONCENTRATOR ASSEMBLY ORU WEIGHTS

ORU	Quantity	Weight per ORU, lb
Reflective surface	1	1940
Strut set	1	133
Two-axis gimbal	1	1199
Linear actuators	2	22
Sun sensors	3	3
Cables	2	5.5
Insolation meter	1	6

TABLE 6.3. – WEIGHT COMPARISON
[Weights are in pounds.]

Component	System requirements review	First interim design review	Reference 6.7
Concentrator	1932.34	2190.0	2077.40
Structure	253.60	284.50	297.92
Cradle	(a)	1347.00	1383.86
Integration hardware	(a)	248.00	962.00
Flight support equipment	---	(a)	67.25
Launch package	---	(a)	[b]7162.46

[a]Not estimated at that time.
[b]Two concentrators, two structures, and one each of remaining items.

TABLE 6.4.– PRELIMINARY CONCENTRATOR POWER PERFORMANCE ASSESSMENT

	Phase B study[a] (minimum)	System requirements review on 2/1/89[b] (minimum)[c]	Concentrator update on 8/6/90[d] (minimum)[e]	Latest projection 11/13/90[f]	
				Minimum[e]	Maximum
Facet projected area, m^2	172.42	189.49	182.7	177.50	177.34
Solar insolation, kW/m^2	1.323	1.323	1.326	1.326	1.418
Power from Sun, kW	228.1	250.7	242.26	235.37	251.47
Primary blockage, kW:					
Radiator	---	6.2	1.36	1.36	1.11
Receiver	---	0.1	0.0	0.0	0.0
Struts	16.4	10.0	8.79	8.77	9.37
Beams	---	---	2.17	1.89	2.02
Facets	---	7.5	1.09	0.85	0.91
Incident power, kW	211.7	226.9	228.86	222.50	238.05
Optical reflectivity[g]	0.90	0.90	0.88	0.893	0.923
Reflected power, kW	190.5	204.2	201.39	198.69	219.72
Secondary blockage, kW:					
Facets	(h)	(h)	1.30	1.34	1.49
Beams	(h)	(h)	1.62	1.63	1.80
Struts	(h)	(h)	3.75	3.91	4.34
Power to focal plane, kW	190.5	204.2	194.73	191.82	212.10
Spillover, kW[i]	5.7 (3%)	12.2 (3%)	6.23	2.21	2.68
Power to receiver, kW	184.8	192.0	188.5	189.6	209.4
(Specification, kW)	(188.0)	(188.0)	(188.0)	(188.0)	(209.0)

[a]Did not include edge wedges.
[b]Included partial edge wedges per recommended baseline.
[c]This minimum-power case assumes 2.0° beta gimbal error and no fine-pointing error.
[d]Includes 19 full panels and 4 edge wedges.
[e]This minimum-power case assumes 0.1° beta gimbal error and 0.1° fine-pointing error.
[f]Includes 19 full panels and 2 edge wedges.
[g]Value for reflectivity at end of life could be as low as 0.85.
[h]Included in primary.
[i]Spillover includes slope error, 0.1° mispointing (off Sun), and facet pointing to accomplish flux tailoring.

6.1.6 Optical Performance

The solar dynamic concentrator power and performance predictions have been continually updated throughout the program. These updates have been required because of changes in the size and spacing of the panels (ref. 6.13), the number of edge wedges (refs. 6.14 and 6.15), the flux tailoring (refs. 6.16 and 6.17), and the revised pointing control system (ref. 6.18). The evolution of the performance is documented in references 6.19 to 6.21 and shown in table 6.4.

The most current performance summary (ref. 6.21) is for the solar dynamic concentrator with one edge-wedge pair (fig. 6.12). The summary bounds the performance with a minimum- and a maximum-power case. The minimum-power case analysis assumes end-of-life reflectivity of 89.3 percent, 0.1° each of beta and fine-pointing error, and minimum insolation of 1.326 kW/m^2. The maximum-power analysis assumes beginning-of-life reflectivity of 92.3 percent, 0.0° each of beta and fine-pointing error, and maximum insolation of 1.418 kW/m^2. Receiver flux distribution plots for the current projections are tabulated in table 6.5 and are shown in figures 6.13 and 6.14. In addition to total power to the receiver the profile of the power flux is also critical to the receiver design. Reference 6.3 sets the design goals for the flux values.

In addition to the steady-state performance, optical power versus mispointing (ref. 6.22) and flux profile characteristics as a result of external disturbances (ref. 6.23) were evaluated.

6.1.7 Reliability and Maintainability

The solar concentrator reliability and maintainability allocations have been identified for the baseline configuration and are documented in reference 6.24 and shown in table 6.6 for the constituent ORU's.

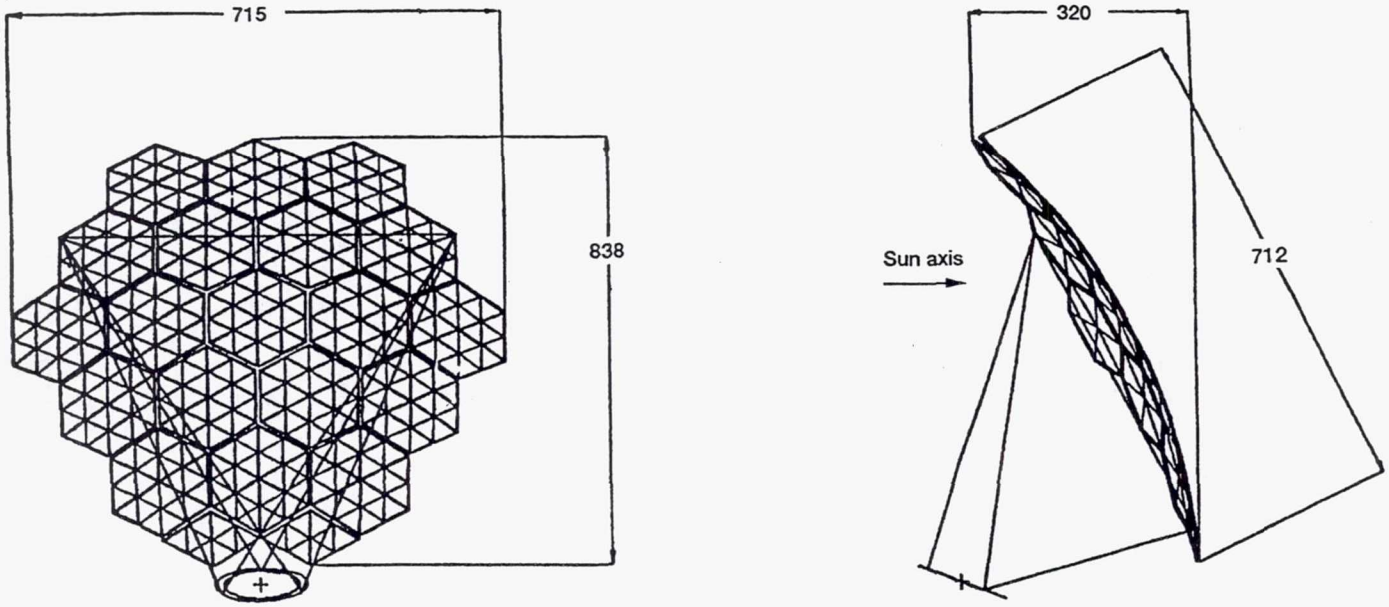

Figure 6.12.—Baseline configuration of solar dynamic concentrator. (One edge-wedge pair; dimensions are in inches and are to hexagonal structure centerlines.)

TABLE 6.5 – CURRENT CONCENTRATOR PERFORMANCE

Flux	Minimum power[a]	Maximum power[a]
Peak side wall, kW/m^2	35.17	37.38
Peak back wall, kW/m^2	32.94	33.93
Peak focal plane, kW/m^2	6496.91	7063.68
Peak aperture, kW/m^2	112.24	134.76
Average tube, kW/m^2	11.03	12.19
Minimum tube, kW/m^2	8.90 (−19.29%)	11.32 (−7.14%)
Maximum tube, kW/m^2	12.56 (+13.91%)	13.82 (+13.37%)

[a]0.1° each of beta and fine-pointing error.
[b]0.0° each of beta and fine-pointing error.

TABLE 6.6. – PRELIMINARY CONCENTRATOR ORU RELIABILITY AND MAINTAINABILITY ALLOCATIONS[a]

[Mean time to replace by IVA, 0.]

ORU	Minimum design life, yr	Mean time to failure, yr	Number of crewmembers		Mean time (in hours) to replace by–	
			EVA	IVA	EVA	Robotics
Reflective surface assembly	15	15	2	0	8	0
Concentrator strut set	30	30	2	0	12	0
Two-axis gimbal	30	30	2	0	6	0
Linear actuator (inner)	15	10	1	0	1	0
Linear actuator (outer)	15	10	1	0	1	0
Concentrator Sun sensor	15	10	0	1	0	1.5
Beta Sun sensor	15	10	0	1	0	1.5
Sun sensor/utility plate cable	30	30	2	0	2	0
Insolation meter assembly	15	10	0	1	0	1.5

[a]Based on four 25-kW modules.

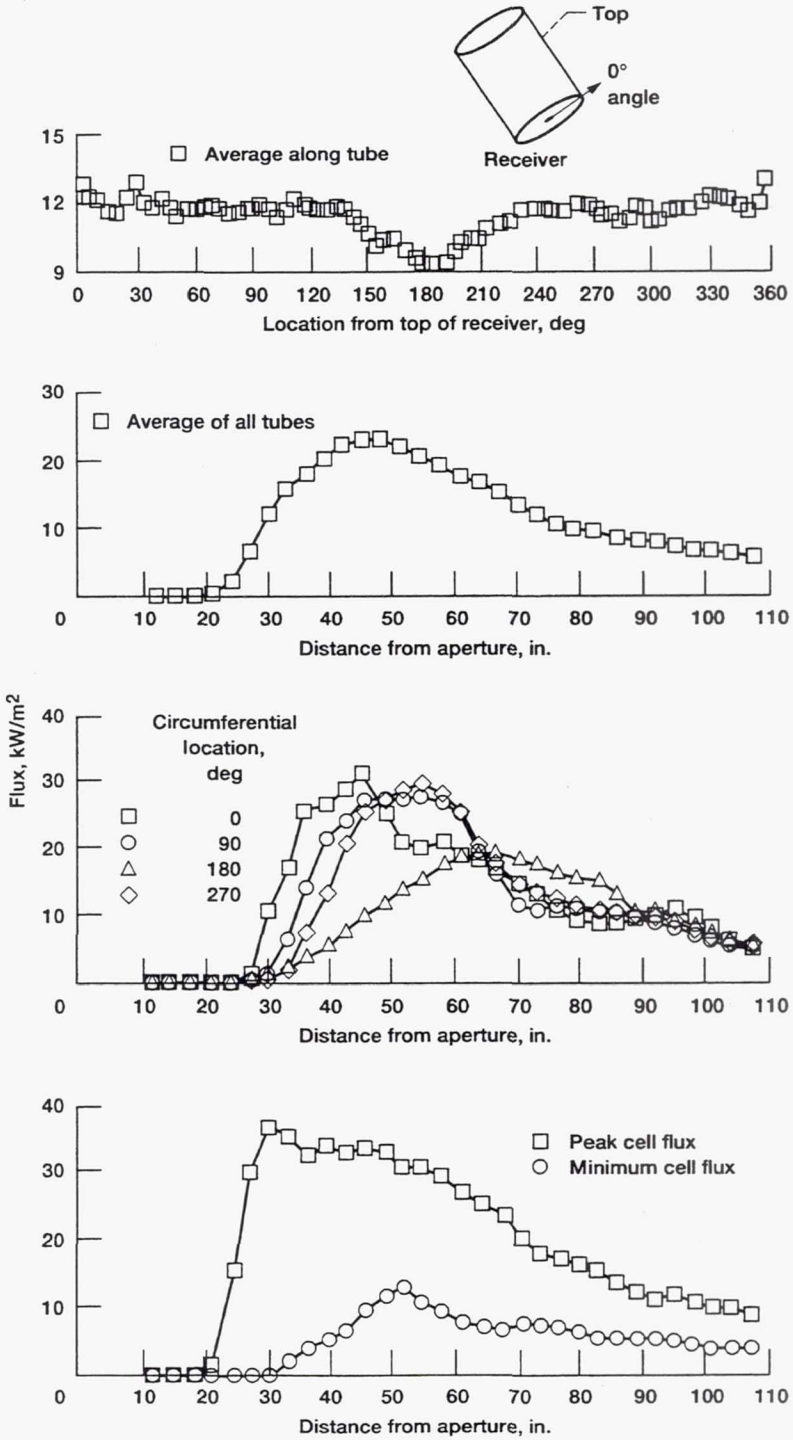

Figure 6.13.—Receiver flux distribution plots for minimum-power case. Fine-pointing error, 0.1°; beta error, 0.1°.

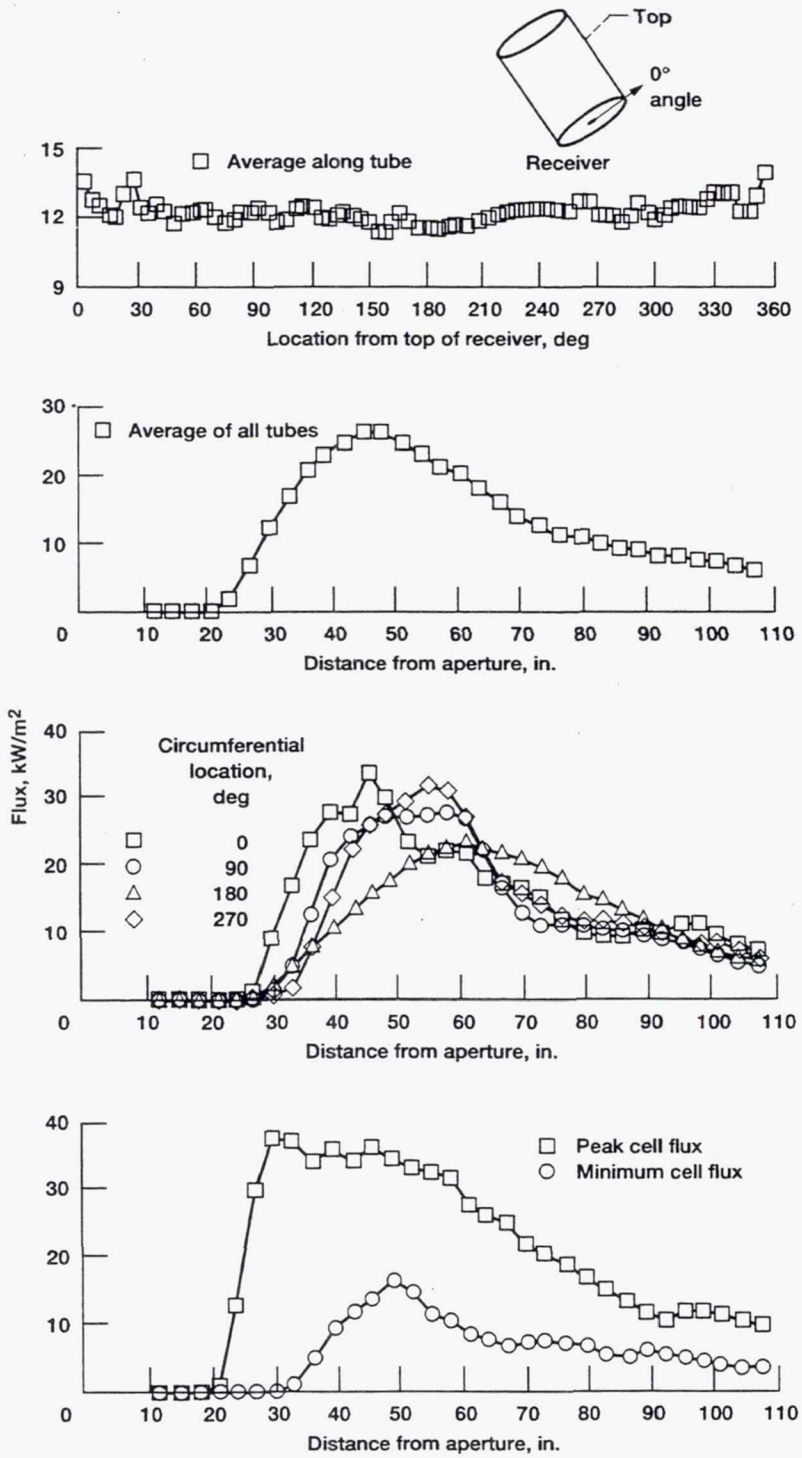

Figure 6.14.—Receiver flux distribution plots for maximum-power case. Fine-pointing error, 0°; beta error, 0°.

6.2 Rationale for Design Selection (Tradeoffs)

6.2.1 Optical Configuration

In a series of tradeoff studies (refs. 6.25 to 6.29) several concentrator concepts and configurations were evaluated, including Newtonian, Cassegrainian, Fresnel, exocentric gimbaled, orthogonal teetered, parabolic offset linear actuated reflector (POLAR), and center-of-mass gimbaled. The POLAR configuration emerged as the preferred concept because it allowed a compact solar dynamic module configuration with minimal receiver and truss blockage, low moment of inertia about the truss, and the lowest mass for growth. Fabrication of the concentrator utilized existing technology.

The truss hexagonal panel reflector was selected as the concentrator concept, primarily because of its technical soundness and design flexibility. The current baseline concentrator structure is defined in references 6.13, 6.15, 6.16, and 6.22. It is composed of 19 hexagonal panels and two edge wedges that are mapped to a spherical contour. Mapping to a spherical contour allows for radial symmetry of the structure and significant commonality of the components. The structure measures 715 in. by 712 in. It is mapped to a sphere that has a radius of 950 in. The spherical contour radius was selected to closely approximate the curvature of the parent paraboloid with which the reflective surface is aligned.

Parabolic mapping of the panels was initially baselined. Each panel would have been tangent at its center to the paraboloid. Parabolic mapping would result in minimum facet tilt angles, which would minimize the panel thickness and therefore the stowed-package volume. However, panel spacing is irregular because the offset parabolic structure is not symmetric. Mapping the panel centers tangent to a spherical approximation of the paraboloid resulted in a symmetric structure and a regular panel spacing. Also shadowing losses are less with this spherical panel mapping. The spherical mapping was chosen to reduce costs because the symmetric structure requires fewer drawings and latch configurations and shorter production time.

The 19 hexagonal panels are arranged in three concentric closed rings. This arrangement provides stiffness, an integral load path, and a closed shell structure. The parabolic optical characteristics are achieved by approximating the parent paraboloid surface with the facets. To do this, the facet surface normal is aligned with the local paraboloid surface normal, and the facet surface is spherically or toroidally contoured with radii that approximate the local curvature of the paraboloid. Translation of the facet in the surface normal direction to fit within the panel envelope has no effect on the optical characteristics.

Concentrator and facet contour studies were conducted and are reported in references 6.16, 6.22, and 6.30. Ideally, for imaging optics, each facet would require a custom contour to match the theoretic paraboloid at that location. In fact, imaging optics are not needed. The facets are divided into families of identically contoured facets. Family contours are defined in each of two orthogonal directions depending on the concentrating power needed and on local facet tilt. The limited number of families relates to production economics, and the choice of toroidal shape relates to sufficient focusing power in the two directions.

6.2.2 Structural Configuration

The structural configuration of hexagonal panels attached at the edges or corners dates to the very early program. The hexagon is a regular polygon that can tile two-dimensional space without leaving gaps. Within the set of those regular polygons that have this property it also tiles the largest proportion of the area of the smallest enclosing circle. This combination of features allows the highest packing density of concentrator surface in the cylindrical orbiter payload bay. Triangular facets were chosen for similar reasons within the context of tiling the hexagonal shape of the hexagonal panels. The choice of 24 facets, as opposed to possibly 6, per panel was driven by the economics of facet mold tooling, minimization of the panel thickness, which is driven by facet bulge, and the convenience of three-point corner support of the individual facets. Corner, as opposed to edge, support of the hexagonal panels themselves is a natural result of choosing the stiffest part of the edge on which to locate the support. The delta frame and truss that attaches the reflector to the rest of the solar dynamic power module is a simple irregular octahedron with truss members at each edge. A study was conducted to determine the best method of attaching the struts to the reflector and the gimbal rings (ref. 6.23). The two methods considered were (1) ball joints at the end of each strut and (2) fixed joints at the gimbal rings and ball joints at the reflector. Analyses indicated that the fixed joint–ball joint configuration produced minimum power losses (~0.79 kW) during docking disturbances. Future investigation should consider how single failures could be tolerated in the support structure members. A series of guy lines may prove helpful in this regard, providing redundant support so that the struts themselves do not become fracture-critical items.

6.3 Concentrator Optical Analysis

6.3.1 Analysis Codes

Four optical analysis codes were developed or modified for simulating *Freedom*'s solar dynamic concentrator optics. Georgia Tech Research Institute (GTRI) developed their OPTIC code (ref. 6.31) for terrestrial concentrators and validated it with experimental data. OPTIC produced focal plane and receiver side-wall flux profiles. The code was modified to model

Freedom's solar dynamic concentrator and was used for optical analysis during the inital concentrator design phase. Harris Corporation developed SOLAR18 (ref. 6.8, pp. 26 to 35), which defines the detailed reflector geometry and also performs optical analysis. On the basis of discussions with GTRI and Harris, NASA developed a similar code called OFFSET (ref. 6.30), which incorporates the optical analysis methods, but not the actual code, from OPTIC and SOLAR18. NASA used the OFFSET code for independent verification, to supplement the contractors' analyses, and to guide the contracted efforts. McDonnell Douglas Space Systems Company later modified the DPAP concentrator analysis code, which they developed and validated for terrestrial concentrators, to model *Freedom*'s solar dynamic concentrator. McDonnell Douglas Space Systems Company used their DPAP code (ref. 6.32) in developing an optical measurement system for experimental testing of concentrator optics.

6.3.2 Results of Analyses

Harris Corporation and NASA have cooperated in optical analysis. As just mentioned, Harris described the analytical methods used in SOLAR18 to NASA. These methods were then incorporated into OFFSET. Additional analytical methods developed for the OFFSET code were later incorporated into SOLAR18. These included an improved pseudorandom method of choosing ray originating points on the Sun (ref. 6.30), use of a two-dimensional normal circular probability distribution for representing facet contour errors, and flux tailoring methods. Analyses done by using one code were evaluated by using the other code. Discrepancies were minor and quickly resolved. Frequently, additional results were achieved when one code was used to extend analysis begun by the other. The solar dynamic development for *Freedom* benefited considerably from this cooperation.

6.3.2.1 OFFSET code.—The OFFSET code determines flux distributions at the receiver aperture, within the receiver, and at other selected locations. It is a ray-tracing optical analysis code that traces rays from 50 selected points on the Sun to 4560 points on the concentrator and traces the 228 000 reflected rays through the receiver aperture to the receiver interior. It uses PATRAN to produce color contour plots of the calculated flux distributions. The code is publicly available through NASA's Computer Software Management Information Center (COSMIC) at the University of Georgia (phone: (404) 542–3265).

6.3.2.2 SOLAR18 code.—The SOLAR18 code has the same optical analysis capabilities as the OFFSET code, but it has additional capabilities to generate precise and detailed concentrator designs. SOLAR18 also has greater flexibility to change the number of computational nodes and to represent a variety of concentrator designs. However, it requires more computer time for each analysis.

6.3.2.3 Concentrator design concepts.—Many of the features of the concentrator design were developed as a result of the optical analyses. These features include spherical mapping of hexagonal panels, dishing of hexagonal panels, toroidal facet contour, offset receiver aperture, and edge wedge panels. See sections 6.1 and 6.2 for descriptions of these features. These features were first introduced as options in the codes. Analysis was then conducted to determine benefits. Finally, the concentrator design was changed to incorporate them.

6.3.2.4 Off-axis analyses.—The term "off-axis" refers to incoming rays that are not parallel to the parabolic axis of the concentrator. This includes solar rays when the concentrator is not properly pointed or any other off-axis radiation that can be focused by the concentrator.

Preliminary off-axis analysis used a code named PIXEL to predict concentration of off-axis radiation. An experimental study reported in reference 6.33 used an 11-m multifaceted dish concentrator to validate the PIXEL analysis. This comparison showed good agreement in average flux, but there were localized hot spots due to individual facets in the experimental data that had not been predicted by the PIXEL model because it does not simulate individual facets.

Subsequent analysis using the OFFSET code, which does simulate individual facets, is reported in reference 6.34. This analysis considered four types of off-axis radiation: (1) small off-axis angles during walkoff, (2) large off-axis angles, (3) an extended off-axis source such as Earth albedo, and (4) miscellaneous off-axis sources including radiofrequency sources and local point sources. The off-axis concerns were not expected to affect *Freedom*'s solar dynamic system. However, the off-axis considerations constitute design constraints for safe operation of the solar dynamic system and for the surrounding region. Additional off-axis analysis was done using the SOLAR18 code and is reported in section 6.6.1.

6.3.2.5 Digital image radiometer configuration change.—A code derived from the OFFSET code was used to evaluate different concentrator and optical system configurations for the digital image radiometer (DIR) optical measuring system that was developed for concentrator testing. Problems with the previous configuration and possible alternative configurations had been identified by McDonnell Douglas Space Systems Company and by NASA. Over 100 possible configurations were evaluated and an optimum configuration was chosen (ref. 6.35). This configuration reduced the size of the light panel from 988 ft^2 to 416 ft^2, increased the accuracy of the optical measurements, and moved the light panel out of the path of the concentrator support cables. This configuration was installed at NASA and used for optical testing of the concentrator.

6.3.2.6 Offset receiver aperture.—In examining receiver flux distributions produced by the OFFSET code, the irregular

flux distribution due to the *offset* parabolic concentrator geometry was noted. A corresponding offset of the receiver aperture was analyzed as a means of canceling this effect, but it made the flux distribution worse. However, offsetting the aperture in the opposite direction improved flux distribution (ref. 6.36). With this aperture offset the peak flux decreases because flux is moved into the dark area near the receiver aperture. This increases the effectiveness of thermal energy storage material in this region and improves the receiver heat transfer. The OFFSET code was used to select an optimum offset of the receiver aperture and an optimum receiver tilt angle. These values were incorporated into the reference receiver design (ref. 6.11).

6.3.2.7 Toroidal facet design. — The concentrator surface is subdivided into 456 (or more if the concentrator includes edge wedges) individual reflectors called facets. In the original concentrator design the facet contours were spherical. Four different spherical radii were used that were based on the distance of the facets from the focal point. Facets with the same radii were identical and interchangeable. However, the facets farthest from the focal point did not accurately match the complex curvature of the parabola. Much of the light reflected by the corners of these facets did not pass through the receiver aperture.

The OFFSET code evaluated an alternative facet design with a complex contour (ref. 6.36). The facet contours had a different radius of curvature in the direction along one side of the facet than in the direction perpendicular to this side. These contours were called toroidal because they are similar to the contour of the outer edge of a donut shape. Power reflected into the aperture was evaluated for a variety of possible toroidal contours. Four groups of optimally contoured toroidal facets were selected. Facets within a group are identical and interchangeable, but the facets must be mounted so that the direction of the longest radius of curvature is approximately radially outward from the parabolic axis. (Additional improvement of focusing is possible if the direction of the radius of curvature is exactly radially outward from the axis. It would still be possible to use the same mold to produce all of the facets in a given group, but the facets within a group would not be identical and interchangeable.) The facet grouping for identical facets and the radii of curvature selected by using the OFFSET code were incorporated into the concentrator design.

6.3.2.8 Circumferential flux tailoring method. — Heat transfer tubes are positioned around the circumference of the receiver interior and are parallel to the receiver axis. Tube-to-tube variations of flux limit the heat transfer performance of the receiver and may shorten the receiver life. In order to improve circumferential flux distribution, the concentrator facets are aimed to selected points within the receiver aperture rather than to the focal point at the center of the aperture.

The following method for aiming the facets to improve circumferential flux distribution was developed at NASA and added to the OFFSET code: The circumferential position inside the receiver of each facet image is first determined by assuming that the facet is aimed at the center of the aperture. The facets are then listed in the order of the circumferential position of their images, starting at a point of symmetry. Keeping this order, new circumferential positions are calculated for each facet image so that the circumferential angle between any two consecutive facet images is proportional to the sum of the power that the facets reflect into the receiver. Aim points within the receiver aperture are calculated for each facet so that the facet image will appear at the selected position. This method produced a major improvement in receiver circumferential flux distribution. Harris Corporation incorporated this method into the SOLAR18 code and confirmed the improvement in circumferential flux distribution (ref. 6.17).

6.3.2.9 Axial flux tailoring method. — High-flux regions within the receiver are within a circumferential band that is between 30 and 54 in. from the aperture end of the receiver. In order to reduce the flux in this band, the axial aim points of each facet were changed. This was accomplished by a linear mapping of the axial position of the facet image with no flux tailoring into a flux-tailored axial position. The flux in this band was stretched by a factor of 4/3 to occupy the band between 26 and 58 in. from the aperture end, thereby decreasing flux density in this band. Neighboring bands with lower flux were compressed by a factor of 5/6, which increased flux in these bands. This axial method was developed by using OFFSET. Harris Corporation incorporated it into SOLAR18 and improved it by choosing the optimum axial stretching at each circumferential location (ref. 6.17).

6.3.2.10 Beta fine pointing. — Analyses of receiver flux distribution that assumed beta pointing errors which were corrected by fine pointing showed that there would be considerable maldistribution of this flux. Because the fine-pointing mechanism does not correct the radiator orientation, the shadow of the radiator on the concentrator becomes larger with beta mispointing. A few receiver tubes that would have received flux from the shadowed area have greatly reduced flux. Also, the beta fine-pointing correction introduces a tilt angle between the concentrator and the receiver. This tilt moves flux from one side of the receiver to the other, thus causing additional flux maldistribution. Because the beta fine-pointing axis is in the plane of the receiver aperture, which is tilted 65° with respect to the beta axis, the beta fine-pointing correction is much greater than the beta pointing error. Harris Corporation reported (ref. 6.22, pp. 122 to 134) that 2° of beta gimbal mispointing corrected by beta fine pointing would result in a circumferential flux maldistribution of ±50 percent. The solar dynamic pointing system is described in detail in section 5.7.

6.4 Concentrator Performance

6.4.1 Optical

Concentrator optical analysis is discussed in section 6.3 and concentrator optical performance is discussed in section 6.1.6. This section discusses the results of the analysis as it applies to the optical performance of the concentrator. The last detailed error budget breakdown is contained in reference 6.19.

Reflectance issues were to be addressed during the facet development portion of the program. A beginning-of-life (BOL) solar hemispherical reflectance of 0.93 and an end-of-life (EOL) reflectance of 0.90 had been used to calculate solar dynamic power module energy balances for these two modes of operation. The range of reflectance from BOL to EOL affects the sizing of some engine components, such as the accumulator tank. Thermal management of the engine is affected if the BOL reflectivity is higher than specified. Performance minimums are affected if the EOL reflectivity is below the specified value. Within some limits, accumulator gas charge could be adjusted relatively late in the program to accommodate a range shift in achievable reflectivity, but it is much preferred to have high-confidence data going into full-scale development.

Flux distribution was a significant factor in the design of the concentrator because of its effect on the receiver's design and performance. The distribution determination and shape modification was an iterative process that was affected by many considerations. The major considerations are listed here with a corresponding reference for further details:

(1) An advanced flux tailoring technique is detailed in reference 6.17. The last flux tailoring report is reference 6.21.

(2) Shadowing and alignment effects are detailed in references 6.22 and 6.37.

(3) Elasto-optics analyses supplied to Rocketdyne are detailed in references 6.38 to 6.40. The Rocketdyne report on elasto-optics is reference 6.23.

(4) Off-axis images analysis and results are detailed in reference 6.41.

(5) The concentrator tradeoff studies are summarized in reference 6.16.

(6) Performance sensitivities are detailed in reference 6.22.

6.4.2 Structural

Structural analysis on the solar concentrator was performed by the Harris Corporation; they calculated dynamic modal shapes, natural frequencies, and structural element stress. The dynamic mode shapes and corresponding frequencies of the concentrator as stowed for NSTS launch are described in reference 6.42. The lowest stowed natural frequency, which was set at 10.0 Hz, was considered a design driver. Deployed on-orbit dynamic mode shapes and natural frequencies considered in the design were evaluated, with the results contained in reference 6.41. The lowest on-orbit deployed natural frequency, which was set at 1.0 Hz for *Freedom* control considerations, was also considered a design driver.

6.4.3 Thermal

Thermal analysis for a reflective facet was performed to assess contour distortions and resulting optical effects. The results of the analysis indicated no problem. The facet thermal analysis and results are described in references 6.43 and 6.44.

6.5 Component Development, Tests, and Test Results

6.5.1 Solar Concentrator Advanced Development Project

The objective of the Solar Concentrator Advanced Development Project was to develop the technology of solar collectors that would be used in a power generation system for Space Station *Freedom*. The development effort for this project was performed by the Harris Corporation, Government Aerospace Systems Division, under NASA Lewis Research Center contract NAS3–24670. The effort was completed in May 1989.

The work performed in this project is well documented in references 6.8 and 6.45.

6.5.2 Facet Development

There were several concurrent efforts to develop and economically produce optically suitable facets for the solar concentrator. These efforts were directed through the prime program and the supporting development program. The facet development work reported in references 6.46 and 6.47 addresses mainly the work performed through the prime program by Harris Corporation and Harris' subcontractors. The purpose of the facet development work was to begin development of a flight facet and to provide support for the solar thermal advanced reflector (STAR) facet program. Most of the work concentrated on the graphite-fiber-reinforced plastic (GFRP) facet with an aluminum reflective coating. Both the conventional and replication processes were investigated.

The prime program incorporated a material and process improvement (M&PI) task directed toward production of flight hardware. The following technical problems were identified and/or worked during the round 1 M&PI effort: (1) facet surface defects and (2) facet slope error and radius-of-curvature changes caused by moisture absorption. The round 1 M&PI results are described in detail in reference 6.46. The round 2 M&PI results are contained in reference 6.47.

The results of STAR tasks.1 and 2 are given in references 6.48 and 6.49. Tasks 3 and 4 resulted only in long-lead-time procurement of the aluminum facet mold and facet materials

(aluminum sheet, honeycomb, and adhesive). No reportable facet development or analysis occurred. Monthly program management review (PMR) briefings from Harris provided insight into the task status until work stopped in September 1990. The facet mold and materials from tasks 3 and 4 of the STAR program were sent to Solar Kinetics Incorporated (SKI) in support of a planned all-aluminum facet development task. Thermoelastic analysis of the proposed facet is discussed in reference 6.44. Although the *Freedom* solar dynamic program was terminated, SKI is continuing development of the all-aluminum facet for other NASA Lewis contracts.

6.5.3 Concentrator Optical Testing

6.5.3.1 Optical measuring systems. — Optical testing of the solar concentrator advanced development (SCAD) concentrator was performed at NASA Lewis by Harris Corporation and NASA personnel. The Harris testing used a laser system to verify optical repeatability following disassembly and reassembly of concentrator panels. NASA continued concentrator optical testing, using the laser system, a digital image radiometer (DIR) system, and a projected image system to further evaluate repeatability, to test sensitivity to counterbalance errors, and to determine the accuracies of the three optical systems.

Laser system: For laser testing the concentrator was installed with the parabolic axis vertical. A target was mounted at the focal point, where the receiver aperture would be located during system operation. A laser was mounted above the concentrator on an apparatus that operates like an x–y axis overhead crane. The laser was on a motor-driven cart that moved along a beam (gantry) which was motor driven to move along parallel tracks. The laser beam was directed vertically to the concentrator and reflected by the concentrator to the target. Concentrator surface errors were calculated on the basis of the deviations of the reflected beam from the target center. The laser optical testing system hardware, installation procedure, and Harris test results are discussed in detail in reference 6.8.

DIR system: The DIR optical alignment system was developed by McDonnell Douglas Space Systems Company for concentrator alignment in their terrestrial solar dynamic program. This system was called a digital image radiometer because digital images of the concentrator were processed to measure the concentrator optical alignment and to predict performance with solar radiation. The DIR system uses a panel of small lights, a video camera, an image processor, and a computer system. Each light illuminates the entire concentrator, but only small areas of the concentrator reflect this light back to the camera. The computer system determines the orientation of these small areas that reflect each light back to the camera on the basis of the location of each light, the locations of the small areas, and the location of the camera. The lights are sequentially turned on, and by combining the orientations of each small area, the contour of the entire concentrator is determined. The DIR optical system and preliminary test results are described in reference 6.50.

Projected image system: Because the DIR system indirectly measures concentrator properties, a simple, direct checking system was needed to verify the results. A projected image system was developed at NASA for this purpose. In this system a high-intensity light source at the concentrator focal point shines on the entire concentrator and is reflected by each concentrator facet to form facet images on the ceiling of the test cell. If the facet contours exactly match the ideal parabola, the reflected rays will all be parallel and the projections will be exactly linear. Deviations of the ceiling images from the linear projections represent deviations of the facet contour from the ideal parabola. These images are photographed and analyzed to determine concentrator optical characteristics. The projected image system is described in reference 6.51.

6.5.3.2 Laser testing. — Testing with the laser system was accomplished by Harris Corporation and NASA. The Harris testing verified structural repeatability and provided an indication of facet optical characteristics. Subsequent NASA testing (ref. 6.52) further evaluated facet specularity, contour, and slope error and measured sensitivity to the counterbalance system that was used to simulate zero gravity. An additional laser reading of the alignment of all facets was taken after a counterbalance weight fell and damaged one of the concentrator panels.

Structural repeatability: These tests were conducted to ensure that the concentrator could be aligned before launch, disassembled by unlatching the panels from each other, and reassembled in space and still retain proper optical alignment for operation in space. The concentrator was assembled by latching the 19 panels to each other. Each panel was supported at its center by a counterweight to approximate zero gravity. Each facet was aligned by adjusting the facet standoffs until a small optical-quality mirror at the facet center reflected the laser to the center of the target. The optical-quality mirrors enabled greater accuracy in measuring alignment repeatability. The 19 panels were unlatched from each other and then the concentrator panels were reassembled and again counterbalanced. Laser readings of the 48 facets taken after reassembly had an average slope error of 0.321 mrad. After throwing out five anomalous readings, the corrected average slope error was determined to be 0.159 mrad (chapter 5 of ref. 6.8). Theodolite measurements of three locations on each panel were also taken for this test and showed an average panel slope change of 0.115 mrad.

Facet specularity: Specularity of a mirror refers to the sharpness of the reflection. The small optical-quality mirrors were able to reflect the laser to a spot about $\frac{1}{4}$ in. in diameter at the focal plane target. The facet surfaces were less specular and produced irregular focal plane images that were typically 2 in. in diameter. Improved specularity has been achieved in facets produced after the laser testing was completed.

Facet contour and slope error: Laser readings were taken

at selected points on each facet. The number of points varied from 13 to 86 per facet, and the points generally were spaced on a regular grid pattern. Data from this test were recorded in reference 6.52. Random irregularities in the laser readings indicated about 2 mrad of surface slope error. The facets were designed to have a curvature best suited for the facets farthest from the concentrator axis. The laser readings showed the best focusing for facets near the center of the concentrator, indicating that the actual curvature of the facets was greater (i.e., smaller radius of curvature) than their design curvature.

Counterbalance test: Laser readings were taken (ref. 6.53) to determine sensitivity to the counterbalance weight simulation of zero gravity. Each panel is supported at its center by using a weight-and-pulley system to balance the panel weight. The concentrator's tolerance to incorrect offloading was tested by attaching a 9-lb weight to the hexagonal panel centers. The weight was successively attached to each of the seven panels nearest the floor while laser measurements were made at the aperture plane. Similar readings were made for a total of five facets. Accurate and consistent readings were possible with this test because the laser was not moved between the eight readings on each facet. The movement of the reflected beam at the aperture plane was generally small. The largest motion recorded was 0.75 in., which corresponds to a facet tilt of 0.7 mrad. This indicates that the concentrator is not sensitive to small errors in offloading.

Although the largest linear motion of the concentrator appeared to occur between the support points, the largest angular change as determined by laser measurements at the aperture plane was for facets close to the support points, where ball-and-socket connections allowed rotational freedom. This indicates that a preferred location for instrumentation that depends on angular alignment, such as Sun sensors, is between the support points.

Counterbalance accident: An accident occurred during concentrator disassembly. A 26-lb counterbalance weight was pulled over its pulley and fell 30 ft in a pendulum arc before colliding with two box beams of a hexagonal panel. There was visible tearing and splitting of the graphite epoxy over a 1-ft length of one of these beams.

The concentrator was reassembled and additional laser test data were taken. The laser test data showed no significant change from previous laser data, except for a systematic ¼-in. shift. After these data were taken, it was discovered that the laser was miscalibrated in the same direction and magnitude as the systematic shift. The concentrator was disassembled and stowed without further incident.

6.5.3.3 DIR testing. — Testing with the DIR system was accomplished by NASA following installation and checkout by McDonnell Douglas Corporation. For DIR testing the concentrator was positioned horizontally with the vertex to the east and the focal point above the concentrator.

Agreement with laser facet pointing: Good agreement was achieved with the results of previous laser testing. The laser results for the contour of each facet were averaged to determine the average orientation of the facet surface in the x and y axes. These were compared with the DIR test results. The differences had an average magnitude of 0.85 mrad in the x axis and 1.27 mrad in the y axis. These differences would cause a beam displacement of 1 to 2 in. This is a small change within the 17-in. receiver aperture. A portion of these differences may be caused by inaccuracy of the DIR system due to camera drift, camera resolution, and calibration error.

Camera drift and resolution: This DIR system was significantly more sensitive to camera drift and resolution than an earlier DIR system developed at McDonnell Douglas because of the optical characteristics of the offset parabolic concentrator and because the 60-ft ceiling height of the NASA Lewis Power Systems Facility (PSF) was not sufficient to optimally locate the DIR light panel. Determining the location of light reflections on the concentrator was limited by the pixel size, which was about 3/4 in.

In order to determine the sensitivity of the DIR data to camera resolution, data were taken with the field-of-view edge markers intentionally misread. Ten pixels of intentionally introduced calibration error in the southerly direction increased the x–z facet cant readings by 1 to 4 mrad. Calibration error in the easterly direction had a smaller and variable effect on the facet cant readings. Thus, a one-pixel error in the DIR system could cause as much as 0.4 mrad of output error.

The camera on several occasions changed in calibration by a few pixels. In general this was corrected by the field-of-view edge markers. However, severe errors in some facet orientation readings occurred because the camera did not know where the facets were and accepted, as data, stray light reflections from the floor below the concentrator. In order to correct for this drift, it was necessary to manually locate the corners of every facet in the camera field of view.

DIR counterbalance test: Counterbalance sensitivity testing, which had been performed with the laser system, was also attempted with the DIR system (ref. 6.54). Although meaningful results had been attained using 9-lb weights with the laser system, it was necessary to remove the entire counterbalance weight (about 49 lb) to achieve consistent readings with the DIR system. Two tests were conducted, one by removing the counterbalance weight from panel 9, the other by removing the weight from panel 10. Facet pointing errors due to removing the counterbalance weights ranged from zero for facets remote from panels 9 and 10 to 8 mrad near the point that had been supported by the counterbalance. There was significant variation of facet readings within some panels, indicating that the hexagonal panels were twisting.

Facet removal test: Twenty-four facets were installed to fully populate panel 1. The facets were aligned by using the DIR system. An initial DIR reading of the aligned facets was then recorded. The facets were each removed from the hexagonal panel and then reinstalled. A second DIR reading was taken after the facets had been reinstalled. The average magnitude of the difference between these two readings was 0.19 mrad in the x–z plane and 0.13 mrad in the y–z plane. A third DIR reading was taken without disturbing the facets. The differences between the second and third readings were 0.41 mrad in the x–z plane and 0.13 mrad in the y–z plane. Note that the readings changed more when nothing was done than when the facets were removed and reinstalled. It was concluded that the orientation change due to removing facets from the panel and reinstalling them in the same position was too small to be determined by using the DIR system (ref. 6.55).

Comparison with projected image system: DIR readings were used to generate a map of expected images of facets projected onto the ceiling. This map was compared with a photograph taken of the ceiling with the light source installed. A systematic error in the photographed images relative to the predicted images was traced to the light source being incorrectly installed 8 in. from the actual parabolic focal point. After correcting for this error, good agreement was achieved.

Evaluation of STAR facets: Improved concentrator facets with a significantly more specular surface were produced by the solar thermal advanced reflector (STAR) facet development effort. These facets were tested in several arrangements by using the DIR system. Surface contour radii of curvature were measured in six directions relative to the facet surface (parallel and perpendicular to each of the three sides). The facets were then tested on Sun at Sandia National Laboratories (ref. 6.56). In the Sandia tests the facets were mounted at specified angles relative to the sunlight, and the reflected flux distribution was measured at a target. Additional DIR readings and projected image testing of facet contours were taken following the Sandia tests (ref. 6.57). Changes noted in the facet contours were attributed to changes in the moisture content of the facets' epoxy substrate. There was reasonable agreement between the on-Sun measurements of reflected energy and the optical test measurements of facet contours.

6.5.3.4 Projected image testing. — As mentioned, the projected image system was developed as a means of checking the DIR system. After an initial light source position error was corrected, good agreement was achieved between the DIR and the projected image system. In addition to checking the DIR the projected image system also provides information about the contour and alignment of facets.

Facet rotation testing: Irregularities were noted in the ceiling images of facets. These irregularities appeared to represent facet surface contour characteristics rather than characteristics of the position on the concentrator where they were installed. In order to verify this, six facets were installed in the centers of the six pie sectors of one hexagonal concentrator panel. Ceiling images were photographed for an initial position and two rotations of the facets. Each facet was left in the same location on the concentrator panel, but it was rotated so that its corners were in different positions. There were major changes in the photographed images, indicating nonsymmetric variations of facet contours. This testing was reported in reference 6.51.

Panel 14 alignment: STAR facets were evaluated after the Sandia testing and were determined to have a complex curvature (ref. 6.57). The contour of most of these facets had the longest radius of curvature in the direction perpendicular to one of the sides. On the basis of radii of curvature estimated from the ceiling images, panel 14 was selected as the best location for the STAR facets. Three positions and appropriate orientations were selected for each of the eight facets to occupy all 24 positions on panel 14.

The Sandia test results had shown that when tested on Sun, the images of the facet corners were almost always farthest from the center of the test target. This suggested that in aligning facets, it was sufficient to align the corners to reflect into the aperture to ensure that the reflected light from the entire facet would be collected. Computer-generated ceiling image targets showed the ideal facet image, and ellipses indicated the tolerance of each facet corner. Photographs were taken of the facets as aligned by using these targets and as aligned by using the DIR system. Differences between the DIR and ceiling image alignment (up to 2 mrad) were due to the DIR aligning the average surface orientation and the projected image system aligning the corners. An additional 2 mrad of difference between the DIR and ceiling images was traced to an error in the initial alignment of the DIR system. Recalibration of the DIR system, which was needed because the DIR camera had been repaired, corrected the alignment and eliminated this systematic error.

6.5.3.5 Comparison of measurement system accuracies. — The most exact and repeatable measurements were the laser measurements of structural repeatability and counterbalance sensitivity. These two tests appeared to be accurate within about 0.1 mrad. Contributing to this accuracy was the small optical-quality mirror mounted on the center of each facet. All other optical tests relied on the quality of the facet surface, and the surfaces of most facets tested had specularity and surface slope errors greater than 1 mrad.

In addition to the limits due to facet surface accuracy, the accuracy of all three systems was limited by system characteristics. The laser system was limited to about 0.1 mrad by the diameter of the laser beam, the DIR was limited to about 0.5 mrad by the camera pixel size, and the projected image

system was limited to about 0.5 mrad by the size of the light source filament.

Results of the laser and DIR tests are compared in reference 6.50. Projected image system test results are compared with predictions based on DIR data in reference 6.51.

6.5.4 Structural and Thermal Supporting Development

As part of the Space Station *Freedom* supporting development work at NASA Lewis, a concentrator structural testing program was developed as an in-house effort with the Engineering Directorate (ED task 87007) to investigate and characterize the stiffness and dynamics of the solar concentrator. The objective was to develop and verify structural models (finite element), by subcomponents, of the solar concentrator on-orbit configuration. The subcomponents studied included latch mechanisms (first and second generation), a single hexagonal panel (with and without facets), and coupled hexagonal panels (up to 19). The approach taken was to conduct various structural tests with solar concentrator advanced development (SCAD) and concentrator panel assembly test (COPAT) hardware: single-panel modal tests with SCAD hardware (with and without facets), latch stiffness tests on SCAD (first generation) latches and COPAT (second generation) latches, and a three-panel modal test with SCAD hardware and redesigned COPAT latches. The COPAT tests were conducted in the Neutral Buoyancy Simulator Facility at NASA Marshall Space Flight Center.

The justifications for conducting this task were that no similar effort was specified by the prime contractor in phase 1 and that NASA needed to understand the concentrator baseline design in order to manage and verify the prime contractor's design efforts.

6.5.4.1 Background. – The Engineering Directorate task 87007, titled "Solar Concentrator Structural Dynamic Model Verification Testing" was begun in 1987. The primary objective of this task was to provide an indication of the structural and structural dynamic characteristics of the then-baselined solar dynamic power generation system. This was to be accomplished by using hardware developed by Harris Corporation for the SCAD operational and optical repeatability testing. Such an opportunity would allow early identification of any specialized testing technology that would be necessary to conduct the follow-on flight hardware testing.

The structural and structural dynamic characterization task was divided into two primary areas: the hexagonal panel modal characterization and the latch stiffness efforts. Each effort provided insight into quantifying a portion of the overall structure.

The hexagonal panel test and analysis effort involved identifying the subsystem dynamic response by using standard modal test and analysis techniques. The latch test and analysis effort involved identifying the behavior of the mechanism both by static loading and deflection tests and finite element analysis. The end goal of both characterization areas was to provide a test-verified analytical model for the on-orbit configuration of the entire advanced development concentrator structure.

As a result of this task a number of documents were published internally. The most significant of these documents are listed as references 6.58 to 6.63.

6.5.4.2 Hexagonal panel modal effort. – A structural dynamic testing and analysis verification task was outlined for the SCAD hexagonal panel. The purpose of this task was to verify early in the Space Station *Freedom* design effort the analytical models that would be required to adequately transfer the design to flight hardware.

Description of efforts: The methodology applied toward completion of this task was to conduct "modular" tests, gradually building up the tested system complexity. This approach would provide a thorough understanding of where substantial verification difficulties existed. It therefore could aid in the successful planning and implementation of the flight hardware verification testing program that would be required prior to launch and on-orbit operation.

The task was planned to proceed from modal testing of a single empty hexagonal panel through eventual testing of the fully assembled concentrator comprising 19 hexagonal panels interlocked by latches.

Prior to cancellation of this task two specific hardware configurations of a single hexagonal panel were tested. The first configuration was the most basic: A single hexagonal panel (panel 17) with its facets removed was suspended from isolation springs to simulate a free-free configuration while not introducing any effects of facet or latch interfaces. See figure 6.15 for the SCAD panel modal test setup.

This first configuration also provided the opportunity to attempt a hexagonal panel latch interface modal data acquisition. The hexagonal panel latch configuration involved suspension of a 4- by 4-in. square, $\frac{1}{4}$-in.-thick-wall aluminum tube from the two type I latches installed on panel 17 by means of two contact balls. Sine sweep data at three controlled excitation levels for this acquisition were never fully analyzed and thus have not been reported. Data reside on the acquisition system only.

The second hardware configuration to be thoroughly tested was the hexagonal panel–facet variation. Panel 17 was configured with four Silverlux type I facets (all group IV). These facets were all installed in the same quadrant of the hexagonal panel in an effort to provide information on the relative facet-to-facet interaction and facet-to-hexagonal panel coupling and decoupling present. Once again, the system was suspended in a free-free configuration.

Summary of testing and results: The modal test results obtained were characterized in two ways: The first was a tabular expression of modal parameters of frequency and damping. The second was in descriptive terms dealing with the deformed mode shapes corresponding to each frequency. Testing on the empty hexagonal panel configuration has been thoroughly reported in reference 6.61. Testing was

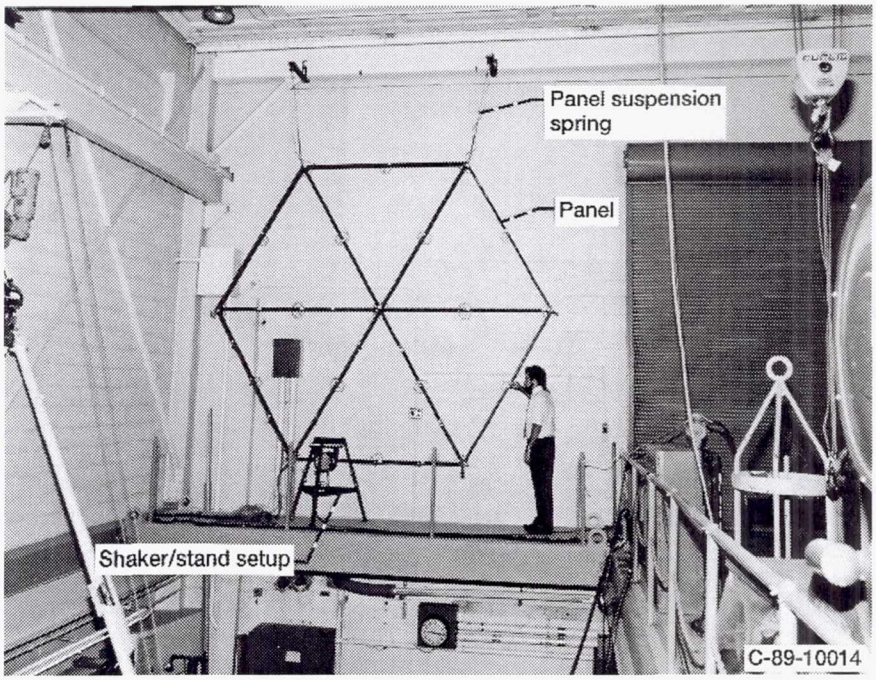

Figure 6.15.—SCAD panel modal test setup.

completed in November 1989. In support of this test configuration a finite element analysis (NASTRAN analysis) was conducted and correlated with the test configuration. It was reported in reference 6.62. The finite element model for the empty hexagonal panel configuration is on the VAX/VMS archive tape (ref. 6.64) under a saved set entitled SCADMODALTEST.BCK.

At the time of SD program cancellation the hexagonal panel–facet test configuration was undergoing testing. Data were being acquired according to the test plan. A fourth, originally unplanned, excitation direction and location was the last set of broadband random modal data to be acquired. Preliminary curve-fit analyses were done on the first three excitation location data sets. This analysis justified the need to acquire data at the fourth location. The raw modal-plus (binary format) data files for this test configuration and the preliminary test mode computer files are on a VAX/VMS archive tape (ref. 6.64) under one saved set called HEXFACETDATA.BCK. These files include the test geometry model file information generated by the Structural Dynamics Research Corporation Test Data Analysis program as well as the parameters and mode shape information obtained at termination. They are provided as raw IDEAS–IV (binary format) files as well as universal (ascii format) files (ref. 6.64).

The hexagonal panel–facet finite element analysis configuration was presented in a preliminary form within reference 6.62. The test plan for the modal test of the solar concentrator panel hardware with facets can be found in reference 6.65. The analysis files for the empty hexagonal panel and for the hexagonal panel with varying degrees of modifications implemented are provided on the same VAX/VMS archive tape (ref. 6.64) under the saved set entitled HEXFEMMODELS.BCK. They consist of the NASTRAN bulk data input decks for each run configuration. Comment statements are provided throughout these input decks to aid in their interpretation.

6.5.4.3 Latch stiffness effort. — A stiffness testing and analysis task was outlined for the SCAD latch mechanisms. The purposes of this task were to investigate and characterize the stiffness and to develop and verify structural models (finite element) of the solar concentrator latch mechanisms.

Description of efforts: An analysis was performed to investigate, both experimentally and analytically, the deflection and stiffness for the solar dynamic concentrator latch mechanisms. The latch mechanisms, which are a self-locking ball-and-socket type, are located at the panel corners and connect the panels together to form the complete reflector. Figure 6.16 shows the type I latch assembly. These latches consist of four types (types I, II, III, and IV). Each type varies in size and angle, forming the shape (curvature) of the concentrator. The concentrator and latches are described in more detail in section 6.1.3.

The engineering development consisted of the design and fabrication of a latch test rig, procurement of load application and displacement measurement transducers, and the development of data acquisition and reduction software for an existing data acquisition unit. Testing involved cyclic application of both tensile and compressive uniaxial forces while measuring resulting displacements with linear variable differential transformer (LVDT) displacement transducers. These

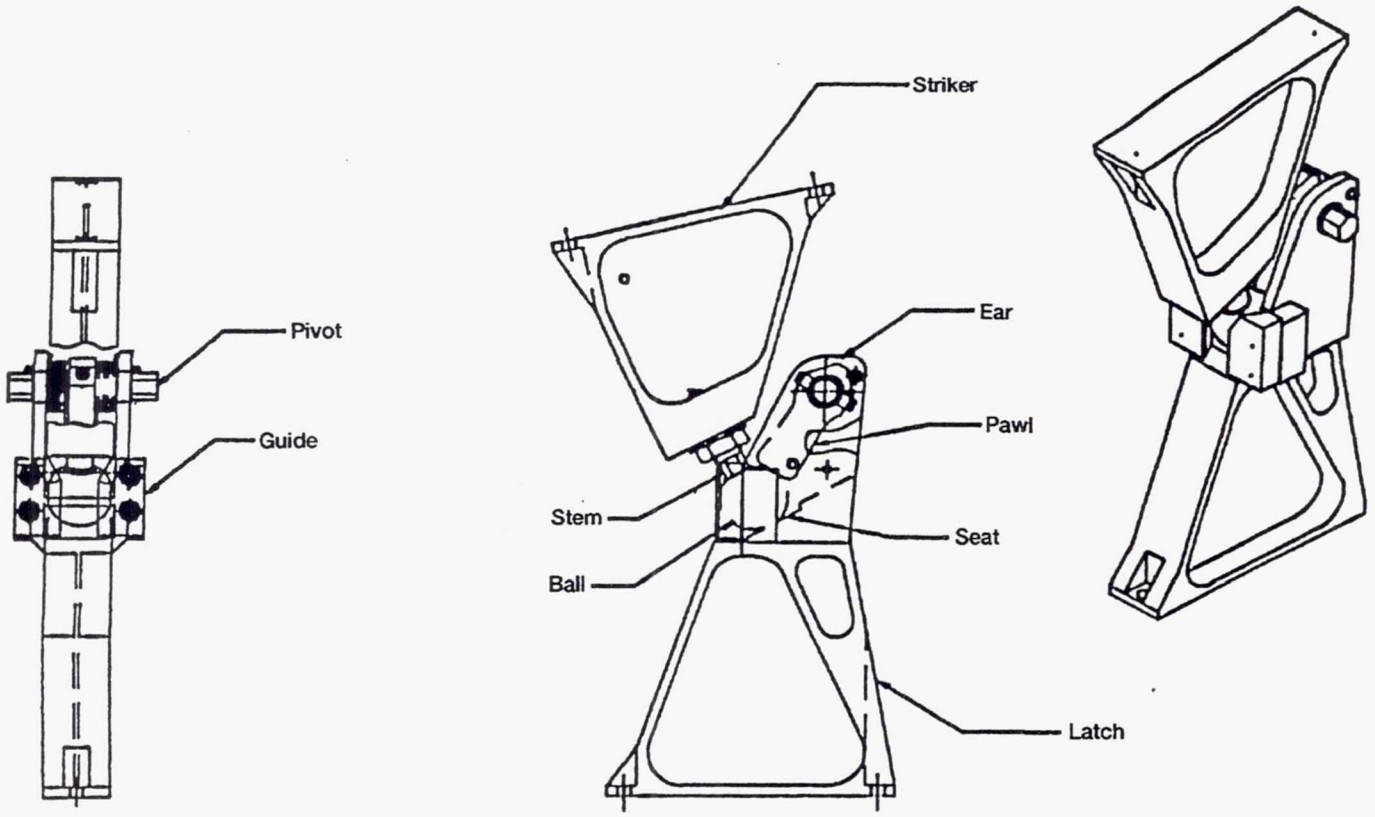

Figure 6.16.—Type I latch assembly kinematics.

measurements were then resolved into resultant translations and rotations of the latch under test. The data then would be evaluated to assess the linearity of the latch mechanism.

The test rig was constructed of welded steel I-beams and plates. Additional hardware was developed to account for the latch-to-latch variation needed in mounting each latch type to the test rig. Additionally, instrumentation towers to support the LVDT transducers were fabricated. The load application originally was planned to be a single pull and push. This plan was modified to include multiple cyclic load applications. Throughout the testing, however, the load application was adjusted manually. Figure 6.17 shows the latch stiffness test rig setup.

Summary of testing and results: Data were gathered for latch types I and II (first generation), and on the basis of these results latch types III and IV were not tested. Load application magnitudes were varied in an effort to determine, over a reasonable estimate of on-orbit loading, if nonlinear effects could be detected. The latch stiffness data were found to exhibit bilinear characteristics and to be linear for the on-orbit load range. Results, including recommended hardware modifications, for the latch testing effort and for testing and analysis correlation for latch type I, have been reported in reference 6.59. A memorandum was also generated that discusses the results of the type II latch tests (ref. 6.60).

Analysis summary: In support of the test results, latch solid and finite element models were generated for each of the four latch types (first generation). (Different degrees of modeling fidelity exist for each latch type model.) These models were to create a verified prediction tool for use in the analytical modeling of an assembled concentrator system. A second analytical model, of latch type II, was created, but the results were not officially reported.

Planned work: The testing and associated analysis efforts have provided the opportunity to assess the first-generation latch design. Numerous design changes were suggested and implemented into the redesigned latches (second generation). Some of the modifications made included adding a hard spherical steel seat and increasing the spring rate of the pawl spring. The redesigned latches (types I and II) were fabricated by Harris Corporation in January 1990 and evaluated in the neutral-buoyancy COPAT conducted in August 1990. (Section 6.5.5 gives the results of this test.) At the time of SD program cancellation a latch retest program was being planned. This program would have automated the load application during testing of the newly designed latches. Goals similar to those in the previous test program were stated for this test program as well.

An additional effort had also been originally planned that would have involved conducting stiffness verification tests on the hexagonal panel elements themselves. Similar to the modular approach of the modal tests, these stiffness verifications would start with a single panel and proceed upward in complexity to the full concentrator assembly. No in-depth

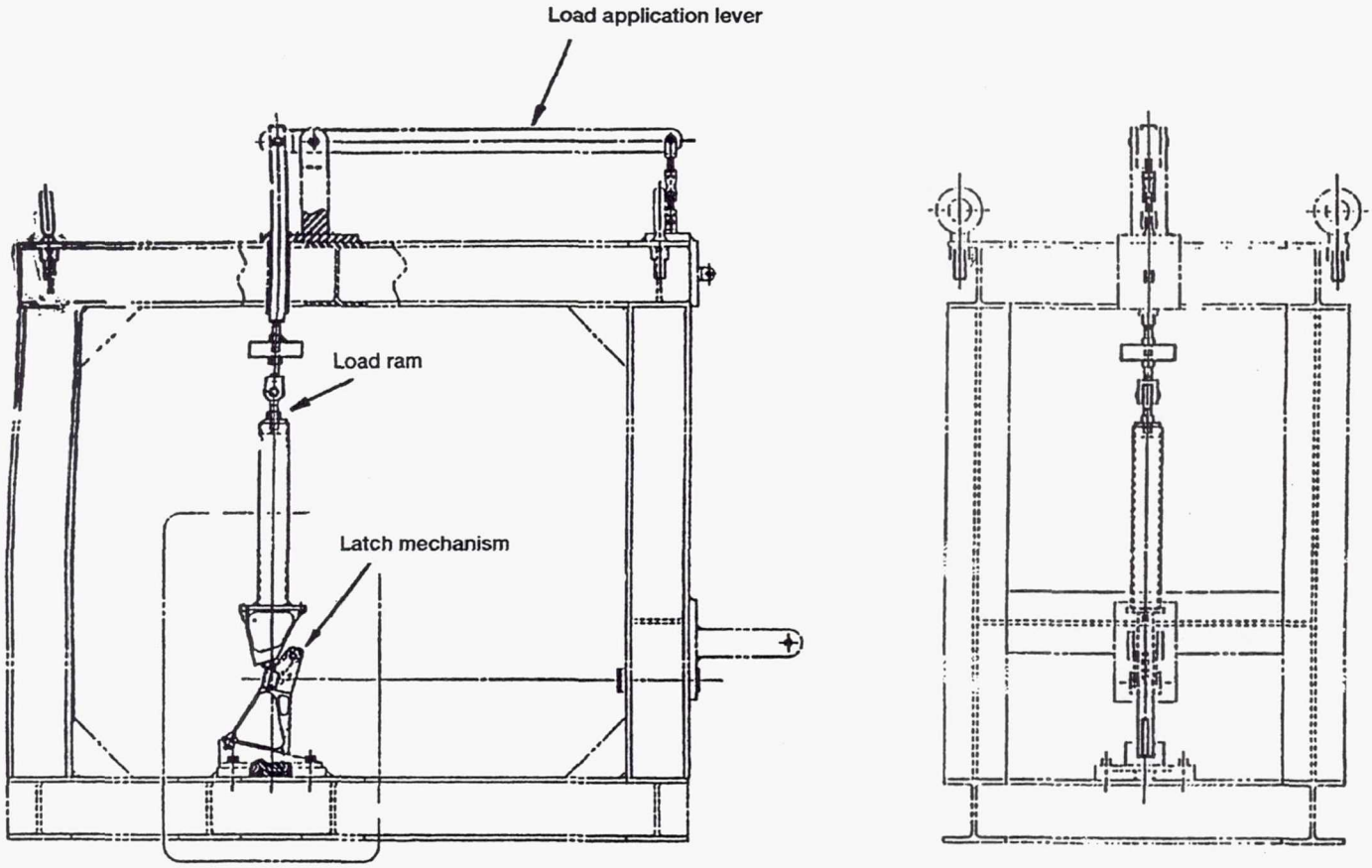

Figure 6.17.—Latch stiffness test rig setup.

work was accomplished in support of this task at the time of SD program cancellation.

Documentation: Detailed drawings of the design for the latch stiffness load application devices exist for both the first- and second-generation designs. The drawings for the as-built original test rig are in reference 6.66, and the drawings for the preliminary redesigned rig with the hydraulic load system are in reference 6.67. These drawings are also filed in the NASA Lewis Engineering Directorate CADAM release system. Files of the finite element models have been supplied on the digital VAX/VMS archive tape (ref. 6.64) under the saved set SCADLATCHFEMS.BCK. A catalog of all existing models created in support of the SCAD program, as of August 14, 1989, is reference 6.68.

6.5.4.4 Solar concentrator structural dynamic model—wind loading analysis.—An analysis was performed to calculate the deflection and stresses in the solar concentrator's single hexagonal panel components under the NASA specified wind pressures and boundary conditions. A finite element model of the hexagonal frame was used in the analysis. Development of the finite element model is documented in reference 6.69. The primary concerns in the test were (1) the deflection of the facets and (2) the stresses in the flexure assemblies that were used to attach the facets to the hexagonal panel beams. The results of the wind loading analysis on a single hexagonal solar concentrator panel can be found in reference 6.58.

6.5.4.5 Summary.—An in-house testing and analysis task was conceived and partially executed in support of the *Freedom* solar dynamics technology development program. This effort consisted of a structural evaluation of the advanced development solar concentrator hardware developed by the Harris Corporation for NASA Lewis. Modal testing and normal mode dynamic analyses were conducted on the hexagonal panel elements of the concentrator. Configurations tested included an empty hexagonal panel in the free-free support condition as well as a panel containing four facets within one of its six quadrants, also freely supported. Stiffness testing and static analyses were conducted on the latch elements of the concentrator. Design changes were implemented on the basis of the initial test results. Follow-on test validation of the success of the changes was being planned at the time of SD program cancellation.

Dynamic testing plans at program cancellation included completion of the four-facet hexagonal panel modal test and continuation of the piecewise buildup of hardware test configurations and the understanding of subsystem dynamic responses. The evolution sequence would probably have included a three-panel test using latches, a seven-panel test, and finally a full concentrator (19 panel) test program. This

final test program configuration will be needed to ensure flight analytical model accuracy for any pointing and dynamic control response analyses that may be conducted in the future.

Follow-on static testing planned at program cancellation included validation of design changes made to the latches as well as static model validation of a single hexagonal panel and of the fully assembled concentrator stiffness distribution by means of an influence coefficient type of test on all 19 panels assembled together.

6.5.5 Neutral Buoyancy Assembly

6.5.5.1 Prime contractor. – NASA Lewis' (WP–04) prime contractor, Rocketdyne Division of Rockwell International Corporation, and their subcontractor, Harris Corporation, participated in a neutral buoyancy panel assembly simulation for the solar dynamic concentrator. This simulation (COPAT) was developed and conducted under a supporting development task at NASA Lewis. For more details of this task see section 6.5.5.2.

Rocketdyne's main responsibilities within this task were to furnish the latch and latch guide mechanisms (second generation) that were designed to aid in the assembly alignment process. Harris Corporation was responsible for the latch-to-panel interface alignment requirements and installation. They participated in a normal-gravity (1-g) test at NASA Lewis to check out hardware prior to testing and as space-suited test subjects in the actual conduct of the test series at NASA Marshall's Neutral Buoyancy Simulator (NBS) Facility.

6.5.5.2 Supporting development. – As part of the supporting development work at NASA Lewis, concentrator panel simulation hardware was developed in-house to allow the assembly process for the concentrator structure to be investigated in a neutral buoyancy facility. The primary objectives of the COPAT series were to evaluate and demonstrate the performance of the current concentrator latch and latch guide (second generation) mechanism and to evaluate assembly procedures and astronaut positions for an on-orbit (erectable scenario) assembly of the concentrator. Secondary objectives included assessing handhold locations and positions to gain the required leverage and line of sight for assembly and obtaining a rough order-of-magnitude estimate of test times for specific tasks.

The approach taken was to conduct a three-panel assembly test with support from the prime contractor (latches, procedures, and test participation) in order to evaluate three panel-to-test-subject orientations (perpendicular, parallel, and combination), to evaluate a total of 10 different test subject positions, and to evaluate two out of the four latch types (types I and II, second generation) required for on-orbit assembly.

COPAT was considered to be a critical part of the early design evaluation process that allowed for reduced technical and schedule risks for the latch mechanism and guide effort, the development effort for the baseline solar dynamic concentrator configuration, and anticipated flight operations and procedures. Flight experience has indicated excellent correlation between the effects of neutral buoyancy simulations and the effects of actual weightlessness.

Background: The solar dynamic concentrator is a large erectable structure that was designed to be assembled by astronauts on orbit. It consists of 19 hexagonal panels with self-locking, ball-and-socket latches located at the panel corners. These latches connect the panels together to form the complete reflector. Figures 6.16 and 6.18 illustrate latch kinematics and components. First-generation latches were fabricated and tested as part of the SCAD program. (Sections 6.5.4 and 6.1.3 give more information on the first-generation latches.) Latch guides (fig. 6.19) to aid in alignment were fabricated and installed on the neutral buoyancy panels. The on-orbit assembly of the solar dynamic concentrator is described in section 5.10 of this report and in reference 6.71.

The COPAT task was begun in 1987. The Solar Dynamic Power Systems Branch was responsible for all phases of the project: management, hardware design and fabrication, test operations, and test conduction. The hardware was built in-house by the Fabrication Branch at NASA Lewis. The underwater mockup's concentrator panels were designed to simulate the baseline concentrator panels. The Engineering Directorate (ED task 87008) provided design services, drafting services, and stress analyses (ref. 6.72) to support the

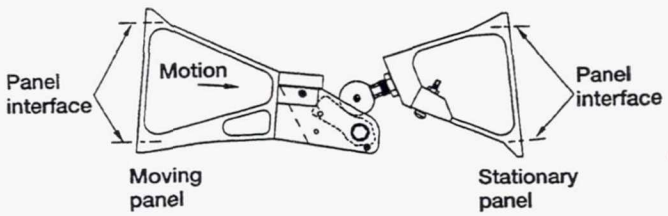

(a) Initial contact.

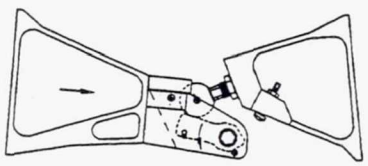

(b) Ball-plate contact.

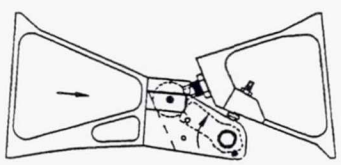

(c) Locked configuration.

Figure 6.18.—Latch components.

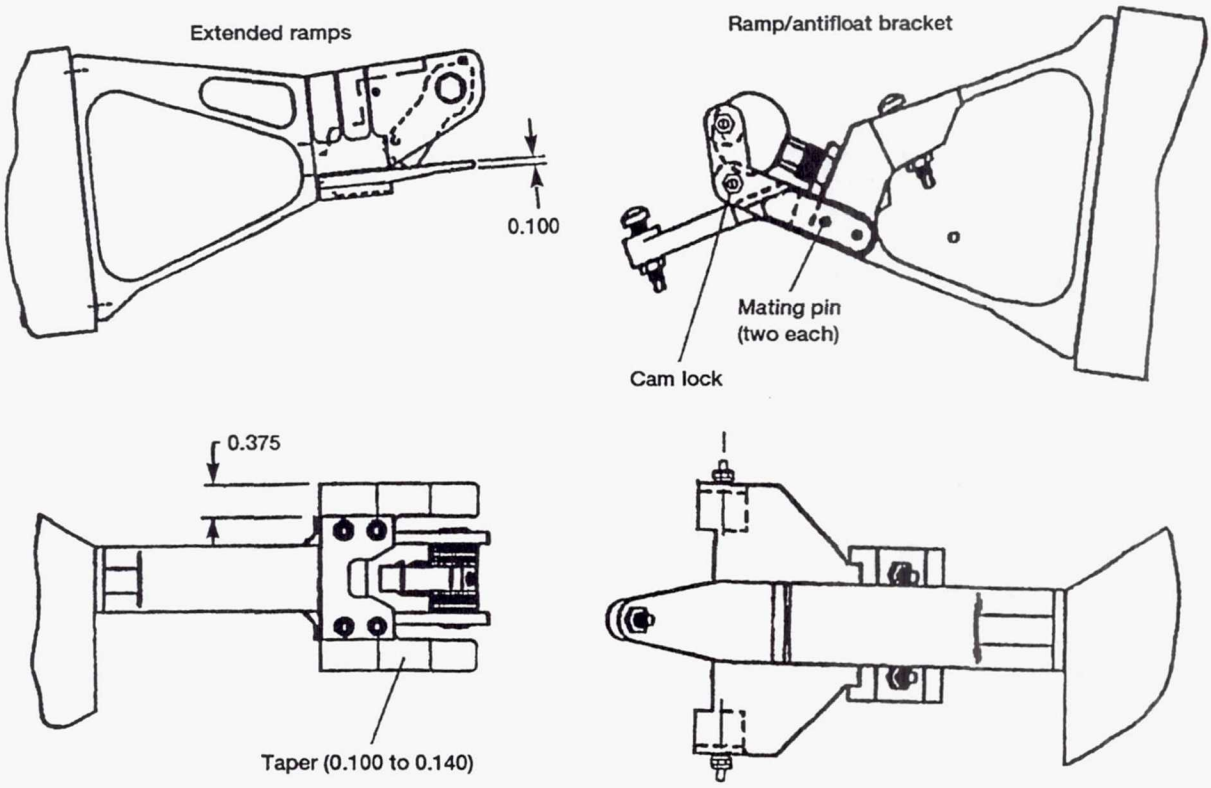

(a) Fine.

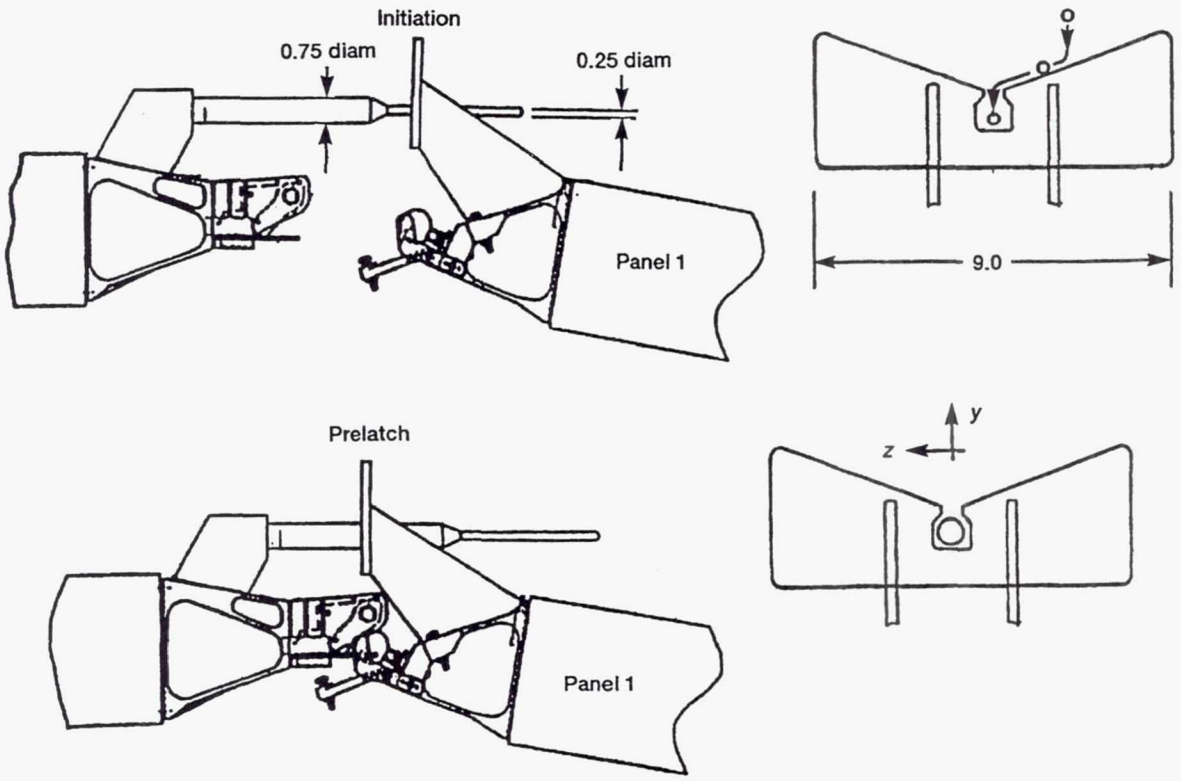

(b) Gross.

Figure 6.19.—Gross and fine latch guides. (Dimensions are in inches.)

fabrication of a concentrator test article, test support equipment (1-g and 0-g tests), and shipping container designs. Latch and latch guide mechanisms were furnished by Rocketdyne and the Harris Corporation. Detailed drawings of the design of the COPAT hardware and the second-generation latch and latch guide mechanisms can be found in references 6.73 and 6.74, respectively.

Assembly test setup and procedures: The COPAT hardware consisted of three solar dynamic concentrator panels and two out of the four latch types required for on-orbit assembly. This hardware was designed and built at NASA Lewis for 0-g evaluation. Latch and latch guide mechanisms that were designed to aid in the assembly alignment process were furnished by Rocketdyne and Harris Corporation as part of the EPS contract. The test hardware and its features are described in detail in references 6.75 and 6.76. Test requirements and procedures are also stated in these references and in reference 6.72.

1-g evaluation: A 1-g checkout of the three COPAT hexagonal panels and assembly techniques was conducted at NASA Lewis' Power Systems Facility during February and March 1990. The 1-g checkout test minimized the effects of gravity as much as possible by counterbalancing the COPAT concentrator panels. The panels were assembled to evaluate the test assembly procedures. The test was conducted by attaching the central panel to a stationary support fixture that held the panel parallel to the floor and then latching the two remaining counterbalanced panels into place.

Neutral buoyancy simulation: The COPAT was conducted from July 11 to September 18, 1990, at the Marshall Space Flight Center's NBS Facility. This underwater test series demonstrated the latch and latch guide mechanism's performance and evaluated assembly procedures and astronaut positions for an on-orbit assembly process by using mockups of three solar dynamic concentrator panels and a NSTS orbiter remote manipulator system (RMS) arm. In addition to the functioning of the latch and latch guide mechanisms, 10 astronaut positions and orientations were evaluated by two space-suited test subjects (fig. 6.20). Three test configurations were evaluated: astronauts and panels perpendicular to each other (configuration 1), astronauts and panels parallel to each other (configuration 2), and a combination of one astronaut perpendicular and one astronaut parallel to the panels (configuration 3). Several astronaut positions in relation to the panel were investigated for each test configuration. The test program was successfully completed and concluded with astronauts in scuba gear assembling the panels.

During each test run the test subject assembled three concentrator hexagonal panels. The central panel (panel 1) was attached to the RMS arm by a grapple fixture through its center. Panel 2 was then latched to panel 1 and rotated 60° to proceed with the assembly procedure. Panel 3 was then latched to panels 1 and 2, thus assembling a ring of three concentrator panels (fig. 6.21). Disassembly was performed by support divers and was not a part of this test.

Throughout the test, time-tagged audio/video and still photographs were recorded. After each simulation, key test personnel participated in a debriefing, during which the test subjects' observations were recorded. Their comments provided a primary source of data in support of engineering assessments of on-orbit assembly.

6.5.5.3 Results. — In the COPAT program the operation of the latch and latch guide mechanisms was evaluated in conjunction with 10 astronaut orientations by two space-suited test subjects. The latch guide system, which consisted of panel-to-panel gross guides and latch-to-latch fine guides, worked well. An orientation where the panels were perpendicular to the test subjects (configuration 1, test 2), was selected as the best test assembly orientation. Figure 6.22 shows the two space-suited test subjects connecting a third panel during a test run of COPAT in NASA Marshall's NBS Facility. This test configuration offered good handling control of the panels and a good view of the latches. This precision latch and guide concept and the assembly orientations and procedures worked out during this test will enable successful on-orbit assembly of large erectable space structures.

The chosen configuration was evaluated for latch/striker performance, the latch guide system (including gross and fine guides), and assembly procedures and astronaut positions (including visibility and maneuverability). Assessments were also made of handrails, RMS capabilities, and assembly timelines. Reference 6.75 gives a more detailed evaluation. A time-tagged video/audio tape (raw footage) of test configuration 1, test 2 (August 24, 1990) can be obtained as reference 6.77 from the NASA Lewis Space Station *Freedom* library.

The latch and latch guide evaluation produced the following results:

Latch and striker performance (latch reliability): The latches and strikers functioned well throughout the testing. A fair estimate is that the latches were engaged and disengaged approximately 50 times during 1-g and COPAT testing. Tolerances for slight misalignment were demonstrated. Tolerances for nonsimultaneous latchup were also demonstrated. No problems were encountered in generating the forces necessary to latch.

Latch guide system: Both gross guides and fine guides were evaluated. The panel-to-panel gross guides worked well, and alignment during some of the test configurations would have been difficult without them. The guides functioned as intended without failure and aided in determining and attaining the correct angle between panels 1 and 2. The gross guides limited panel motion during latch engagement. They also ensured nearly simultaneous engagement of latches and did not present any safety hazards at any point during testing.

The latch type I fine guides performed well throughout the

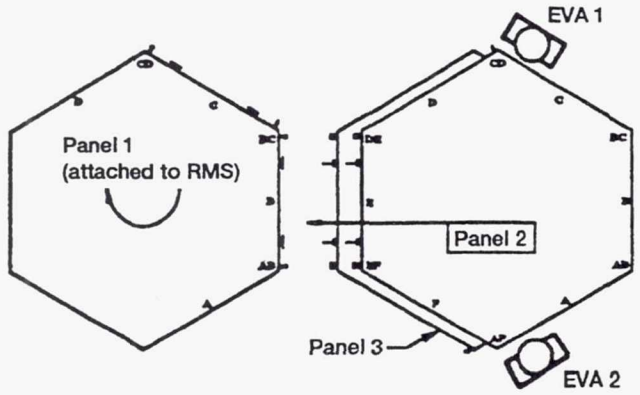

(a) Test 1, configuration 1.

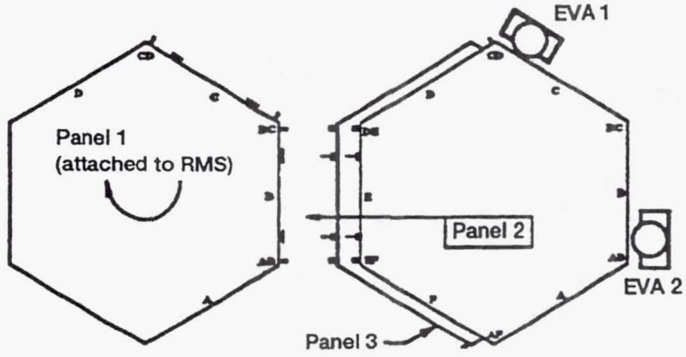

(c) Test 3, configuration 1.

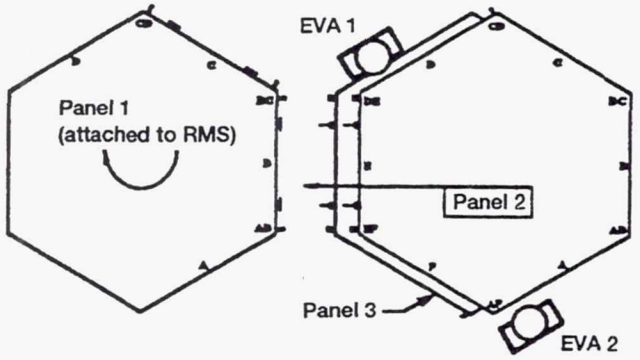

(b) Test 2, configuration 1.

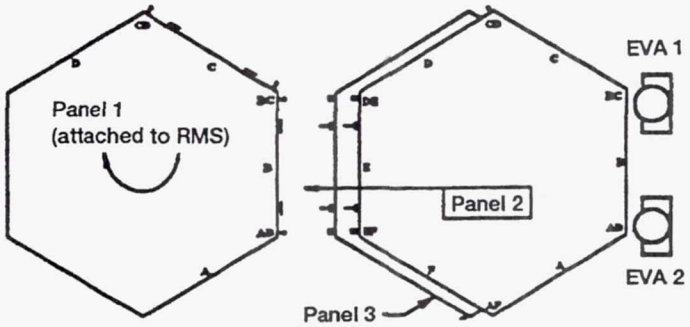

(d) Test 4, configuration 1.

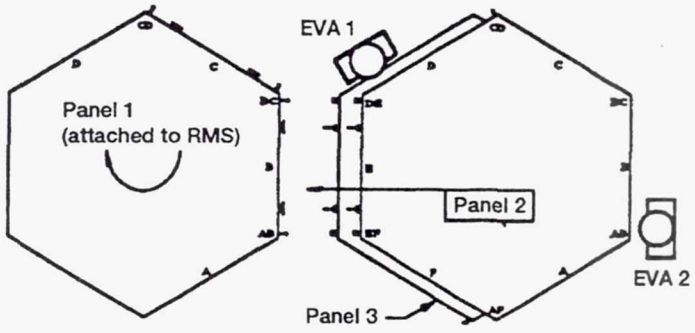

(e) Test 5, configuration 1.

Figure 6.20.—Test configuration summary.

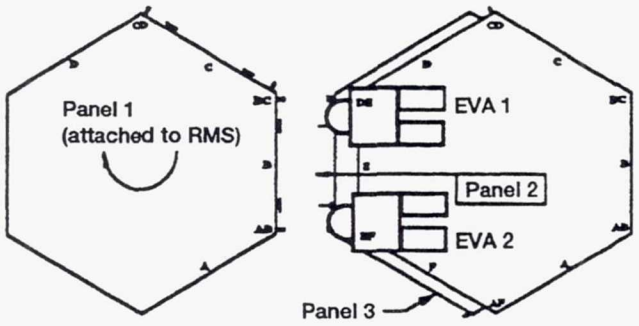

(f) Test 6, configuration 2.

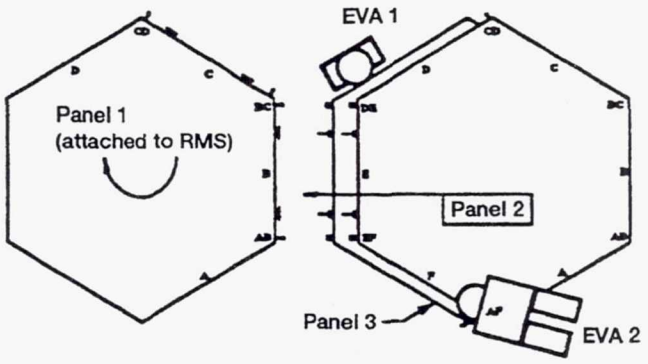

(h) Test 8, configuration 3.

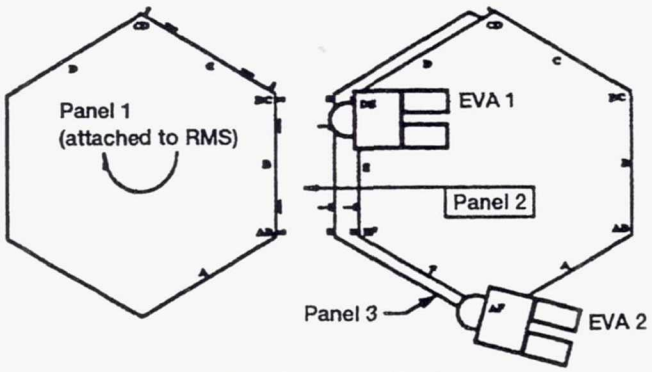

(g) Test 7, configuration 2.

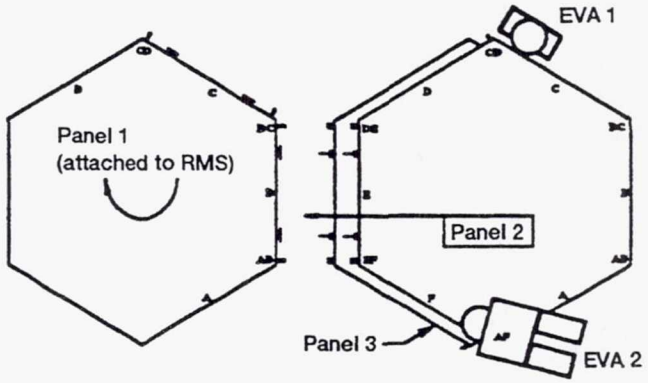

(i) Test 9, configuration 3.

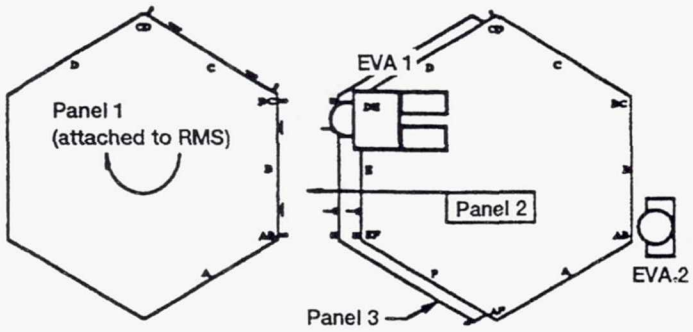

(j) Test 10, configuration 3.

Figure 6.20.—Conclusion.

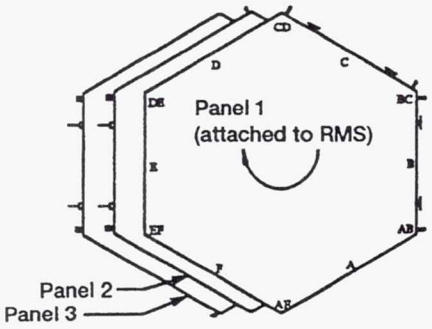

(a) Attach panel 1 to RMS.

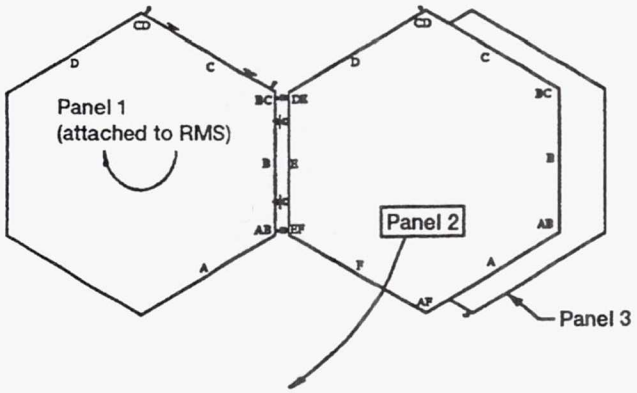

(c) Rotate.

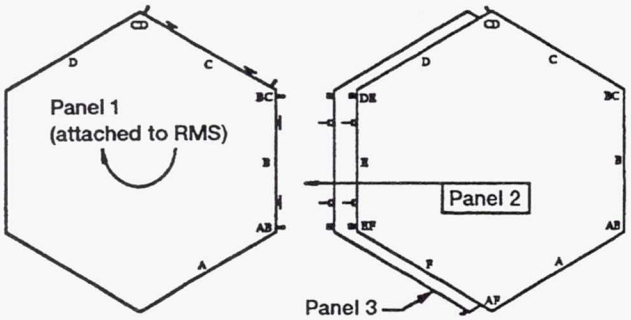

(b) Latch panel 2.

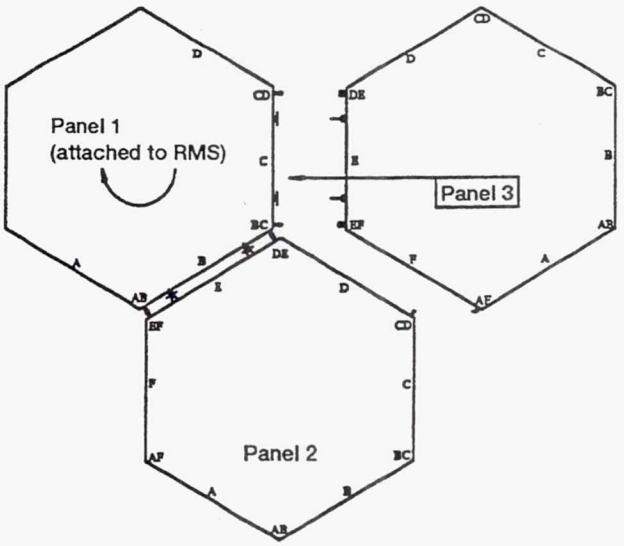

(d) Latch panel 3.

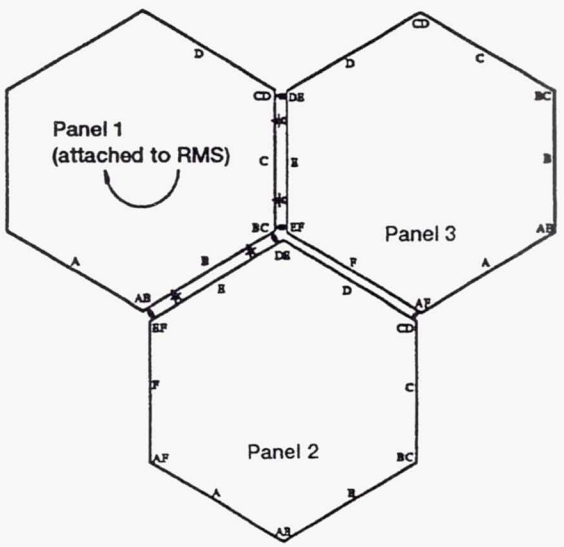

(e) Assembled.

Figure 6.21.—Panel test assembly sequence.

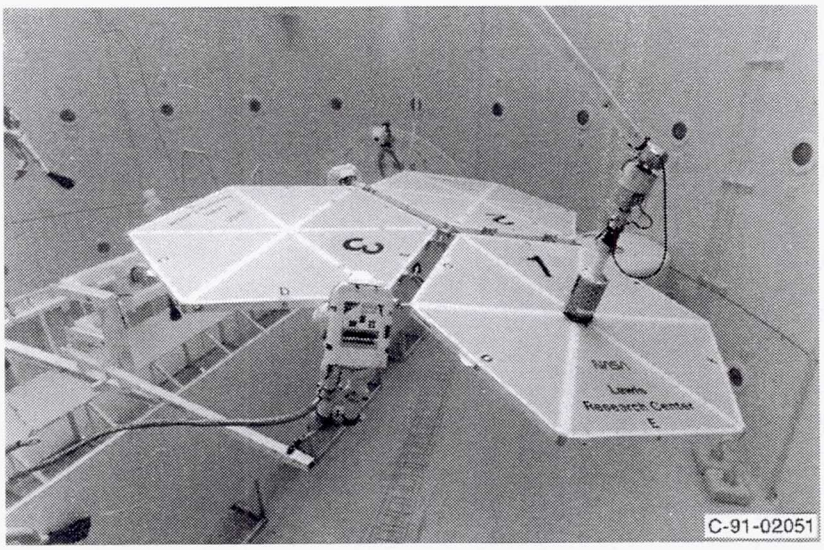

Figure 6.22.—Concentrator panel assembly test run (test 2, configuration 1).

testing. Some wear was observed along the guide ramp surfaces, but they continued to function despite the many repetitions and some rather rough handling. The extended ramps of the latch type II fine guides made it easy to align the type II latch and striker.

Assembly procedures and astronaut positions: The orientation evaluation produced the following results: Test 2 was selected as the best configuration and astronaut position. A mnemonic lift, align, move, and push (LAMP) procedure was developed to aid in the assembly process and worked well. Test subject 1 (EV1) was best suited to give the commands, but a continual exchange between subjects provided the most orderly assembly. Working with the panels at about chest height seems to provide the best combination of visibility and maneuverability. Attaining angular alignment of panels 1 and 2 was the most difficult part of the assembly process, but it became easier with practice. Handhold locations on the panel sides provided good leverage, but they did not permit panel stowage.

Views: Views were determined to be excellent for type I latches and guides and type II latches. Correct angles were determined for latchup. EV1 had an excellent view of both type I latches and guides and was able to determine the correct angle for latchup of panels 1 and 2. Test subject 2 (EV2) had an excellent view of the type II latches and the type I guides.

Maneuverability: Cross-panel positioning and visibility permitted coordinated movements and control. The EVA subjects were able to remove panels from the cradle and position them for latching. The test 2 configuration allowed the EVA subjects to have handholds on both panels being latched.

Handrails: Handrails provided good gripping and handling capabilities and could be removed (fig. 6.23). Handrails did not permit stowage of panels in the cradle, but alternatives that will permit stowage seem attainable. Some test subjects preferred to grasp the panel edges for handling during some test runs.

RMS simulator capabilities: The RMS simulator provided adequate resistance to permit latching, and the RMS arm rotation time was reasonable. The RMS simulator did not provide positioning feedback to the operator.

Assembly timelines: Although there were insufficient data to construct accurate timelines, the results appear to indicate that initial estimates are reasonable. The time to assemble the three panels was greatly reduced with practice. Best times to complete the three-panel assembly ranged from 4 to 5 min. It is reasonable to expect that a flight RMS will enhance assembly capabilities and may reduce assembly time.

At completion of the initial test program, several runs of the test 2 configuration (fig. 6.20) were made for further evaluation. Tests concluded with a scuba runthrough by astronauts of the best test configuration. On the basis of these runs the astronauts judged that the design of the concentrator latches and the assembly method developed thus far are adequate. (A space-suited astronaut run was canceled because of an air problem at the NASA Marshall NBS Facility.)

Reference 6.75 contains the test results for assembling the three full-scale concentrator panels with the precision latch and latch guide mechanisms. The design of the latch and guide mechanisms is discussed, along with details of the assembly procedures used.

6.5.5.4 Future plans and testing. — Space Station *Freedom* Program plans at the cancellation of the SD program included conducting a seven-panel concentrator neutral buoyancy assembly test that would incorporate more flightlike support hardware designs, such as panel cradle and handhold redesign, latch and guide modifications as needed, latch indicator design, and possible robotic assembly scenarios.

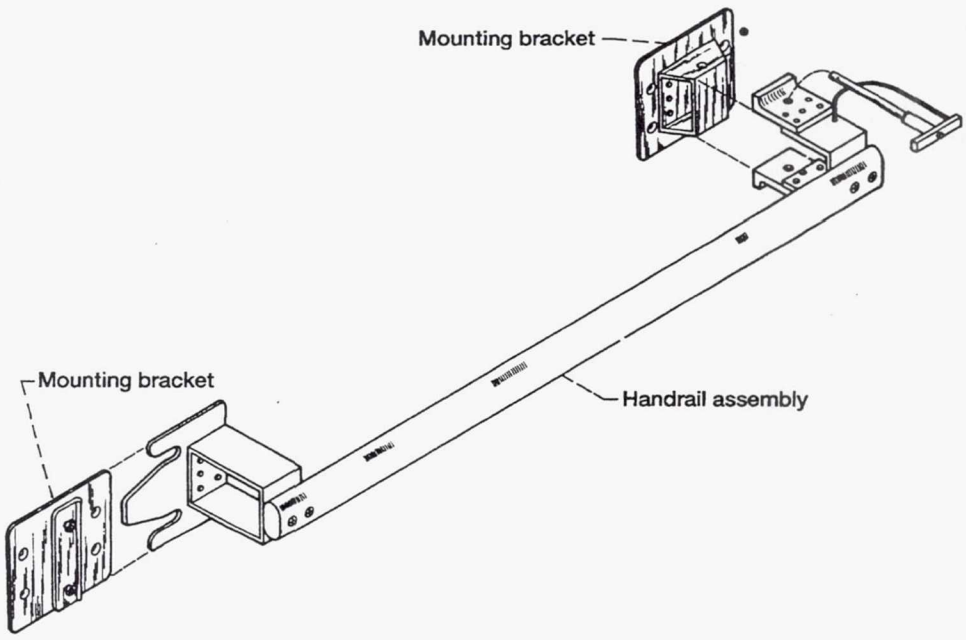

Figure 6.23.—Removable handrail.

6.5.5.5 Summary.—The primary accomplishment from the COPAT series was that the precision latch and guide concept and the associated assembly procedures and orientations were evaluated. It was demonstrated that the concepts tested will enable successful on-orbit assembly of large space structures. This activity addressed a major level I/II concern about the assembly of the solar concentrator.

The latches functioned well throughout the test. They were engaged and disengaged approximately 50 times during testing, and no significant problems occurred. Tolerances for slight misalignment and nonsimultaneous latchup were demonstrated. Gross guides functioned as intended without failure and aided in determining and attaining correct panel angles for latching.

The COPAT underwater test series has provided valuable experience to NASA Lewis and contractor personnel. The tests helped to identify special EVA tools, restraints, and handholds and the necessary hardware design changes to ensure that evolving designs are EVA compatible. These tests were a critical part of the early design evaluation process that will reduce technical risks in the development effort of the baseline solar dynamic concentrator.

6.5.6 Low-Earth-Orbit Durability Evaluation of Solar Concentrator Materials

A program to evaluate the performance and low-Earth-orbit (LEO) durability of solar concentrator facet coupons was conducted by the Electro-Physics Branch of the NASA Lewis Power Technology Division. Effects of atomic oxygen, ultraviolet (UV) radiation, and thermal cycling and the synergistic effects of these LEO environmental conditions on optical performance were evaluated. Solar concentrator facet coupons (approximately 3.75 cm^2) with a sandwich type of structure (two sheets of graphite-fiber-reinforced epoxy bonded to an aluminum honeycomb core) were fabricated at Hercules Aerospace and sent to 3M Corporation for the deposition of protective and reflective thin films (fig. 6.24). Silver was chosen as the reflective material because of its high solar specular reflectance. Because silver does not adhere well to graphite epoxy, an adhesion-promoting layer of copper (200 Å) was first deposited onto the graphite epoxy facesheet, followed by the silver (1000 Å). Two atomic-oxygen-protective coatings were deposited on top of the silver: alumina (Al_2O_3) (200 Å), which is also an adhesion-promoting layer, and then an outer coating of silicon dioxide (SiO_2) (700 Å). The films were deposited by electron beam evaporation. Coupons were exposed to iterative and continuous atomic oxygen exposures for fluences up to 3.1×10^{21} atoms/cm^2. Simulated LEO atomic oxygen exposure was accomplished in a Structure Probe, Inc., radiofrequency plasma asher that operated on air with both continuous and iterative exposures. Effective fluences were obtained by co-ashing Kapton witness coupons and then calculating the fluence from the mass loss of the Kapton and the erosion yield of Kapton in LEO (3.0×10^{-24} cm^3/atom). Plasma ashers produce isotropic arrival of atomic oxygen, whereas the solar concentrator will be exposed to sweeping arrival in LEO, but the undercutting mechanisms are similar. Various coupons were also exposed to 10 vacuum thermal cycles

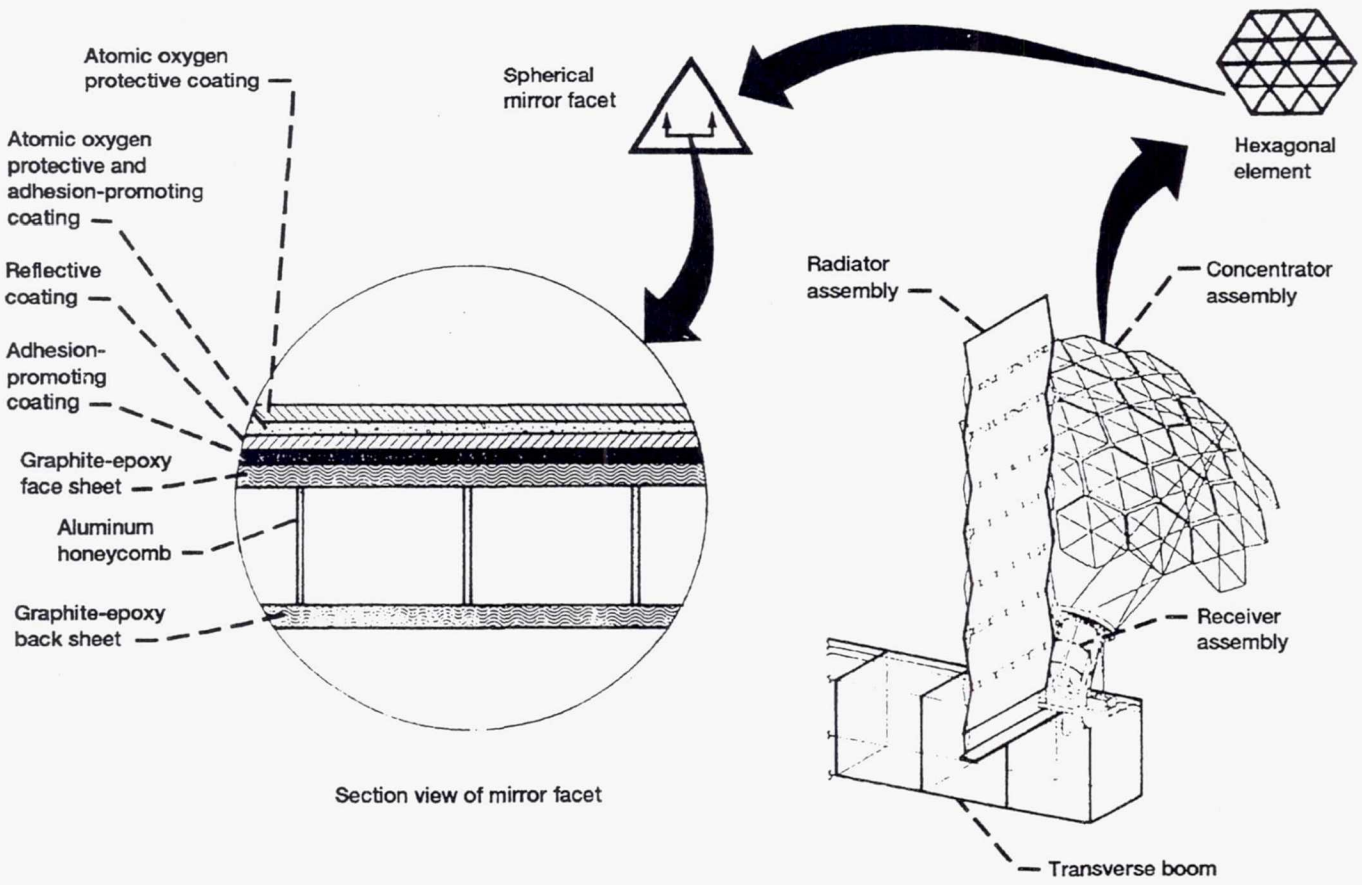

Figure 6.24.—Sandwich construction of solar concentrator facet coupons.

(−18 to 121 °C), 1000 equivalent Sun hours (ESH) of vacuum ultraviolet (VUV) radiation, and 10 and 908 vacuum thermal cycles combined with VUV. Coupons that were vacuum thermal cycled, VUV exposed, and VUV and thermal cycled were then exposed to air plasma ashing for evaluation of the synergistic effects with atomic oxygen. Hemispherical, specular, and diffuse reflectances were obtained before and after simulated LEO exposures by using a Perkin-Elmer λ-9 UV/VIS/NIR spectrophotometer operated with a barium-sulfate-coated 60-mm-diameter integrating sphere. Integrated solar reflectance was obtained by measuring the spectral reflectance over the wavelength range 250 to 2500 nm and convoluting the spectrum into the air-mass-zero solar spectrum over the same range. Solar absorptance was calculated by subtracting the solar hemispherical reflectance from 1 (zero transmittance).

Optical and electron microscopy revealed several types of fabrication and handling defects in the protective and reflective coatings on the pristine coupons. The types of defects (scratches, dendritic regions, porosity and/or bumps, haziness, cracks, and pin holes) and their population varied greatly from coupon to coupon. Microscopic cracks were associated with porous and/or bump defects. Optical micrographs of some typical defect sites are shown in figure 6.25. Coupons that contained more fabrication and handling defects had lower solar specular reflectance than coupons that had fewer defects. Pristine solar specular reflectance varied between 0.832 and 0.887.

Results from simulated LEO exposures indicate a tolerance of the solar concentrator materials to VUV radiation, vacuum thermal cycling, and combined VUV and thermal cycling but not to long-term exposure to atomic oxygen. Atomic oxygen attack at defect sites resulted in oxidation of the silver and erosive undercutting of the graphite-epoxy substrate. Figure 6.26 shows atomic oxygen erosion damage on a concentrator coupon and the corresponding specular reflectance degradation. The mirrored surface is the dark square region in the center. Atomic oxygen erosion sites appear bright. Optical micro-scopy examination and documentation before, during, and after atomic oxygen exposure provided evidence of atomic oxygen attack at protective coating defect sites, particularly at scratches, cracks, porous and/or bump regions, and pin holes. Preferential atomic oxygen attack at a porous defect region can be seen in figure 6.27. Extensive undercutting and curling of reflective and protective coatings were found to be promoted through an undercutting-tearing propagation process. Figure 6.28 shows atomic oxygen undercutting and

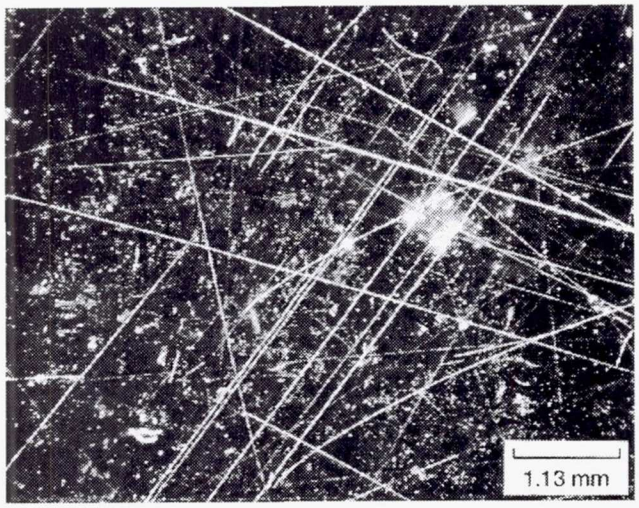

(a) Scratches.

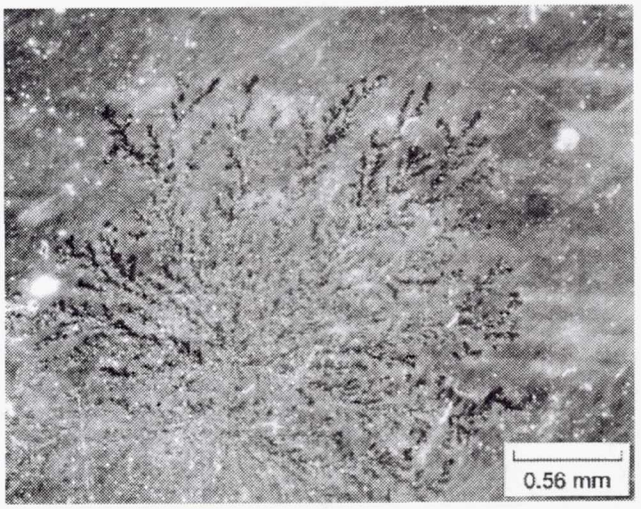

(c) Dendritic region.

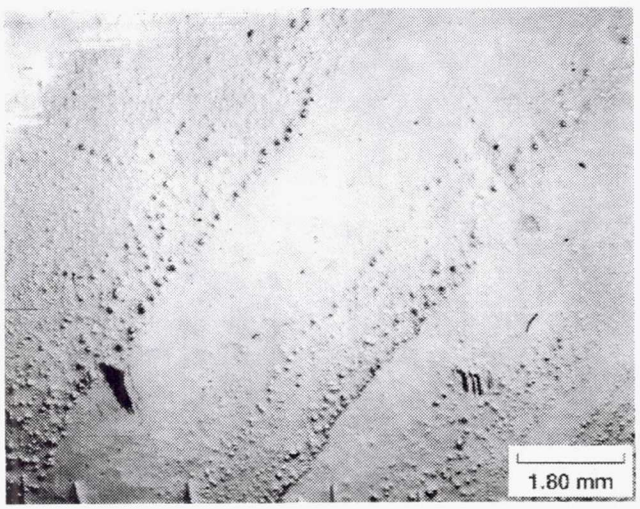

(b) Macroscopic bumps.

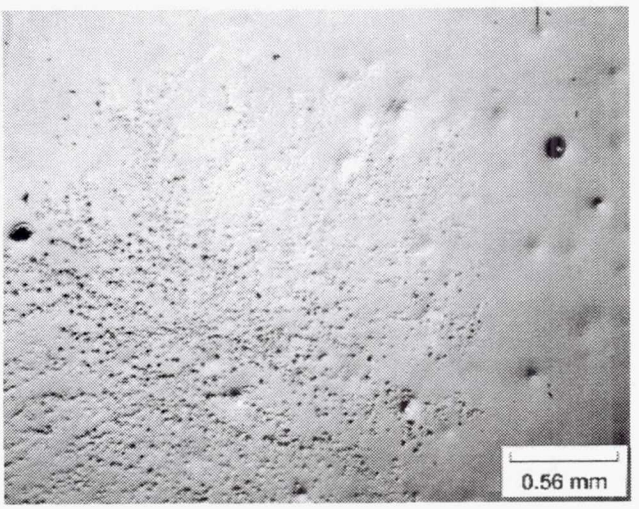

(d) Polarized micrograph of part (c) showing porosity associated with dendritic regions.

Figure 6.25.—Fabrication and handling defects on as-received coupons.

the resulting tearing and curling of the reflective and protective coatings. Iterative air plasma ashing appeared to accelerate the undercoating-tearing propagation process when compared with continuous ashing to the same fluence. Large variations in atomic oxygen damage occurred on various coupons and are attributed to the large variations in defect type and density of the coupons. Thermal cycling and combined VUV and thermal cycling exposure resulted in a negligible change in the integrated solar specular reflectance. Vacuum ultraviolet radiation decreased solar specular reflectance. Coupons exposed to VUV radiation experienced yellowing of the surface with associated spectral reflectance changes in the wavelength range 250 to 500 nm (fig. 6.29). The change in spectral reflectance is attributed to UV darkening. Spectral changes were found to be more pronounced in the absence of thermal cycling or atomic oxygen. Small spectral changes and yellowing were observed on atomic-oxygen-exposed coupons similar to those on the UV-exposed coupons. This result is attributed to either UV effects, since some UV radiation is present in plasma ashers, or atomic oxygen effects. Coloration due to UV effects (solarization) could be attributed to oxide film valency changes or to dissociation of Al_2O_3 bonds allowing the formation of AgO_x. Atomic oxygen interactions may contribute to discoloration through oxide thickness changes or stoichiometric changes. Atomic oxygen bleaching or thermal effects appeared to reverse the spectral damage from VUV radiation.

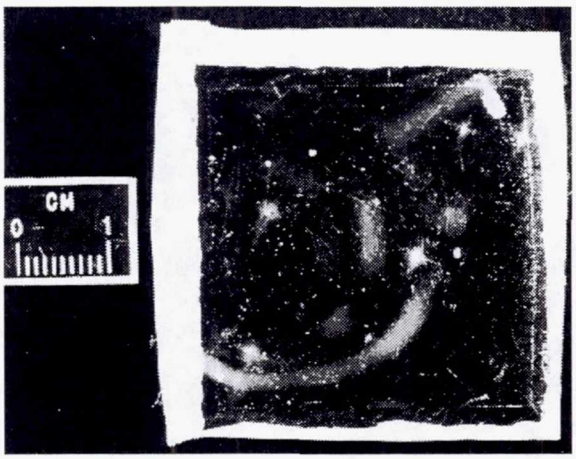

(a-1) Pristine defect.

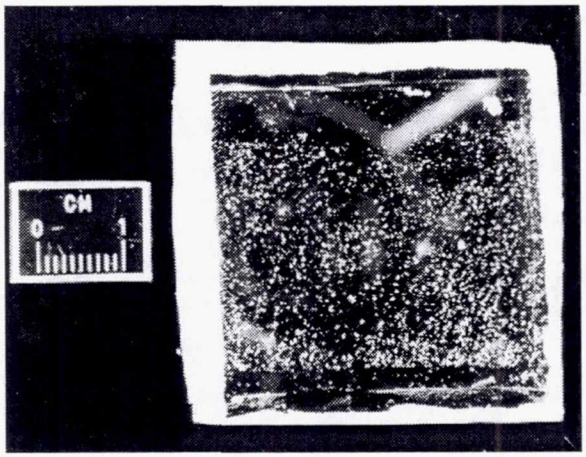

(a-2) Fluence, 1.57×10^{21} atoms/cm^2.

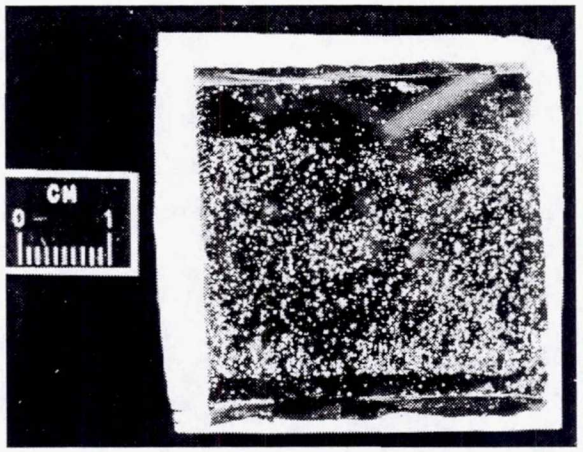

(a-3) Fluence, 3.1×10^{21} atoms/cm^2.

(a) Atomic oxygen erosion damage.

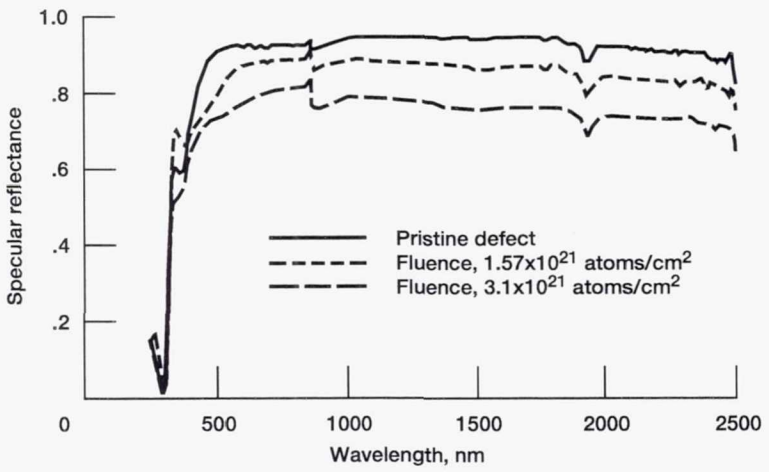

(b) Specular reflectance.

Figure 6.26—Atomic oxygen erosion damage and specular reflectance for coupon D.

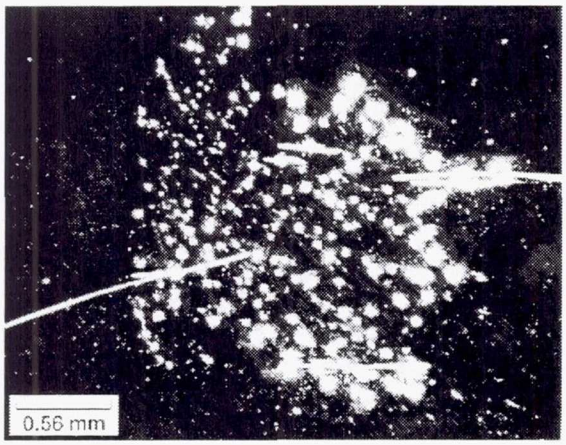

(a) Pristine defect.

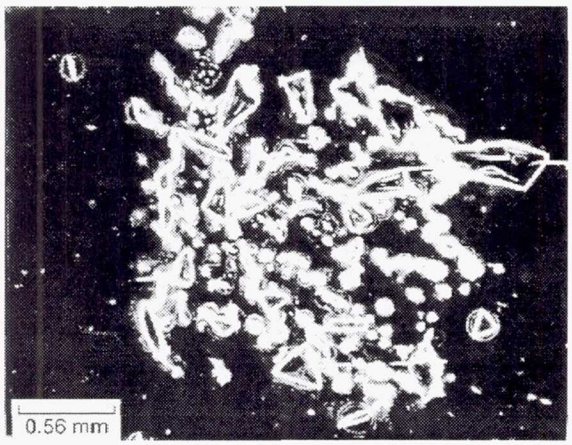

(b) Reflective and protective films over undercut regions have torn (fluence, 1.57×10^{21} atoms/cm^2).

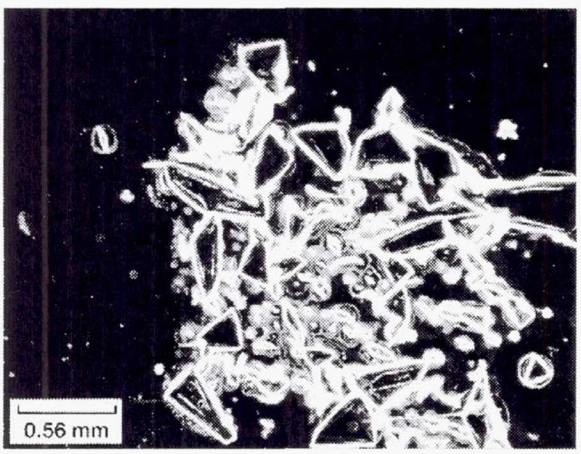

(c) Undercutting and tearing process propagates (fluence, 3.1×10^{21} atoms/cm^2).

Figure 6.27.—Preferential atomic oxygen attack at porous region on coupon C.

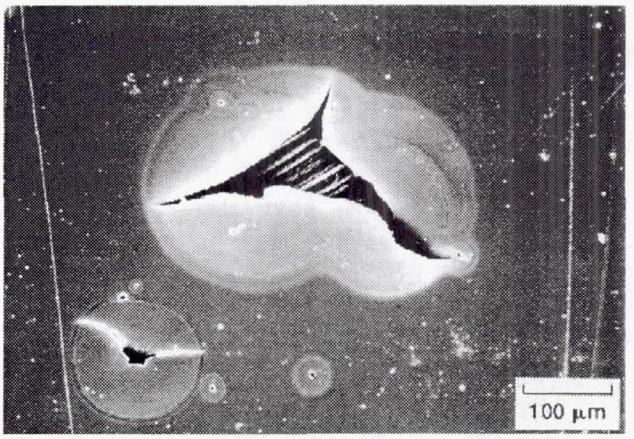

(a) Exposure of graphite fibers due to tearing of reflective and protective films.

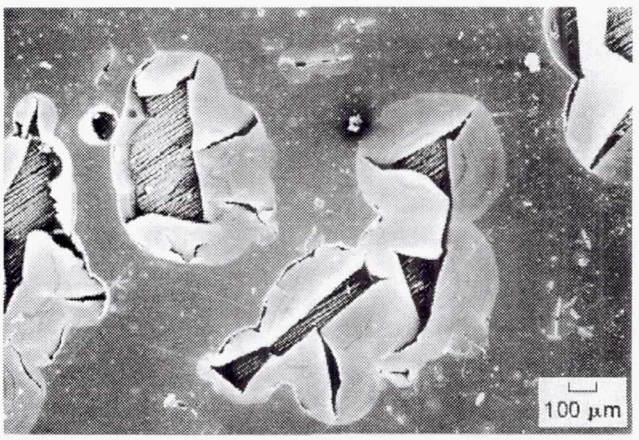

(b) Flaking off of unsupported films at extensively undercut regions.

Figure 6.28.—Scanning electron micrographs of undercut regions.

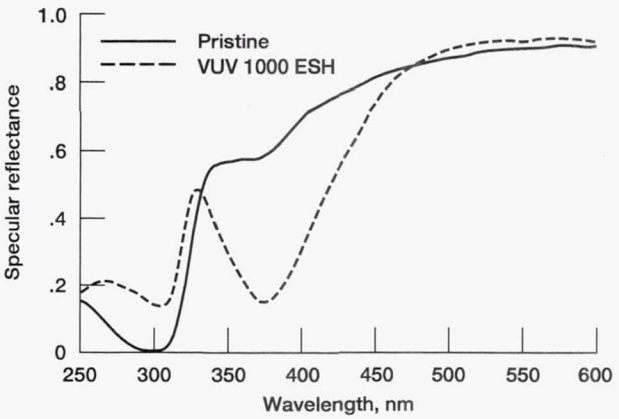

Figure 6.29.—Spectral specular reflectance changes in concentration coupon exposed to 1000 ESH of VUV radiation.

The primary cause of solar concentrator degradation was found to be atomic oxygen undercutting erosion occurring at protective coating defect sites. The extent of optical damage experienced on some of these concentrator coupons after continuous ashing to 1.08 equivalent Space Station *Freedom* years appeared to be unacceptable for the needed 15-year lifetime of the solar concentrators. A 10-point drop in solar specular reflectance was defined to be unacceptable for 15 years.

Therefore, a study was conducted to project the reflectance degradation expected in space from results of plasma asher exposures. A series of conversion factors were computed to account for the differences in atomic oxygen reaction in space and in ashers. The results indicated that the extent of specular reflectance loss will be much less severe than that predicted from simple effective fluence extrapolation of asher results. On the basis of these conversion calculations and the results of concentrator exposure in plasma ashers, after 15 years there would be a drop in solar specular reflectance of 4 to 6 percent. Results on the extrapolation study are presented in reference 6.78.

It was concluded from the LEO durability evaluation that in order to maintain the solar specular reflectance and solar absorptance of concentrator coupons in LEO, the concentration of fabrication and handling defects on the mirrored surface must be decreased. In addition, the ability of the reflective and protective films to resist tearing when undercut should be improved. Leveling coating layers underneath the reflective layer by surface tension curing has been shown to reduce the atomic oxygen defect density by an order of magnitude as well as to improve optical performance (ref. 6.79). Investigation of leveling layers was planned prior to SD program termination. Visible examination of concentrator coupons produced by the replication technique indicated that this technique is very promising for decreasing the defect concentrations. Results of LEO durability evaluation of the solar concentrator coupons are detailed in references 6.80 and 6.81.

An extensive data file containing test information, scanning electron micrographs, and reflectance data is being kept by Kim de Groh of NASA Lewis.

6.6 Interface to *Freedom*

Tasks were included in the Solar Dynamic Concentrator Program to identify and bound interfacing data between solar dynamics and Space Station *Freedom*. The intent is to identify key hardware and software design features (also called hooks and scars) that must be incorporated into the Space Station *Freedom* hardware during the design phase in order for the solar dynamic power systems to be added to the station when required during the growth or evolution phase.

The hook and scar areas examined included system integration (mass properties, moments of inertia, thermal environments, and beta gimbal requirements), assembly, growth considerations (from a thermal environment and an assembly standpoint), and the safety considerations of off-axis reflections when the concentrator is pointed off the Sun.

Detailed results of the hooks and scars studies relevant to the concentrator are described in detail in reference 6.41 and summarized here. Hooks and scars tasks for the remainder of the solar dynamic system are discussed in chapter 12.

6.6.1 Off-Axis Images

Task 1, entitled "Concentrator Solar Flux for Off-Axis Images," evaluated the effects of off-axis incident radiation on the proposed solar concentrator (baseline design, Sept. 1, 1989). Three primary sources of off-axis radiation were defined. The first and most significant is mispointing of the solar concentrator, where the concentrator bore axis is not aligned with the solar direction. The second is energy emitted from the receiver aperture itself, and the third is energy either emitted or reflected from the Earth. The resulting reflected energy can potentially be focused to locations other than the receiver aperture.

In addressing the issue of concentrator mispointing, a systematic set of alpha and beta mispoints was analyzed to present a general view of how the peak flux varies in position and magnitude with respect to the mispointing (ref. 6.82). Within the ranges of alpha and beta mispoints studied, the maximum possible concentration beyond a distance of 108 ft was 2.5 Suns. Regardless of the mispoint angle, a reasonable keepout zone can be identified that does not include any structure other than the concentrator assembly and a small section of the photovoltaic arrays. Within this keepout zone there does exist the potential for regions of considerable flux. However, the problem is controllable, and through appropriate mispointing of one or both of the gimbals the image can be directed along a safe path to a position of zero flux. The off-axis image effect on the photovoltaic modules was analyzed further (ref. 6.83). Reflection of solar radiation from the Earth's surface has been examined by Jefferies (ref. 6.34) and found to be insignificant.

6.6.2 Thermal Environment

Task 2, entitled "Thermal Environment," provided information necessary to determine the thermal effect of the solar dynamic concentrator on other components of *Freedom*. This information includes the area of the concentrator (reflector only, no struts), the outline of the concentrator geometry, the temperature range of the reflector surface (operational and nonoperational), and the thermal loads imposed on other station components.

6.6.3 Station Flight Dynamics

Task 3, entitled "Station Flight Dynamics," provided information necessary to determine the effect of concentrator dynamics on other components of *Freedom*. This information includes the drag area of the concentrator (at various orientations), the outline of the concentrator geometry, the mass properties of the concentrator (mass, moments of inertia, and center of gravity), and the deployed modal frequencies. The drag area of the concentrator was estimated for four orientations. The area varied from a maximum of 423 100 $in.^2$ for planform area perpendicular to the center panel normal to a minimum of 43 500 $in.^2$ for planform area perpendicular to the side axis. The mass of the deployed concentrator was determined to be 2330 lb.

6.6.4 Compatibility

Task 4, entitled "MSC/EVA/IVA Compatibility," compared the capabilities of the current EVA systems against the requirements for the assembly of the solar concentrator. Analysis examined effects on EVA of the mobile transporter, the astronaut positioning system, the *Freedom* remote manipulator system, the mobile servicing center payload accommodations, and the rephased program. The phase 1 equipment was reviewed to determine if any modification would enhance the assembly operations for the concentrator. Although the astronaut positioning system did not reach the two upper concentrator/support structure interface fittings, modifying the APS to gain this capability would reduce its capability elsewhere and therefore did not warrant pursuit. No modification of existing or planned *Freedom* equipment is recommended for solar dynamics at this time.

Task 5, entitled "NSTS Compatibility," provided information regarding the compatibility of the solar dynamic concentrator package with the NSTS. This information includes conceptual layouts of the cradle with conceptual sizing, conceptual-level stowed finite element models and analysis results, and conceptual-level mass properties data.

For complete details of the cradle, see reference 6.84. For complete details of the cradle interfaces, see reference 6.85. The analytical natural frequencies for the cradle concept, which consisted of two reflector stacks installed (full cradle), were 10.38 and 13.22 Hz for the first two modes. Preliminary stress analysis was performed by using internal member loads. Loads applied to the model consisted of the lift-off and landing design load factors from reference 6.86 (tables 4.1.3–1 to 4.1.3.5–1). The cradle beams were reviewed for crippling, local buckling, and beam-column effects as well as static strength at ultimate load. The internal member loads for the restraint system and the hexagonal panel box beams were reviewed as well. One problem identified by the static loads analysis is that the hexagonal panel beam loads nearest the cradle are high owing to the nature of the cradle design and the model uncertainty factor of 2. Also, as explained in the report, a keel spanner bridge is needed for two keel latches to share the large cradle applied load and to allow the entire two-concentrator package to stow within the specified envelope.

6.6.5 Beta Gimbal Requirements

Task 6, entitled "Beta Gimbal Requirements," was established to examine the use of the beta gimbal during the assembly and disassembly of the concentrator and structure. Two different scenarios affect the assembly and disassembly operations of a solar dynamic concentrator:

(1) The assembly and disassembly of a solar dynamic concentrator that is the only solar dynamic power unit on that end of *Freedom*'s main truss

(2) The assembly and disassembly of a solar dynamic concentrator in the presence of a functional solar dynamic power unit on the same end of *Freedom*'s truss (such as a second unit added to obtain the full growth configuration)

These two scenarios provide the beta gimbal requirements for the unit being assembled and the requirements for moving the first unit assembled during the assembly of the second unit. As long as there is not an overwhelming reason to assemble the concentrator parallel to the main truss, the beta gimbal is not needed to support the detailed assembly and disassembly operations. If the unit in question is being assembled in the presence of a functional solar dynamic power unit, it will be necessary to bring the functional unit off line through the use of its beta gimbal so as to preclude any hazard during assembly.

6.6.6 Contamination Effects

Task 8, entitled "Contamination Effects," evaluated the effects of on-orbit contamination on the performance of solar dynamic concentrators. The task was redirected to identify potential risks and to suggest areas for further investigation under the rephased program. Potential contaminants of the solar dynamic concentrator surface have been identified by Rocketdyne (ref. 6.25). Sources of contamination include outgassing from organic materials (chemical composition unknown at present), NSTS orbiter reaction control system (RCS) engines, *Freedom* station reboosting engines, and abnormal sources, such as photovoltaic and solar dynamic module leakage. Only those contaminants with low enough vapor pressures to deposit on the concentrator surface are of concern. Species of interest are thus monomethylhydrazine nitrate (NSTS orbiter RCS engines), ammonia (photovoltaic and solar dynamic modules), potassium hydroxide (photovoltaic module), calcium fluoride (solar dynamic module), and *n*-heptane (solar dynamic module).

6.6.7 Disassembly

Task 10, entitled "Disassembly," addresses the fact that the life expectancy and the possibility of damage to the concentrator while on orbit dictate the requirement for it to have the ability to be removed and subsequently disassembled so that a replacement can be installed. The basic approach used for the disassembly of the solar dynamic concentrator is the reverse of the on-orbit assembly process detailed in reference 6.45. The EVA, IVA, and MSC operations that supported the concentrator assembly will also support disassembly. No additional tooling or modifications to the phase 1 equipment are needed to support just the disassembly process.

6.6.8 Support Equipment Commonality

Task 11, entitled "Support Equipment Commonality," examined the tools required to support the operations centered around the components provided by Harris Corporation of the solar dynamic power system and identified tools available through phase 1 work packages or the NSTS that would support these activities with few or no modifications. The majority of support equipment requirements were met with unmodified or slightly modified equipment available from either the phase 1 work packages or the NSTS. In those cases where new equipment will be needed, the items consisted of removable grapple fixtures, sockets, extensions, crossovers, and pip pins.

References

6.1 SD Power Module System CEI Specification. Part 1, DR E–02[a], rev. B, May 1, 1990.

6.2 Kudija, C.: Power Generation Subsystem, Closed Brayton Cycle. RC1811[a], May 18, 1990.

6.3 Kudija, C.: Reflector/Structure and Launch Cradle Set – Solar Dynamic. RC1812[a], Nov. 26, 1991.

6.4 Young, G.H.: Gimbal Assembly, Two-Axis – Solar Dynamic. RJ00164[a], Sept. 22, 1989.

6.5 Cochran, C.J., Reflector Design Requirements. Harris Corp., SDP–0080[a], June 27, 1990.

6.6 Bunnell, K.G.: Harris Corp. Hooks/Scars and Reflector/Structure Interim Design Review #1 (IDR1). DRR–00268[a], July 9, 1991.

6.7 Cochran, C.J: Weight Summary Update. Harris Corp., R80SIA88561108, SDP–0081[a], June 29, 1990.

6.8 Knasel, D.; and Ehresman, D.: Solar Concentrator Advanced Development Program. Final Report, NASA Contract NAS3–24670, NASA CR–185173, 1989.

6.9 Facet Capture Feature. Harris Corp., SDP–0148[a], Jan. 23, 1991.

6.10 Young, G.H.: Actuator, Linear, Solar Dynamic. RC1819[a], Nov. 9, 1989.

6.11 Thorgusen, R.L.: Receiver Tilt and Aperture Offset. EID–00805[a], Dec. 11, 1990.

6.12 Power System Description Document. Rockwell International, Rocketdyne Division, SE–02[a], June 1, 1990.

6.13 Panel to Panel Spacing Study. Harris Corp., SDP–0147[a], Jan. 23, 1991.

6.14 Cassel, S.D.: Phased Edge Wedge Study. Harris Corp., SDP–0048[a], Apr. 13, 1990.

6.15 Cassel, S.D.: Edge Wedge Elimination Study. Harris Corp., SDP–0112[a], Aug. 29, 1990.

6.16 Cassel, S.D.: Trade Study Report (Flux Distribution Subtask 2). Harris Corp., SDP–0078[a], June 22, 1990.

6.17 Cassel, S.D.: Advanced Flux Tailoring (Flux Distribution Subtask 1). Harris Corp., SDP–0133[a], Oct. 26, 1990.

6.18 Young, G.H.: Pointing and Tracking Subsystem, Design Specification for. RJ00198, key 24282[a], June 1, 1990.

6.19 Cassel, S.D.: Concentrator Performance Update. SDP–0082[a], June 28, 1990.

6.20 Cassel, S.D.: Concentrator Performance Update. SDP–0104[a], Aug. 7, 1990.

6.21 Cassel, S.D.: Concentrator Performance Update. SDP–0144[a], Nov. 15, 1990.

6.22 Cassel, S.D.: Performance Sensitivity Report (Performance Assessment Subtask 1). SDP–0107[a], Aug. 23, 1990.

6.23 O'Brien, D.L.: Interim Servo-Elasto Optics Analysis Report. EID–00739[a], Nov. 27, 1990.

6.24 Marshall, M.; and Papac, T.: Engineering Design Document – WP–04 Power System. Rockwell International, Rocketdyne Division, EID–00259[a], rev. G, Jan. 24, 1991.

6.25 Hallinan, G.J.: Space Station WP–04 Power System Final Study. Report DR–15, (Rockwell International, NASA Contract NAS3–24666), NASA CR–179587, 1987.

6.26 Time-Phased SE&I Study Products. DR–19, Rockwell International, Rocketdyne Division, RI/RD85–194, DP 4.1[a], June 3, 1985.

6.27 Time-Phased SE&I Study Products. DR–19, Rockwell International, Rocketdyne Division, RI/RD85–194–1, DP 4.2[a], July 19, 1985.

6.28 Time-Phased SE&I Study Products. DR–19, Rockwell International, Rocketdyne Division, RI/RD85–194–2, DP 4.3[a], Oct. 3, 1985.

6.29 Time-Phased SE&I Study Products. DR–19, Rockwell International, Rocketdyne Division, RI/RD85–194–3, DP 4.4[a], Nov. 19, 1985.

6.30 Jefferies, K.S.: Ray Tracing Optical Analysis of Offset Solar Collector for Space Station Solar Dynamic System. Proceedings of the 23rd Intersociety Energy Conversion Engineering Conference, Vol. 4, ASME, 1988, pp. 225–232, July 31-Aug. 5, 1988. (Also NASA TM–100853.)

6.31 Elfe, T.: Modeling High Temperature Solar Receivers. Proceedings of Solar Thermal Test Facility User's Association Workshop on High Temperature Materials for Solar Thermal Applications, 1982.

6.32 Blackmon, J.B.; et al.: Design and Performance of a Digital Image Radiometer for Dish Concentrator Evaluation. Solar Engineering 1987, D.Y. Goswami, K. Watanabe, and H.M. Healy, eds., American Society of Mechanical Engineering, New York, Vol. 1, pp. 318–323.

6.33 Holly, S.; Springer, T.; and Jefferies, K.S.: Optical Measurements Pertaining to Space Solar Dynamic Power Systems. IAF Paper 87–229, Oct. 1987.

6.34 Jefferies, K.S.: Concentration of Off-Axis Radiation by Solar Concentrators for Space Power. Proceedings of the 24th Intersociety Energy Conversion Engineering Conference, Vol. 2, IEEE, 1989, pp. 887–893 (Also NASA TM–102052.)

6.35 Jefferies, K.S.: Coordinate Transformations and Analyses of DIR Configurations. Letter to James Blackmon, Nov. 9, 1987.

6.36 Jefferies, K.S.: Offset Optical Code Development. IBR SE–135, key 34889[a], Feb. 8, 1988.

6.37 Cassel, S.D.: Receiver Flux Distribution Sensitivity to Beta Gimbal Mispoint. SDP–0071[a], June 4, 1990.

[a]Space Station *Freedom* library at the NASA Lewis Research Center in Cleveland, OH 44135 (tel. 216–433–5367 and fax 216–433–8050).

6.38 Cassel, S.D.: Concentrator Elasto-Optics Study Input. SDP–0067[a], May 30, 1990.

6.39 Cassel, S.D.: Addendum to Concentrator Elasto-Optics Study Input. SDP–0070[a], June 4, 1990.

6.40 Cassel, S.D.: Deployed Concentrator Finite Element Model Nodal Weight Update With Mid-beam Nodes. SDP–0089[a], July 2, 1990.

6.41 Hooks and Scars Report. SDP–0001[a], Dec. 21, 1989.

6.42 Cochran, C.J.: Launch Cradle Alternatives Status Report. SDP–0031[a], Mar. 5, 1990.

6.43 Cassel, S.D.: Facet Thermal Analysis Report (Thermal Control and Thermo-Elastic Effects Subtask 1). SDP–0114[a], Sept. 11, 1990.

6.44 Eldridge, K.F.: Facet Thermo-Elastic Analysis Report (Thermal Control and Thermo-Elastic Effects Subtask 2). SDP–0123[a], Sept. 24, 1990.

6.45 Solar Concentrator Advanced Development Program Task I. Final Report, (Harris Corp.; NASA Contract NAS3–24670.) NASA CR–179489, 1986.

6.46 Spaunburgh, D.R.: Materials and Process Improvements Round 1 and Environmental Test Report. SDP–0143[a], Nov. 9, 1990.

6.47 Spaunburgh, D.R.: Material Process Improvements Round 2. SDP–0150[a], Jan. 31, 1991.

6.48 Cason, R.D.: Fabrication and Evaluation of Two Full Size Facets Manufactured for STAR. RI–HA–0028[a], Oct. 16, 1989.

6.49 Schumacher, K.M.: Test Report – Star Task I Environmental Coupons. RI–HA–0032[a], Nov. 13, 1989.

6.50 Knapp, W.: The Digital Image Radiometer (DIR) Optical Evaluation System. PIR 189A[a], Apr. 12, 1990.

6.51 Jefferies, K.S.: Concentrator Testing Using Projected Images. Proceedings of the 26th Intersociety Energy Conversion Engineering Conference, Vol. 2, ANS, Aug. 4–9, 1991, pp. 84–89. (Also NASA TM–104349.)

6.52 Gallo, C.: Summary of Results of the Laser Test Data. W.L. Tanksley & Associates, Inc., key 23576[a], Sept. 20, 1989.

6.53 Bachir, M.: Laser Measurement of Slope Variation due to Loading the Solar Concentrator Panels. key 23714[a], June 16, 1990.

6.54 Jamison, M.: DIR Measurement of Solar Concentrator Facet Tilt Error Versus Loading. key 23716[a], June 22, 1990.

6.55 Jamison, M.: Solar Concentrator Facet Repeatability Testing Using DIR System. key 23719[a], Jan. 3, 1991.

6.56 Grossman, J.W.; et al.: Task 3 Report: On-Sun Test and Evaluation of the NASA Star Facets. (Sandia National Laboratories; Contract C–31000–M), key 23679[a], June 1991.

6.57 Gallo, C.; and Jefferies, K.S.: Summary of DIR Testing Performed to Support SD Facet On-Sun Testing at Sandia Labs. IBR SE–338, key 23604[a], July 31, 1991.

6.58 Dalsania, V. : Solar Concentrator Structural Dynamic Model Verification Test Wind Loading Analysis. (W.L. Tanksley & Associates, Inc.; NASA Contract NAS3–24376), key 23575[a], Aug. 15, 1988.

6.59 Roche, J.M.: Solar Dynamic Concentrator Type IA Latch Stiffness Test and Analytical Correlation. (NASA Lewis Engineering Report 87007c001), key 23660[a], May 18, 1989.

6.60 Roche, J.M.: Preliminary Latch Type II Stiffness Test Results. (NASA Lewis memo), key 23568[a], Febr. 22, 1989.

6.61 Sutliff, T.J.: Modal Test Results Report for the Solar Concentrator Advanced Development Hardware – Single Empty Hex Panel Testing. (NASA Lewis Report by Structural Systems Dynamics Branch), key 23664[a], Feb. 28, 1990.

6.62 Sutliff, T.J.; and Ludwiczak, D.R.: Finite Element Modelling Results Report for the Solar Concentrator Advanced Development Hardware – Single Empty Hex Panel Modal Test Configuration. (NASA Lewis Report by Structural Systems Dynamics Branch), key 23663[a], June 20, 1990.

6.63 Sutliff, T.J.: Testing and Analysis for SCAD – E.D. Task 87007. (NASA Lewis Report by Structural Systems Dynamics Branch), key 23569[a], June 25, 1991.

6.64 VAX/VMS Archive Tape. (Label: SCAD; Save sets: (1) HEXFEMMODELS.BCK, (2) SCADLATCHFEMS.BCK, (3) SCADMODALTEST.BCK, (4) HEXFACETDATA.BCK), key 23732[a], Mar. 20, 1991.

6.65 Sutliff, T.J.; and Tamburro, P.: Modal Test Plan for the Solar Concentrator Advanced Development (SCAD) Hardware With Facets. (NASA Lewis Report by Structural Systems Dynamics Branch), key 23662[a], Aug. 23, 1990.

6.66 Drawings of Original Latch Stiffness Test Rig, Dated 1–19–88; Include NASA Lewis Drawings 87007M43A000– 87007M43A017 and 87007M43B000–001. key 23661[a], Jan. 19, 1988.

6.67 Drawings of Preliminary Redesigned Latch Stiffness Test Rig With a Hydraulic Load System, Dated 8–31–90; Include NASA Lewis Drawings 87007M43C000–C009 and 87007M43D000–D002. key 23661[a], Aug. 31,1990.

6.68 Sutliff, T.J.: Analytical Modelling of SCAD Hardware. (NASA Lewis Memo), key 23570[a], Aug. 14, 1989.

6.69 Dalsania, V.: Solar Concentrator Thermal Distortion Analysis. Engineering Memorandum Report, S.O.W. 318-02, NASA Contract NAS3–24376, key 23709[a], May 1987.

6.70 Dalsania, V., Solar Concentrator Thermal Distortion Analysis. Engineering Memorandum Report, S.O.W. 318–03, NASA Contract NAS3–24376, key 23710[a], Sept. 25, 1987.

6.71 Marlatt, W.; Lovely, R.; and Young, G.: Solar Dynamic Module On-Orbit Assembly Sequence. Rockwell International, Rocketdyne Division, EID–00890[a]; Feb. 25, 1991.

6.72 Troung, D.K.: Structural Analysis of Hex Frame Article for Neutral Buoyancy Tests. NASA Lewis Research Center, key 23658[a], Apr. 24, 1989.

6.73 NASA LeRC – Drawing numbers: CF-SS-1001 to CF-SS-1008 (December 1, 1987) and 87008M43A101 to 87008M43A104 (July 13, 1989). Solar Dynamic Advanced Development Hex Panel Assembly Test – Neutral Buoyancy Simulation Test. key 23656[a], Dec. 1987 to July, 1989.

6.74 Harris Corporation Latch/ Latch Guide Hardware Drawing No.'s : NBT101, NBT107, NBT108 and NBT052 through NBT111; Nov. 1989; and Harris Corp. NB Panel ICD Drawing No. NBT020. key 23657[a], Dec. 1989.

6.75 Bartos, L.J.: Solar Dynamic Concentrator Panel Assembly Test. NASA TM–105241, 1991.

6.76 Bartos, L.J.; et al. : Test Plan – Concentrator Panel Assembly Test (COPAT) – Three Panel. NASA Lewis Research Center, key 23659[a], June 22, 1990.

6.77 NASA Lewis Neutral Buoyancy Simulation of Space Station Freedom – Solar Dynamic Concentrator Panel Assembly Test, VHS Videotape of Configuration 1–Test 2A, Runs 1–4. (A list of videotapes of tests 1–10 is included; the 3/4-in. tapes are available from storage (Plum Brook Station).), key 23650[a], Aug. 24, 1990.

6.78 de Groh, K.K.; and Banks, B.A.: Low Earth Orbit Atomic Oxygen Simulation for Durability Evaluation of Solar Reflector Surfaces. 17th Space Simulation Conference, Baltimore, MD, Nov. 9–12, 1992.

6.79 deGroh, K.K.; Dever, T.M.; and Quinn, W.F.: The Effect of Leveling Coatings on the Atomic Oxygen Durability of Solar Concentrator Surfaces. NASA TM–102557, 1990.

6.80 de Groh, K.K.; Terlep, J.A.; and Dever, T.M.: Atomic Oxygen Durability of Solar Concentrator Materials for Space Station *Freedom*. NASA TM–105378, 1990.

6.81 de Groh, K.K.; et al.: Low Earth Orbit Durability Evaluation of Solar Concentrator Materials. Solar Engineering 1992, Vol. 2, The

[a]Space Station *Freedom* library at the NASA Lewis Research Center in Cleveland, OH 44135 (tel. 216–433–5367 and fax 216–433–8050).

6.81 de Groh, K.K.; et al.: Low Earth Orbit Durability Evaluation of Solar Concentrator Materials. Solar Engineering 1992, Vol. 2, The American Society of Mechanical Engineers, pp. 775–782.

6.82 Campbell, J.S.; and Cassel, S.D.: Concentrator Solar Flux for Off-Axis Images (Hooks and Scars Task 1 – Safety). RI–HA–0029[a], Oct. 25, 1989.

6.83 Young, G.; et al.: Solar Dynamic Off-Axis Images Thermal Impact Study. EID–00695[a], Oct. 23, 1990.

6.84 Cochran, C.J.; and Smith, R.T.: Launch Cradle Baseline Design. RI–HA–0030[a], Oct., 1989.

6.85 Cochran, C.J.: Cradle Interfaces. RI–HA–0033[a], Nov. 1989.

6.86 Space Shuttle System Payload Accommodations. National Space Transportation System, NSTS. Report NSTS 07700, Pt.ICD–2–19001, Vol. XIV, Rev. K, Attachment 1: Shuttle Orbiter/Cargo Standard Interfaces. NASA Johnson Space Center, Houston, TX, 1991.

---

[a]Space Station *Freedom* library at the NASA Lewis Research Center in Clevelapd, OH 44135 (tel. 216–433–5367 and fax 216–433–8050).

Chapter 7
Heat Receiver

Two heat receiver designs were developed for the Space Station *Freedom* Program: the baseline design and the advanced development design. The baseline receiver design was developed under contract NAS3–25082 with Rockwell International, Rocketdyne Division, as prime contractor and Allied-Signal Aerospace Company as subcontractor. The advanced development receiver was designed, built, and tested under contracts NAS3–24669 and NAS3–25716 with Boeing Aerospace and Electronics.

7.1 Baseline Receiver Design

7.1.1 Design Description

The heat receiver accepts concentrated solar energy from the concentrator and directly transfers a fraction of this energy to the closed Brayton-cycle working fluid circulating through the receiver. The remaining solar energy is absorbed by a thermal energy storage (TES) phase-change material

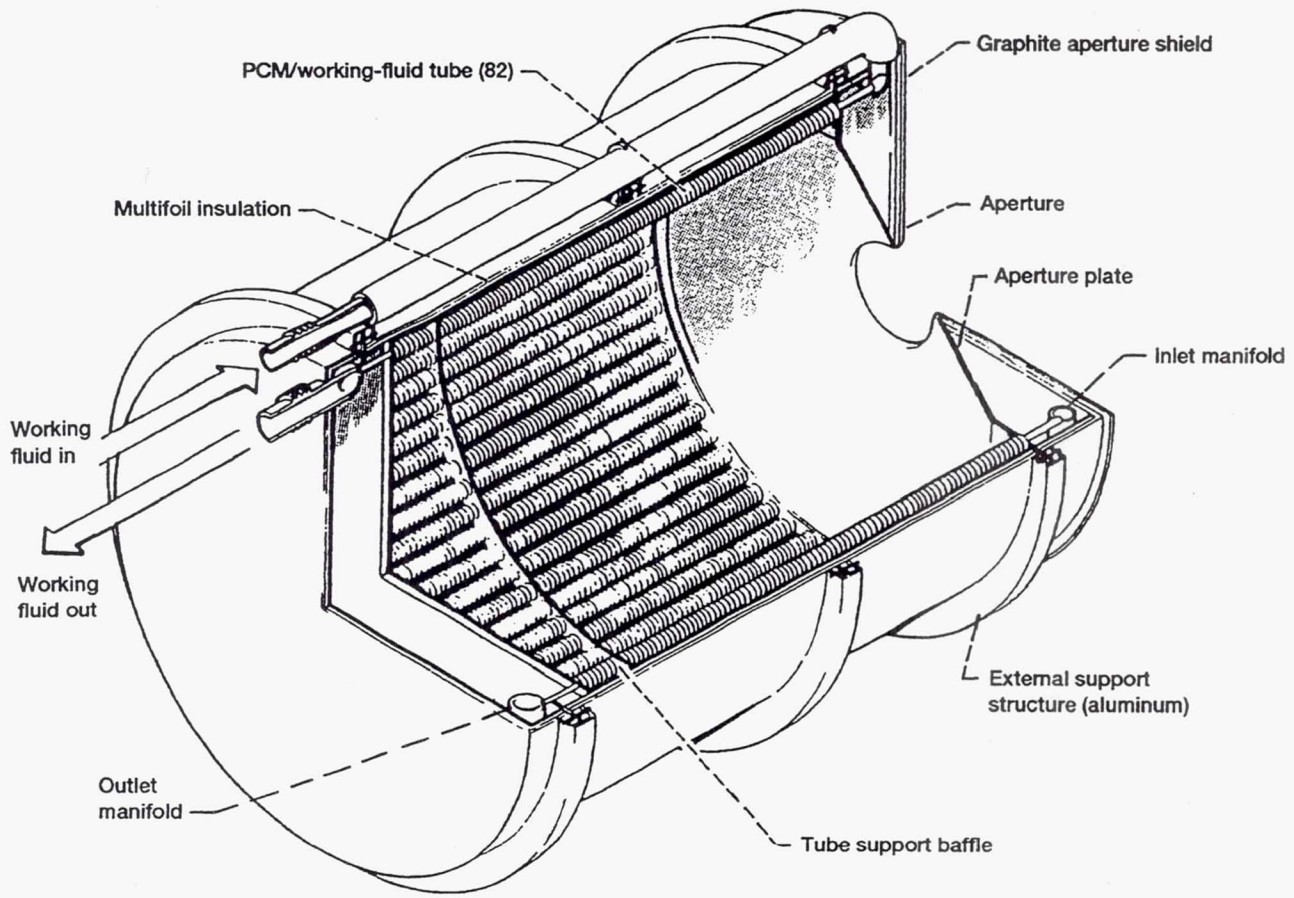

Figure 7.1.—Solar heat receiver concept. Diameter, 6.1 ft; length, 9.8 ft.

(PCM) located within the receiver. TES permits continuous heat engine operation through orbital eclipse periods when solar insolation is not available.

The heat receiver concept is shown in figure 7.1 and is shown in cross section in figure 7.2. The receiver is an insulated cylindrical cavity lined with multiple working-fluid tubes. The cylinder is closed at one end and has a circular aperture at the other end to admit concentrated solar energy. Relatively cool working fluid flows through an external duct to a toroidal inlet manifold at the aperture end of the receiver. After making a single pass through the individual tubes, hot working fluid is collected in a toroidal outlet manifold and is sent to the heat engine turbine. Various receiver design attributes and a receiver mass breakdown are given in tables 7.1 and 7.2, respectively.

Each working-fluid tube is surrounded by multiple PCM containment canisters that are constructed of the cobalt-base superalloy Haynes 188 as shown in figure 7.3. The PCM is a eutectic mixture of lithium fluoride–calcium fluoride (LiF-CaF_2) salt, which has a melting point of 1416 °F. The thermophysical properties of the eutectic LiF-CaF_2 mixture are given in table 7.3. Each canister is individually filled with PCM and hermetically sealed by electron beam welding (fig. 7.4). The canisters are stacked on each working-fluid tube with ceramic paper spacers between adjacent canisters and then brazed to the working-fluid tube. The primary

TABLE 7.1 – CBC RECEIVER DESIGN ATTRIBUTES

Solar dynamic module user power, kW	25
Receiver incident thermal rating, kWt (max.)	209
Working fluid	He/Xe (MW=40)
Receiver inlet temperature range, °F	975–1040
Receiver outlet temperature range, °F	1340–1400
Tube material	Haynes 188
Containment canister material	Haynes 188
Tube support ring material	Haynes 188
Aperture shield material	Graphite
Piping and header material	Haynes 188
External support structure material	Aluminum
Formed insulation	(a)
Multifoil insulation	Nickel, aluminum

[a]To be determined.

TABLE 7.2 – CBC RECEIVER MASS SUMMARY

Component	Weight, lbm
Phase-change material	750
Working-fluid tube	240
Containment canisters	1538
Inlet/outlet manifolds	117
Insulation	438
Shell and structure	516
Aperture plate and shield	263
Total	3862

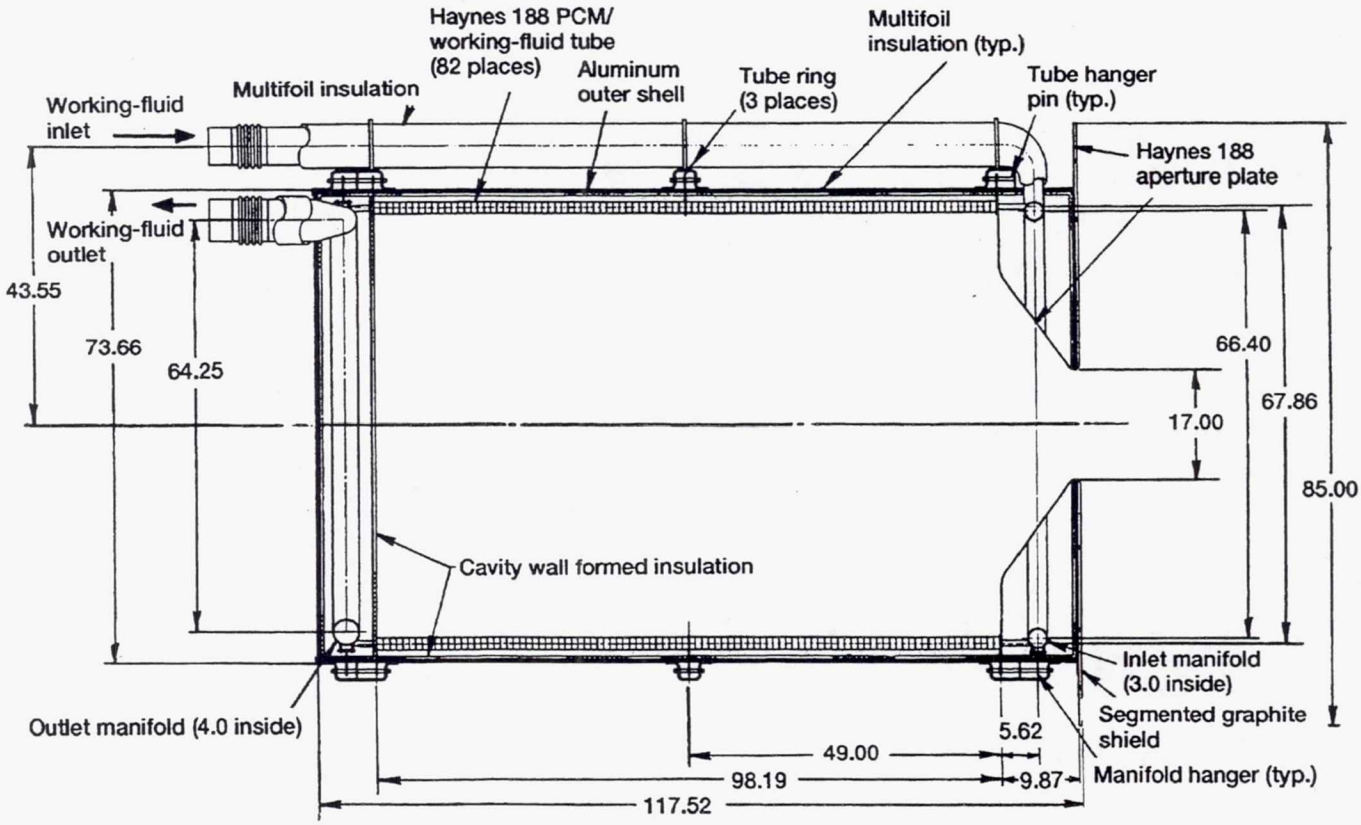

Figure 7.2.—Solar heat receiver layout. (Dimensions are in inches.)

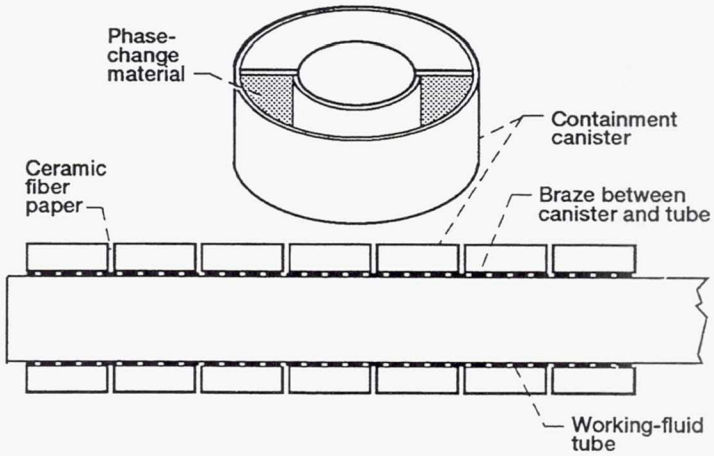

Figure 7.3.—Receiver tube configuration.

TABLE 7.3 – PROPERTIES OF EUTECTIC LiF-CaF_2 MIXTURE

Composition (by mole)	80.5 LiF, 19.5 CaF_2
Melting temperature, °F	1416
Heat of fusion, Btu/lbm	340
Solid density (melting point), lbm/ft^3	167
Liquid density (melting point), lbm/ft^3	131
Solid heat capacity (melting point), Btu/lbm-°F	0.440
Liquid heat capacity (melting point), Btu/lbm-°F	0.471
Solid thermal conductivity (melting point), Btu/hr-ft-°F	3.5
Liquid thermal conductivity (melting point), Btu/hr-ft-°F	1.0

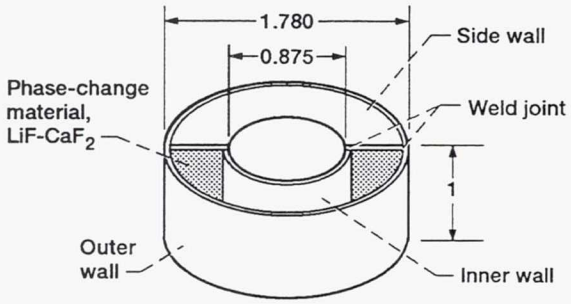

Figure 7.4.—Phase-chance material containment canister (Haynes 188). (Dimensions are in inches.)

purpose of the braze joint is to conduct heat from the canister to the working-fluid tube.

The receiver cavity walls consist of a layer of formed insulation. Energy is reflected and radiated off the cavity side wall to the back side of the receiver tubes to provide relatively uniform heat input circumferentially around the tubes. Blankets of nickel and aluminum multifoil insulation are wrapped around the formed insulation. The insulated cavity walls are enclosed in an aluminum support structure. The tubes are supported in baffles that are connected to reinforced regions of the outer support structure. Tubes fit loosely in the baffles, thereby allowing unconstrained thermal expansion. The cavity back wall moves as the tubes expand, and tube expansion is accommodated by two external baffles. The inlet manifold and the receiver support structure are protected from incident solar flux by a segmented graphite shield (fig. 7.5). The shield is designed to prevent damage from nominal on-Sun flux spillage and short-duration solar beam track-on and detrack events.

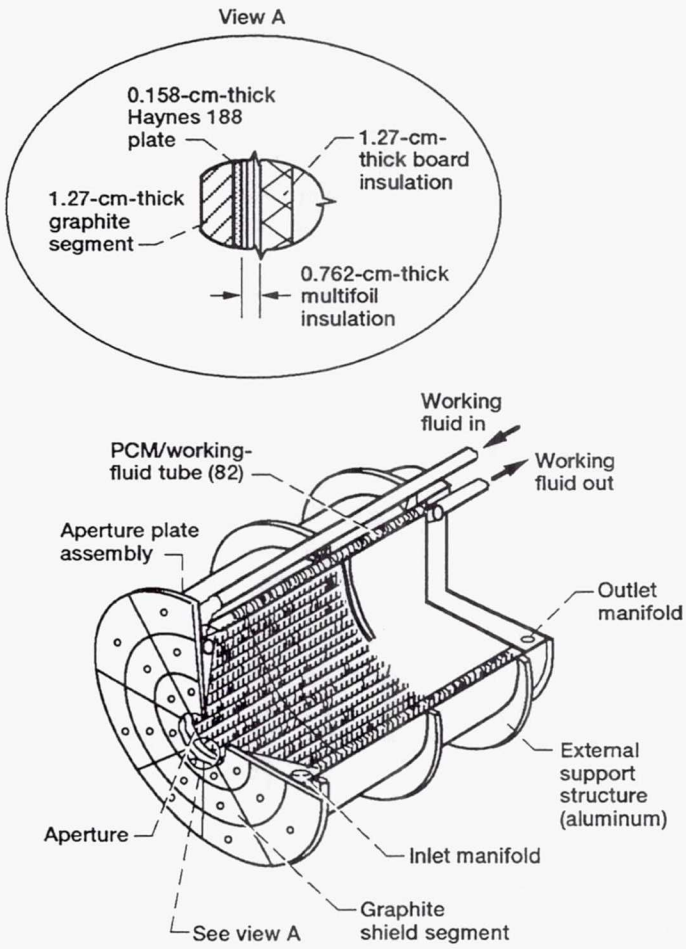

Figure 7.5.—Solar receiver with aperture plate assembly. Overall dimensions: diameter, 1.86 m; length, 2.99 m.

7.1.2 Design Rationale

The receiver design, although not optimized, is the result of a well-balanced approach to fulfilling design requirements under a variety of design constraints. The primary design requirements are to provide thermal power to the heat engine in order to produce 25 kW of continuous power to the user and to meet a 30-year design life. A complete set of design specifications and requirements can be found in reference 7.1. Major design constraints include the given flux input distribution from the offset, segmented surface concentrator (see chapter 6), the allowable working-fluid pressure drop, the cost, and the allowable mass or volume consistent with NSTS launch packaging requirements (see section 5.9).

The receiver cavity length and diameter were chosen to be consistent with the concentrator flux input and the NSTS orbiter packaging guidelines. The aperture diameter was optimized to maximize the net energy that would be retained by the receiver over an orbit. This optimization involved the following time-dependent heat balance terms: solar flux admitted through the aperture, solar spillage flux on the aperture plate, reflected solar flux out of the receiver cavity, and infrared flux radiated out of the receiver cavity (ref. 7.2). The total mass of PCM employed was determined iteratively on the basis of the minimum PCM mass required to make performance (i.e., to deliver the required thermal power to the heat engine).

The PCM selected, a eutectic composition LiF-CaF_2 salt, was chosen on the basis of melting temperature, high heat of fusion, compatibility with the containment material, and experimentally demonstrated, stable thermophysical properties. Other PCM's considered, but eventually dropped, were LiF and the eutectic composition lithium fluoride–magnesium fluoride (LiF-MgF_2). LiF was dropped from consideration because its melting temperature was deemed too high, and LiF-MgF_2 was dropped because of its lack of stable, repeatable properties during thermal cycling tests.

The diameter, length, wall thicknesses, and number of working-fluid tubes and PCM containment canisters were chosen to satisfy several design considerations. Design considerations include adequate heat transfer rates to the salt and the working fluid, conservative canister ullage or void volume to allow for liquid salt expansion, low thermal stresses, low working-fluid pressure drop, and salt compartmentalization. Placing the salt in small volumes or compartments serves two purposes: void volume is localized to accommodate salt melting expansion and thus minimize stress buildup in canister walls, and in the event of a canister leak, only a small portion of salt is lost, reducing the effect of salt contamination and insignificantly reducing receiver thermal storage capacity.

The working-fluid tube and canister material, Haynes 188, was selected for its excellent high-temperature structural properties and its excellent compatibility with the LiF-CaF_2 salt and vacuum environment. Haynes 188 is also readily fabricable and weldable and is available in the required product forms. The nickel-base superalloy Inconel 617 is considered a close backup material to Haynes 188.

7.1.3 Analyses, Tests, and Development Efforts

7.1.3.1 Analyses. – The overall receiver design is based on analyses performed by Allied-Signal Aerospace Company. By using the computer program SOLREC–TSD (Solar Receiver–Thermal Storage Device), the transient thermal performance of the orbital receiver was predicted. For a description of SOLREC–TSD and receiver performance predictions, see references 7.3 and 7.4. Other receiver analyses were performed at Rocketdyne by using the dedicated computer program RECVR (ref. 7.5). In these preliminary studies the performance effects of PCM containment canister dimensions and optical properties, the direction of working-fluid flow, and the recirculation of working-fluid flow were investigated.

Further receiver analyses were also performed at NASA Lewis by using a modified version of SOLREC–TSD that was incorporated into the solar dynamic module performance prediction code CCEP (Closed Cycle Engine Program), see references 7.6 to 7.13. Of particular interest are two view factor calculation computer programs, RADVIEW and VFY, which are contained in SOLREC–TSD and CCEP, respectively. Both of these computer programs calculate three-dimensional geometric view factors for the inside of a diffuse, cylindrical cavity with an aperture at one end (ref. 7.14). Analyses with various PCM mass distributions along the receiver tubes show promising results for reducing maximum tube temperatures and receiver mass (refs. 7.15 and 7.16).

Several detailed canister thermal and structural or life analyses have been performed by the contractor and NASA Lewis. Using the general-purpose computer code ANSYS, Allied-Signal predicted canister thermal stresses that were then used for canister design life prediction (refs. 7.17 and 7.18). NASA Lewis has also performed canister thermal-structural analyses by using the commercially available computer program MARC (refs. 7.19 and 7.20) and has developed viscoplastic constitutive models for Haynes 188 and solid LiF-CaF_2 salt to predict material stress-strain response with improved accuracy (refs. 7.21 and 7.22). In order to improve canister life assessment techniques, a grant (NAG3–1218) with the University of California at Santa Barbara has been established to study high-temperature material damage mechanisms and long-term life assessment techniques that are in use outside the United States (ref. 7.23). Refer to the bibliography for more documentation of canister life analyses.

In addition, dedicated computer programs were developed at NASA Lewis and at Oak Ridge National Laboratory to further analyze the complex, canister phase-change heat transfer; see references 7.24 to 7.28. Parametric analyses

confirmed that the baseline canister is well designed (ref. 7.29). A videotape animation of numerical results was also prepared to visualize the PCM freeze-thaw processes within a TES canister (ref. 7.30).

Preliminary thermal and structural analyses of the receiver aperture plate assembly have been performed by NASA Lewis (refs. 7.31 to 7.33). Studies to date have been performed to determine the aperture plate tolerance to highly concentrated solar flux resulting from optical misalignment of the solar dynamic power module (SDPM). These results, in turn, have been used to guide the design and operating modes of the SDPM pointing and tracking subsystem.

7.1.3.2 Tests.—Several test programs have been conducted with the objectives of demonstrating receiver tube and canister thermal performance, determining long-term canister material compatibility with the LiF-CaF_2 salt and vacuum environments, expanding the existing canister material mechanical property data base, and determining the optical properties of Haynes 188 with various surface preparations.

To demonstrate the receiver salt storage tube concept, Allied-Signal successfully fabricated and tested a full-size, 3-ft receiver tube segment for over 4800 simulated 90-min orbital heating-cooling cycles (refs. 7.34 and 7.35). Other tests at NASA Lewis with three canisters demonstrated the structural integrity of canisters operating under severe heating conditions with deliberately configured adverse salt distributions (i.e., distributions that do not allow the salt to expand while melting (refs. 7.19, 7.20, and 7.36). Valuable information on canister internal salt distributions was obtained through the use of radiography. Further tests with the same canisters demonstrated the relative insensitivity of canister thermal performance to several ground-test orientations (ref. 7.25).

Material compatibility tests were conducted both at the contractor and at NASA Lewis. At Allied-Signal, canisters constructed of Haynes 188 were cyclically heated for up to 20 000 hr. Postexposure metallography revealed an acceptably low corrosion rate (refs. 7.35 and 7.37 to 7.40). At NASA Lewis, 1507 °F isothermal exposures of Haynes 188 have been conducted in environments of salt, vacuum, and air. The longest exposure period (22 500 hr) was completed in late 1991. The nickel-base backup materials, Haynes Developmental Alloy 230 and Inconel 617, have been exposed to these environments as well.

Postexposure metallographic examination of Haynes 188 specimens showed a very low corrosion rate in the salt environment, an acceptably low mass loss in vacuum, and the anticipated stable oxide layer formation in the air environment. Postexposure tensile tests and short-term creep tests (i.e., test durations of less than ~1000 hr) were also performed at 1430 °F . In general, test results from exposed specimens compared well with those from unexposed specimens and with the published data base. A reduction in low-temperature ductility occurred as a result of anticipated thermal aging, but this effect was independent of the exposure environment. For detailed results, see references 7.41 and 7.42 and review the bibliography.

Several NASA Lewis material test programs were undertaken to expand the mechanical property data base of Haynes 188 and, for the most part, are still ongoing. Long-term, monotonic creep rupture tests at various temperatures and stress levels are in progress. Estimated creep rupture times for one-third of the tests are longer than 3 years. In another program, creep threshold, thermal-mechanical, and isothermal, low-cycle fatigue tests of Haynes 188 were performed (ref. 7.43). Strain-controlled, stress relaxation experiments were conducted as well.

Although not funded by the Space Station *Freedom* Program, an important test program was undertaken at NASA Lewis to measure the mechanical properties and stress-strain behavior of the eutectic composition LiF-CaF_2 salt. Tests were performed at a variety of temperatures and strain rates (refs. 7.44 to 7.47). These data are useful for conducting PCM containment canister stress analyses.

A program was also conducted to measure and tailor Haynes 188 radiative characteristics, namely, solar absorptance α_s and thermal emittance ϵ. The goal of this program was to achieve a diffuse Haynes 188 surface with moderate α_s (i.e., ~0.5), high ϵ (i.e., ~0.8 at 1520 °F), and excellent long-term vacuum stability at elevated temperature. This combination of optical properties improves the absorbed flux distributions of receiver tubes, thereby enhancing receiver thermal performance and operational life. Although the stated goals were not achieved within the available program resources, a wide variety of surface treatment techniques were employed and significant data were obtained. For example, pristine and surface-modified coupons of Haynes 188 were exposed to a vacuum environment at 1507 °F for as long as 5215 hr and to an atomic oxygen environment at both 93 and 1520 °F for fluences as high as 5.6×10^{21} atoms/cm^2. After environmental exposure the coupon mass, surface chemistry, surface morphology, and optical properties were evaluated. See reference 7.48 for a detailed discussion of program test results.

7.1.3.3 Development efforts.—Receiver development activities focused on PCM containment canister fabrication, salt filling, and inspection. The goal of these activities was to develop the techniques and processes for cost effectively producing tens of thousands of highly reliable canisters. The Haynes 188 canister fabrication approaches explored included electron-beam-welded construction from rolled and punched sheet, from machined bar stock, and from multistep, cold-formed sheet. Rocketdyne and Allied-Signal undertook efforts in canister weld joint design, weld joint placement, and the combined use of nondestructive inspection and statistical sampling techniques for large production runs.

In efforts to develop canister-filling techniques, salt liquid and compacted solid powder approaches were considered. Two key technical issues were addressed involving the handling of LiF-CaF_2 salt during filling operations: ensuring

adequate off-gassing of water vapor and oxygen from the salt, and minimizing preferential volatilization of the LiF salt component. The former issue is crucial in eliminating all significant salt attack on the containment alloy, Haynes 188. The latter issue is very important in assuring that eutectic composition is maintained so that key thermophysical properties, such as melting temperature and heat of fusion, are not affected.

Detailed information on these developmental efforts can be found in references 7.34 and 7.49 to 7.51.

7.1.4 Required Development

Further receiver development is required in the following areas: canister design and fabrication, cavity and TES tube design, working-fluid flow loop design, aperture plate assembly design, thermal "state-of-charge" determination techniques, and long-term, high-temperature component life assessment techniques. These areas are discussed sequentially at greater length in the following paragraphs.

Further canister fabrication development is needed to refine canister metal-forming operations, weld joint design and welding parameters, weld inspection techniques and approaches, and salt-fill-hole closure weld design. Canister production salt-filling techniques need further work to ensure that a repeatable process is developed which precludes salt contamination and distillation. In addition, a braze material must be selected and a brazing technique developed for attaching the canisters to the working-fluid tubes. The braze joint must provide high thermal conductance between the canisters and the working-fluid tube for the 30-year design life of the receiver.

Further heat transfer analyses are needed to refine the receiver cavity design by studying the effects of cavity length-to-diameter ratio, variable cavity diameter, tube-to-tube spacing, and internal cavity wall radiative properties. In conjunction with these studies, TES tube design refinements could be made to maximize the total mass of PCM melted and to minimize the receiver cavity orbital temperature variation. Tube performance increases could be achieved by considering, as a function of tube length, variable canister diameters, wall thicknesses, contained PCM masses, and void volume fractions (refs. 7.7, 7.15, and 7.16).

The design of the receiver working-fluid flow loop needs further development. Design attributes that require special attention include low fluid pressure drop through ducts and manifolds, high structural compliance to accommodate differential and gross thermal expansion, and working-fluid containment. Although low pressure drop is extremely important for heat engine efficiency, fluid containment is the most important design feature of the fluid flow loop because loss of working fluid constitutes a SDPM single-point failure. Therefore, highly compliant manifold designs that minimize the number and size of weld joints should be developed to preclude large thermal stresses that could fail weld joints. In addition, double containment designs for manifolds and ducts should be considered to further reduce the likelihood of working-fluid leaks.

The aperture plate assembly design requires further development in the areas of material selection, thermal performance, and structural design. The specific graphite shield material chosen requires testing to verify its capacity for withstanding high temperatures, large temperature gradients, and the low-Earth-orbit environment of vacuum and atomic oxygen. The design must incorporate a highly effective, multilayered insulation (composed of high-temperature metal foils or another material) to protect the underlying receiver structural metal from temperature extremes. The insulating performance of the aperture design must be validated through analyses and tests. Lastly, the aperture plate assembly layers must be mechanically supported to allow for unconstrained thermal expansion. This requirement is most critical for the shield layer, which directly receives the highly concentrated solar flux. Analyses and tests are required to determine the extent of shield segmentation and to evaluate a scheme to attach shield segments to the other aperture plate assembly layers.

Techniques are needed to determine the so-called receiver state of charge, or the quantity of stored thermal energy within the receiver. Knowledge of the receiver state of charge is necessary for SDPM operating modes including cold startup and peaking/recovery power production as well as for long-term energy balance maintenance. Basic areas needing further work include identification of robust, long-lived sensors, judicious selection of the receiver parameters to measure, and development of thermal control and state-of-charge algorithms.

The last receiver area requiring further, focused development efforts is the prediction of long-term, high-temperature component design life. Currently, life assessment techniques that specifically address the receiver TES canister design problem (i.e., thermal-mechanical loading of a welded component for 30 years in harsh salt and vacuum environments) do not exist. The best available approach used in the United States is to employ the American Society of Mechanical Engineers (ASME) Code Case N–47 design code. Originally developed for designing terrestrial nuclear powerplant systems, this code is used to very conservatively design components operating under ostensibly isothermal, constant-load conditions. However, the code does not predict component life but instead provides guidelines for making "safe" designs. This can result in overly massive component designs for aerospace systems. Furthermore, the code is based on mechanical property data for only a handful of so-called code-qualified materials that have been extensively tested and on a wide variety of experience factors or safety factors. The canister material of construction, Haynes 188, is not code qualified, nor does it have the necessary experience factor data base. Therefore,

further work on canister life assessment is required in the areas of identifying and understanding applicable material damage mechanisms, developing methods for designing components to survive these deterioration mechanisms, and evaluating the potential use of European or other design methods that better address the canister design problem.

7.1.5 Recommendations and Ideas

In addition to the suggestions given in the preceding section four other recommendations are offered here concerning the development of the solar heat receiver. In short, the recommendations are as follows: modify the multiple layers of construction in the aperture plate assembly, emphasize integration of receiver components early in the receiver design cycle, emphasize integration of the receiver with the SDPM early in the receiver design cycle, and structure future receiver development programs to be hardware intensive (i.e., allocate a large fraction of program resources for the fabrication, inspection, testing, and documentation of full-scale test hardware). Each of these recommendations is discussed more thoroughly in the following paragraphs.

The proposed baseline aperture plate assembly is constructed of four layers (fig. 7.5). From the outside (facing the concentrator) inward (toward the receiver cavity wall), the assembly layers consist of graphite plate segments, Haynes 188 plate, multifoil insulation (MFI) with an unspecified foil material, and unspecified formed insulation board, respectively. On the basis of results from one-dimensional heat transfer analyses (refs. 7.31 and 7.32), the following basic design changes are recommended:

(1) Switch the positions of the Haynes 188 and MFI layers. This protects the Haynes 188 material from exposure to high graphite temperatures that would quickly melt the Haynes 188 after only tens of seconds of worst-case concentrator mispointing.

(2) Construct the MFI from a refractory metal, such as tungsten. Refractory metals have extremely high temperature capability, which increases the allowable high-flux residence time. These metals are well suited for vacuum insulation applications as well.

(3) Utilize two layers of graphite segments around the aperture periphery for a distance equivalent to approximately one aperture diameter (i.e., 17 in.). This portion of the aperture plate must endure the highest temperatures and is thus subjected to the maximum rate of atomic oxygen attack and sublimation mass loss. This simple approach increases the insulating performance of the aperture plate assembly with only a minor mass penalty and conservatively employs a sacrificial layer to combat deleterious environmental effects.

(4) Change the geometry of the aperture plate assembly from a plate to a frustum. This straightforward design modification reduces the amount of absorbed solar energy by a factor of the cosine of the frustum angle while not affecting the ability to dissipate radiant energy. For example, with a frustum angle of 45° the maximum graphite temperature can be reduced by more than 450 deg F during transient concentrator mispointing events (ref. 7.31).

The second recommendation, to emphasize early integration of receiver components, is given because of the inherent interdependence of receiver component performance as well as demanding design requirements. For example, TES canister dimensions and wall thicknesses are restricted by fabrication constraints, environmental durability considerations, and thermal-structural performance requirements. The TES canister must also be compatible with the design of the working-fluid tube and manifold, which is driven by fluid containment, fluid pressure drop, and structural compliance requirements. However, the working-fluid loop design must be compatible with the receiver cavity geometry and the heat transfer environment, which in turn, are determined by TES canister heat transfer. This example illustrates the interdependence of receiver components and suggests that component development should ideally proceed in parallel to avoid integration problems in the later stages of a program.

The third recommendation, to emphasize early integration of the receiver with the SDPM, is substantially similar to the second recommendation, but applies at the module level. The interplay of SDPM components during operation can substantially affect the design of the receiver. In order to avoid SDPM component incompatibilities late in the development program, thoughtful consideration must be given to the effects of receiver interfaces with other components and SDPM operating modes. For example, the concentrator design obviously affects the receiver flux distribution and the resulting cavity temperatures. The power conversion unit state points also clearly affect receiver temperatures in a fairly predictable manner.

However, the heat rejection assembly radiator and the SDPM pointing and tracking subsystem also have an important, but perhaps less obvious, effect on receiver design. By virtue of being collocated, the radiator casts a shadow on the concentrator and affects receiver cavity flux distributions. The pointing and tracking subsystem characteristics affect the time-dependent cavity flux variations in addition to influencing the receiver aperture plate design, which must tolerate highly concentrated solar fluxes during controlled and credible uncontrolled mispointing events.

Another example concerns SDPM operating modes, some of which are not yet totally defined. The receiver must be designed to accommodate off-design and contingency SDPM operating modes such as cold startup, emergency shutdown with and without coolant, and sustained contingency low-power production. Because these operating modes can dramatically affect PCM freezing and melting patterns and receiver temperature distributions, the thermal and structural performance of the receiver will be affected as well.

The last example concerns mutual contamination effects of SDPM components. Because the receiver is the hottest component, it is likely to be the strongest source of contamination. Some issues already identified and initially addressed include chromium sublimation from superalloys and TES canister salt leaks (refs. 7.52 to 7.54). The volatilization of chromium and its subsequent deposition on concentrator and radiator surfaces could impair the performance of these components. The same is potentially true of canister salt leaks as well as mass loss from the graphite aperture shield. These risks, which were initially shown to be minor, should be quantified in greater detail. By using this information, appropriate design choices can be made concerning receiver operating temperature, canister weld reliability, and area margins for the concentrator and the radiator.

The fourth and final recommendation, to structure a hardware-intensive receiver development program in the future, is an outgrowth from experience gained in the latest NASA Lewis receiver programs. In the least mature receiver technological area, the phase-change thermal energy storage subsystem, the task of reliably and effectively fabricating, filling, and sealing PCM containment vessels remains a difficult endeavor. Furthermore, experiments to demonstrate the structural integrity of TES subsystem designs and the long-term chemical compatibility of salt-metal systems proved to be instrumental either in obtaining a high level of confidence in the design or in identifying needed design improvements. Nowhere is this better illustrated than in the largely successful compatibility programs (e.g., refs. 7.37 to 7.40 and 7.42) and in the experience gained from large-scale salt-filling processes and full-scale hardware testing of the advanced-development receiver program (see the following section).

Another important lesson that was learned in the development of TES subsystems is to thoroughly inspect and document the fabrication history of hardware at the *start* of a test program. A concerted effort in this regard makes the task of post-test data interpretation and analysis much easier because documentation of initial salt distributions and the as-built container condition, for example, is available. Should anomalies occur in the data (or salt containers fail), information on how the TES container was built and filled with salt can prove crucial in determining if the anomaly was the result of normal operation or of manufacturing processes.

The results from these hardware programs, whether good or bad, have contributed the most toward improving receiver technology and design. Therefore, further fabrication and performance or endurance testing development work is encouraged not only for the TES subsystem but also for the working-fluid flow loop subsystem, the aperture plate assembly, and the full-scale receiver.

7.2 Advanced-Development Receiver Design

The advanced-development receiver program initially developed and analyzed more than eight conceptual receiver designs that were compatible with either an organic Rankine cycle (ORC) heat engine or a closed Brayton cycle (CBC) heat engine (ref. 7.55). After further analysis and design work for a single ORC and a single CBC receiver concept, the CBC receiver concept was chosen for detailed design, fabrication, and testing of a full-scale unit. This concept was chosen on the basis of predicted performance, fabricability, cost, and technical risk (ref. 7.56). The resulting design of the advanced-development receiver test article is described here.

7.2.1 Design Description

The advanced-development receiver design, which is considered an alternative or backup to the baseline receiver design, is similar to that design in size, mass, design approach, and overall thermal performance. However, the advanced-development receiver design (figs. 7.6 and 7.7) is distinctively different from the baseline design in two areas: the TES container design and the working-fluid tube manifolding design. These differences are highlighted here.

The advanced-development receiver design employs 24 long, tubelike annular PCM containers constructed of Inconel 617 instead of approximately 7800 short canisters made from Haynes 188. A single TES receiver tube, measuring approximately 2 in. in inner diameter, 4 in. in outer diameter, and 60 in. in length, is shown in figures 7.8 and 7.9. The annular tube space is filled with 20-percent-dense nickel-felt matrix material that is impregnated with an eutectic composition LiF-CaF_2 salt. The outer tube wall consists of a $\frac{1}{4}$-in.-pitch bellows that is designed to accommodate large thermal strains. The heat engine working fluid, a 40-molecular-weight helium-xenon gas mixture, flows around a 1-in.-diameter cylindrical spud positioned inside the inner receiver tube. The spud effectively increases the gas Reynolds number, thereby increasing the forced-convection heat transfer coefficient while incurring a slight pressure drop penalty.

The working-fluid manifold design consists of long, spider plumbing runs from domed, cylindrical inlet and outlet plenums (fig. 7.10). This is in direct contrast to the baseline receiver design, which utilizes toroidal inlet and outlet headers and short, straight plumbing runs. The cylindrical plenums distribute flow uniformly between receiver tubes with a very low pressure drop (i.e., 2.5 percent of the inlet pressure (92 psia)). The long plenum radial extension piping readily accommodates differential expansion between

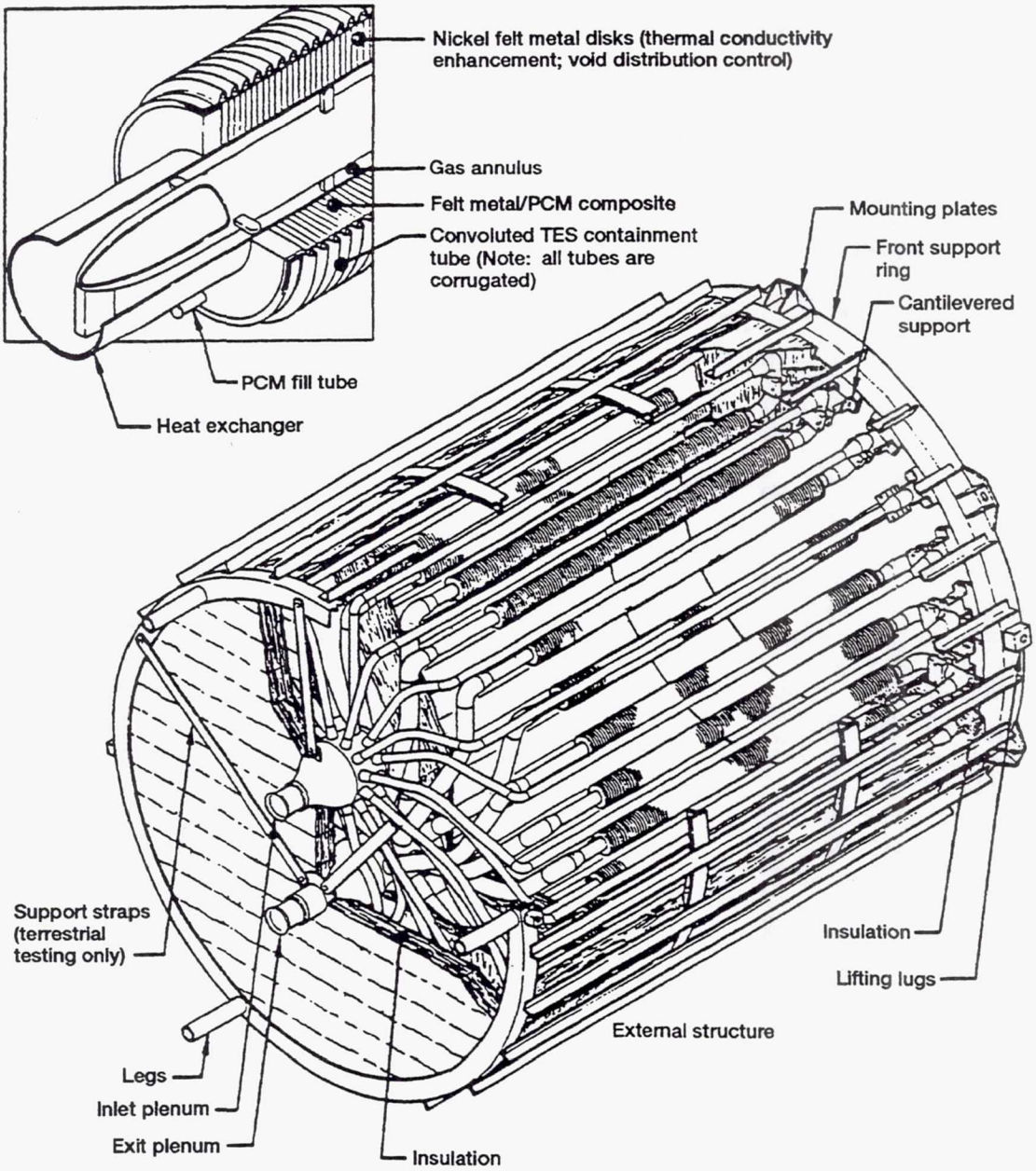

Figure 7.6.—Advanced-development receiver design configuration.

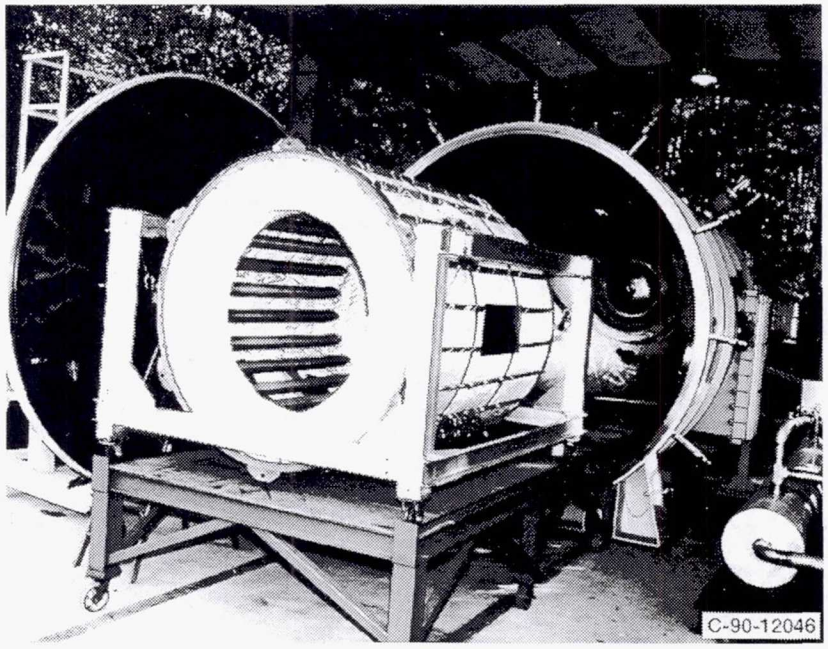

Figure 7.7.—Advanced-development receiver prior to testing in vacuum chamber.

receiver tubes. To accommodate gross thermal expansion, the entire receiver tube and manifold assembly is cantilever supported at the aperture end by saddle clamps attached to the front structural ring. The receiver structure consists of stainless steel front, midspan, and back structural rings connected by longitudinal angle irons (figure 7.11). The receiver tubes are insulated by ceramic fiber blanket insulation that also forms the cavity walls.

A third, perhaps more subtle, difference in the respective receiver designs is that the advanced-development receiver was designed to meet early SD program requirements (circa 1985) and was fabricated as a ground test article (with a 1000-hr test life). As such, the advanced-development receiver design was based on solar input from a continuous-surface Newtonian concentrator and on a constant working-fluid inlet temperature and did not have to accommodate SDPM peaking or startup operating modes. An aperture plate assembly was not designed or built because an internal cavity heat source would be used during ground vacuum testing. Additionally, less expensive materials were permitted for fabricating receiver insulation, structure, and working-fluid plumbing and manifolding hardware.

The advanced-development receiver design and fabrication methods are thoroughly described in references 7.57 and 7.58. Its dimensions, a thermal performance summary, and a mass breakdown are given in tables 7.4, 7.5, and 7.6, respectively.

7.2.2 Design Rationale

The key feature of the advanced-development receiver is the TES tube design. The motivation for using the felt-metal matrix material in the PCM containment volume is twofold. First, the nickel felt enhances conduction (and radiation) heat transfer through the otherwise poorly conducting salt. This reduces the temperature gradients (and associated thermal strains) dictated by TES tube charge and discharge requirements. Second, the nickel felt localizes salt freezing and void formation due to individual fiber wetting characteristics. Because the felt-metal wicking height (against gravity) is greater than the 4-in. outer diameter of the TES tube, the liquid salt uniformly wets the entire volume of felt metal (ref. 7.59). In addition, the felt metal eliminates buoyancy-driven flows within the liquid salt. Thus, the salt melting and freezing behavior is essentially independent of gravity when ground tested in a horizontal orientation. Hence, by means of ground tests (in normal gravity), flight performance (in microgravity) can be readily verified without the need for expensive flight testing.

Other benefits of the advanced-development receiver TES tube design approach (when compared with the baseline receiver approach) include fewer PCM containers to be filled and less welding and inspecting of both PCM containers and working-fluid plumbing and manifolding. However, both these benefits come at the expense of less redundancy in the

Figure 7.8.—Thermal energy storage tube and flow spud.

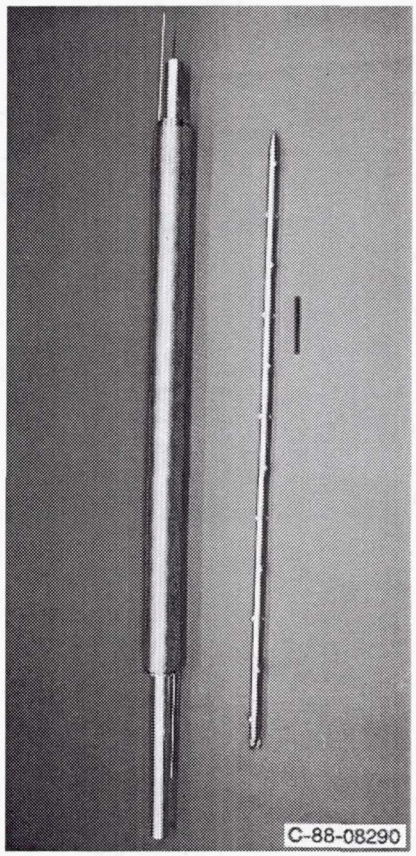

Figure 7.9.—Thermal energy storage tube.

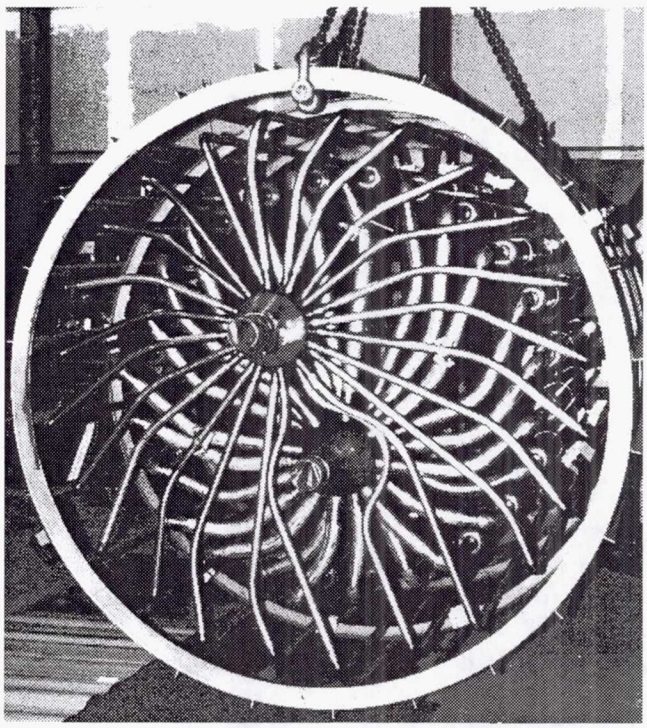

Figure 7.10.—Receiver manifolding.

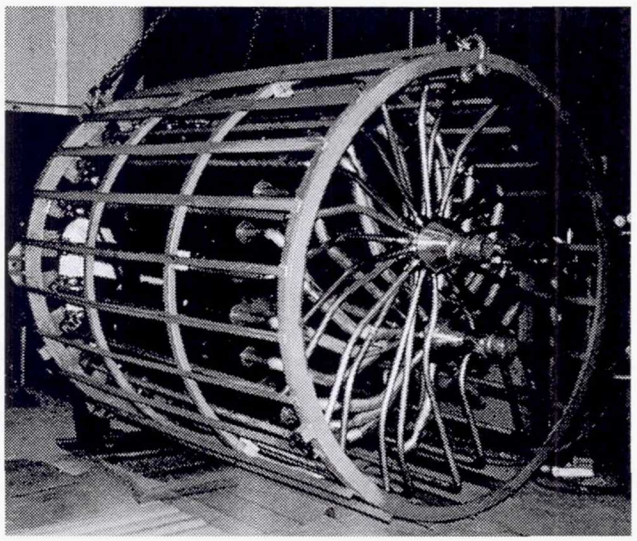

Figure 7.11.—Receiver structure.

TABLE 7.4 – RECEIVER DIMENSIONS

Subsystem	Component or parameter	Dimensions	
		mm	in.
Receiver cavity	Cavity diameter	1778	70
	Cavity length	2032	80
	Receiver outer diameter (OD)	2184	86
	Total receiver length	2794	110
	Aperture diameter	330	17
Heat exchanger	HX/TES tube centerline diameter	1575	62
	HX tube OD	51	2
	Spud tube OD	25	1
	HX tube wall thickness	1.5	0.06
Corrugated TES containment tube	Wall thickness	0.25	0.01
	Convolution OD	100	3.94
	Convolution ID	91	3.58
	Convolution pitch	6.4	0.25

TABLE 7.5 – RECEIVER THERMAL PERFORMANCE SUMMARY

Total solar input to receiver, kW	184.9
Minimum receiver efficiency, percent	91.3
Maximum receiver thermal loss, kW (percent of total)	13.7 (7.4)
Reflection	0.8 (0.4)
Reradiation	9.0 (4.9)
Conduction through insulation	3.9 (2.1)
Sensible energy source, kW (percent of total)	2.4 (1.3)
Temperatures (nominal quasi-steady operation), °C (°F):	
Control of turbine inlet temperature	705 (1300); −9 (−15); 16 (30)
Maximum TES containment temperature	896 (1645)
Maximum TES temperature gradients:	
Circumferential	72 (162)
Axial	116 (241)
Maximum heat exchanger tube temperature	822 (1512)
Maximum insulation temperature	955 (1751)
Pressures:	
Pressure loss, percent of inlet	2
Maximum variation between heat exchanger tubes, percent	0.4

TABLE 7.6 – RECEIVER MASS BREAKDOWN

Receiver subsystem or component	SDHRT[a] weight		Flight weight	
	kg	lb	kg	lb
Heat exchanger/TES heat storage tubes:	759	1673	759	1673
PCM/LiF-CaF_2	319	703	319	703
Nickel felt-metal disks	298	657	298	657
TES containment	46	101	46	101
Heat exchanger tubing	96	212	96	212
Receiver insulation	454	1000	227	500
Heat exchanger tubing and pipe	338	745	49	108
Inlet and exit plenums	82	181	82	90
Receiver structure	545	1202	272	600
Total receiver weight	2178	4801	1389	2971

[a]Solar dynamic heat receiver technology contract.

TES subsystem (i.e., fewer salt containers) and an arguably more involved salt-filling procedure.

7.2.3 Analyses, Development Efforts, and Tests

7.2.3.1 Analyses. – Receiver and TES tube thermal analyses were performed by Boeing using several dedicated Fortran thermal analysis computer codes. The receiver TES tubes, manifolds, piping, insulation, and structure were modeled and analyzed. Diffuse, gray receiver cavity radiation heat transfer was analyzed by using the Boeing proprietary computer code RADSIM with an axisymmetric assumption (i.e., that each TES tube experiences the same radiative environment). PCM heat transfer was analyzed in three dimensions. Receiver analyses were performed both for flight operation and for the actual ground test configuration including test support hardware. In addition, TES tube heat transfer was analyzed for later comparison with data from initial, benchtop tests with subscale length (6 in.) test articles. See reference 7.59 for detailed information concerning these computer codes.

Thermal-stress analyses of receiver tube and structural components were performed by using the general-purpose computer codes ANSYS and NASTRAN (ref. 7.59). Analyses were also performed to predict receiver survivability in a micrometeoroid and space debris threat environment (ref. 7.60).

7.2.3.2 Development efforts. – Major development activities were undertaken in TES tube materials and fabrication, TES tube salt filling, and test support hardware. In TES tube materials and fabrication, the compatibility of several potential containment alloys with the salt was investigated.

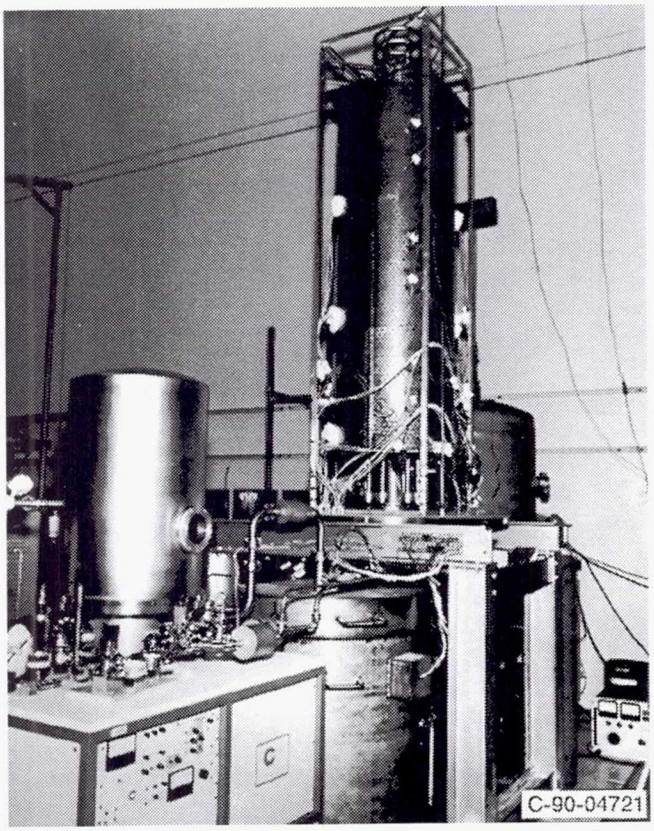

Figure 7.12.—Salt-filling facility used for thermal energy storage tubes.

Thermal exposure periods up to 10 000 hr were completed and then metallographic analyses were performed. Various felt-metal matrix materials were tested to determine liquid salt wicking characteristics. Significant advancements were also made in methods of heat treating felt metals to remove contaminants and improve molten salt wetability. Methods for laser welding thin Inconel 617 sheet to a thick, TES tube end cap made from Inconel 617 were developed as well. Results from these activities directed the eventual material selection and design of advanced-development receiver TES tubes. See references 7.57, 7.59, and 7.61 for detailed information regarding these efforts.

Methods and a facility for casting salt into full-size TES tubes were developed. The salt-filling facility is shown in figure 7.12. Key attributes of this facility include the ability to accurately batch-fill TES tubes with a specified mass of salt while maintaining salt eutectic composition and a high degree of cleanliness. An improved method for electron-beam welding of the TES tubes was developed as well (ref. 7.57).

In order to simulate the incident solar flux distribution on the internal walls of the receiver cavity, a solar simulator lamp array was developed to provide thermal input for receiver vacuum testing. The lamp array (fig. 7.13) is a nearly cylindrical plug that fits into the receiver cavity through the aperture end. The frame is constructed from the niobium alloy C–103 because of this material's superior

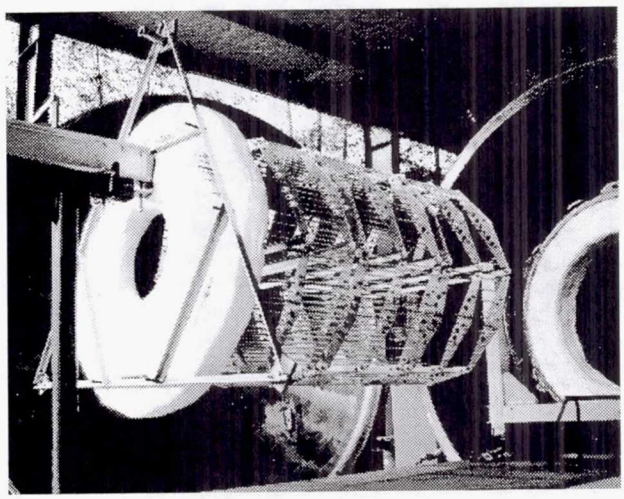

Figure 7.13.—Quartz lamp array.

creep properties and vacuum compatibility in the 1700 to 1880 °F operating temperature range (refs. 7.62 and 7.63). The array has 30 zones, 5 axial and 6 circumferential, each of which has multiple, 1-kW linear quartz lamps that serve as the heating elements.

The electric power to each zone was independently controlled during receiver testing. Because these lamps had no prior history of extended use in high-temperature vacuum environments (where lamp-end-seal temperature limits are exceeded), the suitability of lamps for this application was questionable. Hence, an endurance test was conducted, prior to lamp array design, that conclusively demonstrated the long-term integrity of several lamps when operating continuously at 1700 °F in vacuum (see ref. 7.59 for details).

In addition to the solar simulator heat source described in the preceding paragraph, the other major piece of test support hardware fabricated was the SDPM power conversion unit (PCU) simulator. The PCU simulator (fig. 7.14) employs heat exchangers, valves, supply tanks, and a blower configured in a closed loop. The sole purpose of this hardware is to provide the advanced-development receiver inlet plenum during testing with the proper helium-xenon gas mixture composition, flow rate, temperature, and pressure that emulates what an actual SDPM PCU would provide during operation on Space Station *Freedom*. A detailed description and schematic of the PCU simulator are given in references 7.62 and 7.63.

7.2.3.3 Tests. – Several performance tests were conducted with subscale-length TES tubes. Various methods for enhancing salt heat transport (e.g., fins or felt metal) and various salt container designs (straight wall or bellows) were tested. Computed-tomography TES tube inspection techniques were effectively used to examine internal salt distributions and the condition of the felt metal. Results from these tests verified the thermal performance attributes of the final TES tube design adopted, which employs nickel felt metal and a small-

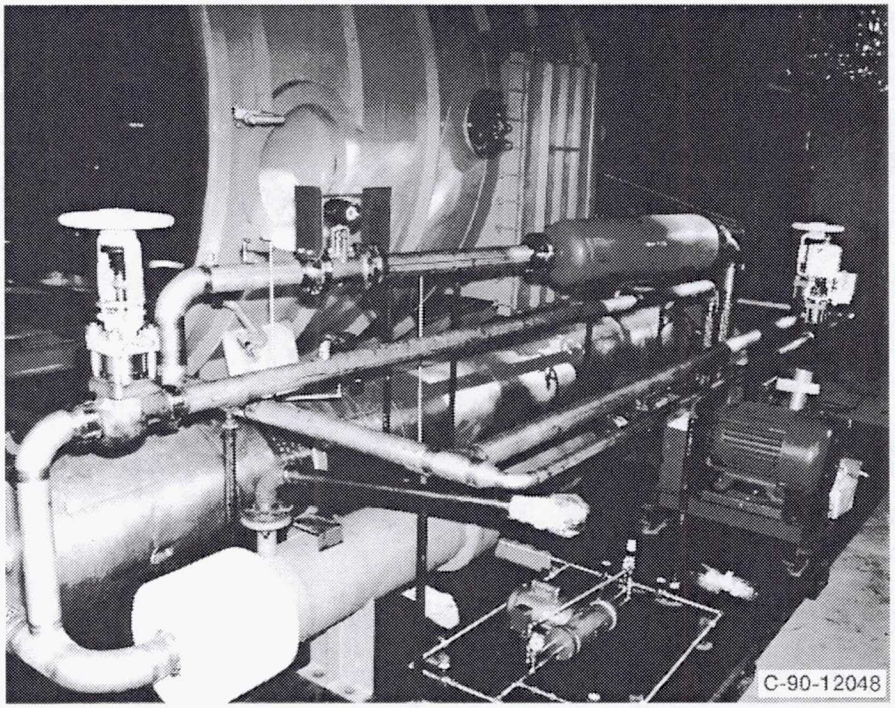

Figure 7.14.—Power conversion unit simulator.

pitch-bellows outer wall. A detailed account of performance testing and inspection results is given in reference 7.59.

The major test activity of the advanced-development receiver program was the thermal-vacuum performance testing of the full-scale receiver. This testing took place at Boeing's Tulalip Test Site in Marysville, Washington, from October 9 to November 3, 1990. During the test campaign, 58 simulated Space Station *Freedom* orbital cycles and various cold startup and shutdown operating modes were successfully completed. Table 7.7 lists and describes the test modes conducted. The measured receiver thermodynamic performance was closely matched by pretest analytical predictions. Hence, the thermal performance computer code developed in the advanced-development receiver program, and now validated with test data, is available to support further receiver studies. See references 7.62 and 7.64 for detailed test results.

The solar simulator and the PCU simulator performed well during the 4-week testing period. Occasional minor problems were corrected quickly with minimal or no loss of data. Post-test inspections revealed no apparent damage to the receiver insulation, structure, or working-fluid piping and manifolding. However, two types of damage to several receiver TES tubes were visually observed: four TES tubes had 11-in.-long kinks where the bellows outer wall was radially displaced by a distance of up to one quarter of the bellows outer diameter, and 10 TES tubes had cracks at the peak of the first bellows convolution adjacent to the TES tube exit or inlet end cap. A small amount of salt did leak out of the cracked TES tubes but did not produce any visible corrosive attack of any materials within the receiver cavity. Furthermore, no receiver performance degradation was measured as a consequence of the salt leakage, which suggests that such leaks can be benign (ref. 7.62).

The cause of TES tube damage is currently under investigation. The fabrication and operational histories of damaged tubes were investigated and compared with those of undamaged tubes. Three TES tubes were removed from the receiver after testing was completed: one tube with a convolution crack, one tube with a kink, and one undamaged tube. The tubes were then balanced (to determine the longitudinal center of gravity) and segmented for computed-tomography inspection and metallographic analysis. An additional nine tubes were radiographed while installed in the receiver to complement the computed-tomography data. Unused bellows were metallographically examined as well. The findings to date are summarized in the following paragraphs.

The only noteworthy observation concerning tube fabrication and operational histories was that all four tubes with kinks underwent a double salt-filling process. Therefore, these tubes experienced greater time at high temperature than single-fill tubes. At the 1700 °F fill temperature the nickel felt disks have low strength and, given sufficient time, can compact (translate down the tube) under their own weight. Measured center-of-gravity data from the three tubes removed were generally within 1/4 in. of the calculated values. These data are significant because they show that cyclic migration of the salt did not occur and that the salt remained stably configured within the tubes.

Seven-inch segments at the ends and middle of two removed tubes and the kinked region of the third removed tube were inspected by computed tomography. Ten-inch segments

TABLE 7.7 – RECEIVER TEST MODES

Test condition	Priority test modes (in order)	Test mode parameters								
		Sun-light time, min	Eclipse time, min	Total heat transfer, kW	Power distribu-tion	Flow, lb/s	Inlet temp-erature, °F	Inlet pressure, psia	Number of orbits	Change in time, Δt, hr
VT.1	Steady-state heat balance 1	(a)	0	3.876	1	0	--	--	--	120
VT.2	Steady-state heat balance 2	(a)	0	10.032	2	0	--	--	--	72
VT.3	SDHRT[b] baseline orbit	58	36	197.880	3	1.95	900	92	10	16
VT.5	Gas flow variation 2	58	36	197.880	3	2.75	900	92	4	7
VT.6	Orbital variation	66	28	197.880	3	2.75	900	92	4	7
VT.8	Maximum insolation orbit 2	66	28	224.960	4	2.75	915	92	4	7
VT.12	Peaking orbits	58	36	197.880	3	(d)	900	92	8	13
SS.1	Axisymmetric flux	58	36	197.880	5	1.95	900	92	4	7
SS.4	Circumferential variation 3	58	36	197.880	8	1.95	900	92	4	7
VT.3	SDHRT baseline orbit	58	36	197.880	3	1.95	900	92	6	10
CS.1	Shutdown to cold soak 1 (60 °F)	--	(a)	0	--	1.20	(d)	--	--	30
CS.3	Cold sink startup to nominal 2	58	36	197.880	3	1.95	900	92	10	16
CS.6	Coolant loss shutdown to ambient	(c)	(c)	197.880	3	0	--	--	--	30
								Total high-priority test mode duration		349

[a]Complete.
[b]Solar dynamic heat receiver technology contract.
[c]To be determined.
[d]Variable.

of the tube inlet end of nine tubes and the exit end of two tubes were radiographed. These inspections revealed four regions where felt-metal disks were displaced down the tube from 2.5 to 5 in. In these regions void of felt metal, salt formed on the inner tube extending out 25 to 75 percent of the annular gap thickness. The felt-metal compaction most likely occurred during salt-filling operations when the tube was oriented vertically. Minor bending or buckling of individual felt-metal disks was observed in about half of the radiographs. There was no direct relationship between the occurrence of displaced felt-metal disks and the first convolution cracks. This indicates that the tube failures were not a result of the expansive forces of melting salt.

In the kinked tube region the felt metal was displaced 7.5 in. with about one-third of the annular gap filled with salt on the inner, convoluted tube surfaces. Lacking the support of felt-metal disks, this region of the bellows buckled from thermal stress and the bellows nearly touched the inner tube. The direction of the bellows outward buckling was generally down, suggesting that gravity was the perturbing force.

Metallographic results show general intergranular corrosion to a depth of about 0.001 in. (one-tenth of the bellows wall thickness) on all internal tube surfaces regardless of location. The exact cause of this corrosion is under investigation. Exterior tube surfaces appeared unaffected from testing. The first convolution adjacent to either end cap on all tubes had intergranular cracks around more than half the circumference with depths running from 25 to 100 percent of the wall thickness. High stresses are possible in the first convolution because it is attached to the rigid end cap. The second convolutions showed little signs of intergranular cracking, indicating that the failure mode is highly stress dependent.

On the basis of the data collected thus far, the most likely cause of bellows failure is stress rupture. The intergranular corrosion hastened the time to failure because of a notch effect.

7.2.4 Required Development

Because of limited program resources, TES tube engineering development was somewhat restricted, making this area fertile ground for more development work. Specific TES tube design features to further develop include the following:

(1) Bellows: Greater effective compliance and durability are required as well as an improved method for terminating the bellows at the tube end cap without affecting the bellows structural characteristics. The bellows design should also accommodate a continuous matrix material that completely fills the convolution volumes to mitigate matrix material deformation or translation and the adverse void effects that are encountered when using felt-metal disks.

(2) Matrix material: Long-term cycling tests are needed to demonstrate salt distribution stability within the matrix, matrix structural integrity, and matrix material chemical compatibility with salts. Matrix materials to consider include metal felts (other than nickel), ceramic and graphite fibers, and various material foams. These materials offer potentially lower mass and better wicking and thermal transport enhancement than nickel felt, which was chosen in large part due to advanced-development receiver program constraints.

7.2.5 Recommendations and Ideas

Given that the development work suggested in the preceding section showed promising results, it is recommended to directly incorporate the matrix material technology of the advanced-development receiver program into the baseline receiver design. The resulting hybrid receiver design would have fewer, larger TES canisters with thinner walls (when compared with the current baseline receiver design), would possibly even have bellows, and would contain a salt-impregnated matrix material. This hybrid design conceivably would have lower mass and higher thermal efficiency than either the baseline or advanced-development receiver designs while maintaining gravity-independent operation and TES subsystem redundancy. Furthermore, if the number of canisters is sufficiently reduced, the number of working-fluid tubes could be reduced to enable either manifolding approach (i.e., toroidal or cylindrical spider plenum designs).

Another recommendation, for future receiver hardware development programs, is to thoroughly document fabrication histories and fully inspect hardware *before* testing commences. An example of this would be a full pretest computed-tomography inspection of each TES tube to document the initial condition of the salt-impregnated matrix. This becomes very important for gaining needed information on the performance of the TES subsystem, whose detailed characteristics heretofore have not been well explored. This documentation also greatly simplifies post-test assessment of hardware thermal and mechanical performance. Although this appears to be a basic recommendation, it is one easy to overlook or relinquish when budgetary and schedule pressures are encountered during the planning and/or implementation stages of a program.

References

7.1 Kudija, C.: Power Generation Subsystem, Closed Brayton Cycle, Rocketdyne Document. Allied-Signal Procurement Specification RC–1811[a] rev. D, May 18, 1990.

7.2 Jefferies, K.S.; and Gallo, C.: OFFSET Runs to Verify Analysis of Concentrator Mispointing Effects on Net Flux Input. IBR SE–247, key 23273[a], Apr. 4, 1990.

7.3 Strumpf, H.J.; and Coombs, M.G.: Solar Receiver for the Space Station Brayton Engine. ASME paper 87–GT–252, 1987.

7.4 Strumpf, H.J.; and Coombs, M.G.: Solar Receiver Development for Space Station *Freedom* Solar Dynamic Power System. 2nd Annual Space Conference, California State University–Long Beach, Sept. 22, 1990.

7.5 Chung, D.: Prediction of Thermal Performances of Solar Dynamic Receiver: Case Study Results With RECVR Code. Rocketdyne Internal letter 659–314–IL–90–130 to K. Santarelli, key 23691[a], Oct. 31, 1990.

7.6 Klann, J.L.; Gallo, C.; and Jefferies, K.S.: Up-dated Performance Estimates and Receiver Cavity-Wall Temperature Distributions for the Phase-C Baseline Solar Dynamic Power Module. IBR SE–226, key 23265[a], Jan. 16, 1990.

7.7 Klann, J.L.: Initial Checkout Results for Non-uniform Axial Salt Distribution Within the SD Heat Receiver. IBR SE–293, key 23260[a], Nov. 20, 1990.

7.8 Klann, J.L.; Gallo, C.; and Jefferies, K.S.: Receiver Temperature Distributions at 3 Minute Intervals During Maximum Insolation Orbit. IBR SE–221, key 23258[a], Dec. 6, 1989.

7.9 Klann, J.L.: Solar Heat Receiver Transient Thermal Effects on CBC Module Orbital Performance. PIR 182[a], Nov. 13, 1986.

7.10 Klann, J.L.: Solar Dynamic Heat Receiver Design Tradeoffs. IBR SE–167, key 23259[a], Dec. 5, 1988.

7.11 Klann, J.L.: Preliminary Analysis of Heat Receiver Hot-Spot Temperatures Without Flux Tailoring. IBR SE–171, key 23262[a], Dec. 15, 1988.

7.12 Klann, J.L.: Effects of Tilt Angle on SD Heat Receiver Hot-Spot Temperatures Without Flux Tailoring. IBR SE–176, key 23261[a], Feb. 24, 1989.

7.13 Klann, J.L.: CCEP User's Manual Closed (Brayton) Cycle Engine Program Revision of 7/17/89. IBR SE–199, key 23272[a], July 18, 1989.

7.14 Bruner, S.: RADVIEW – A Radiation View Factor Program for the Space Station *Freedom* Solar Receiver, Design Analyses and Data Report for the CBC Power Generating Subsystem. Allied-Signal Aerospace Co., Report 41–8702–15, key 10544[a], Aug. 23, 1990.

7.15 Klann, J.L: A Partial Design Study of the Heat Receiver for *Freedom*'s Solar Dynamic Power Module. IBR SE–326, key 24404[a], May 6, 1991.

7.16 Klann, J.L.: Some Additional Design Study Results for *Freedom*'s Solar Dynamic Heat Receiver. IBR SE–333, key 24403[a], July 1, 1991.

7.17 Strumpf, H.J.; and Avanessian, V.: Solar Receiver Canister Life Analysis. Allied-Signal Aerospace Co., key 23678[a], Sept. 13, 1990.

7.18 Strumpf, H.J., et al.: Design Analysis and Life Prediction for the Brayton Engine Solar Receiver for the Space Station *Freedom* Solar Dynamic Option. Proceedings of the 26th Intersociety Energy Conversion Engineering Conference, Vol. 1, Aug. 4–9, 1991, pp. 241–247.

7.19 Tong, M.T.; Kerslake, T.W.; and Thompson, R.L.: Structural Assessment of a Space Station Solar Dynamic Heat Receiver Thermal Energy Storage Canister. Proceedings of the AIAA SDM Issues of the International Space Station, Williamsburg, VA, Apr. 21–22, 1988, pp. 162–172.

7.20 Kerslake, T.W.: CBC Heat Receiver TES Canister Thermal Structural Analysis and Test. PIR 196[a], July 22, 1987.

7.21 Freed, A.D.: A Viscoplastic Model With Application to LiF-22%CaF_2 Hypereutectic Salt. NASA TM–103181, 1991.

7.22 Freed, A.D; and Walker, K.P: Model Development in Viscoplastic Ratchetting. NASA TM–102509, 1990.

7.23 Leckie, F.A.; and Marriott, D.L.: Long Term Integrity for a Space Station Power Systems. University of California–Santa Barbara, NASA Contract NAG3–1218, key 34379[a], Jan. 1991.

7.24 Kerslake, T.W.: Multidimensional Modeling of a Thermal Energy Storage Canister. NASA TM–103731, 1991.

7.25 Kerslake, T.W.: Experiments With Phase Change Thermal Energy Storage Canisters for Space Station *Freedom*. Proceedings of the 26th Intersociety Energy Conversion Engineering Conference, Vol. 1, Aug. 4–9, 1991, pp. 248–261. (Also NASA TM–104427.)

7.26 Wichner, R.P., et al.: Thermal Analysis of Heat Storage Canisters for a Solar Dynamic, Space Power System. ORNL TM–10665, 1988.

7.27 Wilson, D.G.; and Flanery, R.E.: Modeling Cyclic Melting and Refreezing in a Hollow Metal Canister. ORNL–6497, 1988.

7.28 Wichner, R.P., et al.: Transient, Three Dimensional Analysis of Thermal Energy Storage Phase Boundary and Void Behavior and

[a]Space Station *Freedom* library at the NASA Lewis Research Center in Cleveland, OH 44135 (tel. 216–433–5367 and fax 216–433–8050).

Canister Stresses. Final Report DOE Interagency Agreement 1819–1819–A, key 23276[a], July 1987.

7.29 Kerslake, T.W.: Parametric Studies of Phase Change Thermal Energy Storage Canisters for Space Station *Freedom*. ASME International Solar Energy Conference, Lahaina, Maui, HI, April 4–8, 1992.

7.30 Kerslake, T.W: Orbital and Ground-Based Freeze-Thaw Cycles of a Space Station *Freedom* Thermal Energy Storage Canister. VHS format, prepared by the NASA Lewis Advanced Graphics Visualization Laboratory and presented at the 25th Intersociety Energy Conversion Engineering Conference, Reno, NV, key 23649[a], Aug. 1990.

7.31 Quinn, R.D.; and Kerslake, T.W., Solar Dynamic Modules for *Freedom*: The Relationship Between Fine-Pointing Control and Thermal Loading of the Aperture Plate. NASA TM–104498.

7.32 Kerslake, T.W.: Solar Dynamic Heat Receiver Aperture Plate Thermal Response to Mispointed Concentrator Flux. PIR 233[a], Oct. 24, 1989.

7.33 Guthridge, K.C.: Status Report of the Thermal Modeling of the Solar Dynamic Aperture Plate. NASA Lewis Memo to T. Kerslake, key 34725[a], Mar. 1, 1991.

7.34 Strumpf, H.J.; and Coombs, M.G.: Solar Receiver Experiment for the Hybrid Space Station Brayton Engine. ASME Solar Energy Division Conference, San Diego, CA, 1989.

7.35 Strumpf, H.J., et al.: Material Compatibility and Simulation Testing for the Brayton Engine Solar Receiver for the NASA Space Station *Freedom* Solar Dynamic Option. Presented at the 24th Intersociety Energy Conversion Engineering Conference, Washington, DC, Aug. 6–11, 1989.

7.36 Kerslake, T.W.: Solar Dynamic Heat Receiver Thermal Energy Storage Canister Short-Term Test Data. PIR 225[a], Apr. 3, 1989.

7.37 Preliminary Report on Space Station Solar Receiver Material Compatibility Testing. Allied-Signal Aerospace Co., Report 88–61967, key 23677[a], Dec. 6, 1988.

7.38 Rubly, R.: Space Station Solar Receiver Material Compatibility Test: Evaluation of 10 000 Hour Exposure Canister. Allied-Signal Aerospace Co., Memo to M. Coombs, key 23677[a], July 26, 1989.

7.39 Preliminary Design of the Salt/Metal Compatibility, 12 000 Hour Exposure, Solar Receiver Thermal Energy Storage Canisters. Allied-Signal Aerospace Co., Report 41–8702–12, key 23677[a], Dec. 8, 1989.

7.40 Solar Receiver Thermal Energy Storage Canisters Compatibility Test—Final Report. Allied-Signal Aerospace Co., Report 41–8702–17, key 23677[a], Jan. 21, 1991.

7.41 Misra, A.K.; and Whittenberger, J.D.: Fluoride Salts and Container Materials for Thermal Energy Storage Applications in the Temperature Range 973 to 1400 K. NASA TM–89913, 1987.

7.42 Whittenberger, J.D.: Tensile Properties of HA 230 and HA 188 After 400 and 2500 Hour Exposures to LiF-22CaF_2 and Vacuum at 1093 K. J. Mater. Eng., vol. 12, 1990.

7.43 Ellis, J.R., et al.: Preliminary Study of Creep Thresholds and Thermomechanical Response in Haynes 188 at Temperatures in the Range 649 to 871 °C. NASA CP–2493, 1987.

7.44 Raj, S.V.; and Whittenberger, J.D.: Intergranular Fracture of Lithium Fluoride–22% Calcium Fluoride Hypereutectic Salt at 800 K. J. Am. Ceram. Soc., vol. 73, no. 2, Feb. 1990.

7.45 Raj, S.V.; and Whittenberger, J.D.: Deformation of As-Cast LiF-22% CaF_2 Hypereutectic Salt Between 500 and 1015 K. J. Mat. Sci. Eng., vol. A124, 1990.

7.46 Raj, S.V.; and Whittenberger, J.D.: The Mechanical Properties of Fluoride Salts at Elevated Temperatures. Presented at the 8th International Conference on the Strength of Metals and Alloys, Tampene, Finland, Aug. 1988.

7.47 Wolfenden, A., et al.: Temperature Dependence of the Elastic Moduli and Damping for Polycrystalline LiF-22% CaF_2 Eutectic Salt. J. Mat. Sci., vol. 26, Apr. 1, 1991, pp. 1793–1798.

7.48 de Groh, K. K., et al.: Low Earth Orbit Durability Evaluation of Haynes 188 Solar Receiver Material. AIAA Paper 92–0850, Presented at 30th Aerospace Sciences Meeting and Exhibit, Reno, NV, Jan. 6–9, 1992.

7.49 Beckwith, M.: Results of Melting of the Eutectic Mixture LiF-CaF_2 Under Controlled Conditions and Supporting Analysis, Design Analyses and Data Report for the CBC Power Generating Subsystem. Allied-Signal Aerospace Co., Report no. 41–8702–14, key 9793[a], July 11, 1990.

7.50 Kudija, C.: Comments on Thermal Energy Storage Development at Allied-Signal. Rocketdyne Internal Memo 659–314–IL–91–012 to K. Santarelli, key 23684[a], Feb. 11, 1991.

7.51 Space Station *Freedom* Solar Receiver Technical Information Exchange Meeting. Allied-Signal Aerospace Co., key 23673[a], Mar. 28, 1989.

7.52 Final Report: High Temperature Vacuum Sublimation Testing of Candidate Space Solar Receiver Materials. Allied-Signal Aerospace Co., Report 41–5586A, key 23669[a], Sept. 22, 1986.

7.53 Kerslake, T.W.: Chromium Contamination of Solar Concentrator. NASA Lewis Memo to S.D. Johnson, key 23694, Dec. 29, 1987.

7.54 Impacts of a Space Station Solar Dynamic Heat Receiver Thermal Energy Storage Canister Leak During On-orbit Operation. NASA Lewis Memo to Space Station Systems Director From Solar Dynamic Power and Propulsion Office, key 23683[a], Sept. 13, 1988.

7.55 Sedgwick, L.M., et al: Solar Dynamic Receiver Designs for Space Applications, key 37946,[a] 1987.

7.56 Solar Dynamic Heat Receiver Technology Preliminary Design Review. Boeing Aerospace Co., NAS3–24669, key 23281[a], July 15, 1986.

7.57 Sedgwick, L.M.: Solar Dynamic Heat Receiver Technology. NASA Contract NAS3–24669, NASA CR–187040, 1991.

7.58 Sedgwick, L.M., et al.: A Brayton Cycle Solar Dynamic Heat Receiver for Space. Proceedings of the 24th Intersociety Energy Conversion Engineering Conference, Vol. 2, Aug. 1989, pp. 905–909.

7.59 Solar Dynamic Heat Receiver Technology Design Analysis Report. Boeing Document D180–29711–1, NASA Contract NAS3–24669, key 23671[a], Sept. 19, 1988.

7.60 Wright, M.A.: Updated Meteoroid/Debris Analysis of the Solar Dynamic Receiver. Boeing Memo 2–3614–PDR–022/87 to L.M. Sedgwick, NASA Contract NAS3–24669, key 23693[a], June 26, 1987.

7.61 Cotton, J.D.; and Sedgwick, L.M.: Compatibility of Selected Superalloys With Molten LiF-CaF2—for Use on Space Station *Freedom*. Proceedings of the 24 Intersociety Energy Conversion Engineering Conference, Aug. 6–11, 1989, pp. 917–921.

7.62 Sedgwick, L.M.: Advanced Development Receiver Thermal Vacuum Tests With Cold Wall. NASA CR–187092, 1991.

7.63 Sedgwick, L.M.; Kaufmann, K.J.; McLallin, K.L.; and Kerslake, T.W.: Ground Test Program for a Full-Size Solar Dynamic Heat Receiver. Proceedings of the 26th Intersociety Energy Conversion Engineering Conference, Vol. 1, Aug. 4–9, 1991, pp. 268–273. (Also NASA TM–104485.)

7.64 Sedgwick, L.M.; Kaufmann, K.J.; McLallin, K.L.; and Kerslake, T.W.: Full-Size Solar Dynamic Heat Receiver Verification Test Results. Proceedings of the 26th Intersociety Energy Conversion Engineering Conference, Aug. 4–9, 1991, pp. 262–267. (Also NASA TM–104486.)

---

[a]Space Station *Freedom* library at the NASA Lewis Research Center in Cleveland, OH 44135 (tel. 216–433–5367 and fax 216–433–8050).

Page intentionally left blank

Chapter 8

Power Conversion Unit

8.1 General Description

The power conversion unit (PCU) consists of a Brayton heat engine including a turboalternator compressor (TAC), a recuperator, gas coolers, ducting, a gas accumulator with valves, and support structure. The Brayton cycle works by extracting useful (electric) work from the difference in the shaft power supplied by heated high-pressure gas expanding through a turbine and the shaft power required to drive a compressor operating on cooled low-pressure gas. The closed Brayton cycle (CBC) working fluid is a helium-xenon (He-Xe) mixture with a molecular weight equal to that of argon (39.94). This mixture functions as the working fluid and has properties approximated by the ideal-gas laws. Those properties affected by temperature are viscosity and thermal conductivity. Values for these properties are listed in table 8.1.

TABLE 8.1.—PROPERTIES OF He-Xe MIXTURE AT MOLECULAR WEIGHT OF ARGON (39.94)

Temperature, °R	Viscosity lbm/ft-hr	Thermal conductivity, Btu/hr-ft-°R
360	0.0462	0.0281
720	.0810	.0450
1080	.1093	.0590
1440	.1339	.0712
1800	.1561	.0824
2160	---	.0928
2340	.1861	---

8.2 Turboalternator Compressor

The CBC turboalternator compressor (TAC), shown in figure 8.1, consists of a single-stage, radial-inflow turbine, a straddle-mounted Rice alternator, and a centrifugal compressor. Design features of this single-shaft unit include radial aerodynamic components integrated with a high-speed, solid-rotor Rice alternator that is supported by foil gas journal bearings. Thrust induced on the shaft by the rotating machinery is supported by a double-acting foil gas thrust bearing. The TAC cooling is provided by *n*-heptane coolant to the alternator stator and cooled bleed gas to the gas bearings and the alternator rotor. TAC rotating speed is 32 000 rpm. This TAC concept is a very rugged single unit that is the only continuously moving part in the CBC receiver/PCU. Table 8.2 shows two extremes of the operating performance envelope.

The CBC turbine consists of a rotor and end bell assembly, a turbine scroll, and a stator assembly. The turbine end of the shaft is sealed by a back shroud and labyrinth seal assembly. The single-stage, radial-inflow rotor is 7.66 in. in diameter. Materials used in the turbine design include Mar-M for the turbine wheel and Inconel for the stator and nozzle assembly of the turbine scroll.

The Rice alternator is an integrated, brushless, four-pole synchronous type of machine. The power windings are a conventional *Y*-wound, three-phase type. The rotor is a composite structure of magnetic and nonmagnetic materials combined through casting and brazing techniques. Each pole element is fitted integrally with the other but is separated from other elements by a nonmagnetic metal piece. The alternator stator assembly has a conventional three-phase winding. The materials and insulation system used throughout the stator and field coils consist of class 220C-rated components for long life and high reliability. Lamination material is 49 percent nickel steel for low core losses.

The outside-coil Lundell type of alternator was selected for use in the solar dynamic power system because it offers the best combination of performance and weight in the general class of solid-rotor synchronous electric machines. A solid-rotor machine is needed because of its ruggedness and relative simplicity, which are essential qualities for the alternator in the PCU turboalternator compressor. Although successfully designed, built, and operated in NASA's dynamic power system development program in the 1960's and 1970's, the outside-coil Lundell machine has not been widely used because it is somewhat heavier than the conventional, wound salient pole machines that are common in aircraft electric power systems. As can be seen in figure 8.1 the Lundell rotor length is approximately the same as its diameter, and the field coils are at some distance from the armature air gap. This configuration results in magnetic leakage paths, armature end effects, and nonuniform air gap flux density more severe than those encountered in conventional machines. Optimization of the alternator design for the *Freedom* solar dynamic power module

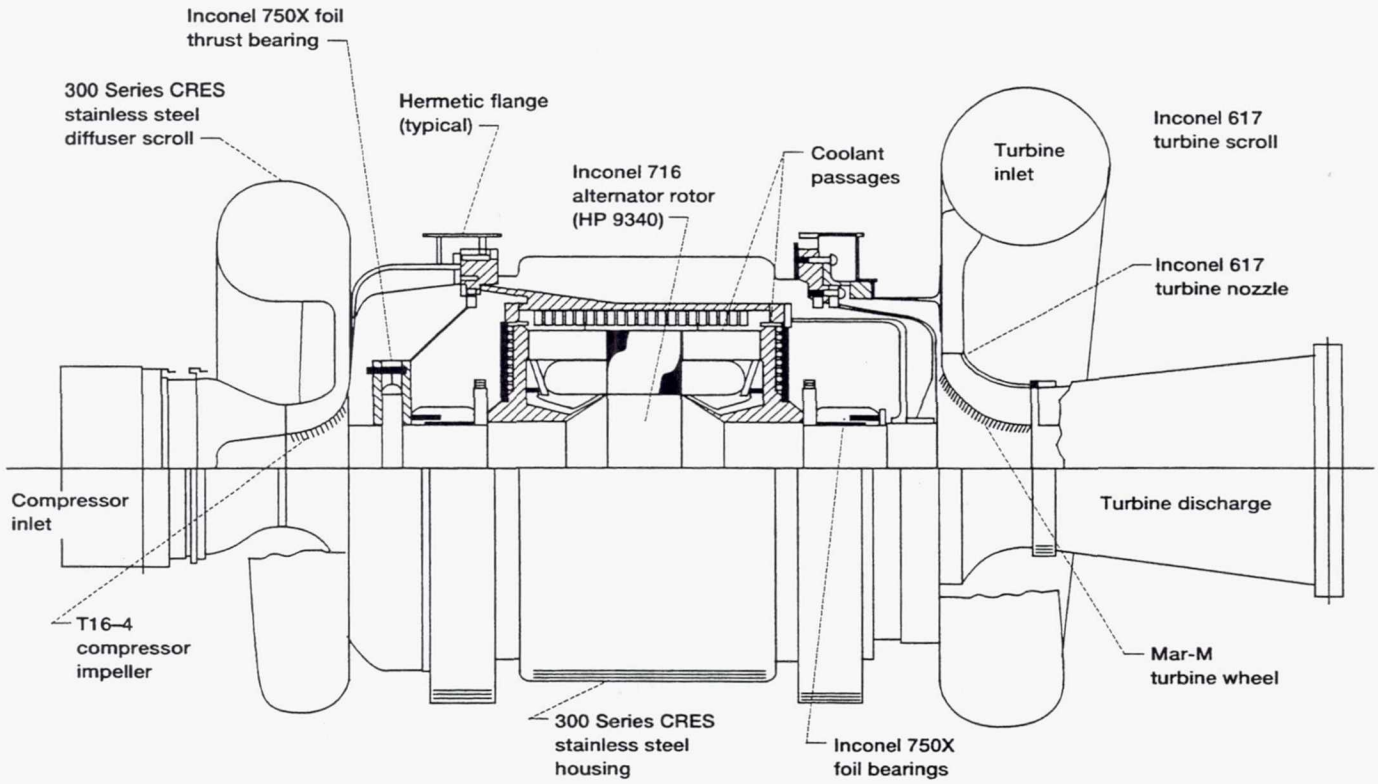

Figure 8.1.—Turboalternator compressor.

TABLE 8.2.—PCU OPERATING PERFORMANCE

Parameters	Minimum insolation (sunrise)	Maximum insolation (sunset)
Alternator electrical output, kWe	32.15	36.42
Net cycle efficiency, percent	33.75	27.6
Turbine inlet temperature, °F	1361.5	1401.6
Turbine efficiency	0.8960	0.901
Compressor efficiency	0.8420	0.847
Alternator efficiency	0.9340	0.927
Recuperator effectiveness	0.940	0.926

is essential to ensure the best possible performance. Design procedures for the Lundell alternator existing at the beginning of the Space Station *Freedom* Program relied on empirical data to account for leakage and the other factors mentioned. In order to allow a more rigorous design, all current paths and magnetic fields, leakage as well as main, need to be understood and quantifiable in three dimensions. Such work had not been done prior to this program, and therefore a task to apply three-dimensional, finite element modeling analysis to the complex electromagnetic structure of a Lundell alternator was pursued by Clarkson University under NASA grant NAG3–818. The results of this grant are documented in references 8.1 to 8.8

The CBC compressor consists of an impeller and end bell assembly, a diffuser scroll, and a back shroud and labyrinth seal assembly. The single-stage, radial-outflow compressor is 6.42 in. in diameter. Materials used in the compressor design include 410C or TI–64 for the compressor impeller and 347 stainless steel for the diffuser scroll.

The TAC common shaft is mounted on foil hydrodynamic gas journals and thrust bearings. The foil gas bearings provide a long-life, low-power-loss bearing system that requires no external coolant or seals. The radial foil bearing journals are 2.726 in. in inner diameter and are located at each end of the shaft near the compressor and the turbine wheels. The thrust bearing, which is located at the compressor end of the shaft, is 0.55 in. thick and has a 4.766 in. outer diameter. The foil journal and thrust bearing material is 302 stainless steel; hydrodynamic foil surfaces are coated with polyimide graphite or a similar material for startup purposes.

8.2.1 TAC Testing

*8.2.1.1 **Background.***—Originally Space Station *Freedom* was going to use an alternating-current distribution system. To determine how difficult it would be to synchronize the output of an operating BRU with *Freedom*'s distribution

system, the division responsible for overall power system architecture resurrected an old Brayton unit. To alleviate the problems associated with running the unit in a hot loop, it was modified so that it could be driven by compressed air.

When the distribution system for *Freedom* was changed to direct current, the need for this paralleling test vanished. And now, since the facility was operational and not being utilized, it was offered to the Solar Dynamic Branch. As a result of discussions and meetings with various organizations, three areas were identified in which testing would provide valuable information. They were electrical characterization, electromagnetic interference emissions while operating, and startup characteristics. When the SD program was shut down, only a portion of the electrical characterization test had been completed.

8.2.1.2 Electrical characterization. — When the Solar Dynamic Branch began operating the BRU simulator facility, NASA also had a 3-year grant ongoing with Clarkson University. This grant was to model the Rice-Lundell generator, part of the TAC, electromagnetically in three dimensions.

In order to verify the model and thus gain better confidence in its results, it was decided to perform some electrical characterization tests of the Rice-Lundell generator that was contained in the BRU simulator. These tests consisted of phase voltage and current waveshapes, under various load conditions, and saturation curves. The results were provided to the principal investigator at Clarkson University and supported his analyses documented in references 8.1 to 8.8.

8.2.2 TAC Recommendations

Startup testing has been identified as an area in which additional data are needed. The following are some of the arguments for and against induction versus synchronous startup of the TAC.

The most important problem associated with induction starting is induced rotor heating. This problem has never been adequately investigated but has been mentioned as a cause for concern. During an induction start some of the energy that could be used for starting is lost in the rotor as eddy-current-induced heating. Not only can this heating be detrimental to rotor life, it requires, for a particular breakaway bearing friction, more massive alternator windings to handle the higher current requirements. Consequently, the energy required for an induction start would be somewhat higher than that required for a similar synchronous start. However, this difference in the total energy required for each startup scenario would be less the shorter the duration of the start cycle.

The advantages of a synchronous startup are no rotor heating, minimum energy requirement, and, for a particular breakaway bearing friction, a possibly lighter TAC. The lighter TAC is a direct result of the lower current requirements allowing for less massive alternator windings. The disadvantage is a more complex system with a likelihood of reduced reliability. This complexity is a result of the need to know shaft position during startup and having the ability to retard or increase field rotational speed. It is not clear whether the decrease in TAC mass would be offset by the mass of the additional components necessary to perform the synchronous start. This may negate the mass advantage.

It comes down to answering the question, What is more important, greater reliability or minimum energy and mass? A test to quantify induction-induced rotor heating would go a long way in helping to find the answer.

8.3 Recuperator

The gas-to-gas recuperator, which receives the turbine discharge, is shown in figure 8.2, with the design summary shown in table 8.3. The recuperator, which was designed for 94-percent heat transfer effectiveness, is a pure counterflow plate-fin unit, with crossflow triangular end sections providing fluid access to the core. The counterflow section has 0.153-in.-high offset fins on the low-pressure side and 0.125-in -high offset fins on the high-pressure side. The offset fin is used to promote turbulence, which in turn enhances heat transfer. The sides of the flow passages are closed by redundant 0.060-in.-wide side bars. Each gas passage has double containment, which means that both bars on a side in the same passage must leak before any external leakage can occur. All fins in the recuperator are 0.006-in.-thick corrosion-resistant steel (CRES) 304L, a material that retains its ductility even after prolonged exposure to temperatures over 1000 °F. The separation plate is 0.010 in. thick, slightly thicker than that used in previous Brayton cycle recuperators in order to reduce the probability of interpassage leakage between the high- and low-pressure gases. The increased thickness, in combination with low operating temperature (1070 °F maximum), will increase the design margin by 50 percent and further enhance the recuperator reliability. The unit will be brazed by using a nickel-based alloy (AMS 4778) applied in powder form.

The inlet and outlet pans on the recuperator are not welded directly to the core but are welded to machined stubs joined to grooves cut into the side bars in a secondary brazing operation. The side bars are specially shaped to optimize the resulting braze fillets. This type of joint has successfully been used on other heat exchangers designed for zero-leakage, long-life space applications.

Between the recuperator and gas cooler is a short transition section that turns and distributes gas flow from the recuperator low-pressure outlet to the gas cooler. It also serves as a rigid structure between the two heat exchangers.

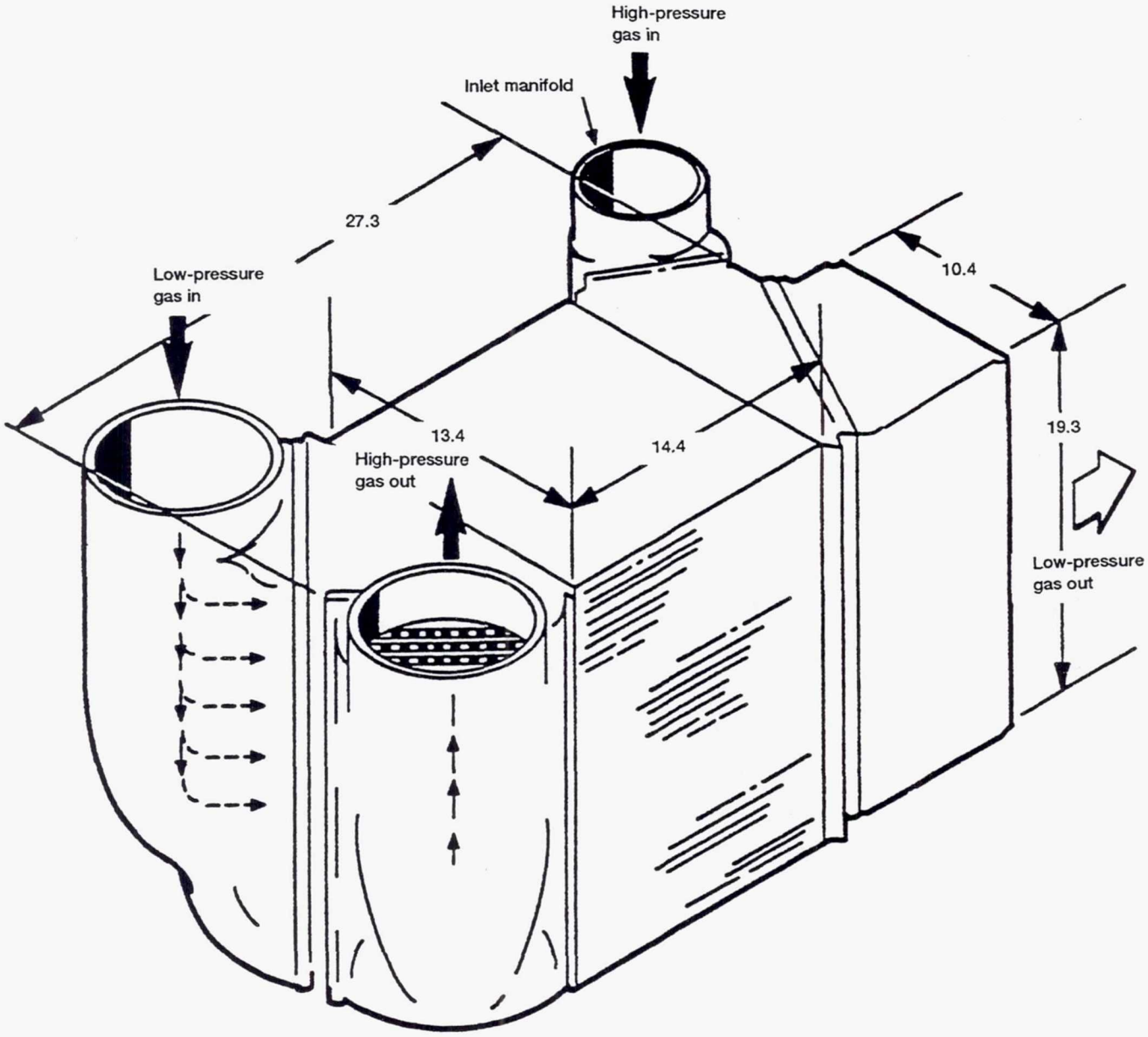

Figure 8.2.—Closed Brayton cycle counterflow recuperator. Weight, 357 lb. (Dimensions are in inches.)

TABLE 8.3.– RECUPERATOR DESIGN SUMMARY

Counterflow section	
Flow length, in.	14.4
Flow width, in.	12.5
High-pressure-side fin:	
Height, in.	0.125
Number of fins per inch	16
Thickness, in.	0.006
Number of sandwiches	62
Type	Rectangular offset
Low-pressure-side fin:	
Height, in.	0.153
Number of fins per inch	16
Thickness, in.	0.006
Number of sandwiches	63
Type	Rectangular offset
Plate thickness, in.	0.010
Stack height, in.	19.3
Side-plate thickness, in.	0.060
Triangular end sections	
Fin configuration:	Same as counterflow section
Height	Same as counterflow section
Number of fins per inch	5
Thickness, in.	0.006
Type	Plain rectangular
Total recuperator weight, lbm	357

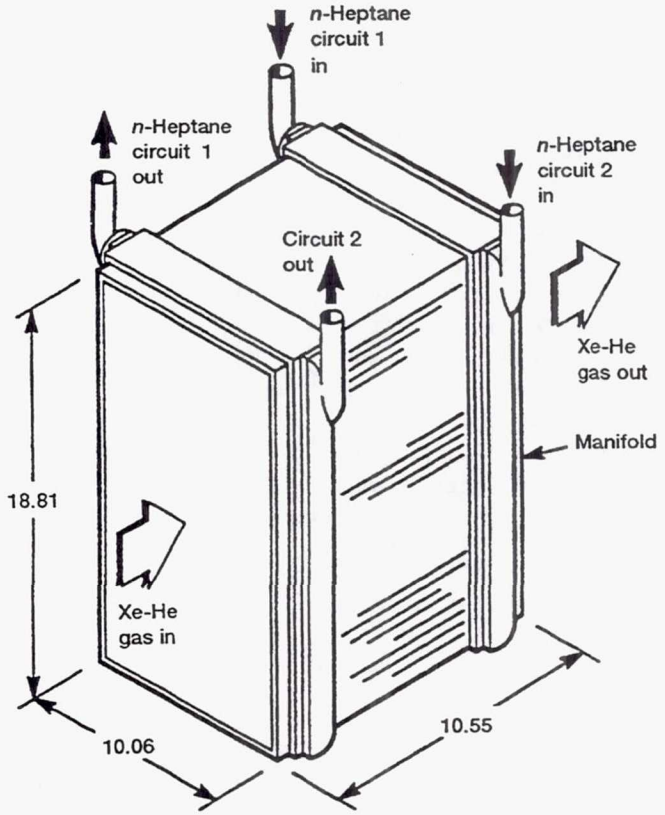

Figure 8.3.—Dual-fluid, eight-pass, cross-counterflow, plate-fin gas cooler. Weight, 188 lb. (Dimensions are in inches.)

8.4 Gas Cooler

The gas cooler is shown in figure 8.3 with the design summary in table 8.4. The gas cooler serves to reject the cycle waste heat to a liquid coolant from the solar dynamic heat rejection assembly. The gas cooler is a gas-liquid heat exchanger that is located downstream of the recuperator and receives the turbine discharge. The resultant low-pressure, low-temperature gas returns to the compressor inlet and is recirculated.

The gas cooler is connected to the recuperator by a short transition section that turns and distributes the gas discharged from the recuperator. The cooler heat exchanger (fig. 8.3) is an eight-pass, cross-counterflow, plate-fin design. The fin sandwiches are rectangular offset, 0.089 in. high on the gas (He-Xe) side and 0.075 in. high on the liquid (*n*-heptane) side in a single sandwich arrangement on both sides. The gas cooler is a redundant alternating sandwich design that connects to independent fluid loops and results in double-sandwich, gas-side passages. In order to maintain separation of the two liquid loops, turning between successive liquid passes is accomplished with mitered fin-turning sections rather than manifolds. These turning sections are triangular sections of fin sandwich, of the same geometry as the remainder of the core and sized to give the same fluid flow area in the turn as in the pass. Successive liquid passes within each sandwich are separated by 0.050-in.-thick splitter bars. Header bars and side bars at the external faces of the core are 0.100 in. thick. Double bars in the liquid passage areas of the manifolds eliminate the possibility of a liquid leak entering the gas stream. Double bars similar to those described for the recuperator are incorporated in all gas passages to meet the requirement for double containment.

TABLE 8.4.– GAS COOLER DESIGN SUMMARY

Gas flow length, in.	10.55
Liquid flow length (per pass), in.	10.0
Number of liquid passes	10
Gas-side fins:	
Height, in.	0.089
Number of fins per inch	12
Thickness, in.	0.006
Type	Rectangular offset
Liquid-side fins:	
Height, in.	0.075
Number of fins per inch	20
Thickness, in.	0.006
Type	Rectangular offset
Plate thickness, in.	0.008
Number of gas sandwiches	103
Stack height, in.	18.8
Side-plate thickness, in.	0.06
Total gas cooler weight (dry), lbm	188
FC–75 inventory mass, lbm	107

8.5 Bleed Cooler

The bleed cooler, shown in figure 8.4, lowers the temperature of the gas that is tapped from the compressor discharge and cools the bearings and alternator winding of the Brayton rotating unit.

The heat is transferred to a liquid coolant (*n*-heptane) in the small counterflow, plate-fin heat exchanger shown in figure 8.5. The fin sandwiches are rectangular offset, 0.077 in. high on the gas side, and 0.100 in. high on the liquid side in a single sandwich arrangement on both sides. The bleed cooler contains redundant liquid sandwiches (in this case, only three of the six liquid sandwiches are active at any given time). Redundancy on the gas side is also provided by incorporating double side bars. This unit is constructed entirely of CRES 304L. The design is summarized in table 8.5.

TABLE 8.5.—BLEED COOLER DESIGN SUMMARY

Gas flow length, in.	4.63
Liquid flow length (counterflow), in.	3.33
Gas-side fins:	
Height, in.	0.077
Number of fins per inch	16
Thickness, in.	0.006
Type	Rectangular offset
Liquid-side fins:	
Height, in.	0.100
Number of fins per inch	20
Thickness, in.	0.006
Type	Rectangular offset
Plate thickness	0.008
Number of gas sandwiches	7
Number of liquid sandwiches	6
Stack height, in.	1.35
Side-plate thickness, in.	0.06
Total bleed cooler mass	4

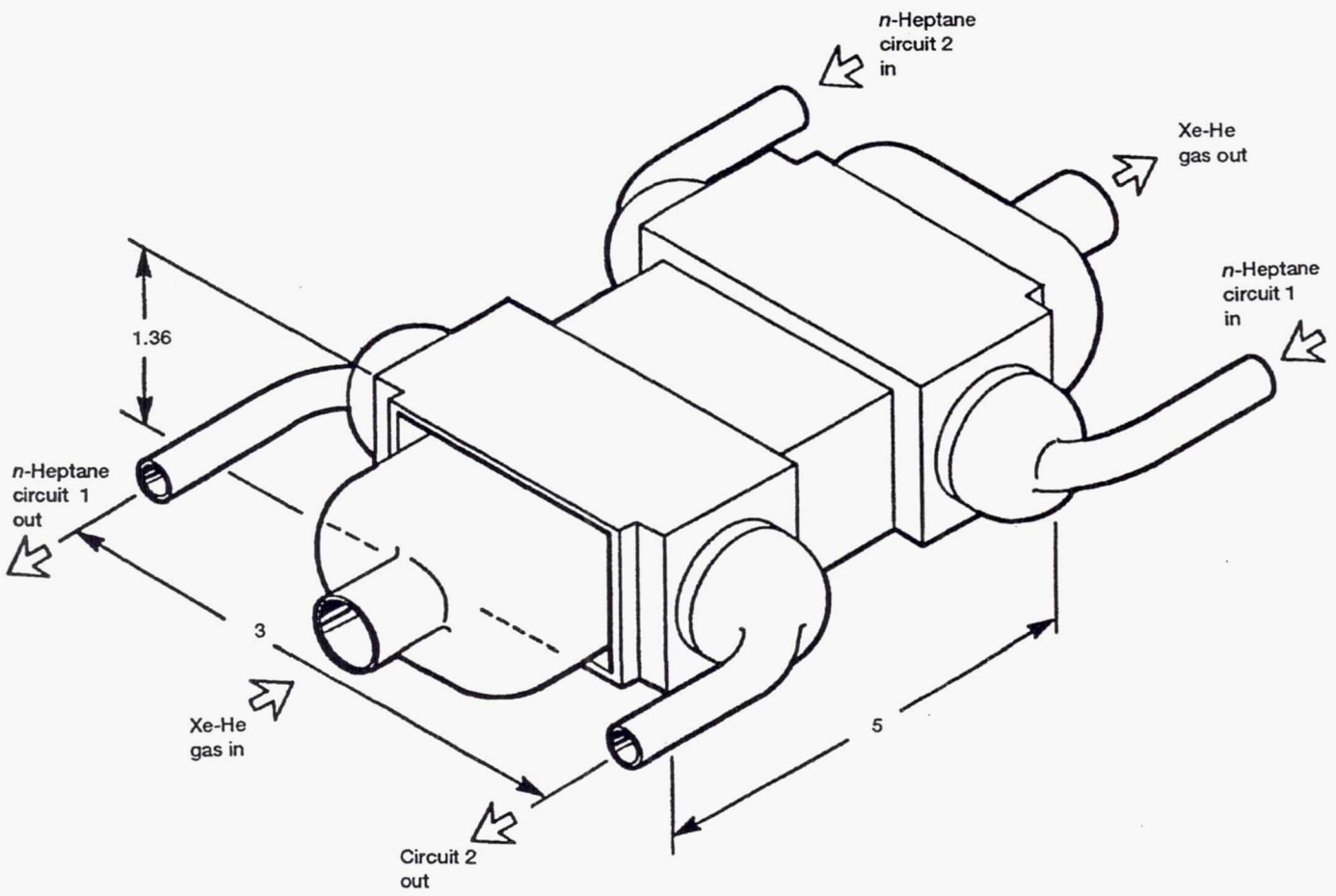

Figure 8.4.—Dual-fluid, counterflow, plate-fin bleed cooler. (Dimensions are in inches.)

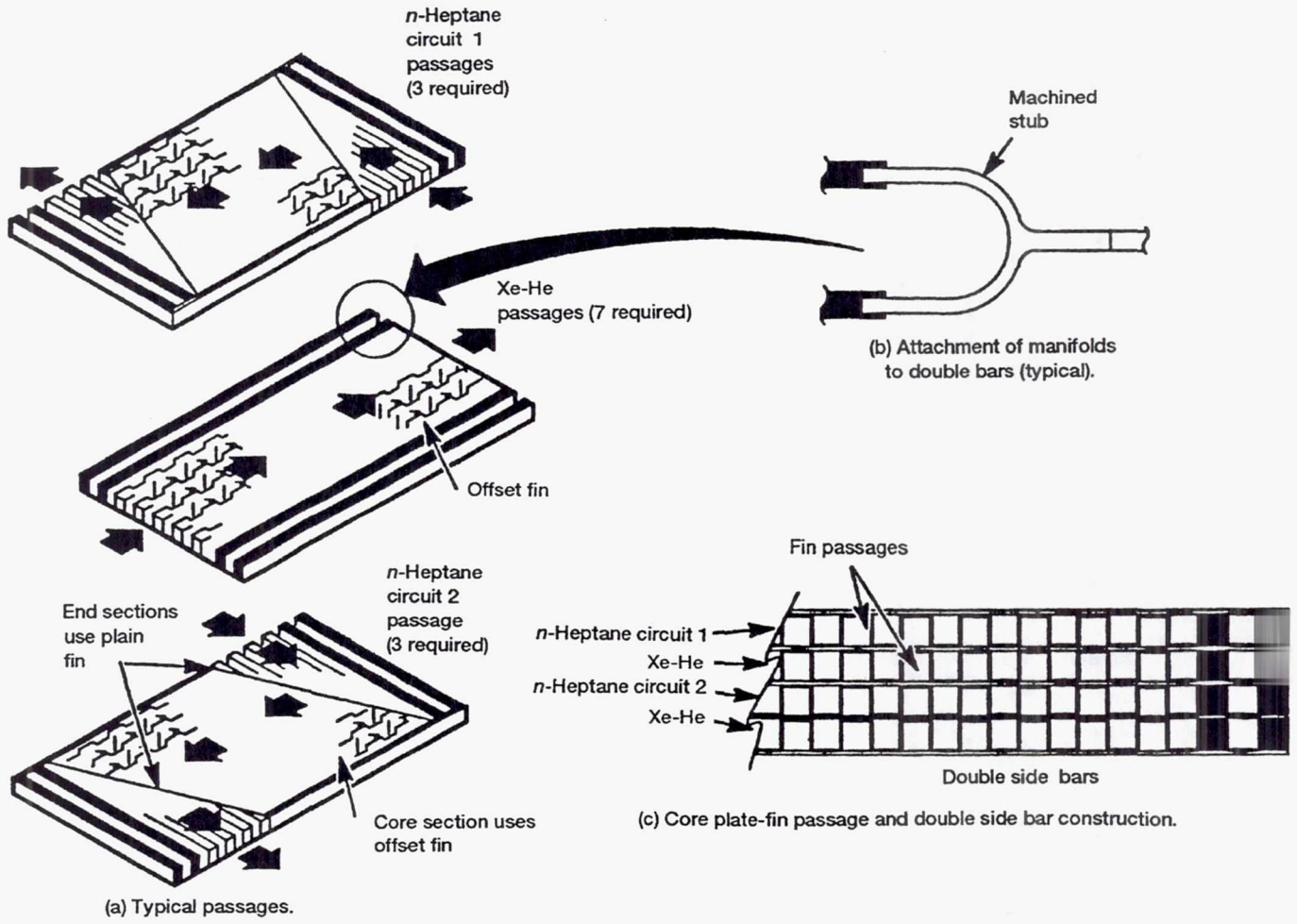

Figure 8.5.—Internal construction (double header bars) of bleed cooler.

8.6 Gas Loop Control Hardware

The gas loop control hardware consists of the inventory control valve with an actuator ORU, which is described in section 8.8, and the ducting and gas inventory accumulator described herein. Fluids are transferred from one component to another through a duct system. The ducts are fabricated from two materials, Hastelloy X for high-temperature applications and 347 stainless steel for lower temperature applications. All joints in the gas loop are hermetically sealed by welding. CBC PCU components or ducts may be removed by grinding down the weld flange. The ducting may then be reassembled by rewelding the flange. Weld joints are either tungsten inert gas (TIG) or E-beam type for discrete ducting details. TIG welds are used for component assembly joints where access is limited.

Multiple bellows are used throughout the ducting system at locations of high relative thermal expansion. In order to minimize the stresses on the interfacing ducts and components, these bellows are always used in pairs. For extreme thermal expansion a link type of bellows will be used for additional safety margin. A typical bellows-to-duct joint may be either welded or brazed, depending on detailed design considerations. The duct configurations and their physical properties are given in figure 8.6.

The amount of He-Xe inventory in the Brayton cycle gas loop is controlled to limit receiver temperature and to provide for peaking power requirements. This provision is accomplished by storing or extracting working fluid from a system accumulator. The accumulator is constructed of formed and welded aluminum alloy. The accumulator volume is yet to be determined.

Because insolation and demand vary simultaneously in orbit, actual cycle operation requires using both inventory control and electric load control at the same time. The He-Xe inventory in the power loop is varied to maintain the TES melt fraction in the desired range of operation, to limit maximum receiver temperature, and to provide peaking power. The receiver temperature measurements taken throughout the orbit reflect the thermal state of the TES material. Excessive

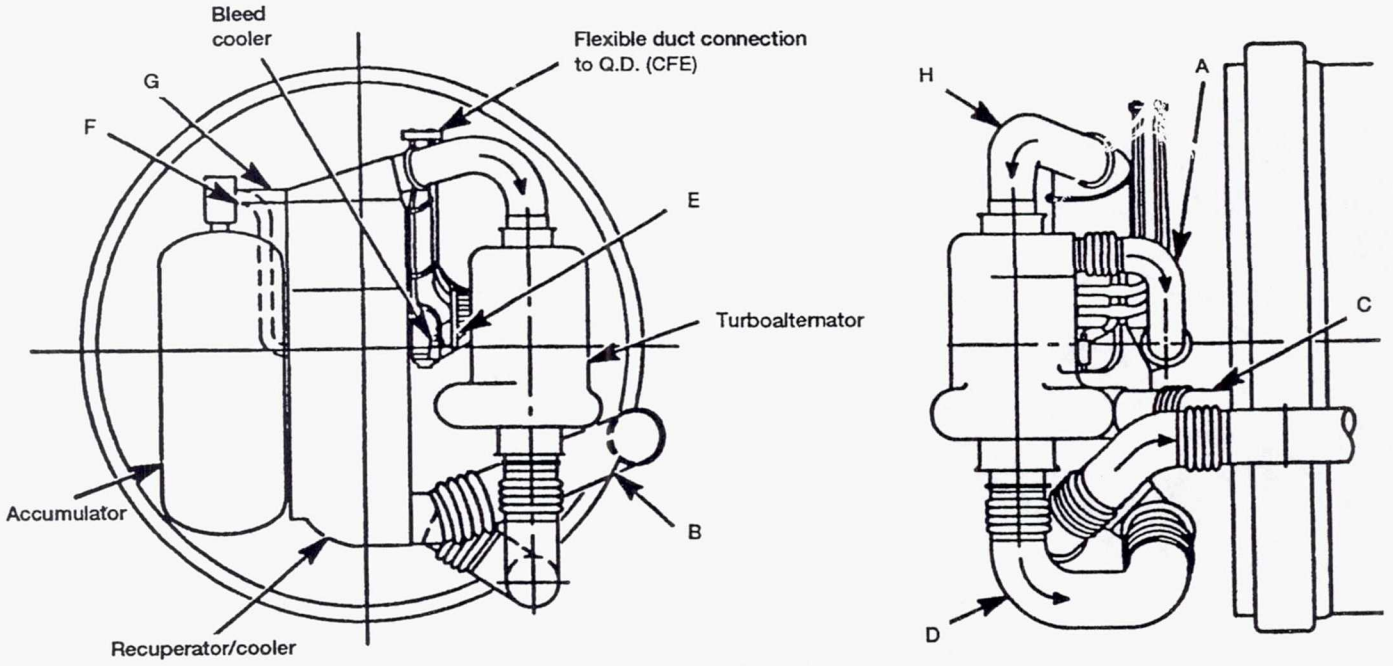

[SS = Stainless steel; Hast X = Hasteloy X; working fluid, Xe-He 40; weights include bellows, insulation, and flanges.]

	Duct designation							
	A	B	C	D	E	F	G	H
	Working fluid characteristics							
Temperature, °F	333	1038	1402	1099	466	333	333	155
Pressure, psia	81	81	78	48	47	81	81	47
	Duct characteristics							
Length, in.	60	70	12	53	46	55	27	33
Diameter, in.	5	7.5	6	8	0.75	2	2	7
Material	347SS	Hast X	Hast X	Hast X	304SS	304SS	304SS	304SS
Thickness, in.	0.062	0.078	0.078	0.062	0.032	0.032	0.032	0.064
Total weight, lbm	36	61	18	66	2	7	4	26

Figure 8.6.—Summary of closed Brayton cycle gas ducting design.

receiver temperature activates the inventory charge solenoid, which opens the valve at the compressor inlet to admit inventory to the system. The time that the valve is open is computed in the inventory control algorithm. The rotor speed is held constant and the mass flow rate through the receiver increases, reducing receiver temperature as more energy is extracted from the receiver. The resulting increased power level is absorbed in the parasitic load or distributed to keep speed constant. A similar adjustment with the discharge control valve is performed to keep receiver temperatures above the minimum value and to provide for receiver recovery during peaking orbits except when gas is taken out at the compressor exit.

8.7 Parasitic Load Radiator

The parasitic load radiator functions as an electrical sink for excess power. This is necessary to provide effective speed control for the turboalternator rotor while managing the excess power in a way that allows fast response to changes in user demand.

The parasitic load radiator is an integral part of the electric loop controls for the CBC power generation subsystem. Its design allows it to passively accept a wide range of power up to the maximum output of the turboalternator, converting the power to heat and radiating it to space. The parasitic load radiator will accept electric power from the power electronics unit.

8.8 Inventory Control Valve Actuator

The inventory control valve actuators provide motive force for opening the solenoid valves that control the flow of gas to and from the inventory accumulator.

The inventory control valve is a dual-solenoid diverter valve, as shown in cross section in figure 8.7. The valve consists of two two-way solenoid valves that are spring-loaded closed. The solenoids are installed in a line-mounted housing that is ported so that the combination provides a closed-center, three-way diverter valve design. When solenoid 2 is deenergized, it shuts off the flow of He-Xe gas from the accumulator to the compressor inlet. When both solenoids are deenergized, the accumulator is isolated from the compressor, maintaining the gas inventory until change is needed for power adjustment.

To open either solenoid, 28-V dc power is applied to the appropriate pins of the electrical connector. Electric current flowing through the solenoid coil generates a magnetic force that is transmitted through the hermetically sealed pressure vessel to the solenoid interior. Magnetic force acts on the solenoid armature to force it down against the solenoid rod and return spring. The rod moves down and strikes the solenoid ball, forcing it off its seat. He-Xe gas under pressure flows from the base of the solenoid, upward past the ball and seat, and out through the solenoid discharge ports.

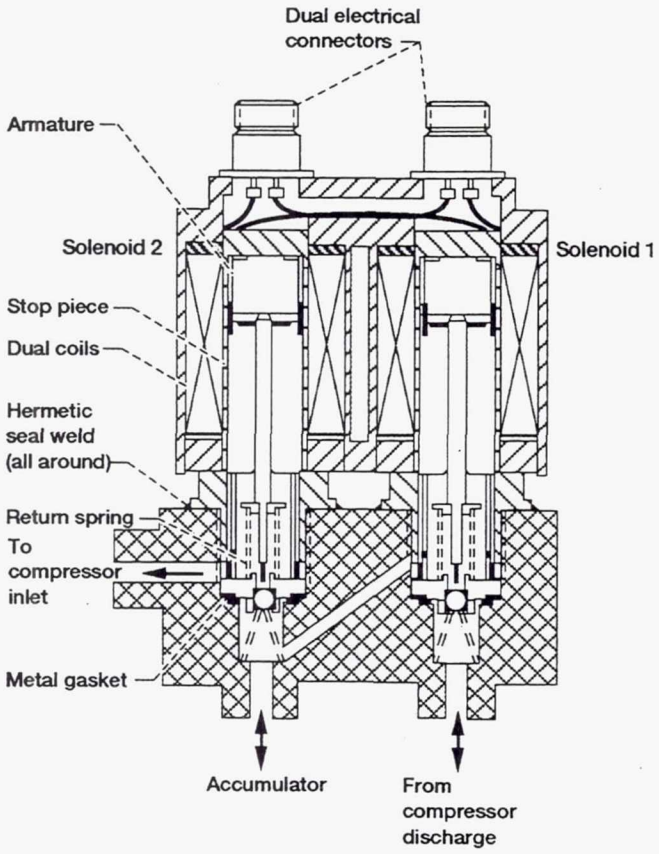

Figure 8.7.—Inventory control valve.

With the removal of the electric power the magnetic field collapses, causing the magnetic force holding the armature down against the lower pole piece to vanish. The force of the return spring then pushes the armature back to the closed position.

The dual-solenoid diverter valve is specially designed for use on Space Station *Freedom* and includes the following design features:

(1) Both solenoids incorporate hermetically sealed pressure boundaries to prevent external leakage for the life of the unit. After assembly, the pressure vessels are welded to the main housing to provide the hermetic seal. In addition, the main housing is welded into the connecting ducts.

(2) The ball valves that control the flow of He-Xe gas are optimized for minimum external and internal leakage for the life of the unit.

(3) The magnetic circuit of the solenoids is designed for the highest efficiency that is consistent with the hermetically sealed design. All parts are coated to prevent galling and corrosion.

(4) The solenoids use only metallic materials inside the pressure boundary. The coil assemblies use only those materials approved for usage in the space environment.

(5) The dual-coil actuator is removable and may be replaced in orbit.

(6) The valve features dual coils in each valve and redundant electrical connectors separately linked to the dual-channel controller to ensure high reliability and fail-safe operation.

8.9 Engine Controller

The controller adjusts rotor speed by modulating the voltage of the parasitic load radiator, adjusts supply voltage by modulating field coil current, and controls the cycled thermal condition by modulating accumulator pressurization through use of the inventory control valve actuators.

The electric loop control equipment consists of dual redundant controllers each having power, logic, signal conditioning, and communications circuitry. The engine controller functionally consists of the electric control unit and the power electronics unit.

The electric control unit can accept instrumentation signals and data bus information and can operate on such information to generate control signals that are appropriate to the functions of output power, alternator speed, voltage control, receiver and PCU startup, shutdown, equipment protection, and EPS information supply.

The power electronics unit conditions and controls power according to commands generated by the electric control unit. These functions include parasitic load radiator power control, speed control, voltage control, and startup power conditioning

References

8.1 Demerdash, N.A.; and Wang, R.: Theoretical and Numerical Difficulties in 3–D Vector Potential Methods in Finite Element Magnetostatic Computations. IEEE Transactions on Magnetics, vol. MAG–26, no. 5, 1990, pp. 1656–1658.

8.2 Wang, R.; and Demerdash, N.A.: On the Effects of Ill-Conditioning in Three Dimensional Finite Element Vector Potential Magnetostatic Field Computations. IEEE Transactions on Magnetics, vol. MAG–26, no. 5, 1990, pp. 2190–2192.

8.3 Demerdash, N.A.; Wang, R.; and Secunde, R.: Three Dimensional Magnetic Fields in Extra High Speed Modified Lundell Alternators Computed by a Combined Vector-Scalar Magnetic Potential Finite Element Method. Paper No. 90WM069–5–EC, Presented at the IEEE Power Engineering Society Winter Meeting, New York, Feb. 3–7, 1991. IEEE Transactions on Energy Conversion, vol. EC–7, no. 2, June 1992, pp. 353–366.

8.4 Wang, R.; and Demerdash, N.A.: Extra High Speed Modified Lundell Alternator Parameters and Open/Short Circuit Characteristics From Global 3D–FE Magnetic Field Solutions. Paper No. 91WM067–9–EC, Presented at the IEEE Power Engineering Society Winter Meeting, New York, Feb. 3–7, 1991. IEEE Transactions on Energy Conversion, vol. EC–7, no. 2, June 1992, pp. 340–341.

8.5 Wang, R.; and Demerdash, N.A.: Computation of Load Performance and Other Parameters of Extra High Speed Modified Lundell Alternators from 3D–FE Magnetic Field Solutions. Paper No. 91WM068–7–EC, Presented at the IEEE Power Engineering Society Winter Meeting, New York, Feb. 3–7, 1991. IEEE Transactions on Energy Conversion, vol. EC–7, no. 2, June 1992, pp. 342–352.

8.6 Wang, R.; and Demerdash, N.A.: A Combined Vector Potential–Scalar Potential Method for FE Computation of 3D Magnetic Fields in Electrical Devices With Iron Cores. Paper No. CA–03, Presented at the Fourth Biennial IEEE Conference on Electromagnetic Field Computation, CEFC '90, Toronto, Canada, Oct. 22–24, 1990. IEEE Transactions on Magnetics, vol. MAG–27, no. 5, 1991, pp. 3971–3977.

8.7 Alhamadi, M.; Wang, R.; and Demerdash, N.A.: Vector Potential 3D Finite Element Modeling of Magnetic Fields in Permanent Magnet Devices, Paper No. FP–17, Presented at the Fifth Joint MMM–INTERMAG Conference, Pittsburgh, PA, June 18–23,1991. IEEE Transactions on Magnetics, vol. MAG–27, no. 6, 1991, pp. 5016–5018.

8.8 Wang, R.H.: Combined Magnetic Vector-Scalar Potential Finite Element Computation of 3D Magnetic Field and Performance of Modified Lundell Alternators in Space Station Applications. Ph.D. Dissertation, Clarkson University, Potsdam, NY, 1991.

Chapter 9
Heat Rejection Assembly

9.1 Introduction

The heat rejection assembly (HRA) has a design heritage that is based on extensive spaceflight experience. Design features have been culled from Apollo, Skylab, and Shuttle hardware (ref. 9.1); performance characteristics are generally well understood. A number of design features, however, are unique either to the solar dynamic heat rejection system or to the requirements of Space Station *Freedom* and therefore lacked the developmental maturity requisite for preliminary design review. The focus of phase 1 efforts for the HRA thus was to develop these less mature aspects of the design and to ensure successful integration with other solar dynamic and station hardware.

The HRA provides the heat sink for the closed Brayton cycle (CBC) of the solar dynamic module. The major components of the HRA are the radiator panel set, the baseplate, the deployment scissors, the flexible hoses, the deployment motor, the utility plate, the fluid management units, and the gas coolers. The remotely deployed radiator panels reject excess heat from the engine cycle, the internal engine components, and the electronic components of the solar dynamic module. A single-phase cooling fluid, *n*-heptane, collects the waste heat generated by the engine and electronic components and convects it to the radiator, where it is radiated to the thermal sink of space. The fluid is circulated throughout the system and controlled by the fluid management unit (FMU), which consists of centrifugal pumps, accumulators, valves, and sensors. Line fittings provide the ability to connect the radiator panel set on-orbit to, and disconnect it from, the CBC receiver and power conversion unit and the FMU. The radiator, the FMU, and the utility plate are designed for on-orbit replacement.

Although the heat rejection assembly is composed of a number of ORU's, work supporting the solar dynamic radiator (SDR) ORU was the primary focus of the HRA development. Fewer programmatic resources have been devoted to HRA development because of its relative design maturity with respect to the concentrator and receiver assemblies.

The following discussion summarizes the HRA system design, requirements, component development, testing, and analyses. Tradeoff studies that had a direct effect on the HRA are outlined; issues and concerns are addressed. Areas requiring further development before the HRA can be safely incorporated into a flight program are included.

9.2 Background

The advanced development work of phase B precipitated the basic design of the SDR. A deployable, redundant, pumped-loop system was selected over various heat pipe and hybrid system concepts. The radiator configuration, location, and fluid (originally FC–75) were chosen by a tradeoff study. Inlet and outlet state points were optimized with the entire solar dynamic system. Preliminary strength and natural frequency studies were performed.

As previously mentioned, several design features emerged that lacked developmental maturity and therefore became the focus of phase 1 efforts. These are listed here along with the related design concerns:

(1) Operating lifetime: The SDR on-orbit design lifetime is much longer than any previous flight experience for similar radiators. As with all station hardware, reliability, maintainability, and performance over years (rather than months or days) creates a major design concern.

(2) Operating temperatures: The power conversion unit (PCU) outlet temperature (radiator inlet temperature) is relatively high in terms of space radiator design experience. Material performance under thermal cycling is a concern. The high temperatures also create a "zone of exclusion" for astronaut extravehicular activities. The difference required between inlet and outlet temperatures necessitates a relatively large heat rejection area. Large surface areas lead to other concerns, such as mass, launch packaging, aerodynamic drag, vulnerability to hypervelocity impact, shadowing of other components, and structural interactions.

(3) Protection from micrometeoroid and space debris impacts: The hazard from hypervelocity impact of micrometeoroid and space debris is directly related to time on orbit and exposed area. Puncture of a flow tube, a flexible hose, or an interconnect line would render an entire flow loop inoperable, necessitating use of the backup system. Adding bumpering to protect flow lines is necessary but increases radiator mass.

(4) Thermal control coating: A coating for the radiator

panels that has a high thermal emittance to minimize surface area and a low solar absorptance to reflect incident sunlight is required for efficient heat rejection. The coating must stand up to thermal cycling and be resistant to degradation due to vacuum ultraviolet radiation and atomic oxygen attack over the radiator lifetime.

(5) Deployment mechanism: Although the deployment mechanism is based on a Skylab design, the SDR panels are much larger than the photovoltaic panels deployed on Skylab. Vacuum welding of the scissor arms is also a concern.

(6) Control and structure interaction: Interaction between large, flexible space structures, such as the SDR, and associated controllers is a concern. The traditional separation between structural natural frequencies and controller frequencies that is used in ground-based systems is usually not available on orbit, primarily because of mass limitations.

(7) Transport fluid: The transport fluid must convect heat efficiently over the operating temperature range (to minimize mass and heat rejection area), must be resistant to thermal degradation, and must remain in the liquid phase between the radiator cold-soak and peak operating temperatures and pressures (i.e., it must not freeze or vaporize). The fluid must also meet material safety requirements.

(8) Transient operation: The heat rejection system must respond effectively during all system transients, including maximum insolation, minimum insolation, startup, shutdown, and both planned and unplanned emergencies.

The HRA portion of the phase 1 program was primarily structured to address these concerns, with both prime contract and supporting development resources, within budget constraints. Many general Space Station *Freedom* reporting requirements were addressed during phase 1 as well.

Approximately two years after preliminary design had commenced on the SDR, a contract for the photovoltaic radiator on *Freedom* was let to the same subcontractor. This radiator has different operating requirements than the SDR but is designed to take advantage of a number of SDR design features. The designs employ similar panels, hinges, flow tubes, and deployment mechanisms. The thermal control coating material is also the same. These similarities, along with the perceived design maturity are believed to have lowered costs and development time for the photovoltaic radiator. It is hoped that effort expended to develop the photovoltaic radiators and related heat rejection system components will in turn benefit future solar dynamic efforts. Development results from and flight experience with the photovoltaic system will greatly assist spacecraft thermal control system programs in the areas of thermal coating performance, durability, hypervelocity impact survivability, remote deployment and retraction system reliability, and fluid management. It is recommended that the photovoltaic heat rejection system utilized in the Space Station *Freedom* Program be reviewed.

9.3 Contractor Team

The Rocketdyne Division of Rockwell International was responsible for developing the fluid management unit, the utility plate, and the interface definitions for structural, electrical, and fluid connections. LTV Missiles and Electronics Corporation, under subcontract to Rocketdyne, was responsible for the SDR ORU, which included the panels, the baseplate, the flexible hoses, and the deployment mechanism. LTV's structural responsibility ended at the baseplate attachment to the interface structure. LTV's fluid and electrical responsibilities ended at their respective interfaces on the baseplate.

9.4 Design and Requirements

Specifications for the various components of the HRA establish the performance, design, manufacturing, verification, and acceptance requirements for the solar dynamic module components. Several components of the HRA have evolved to the point where initial specifications were drafted. Other components were in the early definition phase; their preliminary configurations are summarized.

9.4.1 Solar Dynamic Radiator

Physical requirements imposed upon the solar dynamic radiator were that it not exceed 2600 lb and that it have a deployed drag area no greater than 1600 ft^2. The stowed radiator must fit within the NSTS launch envelope (details of which can be found in section 5.9). The design life is 30 years. Maximum and minimum thermal performance requirements were based upon the extreme conditions that occur during maximum and minimum solar insolation. The maximum insolation case required a heat rejection capability of 99 kW thermal; the minimum case required 68 kW of thermal energy to be rejected. These requirements were derived from a thermodynamic state-point analysis. The radiator was to operate over a nominal fluid temperature range of 16 to 350 °F, corresponding to the maximum outlet and minimum inlet temperatures expected (figs. 9.1 and 9.2). The system was required to endure temperatures as low as −120 °F (cold-soak condition, ref. 9.2).

A summary of the LTV SDR design to meet these requirements follows: The maximum deployed envelope of the assembly has a width of 27.6 ft, a height of 56.0 ft, and a depth of 7.4 ft. Total weight of the assembly is estimated at 2559 lb, and it has a calculated first modal frequency of 0.097 Hz. The baseplate provides structural support to the deployment mechanism and to the radiator panel set and houses fluid and electrical lines. This plate is the mechanical interface with the solar dynamic module support structure.

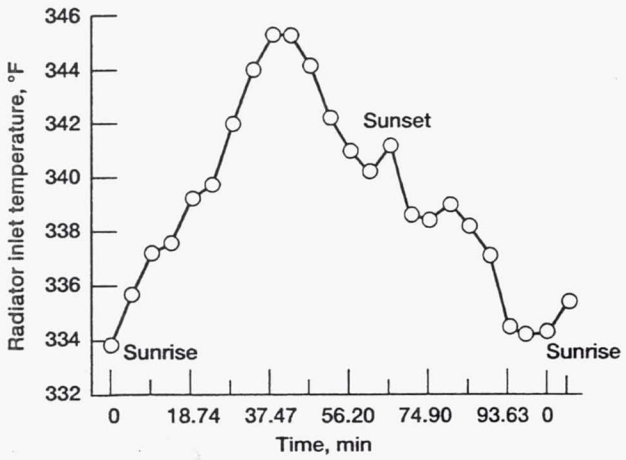

Figure 9.1.—Inlet temperature as a function of time (maximum insolation orbit) for solar dynamic radiator.

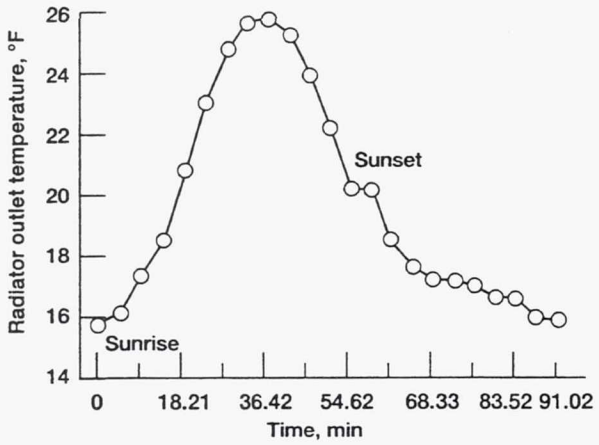

Figure 9.2.—Outlet temperature as a function of time (minimum insolation orbit) for solar dynamic radiator.

The deployment scissors mechanism deploys and retracts the panels between the folded package configuration and the extended operational configuration. Deployment and retraction take place remotely by means of a deployment motor. The system also has a manual backup deployment and retraction capability, which is performed by an EVA crewperson.

The radiator panel set consists of seven panels. Figure 9.3 represents the latest design with panel sizes of 87.24 in. in height and 325.30 in. in width. When deployed, the scissors half-angle between panels is 8°. Each panel consists of face sheets that are 0.010-in.-thick aluminum coated with Z–93 white paint. Between the face sheets is aluminum honeycomb to provide strength and support for the aluminum extruded flow tubes that are embedded in the honeycomb (ref. 9.3) The flow tubes of the primary loop are spaced every 4.854 in., with the redundant tubes spaced equally between the primary tubes (view A–A) (ref. 9.4). The tubes and the face sheet are bonded by using adhesives. The flow tube extrusion is shown in detail B and is 0.67 in. by 0.188 in., with a fluid flow diameter of 0.08 in. The tube incorporates a bumpered design, which provides added protection to the flow path from hypervelocity impacts of micrometeoroids and space debris.

Flow tubes are welded to panel manifolds and each of the panel manifolds is connected to the adjacent panel by flexible hoses. These hoses are constructed of a solid aluminum elbow with flexible aluminum bellows attached to each end (ref. 9.5). These bellows are welded to the fixed manifold pipes, completing the flow path. The bellows portions of the flexible hoses have a double braided overwrap to provide structural support and hypervelocity impact protection. Similar panels and hoses are currently being used in the NSTS orbiter radiator system.

9.4.2 Utility Plate

The utility plate serves as a support structure and an electrical and fluid interface for solar dynamic controllers, FMU's, and power management and distribution system ORU's and is attached to the interface structure. This plate removes the excess heat generated by the solar dynamic module's electronics and coolant fluid pumps. The utility plate provides some cooling to these components and interfaces with the balance of the HRA through the interconnect lines.

The utility plate has a design weight of 170 lb when filled with *n*-heptane. Its maximum envelope is set at 38 by 124 by 6 in. The design life is 30 years. The operating fluid temperatures range from −126 to 70 °F at a maximum pressure of 200 psia. The maximum nominal operating temperature is imposed by the electronic cooling needs. Because the electronics must be maintained between −65 and 120 °F, the utility plate maximum fluid outlet temperature was set at 70 °F. This requirement is based upon simplified calculations involving estimates of electronic heat loads and utility plate design. The entire flow that circulates through the radiator passes through the utility plate; there are no bypass lines in the system. The amount of heat rejected ranges between 2 and 4.7 kW thermal as generated by the ORU's on the plate (ref. 9.6).

9.4.3 Fluid Management Unit

The specification for the fluid management unit was not completed, but the functional description and preliminary component mass estimates were compiled. This unit provides the required coolant pumping and inventory management for the HRA fluid system. Each FMU contains a centrifugal pump, valves, an accumulator, a filter, and coolant line disconnects (fig. 9.4). There are separate ORU's for the

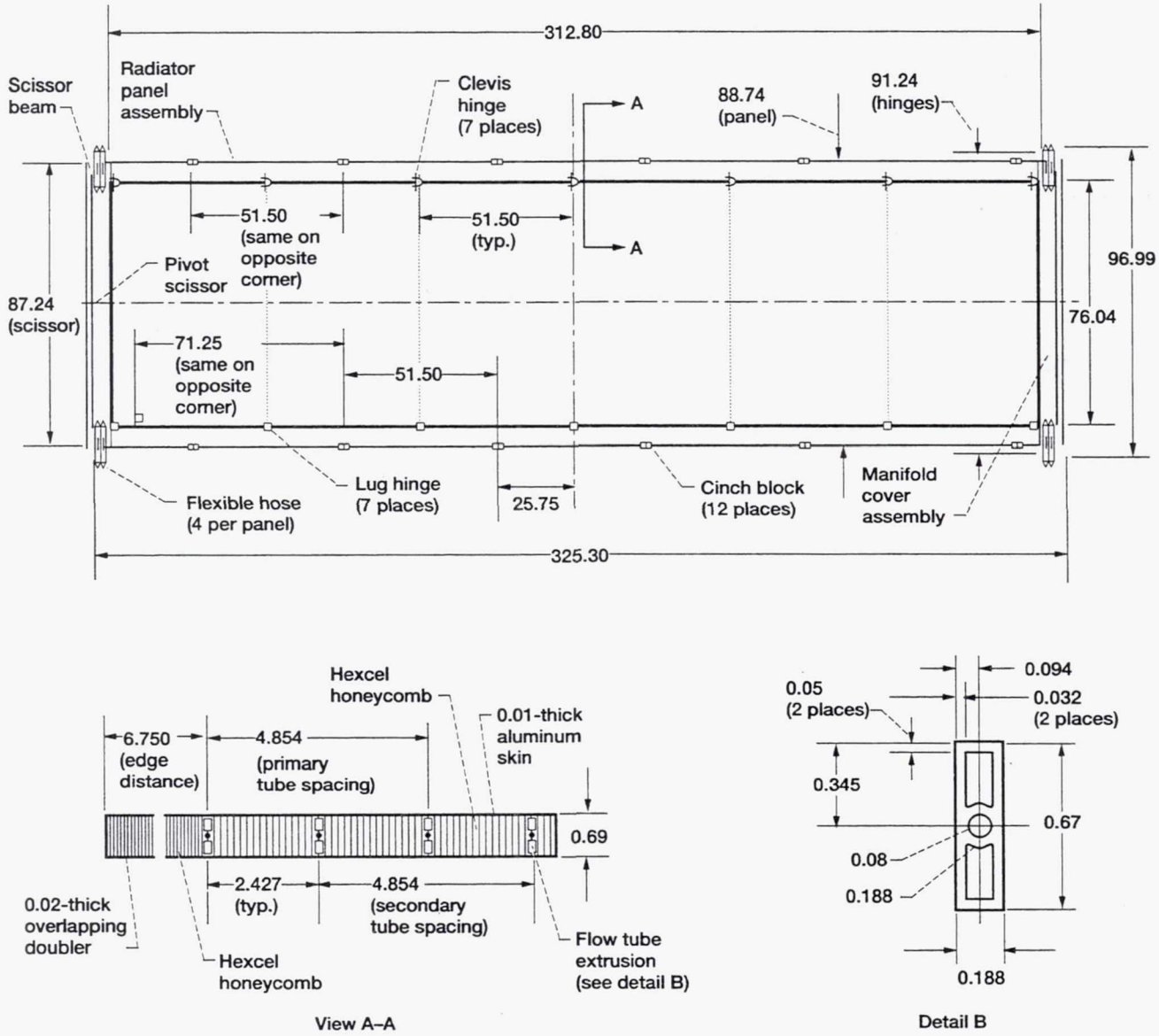

Figure 9.3.—Radiator panel design. (Dimensions are in inches.)

primary and backup systems to provide the necessary system redundancy. The units are designed for EVA or robotic maintenance operations (replacement). The FMU is controlled by the power control unit; the functions controlled include inventory management, leak detection, fault detection and isolation, corrective and protective actions, redundant component management, and pump control.

The weight allocation per ORU is 70 lb, which includes all components and support structure. The most recent design mass estimate for the FMU is about 110 lb (ref. 9.7). For comparison the mass of one pump is roughly 4.2 lb. The ORU was sized to fit into a standard ORU box being designed for the photovoltaic system. This box had overall dimensions of 20 by 38 by 17 in. (ref. 9.8).

The design flow rate of the system varies with the required heat rejection and coolant outlet temperatures. The flow rate ranges from a minimum of about 0.52 lb/s to a maximum of about 0.526 lb/s (fig. 9.5).

9.4.4 Interconnect Lines

The redundant hot interconnect line ORU's are fluid lines with disconnects that provide the flow path between the PCU assembly and the deployable radiator panel subassembly. The redundant cold interconnect line ORU's are fluid lines with disconnects that provide the flow path between the solar dynamic utility plate and the power generation system. The redundant pump interconnect line ORU's are fluid lines with disconnects that provide the flow path between the deployable radiator panel subassembly and the FMU's. No specifications are available for interconnect lines.

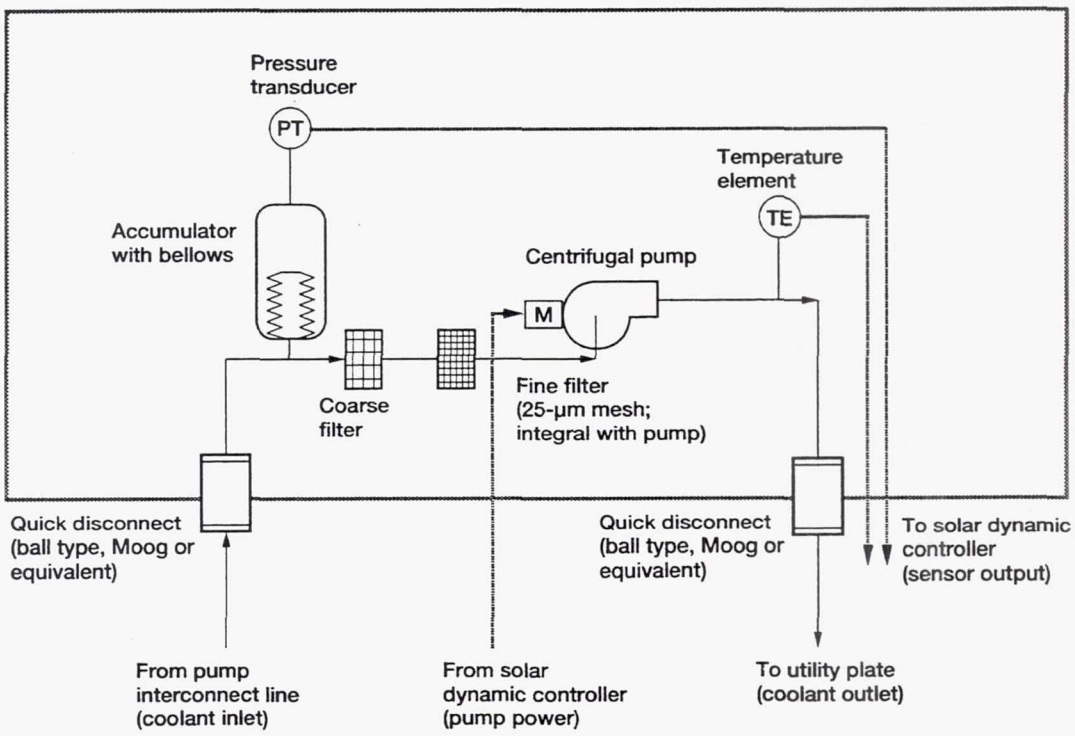

Figure 9.4.—Schematic of alternative fluid management unit.

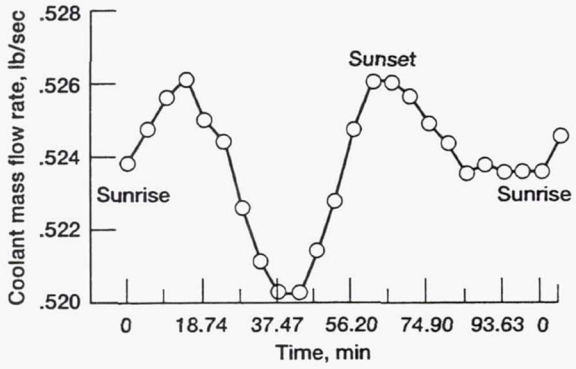

Figure 9.5.—Flow rate as a function of time (maximum insolation orbit) for solar dynamic radiator.

9.5 Preliminary Design

This section summarizes the analyses and tradeoff studies performed to define the HRA preliminary design.

9.5.1 Safety Analyses

Safety analyses of the HRA were performed to satisfy general Space Station *Freedom* reporting requirements and to identify potential design problems as early in the program as possible.

9.5.1.1 Failure modes and effects analysis. — A preliminary failure modes and effects analysis (FMEA) was performed to identify and evaluate the significant SDR potential failures modes and their effect on *Freedom* (ref. 9.9). The FMEA was performed on the design as it existed and was to be revised and updated as the design process proceeded. The study was performed during the early design stage to identify and correct potential design problems as early as possible. The results of the study were the basis for the critical items list (CIL). This list identifies items that are highly critical to *Freedom* and must meet specific conditions (ref. 9.10).

Study results identified no critical items in the SDR on the basis of CIL criteria. Additional observations were that the SDR imposes no special requirements on *Freedom* and requires no EVA for nominal operations.

There was concern that the loss of a radiator would result in the loss of solar dynamic module power-generating capability. This loss could be defined as a loss of critical mission capability, putting the radiator on the CIL. Additional failure effects that should be incorporated into future analyses include the hypervelocity impact results from the completed testing and test results of the flexible hose components when available.

9.5.1.2 Materials safety. — Materials selected for the HRA must be compatible with the space environment. Most materials that are exposed to space are aluminum alloys, corrosion-resistant steel, and stainless steel. Preliminary material assessments of the radiator have been conducted (refs. 9.11 and 9.12). Radiator materials were evaluated for safety in

handling, processing, and fabrication. Results indicated that if materials were processed and controlled by the appropriate specifications, they would be compatible with safe operation.

Eighty-nine radiator components were identified and rated against reference 9.13. Twenty of the components did not receive top ratings and will require more information before a rating can be established. If they still do not receive the top rating, a material usage agreement must be filed and accepted before that particular material can be flown in space.

A preliminary in-house assessment was performed on the HRA, the heat receiver, and the PCU. No material was identified that must be changed to enable these assemblies to be flown.

9.5.2 Reliability, Availability, and Maintainability Analysis

9.5.2.1 Reliability analysis of radiator. – A preliminary on-orbit reliability analysis of the baseline radiator was performed by LTV (ref. 9.14). Radiator components consisting of panels, a baseplate, scissor beams, hinge joints, quick disconnects, flexible hoses, fluid systems, a deployment and retraction motor, a deployment and retraction mechanism, and an EVA deployment and retraction backup were examined. Failure rates of the individual components were created by engineering estimate. The result was a prediction of 39.6 years mean time between failure, which exceeded the 30-year requirement. The analysis should be repeated using more reliable failure rates of the individual components. The degradation characteristics of the thermal control coating over the long-duration exposure to the space environment should be included. A full-scale deployment mechanism should be constructed to perform failure simulations for verifying anticipated failure modes and effects.

9.5.2.2 Reliability analysis of FMU. – A reliability study of the FMU evaluated the baseline configuration, which consisted of two pumps per ORU, against an alternative configuration that only had one pump per ORU. The results were inconclusive. Normally, one would expect a redundant system to have an increased reliability, but this was offset by the redundant system's need for an additional flow control valve. In an attempt to determine the better configuration, the results were converted into life cycle costs. The conclusion was that the single-pump configuration had the advantage. Potential additional savings identified included reduced complexity, which may relieve packaging density problems, reduced size, and simplified checkout procedures and diagnostic instrumentation (ref. 9.15). The disadvantage is the obvious lack of a backup system. Note that a primary driver in the study was the reliability of a flow control valve, which is necessary in the redundant configuration. If a more reliable valve is identified in the future, the FMU configuration should be reevaluated.

Mainly on the basis of this study the baseline FMU configuration was changed to the single-pump-per-ORU configuration. Weak links in the system that must be addressed are the fluid quick disconnects and the check valves, which have the lowest reliability of all components in the single-pump FMU.

9.5.2.3 SDR survivability from micrometeoroid and space debris impact. – LTV analyzed the SDR probability of surviving impacts from micrometeoroids and space debris (refs. 9.16 and 9.17) to determine if the preliminary design met the requirement of at least a 0.95 probability of no penetration during a 10-year period that would cause complete loss of heat rejection. A reliability analysis showed that design changes were required for the hard interconnect line in the baseplate and the flexible hose assemblies. Design changes were proposed that added shielding to these components.

9.5.3 Thermal Analyses

The thermal performance of the HRA was modeled extensively during phase 1. Numerical models were built by the prime contracter, by two subcontracters, and at NASA Lewis by using Fortran, SINDA, SINDA85/FLUINT, and other SINDA type of codes. These models were used to evaluate the preliminary design and to perform tradeoff studies for both steady-state and transient operation. Several models were integrated into system-level models of the solar dynamic power cycle. The codes were frequently crosschecked to identify discrepancies.

The codes are briefly described in this section. Major tradeoff studies that used these codes are described in sections 9.5.4 and 9.5.5.

Several codes were developed prior to phase 1 and were used in phase A/B studies; later they were refined for use in phase 1 design and tradeoff studies. An early in-house effort modeled the solar dynamic thermodynamic cycle by using the Closed Cycle Engine Program (CCEP) developed by J. Klann (ref. 9.18). Cycle performance calculations were conducted throughout phase 1 that evaluated the performance of the solar dynamic module and the state points that optimized the system. Although the focus of these studies was cycle performance, studies to evaluate the radiator performance were also conducted (ref. 9.19).

9.5.3.1 Contractor thermal modeling. – LTV first modeled the preliminary design of the SDR with a SINDA code during phase A/B. The code was later refined during phase 1. A general description of the model can be found in reference 9.20, and a more current version in reference 9.21. The later version also explains the sizing strategy for the design.

Rocketdyne developed a transient thermal model of the HRA by using Fortran (ref. 9.22). This two-dimensional code used fin efficiencies to obtain the equivalent thermal resistances of the radiator. Sample transient performance runs and weight optimi-

zation were illustrated. This code was intended for the solar dynamic and photovoltaic radiator programs. It was anticipated that this code would be verified against the heat transfer test results that LTV obtained from their radiator panel heat transfer testing. Rocketdyne also developed a radiator model for their cycle performance code (EPSTAM).

Allied-Signal also used a SINDA type of code to model the SDR for cycle analysis of the solar dynamic module.

9.5.3.2 In-house thermal modeling. — In-house thermal models were developed with two purposes in mind. First, since NASA Lewis had a role in phase 1 to provide supporting development for the SD program, simple models were used to perform parametric studies that were difficult to perform on the larger, more complex codes used by the contractors. Second, NASA Lewis performed some preliminary independent verification and validation work on the contractor codes and on the design recommendations resulting from these codes.

A simple and flexible numerical model was developed in-house (ref. 9.23) to simulate steady-state heat transfer and fluid flow performance of the radiator and to calculate area, mass, pumping power, and impact survivability for many combinations of flow tube and panel configurations, fluid and material properties, and environmental and cycle variations. The code was used to study alternative radiator configurations and to evaluate contractor recommendations. Because the code requires very little computer time, many configurations could be evaluated and the best recommended for further study.

In anticipation of the need to have a more detailed performance model of the entire HRA, the Solar Dynamic Office initiated a model development effort with the NASA Lewis Engineering Directorate. Initial efforts were to study the radiator for compliance with required heat rejection and given fluid inlet temperatures and to assist in the heat transfer fluid selection evaluations (ref. 9.24). The SINDA/FLUINT model developed was used to verify contractor design assumptions (e.g., whether heat transfer through the honeycomb was significant). The radiator model was then incorporated as a component into an entire heat rejection assembly model by using the SINDA85/FLUINT code. The status of this effort is documented in reference 9.25. The heat exchangers were modeled to provide heat transfer analysis of each component. Additional components, such as pumps and interconnect lines, were modeled to the greatest extent possible, although very limited design information was available at the time. Where applicable, component models from the photovoltaic program, such as the utility plate, were scaled and used directly for the solar dynamic program.

In general the results from all of the codes agreed well. The most difficult area to reach agreement on was the sink temperature to be used in these models. The ability to generate accurate sink temperatures is dependent upon the ability to model *Freedom*'s varied surfaces and orientations relative to the Sun, the Earth, and itself as it orbits about the Earth (i.e., to determine the effect of surrounding equipment and heavenly bodies on the radiator's ability to reject heat by radiation). Detailed studies were conducted to develop sink temperatures at discrete locations about the orbit, primarily by using the TRAYSYS codes. Because this approach involved considerable computer time, an effective sink temperature was found that was held constant throughout an orbit but resulted in the same heat rejection by the radiator on an orbital average. This approach was considered adequate for preliminary design.

Note that the effective sink temperature is influenced by changes in *Freedom*'s design, in orbital parameters, and possibly in the operating point of the solar dynamic module. However, because of computational limitations the effective sink temperature was not updated with each design change. As a result, sink temperatures obtained for one design were sometimes used in another design in a manner that could yield less accurate results (potentially because of differences in modeling techniques). This area should be carefully examined after preliminary design because it may have a large influence on the heat rejection calculations.

9.5.4 Heat Rejection Fluid Tradeoff Study

LTV and Rocketdyne conducted fluid selection tradeoff studies to determine a heat transport fluid that met the thermal performance and safety requirements for the SDR while minimizing mass, drag, and pumping power (refs. 9.26 and 9.27). Thirteen alternative fluids were identified in addition to the baseline fluorocarbon FC–75 coolant: acetone, cumene, DC–200, ethanol, FC–77, Freon-22, isopropanol, methanol, *n*-heptane, RC–1, Syltherm XLT, Syltherm 800, and toluene. The criteria used for comparison consisted of toxicity, flammability, special handling equipment or procedural requirements, freeze temperature, vapor pressure, reactivity, compatibility, stability, commercial and industrial experience, availability, cost, and design and development impact. From the information available at the onset of the study it was known that major performance improvements were possible by opting for a more hazardous (flammable or toxic) fluid.

A figure-of-merit approach was used to begin the selection process. These parameters were based on thermal transport properties of heat transfer, pumping power, and heat exchanger effectiveness. The alcohols were at the top of the list but were eliminated owing to their incompatibility with aluminum. The hydrocarbons were the next best, with the remainder in the bottom group. The top four candidates (toluene, *n*-heptane, FC–75, and Syltherm XLT) were selected for more thorough consideration. Syltherm was the worst performing and was eliminated early in the study. FC–75 ranked first in safety and flammability, but last in performance, with a radiator mass exceeding the allocation. Normal heptane was demonstrated to be the most effective thermal performer. Studies done at NASA Lewis using in-house programs (refs. 9.23 and 9.24) confirmed this conclusion.

9.5.5 HRA State-Point Tradeoff Study

The HRA acts as the thermodynamic sink of the CBC and is required to carry away enough heat to maintain the cycle gas working-fluid temperature and the alternator operating temperature (at operating pressure). The SDR rejects heat to the thermal sink of space. The effective sink temperature varies due to orbital and seasonal changes. A series of tradeoff studies were performed by Allied-Signal, and desirable state points were determined thus placing performance requirements on the HRA.

LTV, in turn, assessed the expected radiator performance under these conditions, and when deficiencies or positive margins resulted against the baseline design, design changes in the radiator were considered. These changes included varying the fluid flow rate, the flow tube diameter, the number of flow tubes, the flow tube spacing, the flow tube length, and the number of panels.

A number of state-point design studies were conducted throughout phase 1. The most recent state points and SDR design-point conditions for steady-state operations are listed in table 9.1. Rocketdyne directed LTV to evaluate the state-point performance for the baseline design with pressure drops of 11.5 and 26.8 psi. Their analysis concluded that the baseline configuration satisfied the latest state-point conditions, but that raising the pressure drop allocation reduced overall system mass. Because the solar dynamic module was over its mass allocation, all methods of mass reduction were being explored (ref. 9.28). Reference 9.28 evaluates the performance of the radiator against the state-point requirements at that time.

TABLE 9.1.—SDR STATE-POINT EVALUATION AND DESIGN-POINT CONDITIONS

Orbital altitude, n mi	250
Beta angle, deg	52
Orbit time	Solar noon
n-heptane flow rate, lb/sec (lb/hr)	0.7122 (2563.9)
Fluid inlet temperature, °F	244.2
Fluid outlet temperature, °F	57.6
Fluid heat rejection, Btu/sec (kW)	76.6 (80.8)

9.5.6 Structures and Dynamics

The structural design criteria are summarized in reference 9.29. The structural environments (structural stiffness, loads, acoustics, shock, and temperature) that the radiator must survive for the design life of 30 years are defined. Factors of safety and margins of safety are also defined.

The first modal frequency of the on-orbit deployed radiator was a contentious design issue because it was thought to have a significant effect on the module's pointing and tracking control system. The initial modal frequency of the radiator was 0.1 Hz. The contractor recommended stiffening the radiator to at least 1.0 Hz to avoid control-structure interactions and proposed several modified radiator configurations. The Solar Dynamic Office contended that a properly designed control system would preclude control-structure interactions. Changing from the lower to the higher frequency prohibitively increased radiator weight and complexity. When the magnitude of these increases was realized, serious attention was given to the driving requirements of the control system. Changes were proposed by NASA Lewis, and after being studied both in-house and by the contractor, the pointing system was changed. The effect was a less stringent requirement on the radiator first modal frequency. With these relaxed requirements, the radiator 0.1-Hz design was retained. Details of the frequency issue can be found in section 5.7.

In the stowed (or launch) configuration, the radiator must meet specific structural requirements to avoid the possibility of mechanical interferences with the orbiter, other components, and itself. The design was analyzed and presented at the LTV interim design review (ref. 9.30) for compliance with a (derived) stowed frequency requirement of 10 Hz and response to the cargo bay internal acoustic environment. Also analyzed was the response to the random vibration levels specified at the supports when stowed for NSTS launch. The panel was supported at the four corners initially, and two supports were added at the midpoint edges to raise the frequency. The resulting panel deflections were small enough that there was no danger of adjacent panel contact. Adding the supports in the middle of the base structure raised the stowed fundamental frequency to 11.4 Hz, satisfying the requirement.

Although this study shows that the radiator by itself meets the requirements, further analysis must be conducted on the payload as a whole because the support points available for the radiator may vary significantly from what was assumed.

9.5.7 Plume Loads

When the orbiter is in the vicinity of *Freedom*, its reaction control system (RCS) plumes could impact the solar dynamic module. LTV assessed these effects for the maximum RCS plume loads identified. These loads were translated into a back-to-back square pulse forcing function tuned to the radiator's fundamental frequency (considered the worst case). Maximum transient load and displacement magnitudes were predicted in critical areas of the model and then compared with a static loading of 0.04 g resulting from typical orbit dynamics. The 0.04-g load was derived for the photovoltaic radiator specification and was considered to be a very conservative number relative to the SDR. This static load was applied normal to the SDR long axis. The static load resulted in displacements up to six times greater that the plume loads (ref. 9.31); see table 9.2.

TABLE 9.2.—COMPARISON OF SDR DISPLACEMENTS FOR PLUME IMPINGEMENT AND 0.04-g LOAD CASES

[The 0.04-g load was arbitrarily applied in the positive y direction. It is actually a reversible load.]

Location	Plume impingement displacements, in.			0.04-g load displacements, in.		
	x	y	z	x	y	z
End of seventh panel	−0.4	−10.1	−0.3	0.1	60.8	1.0
	−.4	−11.1	−.3	.1	65.1	1.2
	−.4	−11.5	−.2	.1	68.0	1.1
Fifth panel	−.3	−6.7	−.2	.1	40.5	1.0
Third panel	−.2	−3.0	−.2	0	18.9	.8
First panel	−.1	−.5	−.2	0	3.3	−.5

9.5.8 Contamination

The Space Station *Freedom* Program has specific requirements governing contamination of, and due to, its many components (ref. 9.32). Activities that contribute to contamination include manufacturing, launch preparation, execution, and orbital operation.

An assessment was conducted on the radiator for the orbital operation conditions (ref. 9.33). It was assumed at this time on the basis of previous flight program experience with the NSTS that manufacturing and launch requirements would be met. (This of course should be stringently analyzed as design progresses.) Specific limits were placed on molecular efflux (molecular column density), particulate background, and induced contamination or deposition. The radiator panels were identified as the major source of molecular species because panel manufacture traps air in the honeycomb construction and makes use of adhesives and paint. These may release infrared or ultraviolet active species, or both. Honeycomb panel construction creates a sealed container that will contain these molecules unless struck by space debris. The only source of contaminant with large exposure to space would be the white paint. This surface will be thermal vacuum baked to remove all evaporable species.

The white coating itself has been shown to degrade when contaminated (section 9.7.4). Deposition effects, especially from sources such as the NSTS thrusters during docking operations, will need to be addressed when view factors and relative positions of all components are known.

The initial look into the contamination area concerning the HRA indicated that the requirements imposed by the program will be met without any exemptions necessary.

9.5.9 Mass Properties

Mass properties for the HRA consist of weight, center of gravity, and moments of inertia. Only the radiator has received detailed analysis that has been documented. Other component mass estimates are summarized here. Current design weight of the radiator is 2559 lb; this does not include the mass of the heat transfer fluid, which is included under the FMU allocation. Stowed and deployed configurations have the same mass. Detailed radiator mass properties can be found in reference 9.34, which breaks down the component masses that form the radiator ORU. Table 9.3 lists the ORU's center of gravity and moments of inertia. The coordinate system used is shown in figure 9.6.

TABLE 9.3.—MASS PROPERTIES SUMMARY FOR SDR LOW-FREQUENCY DESIGN

Property	Condition	
	Folded	Deployed
Weight, lb	2598.42	2598.42
Center-of-gravity locations, in:		
x	165.12	165.12
y	44.49	44.49
z	13.23	282.63
Moments of inertia, lb/in.^{2}:		
I_{xx}	1.80×10^6	119×10^6
I_{yy}	25.4×10^6	143×10^6
I_{zz}	27.0×10^6	25.7×10^6
I_{xy}	−206	−4984
I_{xz}	5260	133 768
I_{yz}	2784	76 222

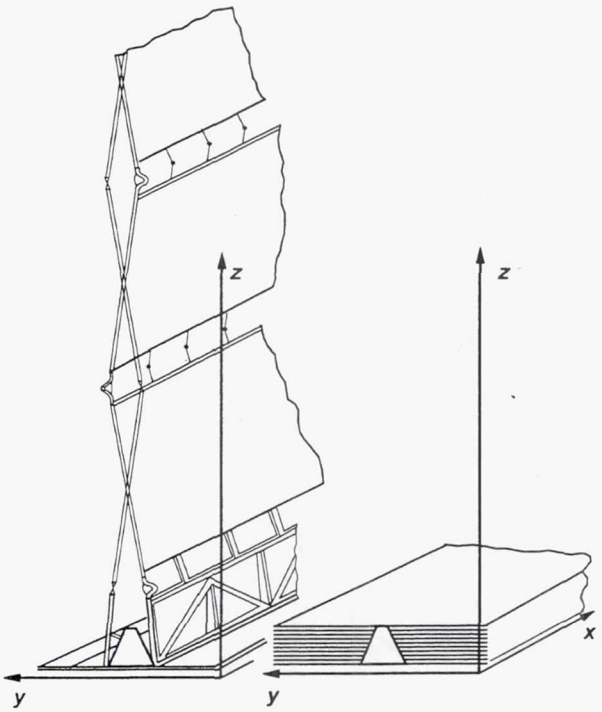

Figure 9.6.—Solar dynamic radiator coordinate reference system.

9.6 Module Interface Definition and Effects

9.6.1 Shadowing of Concentrator

In the module configuration that places the radiator in front of the concentrator, the radiator casts a shadow on the concentrator. This shadow has an effect on the solar flux delivered from the concentrator to the receiver. When the radiator has its edge to the Sun, the beta angle determines the magnitude of the shadow that is projected by the seven panels onto the concentrator mirrors. When pointing is perfect, the beta mispoint angle is zero, projecting the minimum shadow onto the concentrator. The worst condition, a mispoint angle of 2°, would result in the largest shadow projection onto the concentrator. The calculated shadow areas for the 0° and 2° positions are 17.0 and 69.3 ft^2, respectively (ref. 9.35).

9.6.2 Radiator Attachment

The method used to attach the radiator to the baseplate was influenced by how the solar dynamic module was to be pointed (i.e., accurate pointing reduces radiator shadow on the concentrator and has less effect on flux distribution to the receiver). A study was conducted to determine a preferred SDR attachment concept (ref. 9.36). Factors that were looked at were mass, structural integrity, deployability, reliability, and maintainability. The recommended concept was a single gearbox-driven deployment hinge and four attachment points for two inboard and two outboard struts that support a vertical SDR. A canted orientation was also examined. The flux distribution section of reference 9.36 contains details on the effects of radiator position on the concentrator and receiver; the fine-pointing and tracking section details the effect of the radiator on module pointing.

The attachment study referenced here required numerous key assumptions and was not fully approved at NASA Lewis. Attention should be focused on this area of component interactions if the program is resumed.

9.7 Component Development

This section addresses testing performed to advance the preliminary design of specific components of the HRA during phase 1 of the program.

9.7.1 SDR Hypervelocity Impact Testing

The approach to assessing the survivability of the solar dynamic radiator to micrometeoroid and space debris impacts included analysis (section 9.5.2.3) and hypervelocity impact testing of radiator panel samples. The specific details can be found in references 9.17 and 9.37; a summary is included here. The intent was to quantify the type of particle and the particle population expected to penetrate the radiator flow tube. Two phases of testing were conducted.

The first phase consisted of 12 shots using aluminum spheres with diameters of 1.0 to 1.6 mm and impact angles normal (0°) and at 45° to the panel surface. Velocities ranged from 6 to 7 km/sec. Test results indicated that a 1.59-mm aluminum particle traveling at 6.9 km/sec will penetrate the tube wall. Calculations to translate the test data to average orbital debris velocities showed that a typical space debris particle of 1.09-mm diameter with a density of 2.8 g/cm^3 traveling at 10 km/sec would penetrate the tube. Survivability calculations for a solar dynamic radiator indicate a 0.966 probability that both the primary and secondary loops would not be penetrated over a 10-year period. Additional observations indicated that the aluminum honeycomb channeled the particle through the panel, tending to reduce the number of oblique impacts that could reach the flow tube after passing through the honeycomb. Secondly, the foam adhesive that binds the honeycomb to the flow tube extrusion provided additional protection from oblique impacts.

The second phase of testing was conducted to refine the initial assessments. Specific goals were to determine the penetration limit of the flow tubes and to determine protection benefits from increasing the tube wall thickness (ref. 9.37). Thirty-three shots consisting mainly of aluminum spheres (two were nylon) ranging from 1.0 to 2.4 mm in diameter were shot at oblique angles of 0° to 75° from the panel surface normal. The maximum velocity was 7.8 km/sec. Some samples were coated with the thermal control white paint to investigate the spalling characteristics of the paint. Flow tubes were leak checked with water under ambient conditions to determine if the tubes had been perforated. Results indicated that when the SDR is considered as a system (primary and redundant flow tubes), there is a 0.992 probability of survival over a 10-year period. These calculations were performed by using the baselined (ref. 9.38) orbital debris model. An updated debris model that predicts a more severe environment (ref. 9.39) is pending approval by the level II program office. This model predicts an increase in orbital debris as a function of time, depending on the number of spacecraft launches, etc. With this new model the survivability of the radiator is reduced to 0.97 for the years 2001 to 2010 and to 0.96 for 2011 to 2020. Details of the LTV analysis of the test results can be found in reference 9.40. Other observations were that the coated specimens showed spalling on the order of 4 to 6 times the diameter of the impacting projectiles.

Future tests were planned with the hard and flexible interconnect lines for the HRA. Although the hard lines lend themselves fairly well to existing analytical methods of predicting penetration, the flexible lines do not. Their cross sections consist of complex layers of wire mesh and bellowed flow tube that cannot be modeled analytically. It will be necessary to thoroughly test them to determine the particle size that will penetrate them.

9.7.2 Panel Heat Transfer Testing

LTV conducted thermal testing of panel elements in a vacuum chamber with a cold wall for steady-state and transient load conditions and two test fluids, *n*-heptane and FC–75. The test objectives were to verify the thermal perform-ance of the panels against numerical predictions and to eval-uate the benefits of installing helical coiled wire turbulator inserts in the flow tubes to enhance convective heat transfer. Pressure drops were measured over ranges of flow rates: 5 to 45 lb/hr for *n*-heptane and 10 to 100 lb/hr for FC–75, both for ambient and 350 °F inlet temperatures. Heat transfer was measured at flow rates of 25 to 45 lb/hr and 40 to 80 lb/hr, respectively, for the two fluids. Inlet temperatures were 250, 300, and 350 °F. These flow rates were selected to obtain the same Reynolds numbers for the two fluids in order to facilitate comparisons. The test configuration was arranged so that three panel elements measuring 10 in. wide by 60 in. long were connected in series. Each panel contained four flow tube extrusions, two with turbulators and two without.

Steady-state heat transfer test data compared well with predictions; the transient comparison was not completed by the end of the program. No significant differences in heat transfer between the two fluids were seen when they were compared at the same Reynolds number. A small difference was predicted but was probably not detectable within the accuracy of the instrumentation. The test results showed that heat transfer in the tubes with turbulators increased by a factor of 2 but that the friction factor increased by a factor of 6 to 7, which roughly corresponds to a six- to sevenfold increase in the pressure drop. Details of the test can be found in reference 9.41.

The final test report (ref. 9.41) contains a significant amount of unanalyzed data that could help in the future design of radiator panels.

9.7.3 Adhesive Structural Test

Limited strength data existed on the adhesive planned for use in the SDR to bond the aluminum honeycomb and flow tube extrusions to the aluminum facesheets, especially at the elevated temperatures at which the SDR operates. The test objective was to verify the high-temperature performance of the adhesive, but because of budget constraints the program was combined with the photovoltaic radiator testing and the test matrix temperature conditions were thus extended to the higher solar dynamic operating temperatures. Testing was performed over a temperature range of −120 to 350 °F for flat tensile, climbing drum peel, and lap shear testing modes. A set of test points was also conducted at 70 °F after a simulated 30-day salt spray. Results provided enough information to accurately establish the acceptance levels for the adhesive. The mechanical properties of the system varied with temperature in a predictable manner. When the honeycomb cell size was reduced from 3/8 to 1/8 in., the flat tensile strength was much higher than expected. Salt spray did not damage the bonded honeycomb structure as evidenced by the drum peel and flat tensile tests (ref. 9.42).

9.7.4 Thermal Control Coating Screening Tests

Thermal control materials used previously on space radiators have not been qualified for the extended life that *Freedom* requires or qualified for the elevated temperatures imposed by the CBC. A program was undertaken to perform screening tests on candidate materials that had potential to perform as desired and survive the low-Earth-orbit environment. The goals were to identify coatings with an initial emittance of at least 0.9 and a solar absorptance equal to or less than 0.2. Postexposure requirements were no change in emittance and a final solar absorptance of less than 0.3. Eleven coatings were exposed to 1000 equivalent Sun hours (ESH) of vacuum ultraviolet (VUV) radiation, in the range 100 to 200 nm, for 25 vacuum thermal cycles and with atomic oxygen exposure to a total fluence of 2×10^{21} atoms/cm^2 in air plasma ashers. Of these, 10 coatings were exposed to 1000 ESH in the ultraviolet range (200 to 400 nm). The top-performing coatings in descending order were Z–93, YB–71, and S13G/LO–41. Details of the test program and results can be found in reference 9.43.

A sulfuric-acid-anodized aluminum material prepared by McDonnell Douglas (ref. 9.44) was also tested and was found to meet the optical property requirements upon exposure to 1000 ESH for 15 vacuum thermal cycles and an effective atomic oxygen fluence of 2×10^{21} atoms/cm^2 in an air plasma asher (ref. 9.45).

The top four candidates were to be evaluated in a longer duration, synergistic exposure test to atomic oxygen and VUV radiation with in situ solar absorptance measurements. This testing would have provided important information to be used in investigating recent findings from the Long-Duration Exposure Facility and other ground tests which indicate that synergistic effects may occur when materials are exposed to atomic oxygen and ultraviolet radiation. Specific effects may be a "cleaning" or "bleaching" of surfaces that had been darkened by ultraviolet radiation upon exposure to atomic oxygen. At the writing of this paper the photovoltaic radiator program plans to proceed with the evaluation of the top four coatings. The test results should yield valuable information on coating performance and durability in the low-Earth-orbit environment.

9.7.5 Flexible Hose Testing

The flexible hoses that are used to connect adjacent panels of the SDR will require testing to develop the analytical relationships so that pressure drop, bending force, flexible life,

and hypervelocity impact survivability can be accurately modeled. Hypervelocity impact was previously addressed. The pressure drop needs to be obtained experimentally because of the bellows design of the tubing. The bending forces must be known in order to analyze the stowed configuration stress and the resultant spring force that is imparted to the radiator during deployment. The ability of the hoses to meet the flexible life requirement of 100 cycles needs to be demonstrated even though NSTS program experience indicates that it will not pose a problem. Plans were being drafted to address all of these areas when the SD program was terminated. Because the photovoltaic radiator system also has flexible hoses, some information obtained during that program should be useful. The major difference is that photovoltaic radiator hoses are planned to be constructed of stainless steel, but the solar dynamic hoses were planned to be constructed of aluminum.

9.8 Assessment of Status

The primary objective of the phase 1 work on the heat rejection assembly has been to develop the design maturity requisite for preliminary design review. Major extant or unresolved design concerns are as follows:

(1) Deployment mechanism: No deployment testing was planned or performed because of budgetary constraints; therefore the original concern remains. Deployment testing is planned for the photovoltaic radiator program, although in making comparisons between the two systems, it should be noted that the photovoltaic radiator is smaller (and thus easier to deploy) than the current SDR.

(2) Heat transfer fluid: Although *n*-heptane is a good thermal performer, safety concerns remain.

(3) Transient operation: Performance under transient conditions has not been well studied.

(4) Integration: Integration issues were not recognized early in the phase 1 program but became apparent as the module design progressed. Concerns such as radiator shadowing of the concentrator, control-structure interactions, and launch packaging have been addressed but are not sufficiently resolved.

Although solar dynamic phase 1 work was suspended prior to completion, much of the development work in the heat rejection area is continuing under the photovoltaic radiator effort. When evaluating the maturity of any future solar dynamic heat rejection design, the photovoltaic work should prove invaluable. However, the major *differences* between the two systems should be held in mind (i.e., size, area, stainless steel versus aluminum tubing, operating temperature range, operating pressure, working fluid, etc.). It also should be recognized that the preliminary design review for the photovoltaic radiator was conducted with many of the same unanswered or unaddressed design concerns as exist for the SDR at this writing.

References

9.1 McLallin, K.L., et al.: The Solar Dynamic Radiator With a Historical Perspective. Proceedings of the 24th International Energy Conversion Engineering Conference, Vol. 1, IEEE, Piscataway, NJ, pp. 299–307.

9.2 Howerton, R.L.: Procurement Specification Panel Assembly, Radiator, Deployable-Closed Brayton Cycle, Solar Dynamic. Rockwell International, Rocketdyne Division, RC1815, rev. E, Jan. 29, 1990.

9.3 Mechanical Properties of Hexcel Honeycomb Materials. TSB120, Hexcel Co., 1984.

9.4 Hofstad, R.B.: Solar Dynamic Radiator Low Frequency Design Definition. LTV Missiles and Electronics Group, Missiles Division, 3–44100/0DIR–026, Apr. 5, 1990.

9.5 Hofstad. R.B.: Solar Dynamic Radiator Flex Hose Test Requirements. LTV Missiles and Electronics Group, Missiles Division, 3–47300/0DIR–029, June 25, 1990.

9.6 Young, G.H.: Plate, Utility, Solar Dynamic. Rockwell International, Rocketdyne Division, RJ00176 Design Specification, Nov. 10, 1989.

9.7 Howerton, R.L.: Personal letter to J. Rhatigan (NASA Lewis). Rockwell International, Rocketdyne Division, 90RC10825, Aug. 16, 1990.

9.8 Engineering Design Document WP–04 Power System. Rockwell International, Rocketdyne Division, EID–00259, rev. G, Jan. 24,1991.

9.9 Clark, J.D.: Preliminary SDR FMEA. LTV Missiles and Electronics Group, Missiles Division, 3–44000/9DIR–030, Nov. 8, 1989.

9.10 Instructions for Preparation of Failure Modes and Effects Analysis and Critical Items List for Space Station. Space Station *Freedom* Program Office, SSP 30234[a], Sept. 1992.

9.11 Stoyack, J.E.: Solar Dynamic Radiator Preliminary Material Safety Evaluation. LTV Missiles and Electronics Group, 3–44000/9DIR–026, Missiles Division, Aug. 30, 1989.

9.12 Solecki, L.B.: SDR Baseline Material Review. LTV Missiles and Electronics Group, 3–44000/8DIR–12, Missiles Division, Dec. 7, 1989.

9.13 Materials Selection List for Space Hardware Systems. NASA Marshall Space Flight Center, MSFC–HDBK–527, rev. F[a], Sept. 30,1988.

9.14 Qualls, G.L.: SDR Preliminary Reliability Analysis. LTV Missiles and Electronics Group, Missiles Division, 3–47300/SDR/0DIR–043, June 15, 1990.

9.15 Burgess, D.S.: Reliability and Life Cycle Cost Assessment of Solar Dynamic Fluid Management Unit Configuration. Rockwell International, Rocketdyne Division, EID 00677, June 26, 1990.

9.16 Documentation of Micrometeoreid/Space Debris Impact Analysis of the SDR. DIR 3–46200/9DIR–003, Feb. 1, 1989.

9.17 Rhatigan, J.L.; Christiansen, E.L.; and Fleming, M.L.: On Protection of *Freedom*'s Solar Dynamic Radiator From the Orbital Debris Environment, Part 1: Preliminary Analyses and Testing. NASA TM–102458, 1990. (Also ASME Journal of Solar Energy Engineering, vol. 114, Aug. 1992, pp. 135–141.)

9.18 Klann, J.L.: Presentation: CCEP Computer Code Description and Status. IBR SE–159[a], Aug. 19, 1988.

9.19 Gallo, C.: A Comparison Between Design Point Radiator Results for the Rephased Solar Dynamic Power Module. IBR SE–291[a], Nov. 13, 1990.

9.20 Solar Dynamic Radiator. LTV Missiles and Electronics Group, 3–12450–8DIR–7[a], Aug. 19, 1988.

9.21 Flores, R.R.: Solar Dynamic Radiator Low Frequency Sizing Analysis. LTV Missiles and Electronics Group, Missiles Division, 3–44100/0DIR–011, Feb. 7, 1990.

---

[a]Space Station *Freedom* library at the NASA Lewis Research Center in Cleveland, OH 44135 (tel. 216–433–5367 and fax 216–433–8050).

9.22 Chung, D.K.: Transient Thermal Model of Solar Dynamic Radiator. EID–00697[a], Aug. 24, 1990.

9.23 Rhatigan, J.L.: Numerical Model of Solar Dynamic Radiator for Parametric Analysis. NASA TM–1020543. (Also Proceedings of the 24th Intersociety Energy Conversion Engineering Conference, Washington, DC, Aug. 1989.)

9.24 Guthridge, K.C.: Thermal Analysis of the Solar Dynamic Radiator. TFAB Report 90–003, July 1990.

9.25 Guthridge, K.C.: Thermal Modeling of the Solar Dynamic Radiator. TFAB Report 91–002, Apr. 1991.

9.26 Flores, R.R.: Solar Dynamic Radiator Fluid Trade Study Results. LTV Missiles and Electronics Group, Missiles Division, 3–12450–8DIR–19[a], Jan. 19, 1989.

9.27 Howerton, R.L.: Heat Rejection System Fluid Trade Study (Solar Dynamic System). Rockwell International, Rocketdyne Division, DRD SE–03, TSR–00055, key 35345[a], Mar. 1, 1989.

9.28 Flores, R.R.: Solar Dynamic Radiator CBC State Point Analysis. LTV Missiles and Electronics Group, Missiles Division, 3–47300/0DIR–057, Sept. 12, 1990.

9.29 Miniatas, J.B.: SDR Structural Design Criteria. LTV Missiles and Electronics Group. 3–46200/9DIR–021, Missiles Division, June 1, 1989.

9.30 Fleming, M.L., et al.: Solar Dynamic Radiator First Interim Design Review. LTV Missiles and Electronics Group, Missiles Division, 3–44000/9R–042, Jan. 17, 1990.

9.31 Fearing, P.D.: Summary of LTV Dynamic Analysis of RCS Plume Impingement Loads on SDR. LTV Missiles and Electronics Group, Missiles Division, 3–47300/0DIR–059, Sept. 25, 1990.

9.32 Space Station External Contamination Control Requirements. Space Station *Freedom* Program Office, SSP 30426, rev. B[a], July 1991.

9.33 Stoyack, J.E.: Solar Dynamic Radiator Preliminary Contamination Assessment. LTV Missiles and Electronics Group, Missiles Division, 3–44000/9DIR–027, Sept. 29, 1989.

9.34 Pierson, J.L.: Solar Dynamic Radiator, Low-Frequency Design Mass Properties. LTV Missiles and Electronics Group, Missiles Division, 3–47300/0DIR–027, Apr. 9, 1990.

9.35 Hofstad, R.B.: Solar Dynamic Radiator Low Frequency Design Shadow Definition. LTV Missiles and Electronics Group, Missiles Division, 3–44100/0DIR–018, Mar. 14, 1990.

9.36 Howerton, R.L., SDR Attachment Study Results. Rockwell International Corp, Rocketdyne Division, EID–00625, rev. A, Apr. 5, 1990.

9.37 Rhatigan, J.L., et al.: On Protection of *Freedom*'s Solar Dynamic Radiator From the Orbital Debris Environment, Part 2: Further Testing and Analyses. NASA TM–104514, 1991. (Also ASME Journal of Solar Energy Engineering, vol. 114, Aug. 1992, pp. 142–149.)

9.38 Kessler, D.J.: Orbital Debris Environment for Space Station. NASA Johnson Space Center, JSC–20001, 1984.

9.39 Kessler, D.J.; Reynolds, R.C.; and Anz-Meador, P.D.: Orbital Debris Environment for Spacecraft Designed to Operate in Low Earth Orbit. NASA TM–100471, 1989.

9.40 Urbanowicz, J.P., et al.: Solar Dynamic Radiator Hypervelocity Impact Test Analysis Update. LTV Missiles and Electronics Group, Missiles Division, 3–47300/0DIR–056, Aug. 31, 1990.

9.41 Flores, R.R., et al.: Solar Dynamic Radiator Element Panel Thermal Test Report. LTV Missiles and Electronics Group, Missiles Division, 3–47300/1DIR–019, Mar. 4, 1991.

9.42 Miranda, J.H., et al.: Evaluation of EA 9689/EA 9205R Adhesive System, LTV Missiles and Electronics Group, Missiles Division, 3–47300/1DIR–011, Feb. 7, 1991.

9.43 Dever, J.A., et al.: Evaluation of Thermal Control Coatings for Use on Solar Dynamic Radiators in Low Earth Orbit. NASA TM–104335, 1991.

9.44 Simpson, K.E.: Beginning and End of Life Optical Properties of Sulfuric Acid Anodized 5657–H25 Aluminum for the Active Thermal Control System Radiators. McDonnell Douglas Memorandum A95–J849–KES–M–9005089, Aug. 2, 1990.

9.45 Dever, J.A.: Personal letter to H. Le (McDonnell Douglas) from NASA Lewis Research Center. Nov. 19, 1990.

---

[a]Space Station *Freedom* library at the NASA Lewis Research Center in Cleveland, OH 44135 (tel. 216–433–5367 and fax 216–433–8050).

Page intentionally left blank

Chapter 10
Interface Structure and Integration Hardware

10.1 Interface Structure

The interface structure is the structure to which all of the major solar dynamic assemblies are attached when the module is on orbit. For the baseline two-axis gimbal concept the interface structure is attached to the beta gimbal, the deployable radiator subassembly, the receiver/ power-conditioning unit (PCU), and the fine-pointing subassembly (which interfaces with the concentrator assembly). Various other components may be attached to the interface structure, including Sun sensors, the insolation meter, the parasitic load radiator, and the electrical equipment assembly. Figure 5.21 shows how the interface structure fits into the baseline concept.

Within the orbiter cargo bay the receiver/PCU and the radiator subassembly are attached to the interface structure, which acts as a launch cradle and interface with the orbiter. At the start of phase 1 of the SD program the interface was estimated to have a mass of 828 lb. The estimate was revised (but not baselined) to 1328 lb near the end of the SD program.

Other solar dynamic gimbaling concepts would have different requirements for an interface structure. Little has been done to develop these concepts. An early mass estimate of the interface structure for the beta fine-pointing concept was about 440 lb, a significant saving on the basis of the information in reference 10.1[1].

Irrespective of the configuration, the interface structure must be relatively stiff to minimize relative motion among the various solar dynamic assemblies, to aid in accurate pointing of the solar dynamic module, and to reduce the possibility of controls-structure interaction. The actual stiffness requirement must be based on analysis of a particular configuration. The interface structure must be able to withstand the natural and induced environments.

One consideration that should be made in designing the interface structure is its capability for replacement. Because many other assemblies are attached to it, the interface structure may prove to be very difficult to remove and replace should it become damaged (perhaps due to a meteoroid). Before too much effort is expended on this issue, the credibility of such failures needs to be evaluated.

[1]The mass tabulation in ref. 10.1 contains an error.

10.2 Integration Hardware

The integration hardware includes the truss structure, the extravehicular activity rails, and the cable trays. The integration hardware was identically common with other Space Station *Freedom* erectable truss hardware. The solar dynamic and outboard photovoltaic modules will be separated by about six bays of truss. Each bay is a cube, 5 m (16.4 ft) per side. If growth solar dynamic modules are added to *Freedom* after the first port and starboard solar dynamic units, they would be added at the outermost truss bays, directly opposite the initial modules. Thus, each assembly of integration hardware (six bays) can support two solar dynamic modules. Growth beyond two modules per side would require adding more integration hardware to space the modules apart along the solar power module boom.

The truss bays are built up from individual truss members with end fittings that attach to node fittings at each corner of the bay. The truss members are hollow tubes, 2 to 2.5 in. in diameter, that are made of graphite-epoxy composite or possibly aluminum alloy. Design considerations for the truss include stiffness, thermal stability, and survivability in an atomic oxygen environment.

The concept for a Space Station *Freedom* structure using a preintegrated truss as an alternative to an erectable truss was developed during program restructuring, early in 1991, after the halt to solar dynamic activities. The preintegrated truss is preassembled and integrated with truss-mounted hardware, including all utility lines, on the ground and launched as an integrated unit. Its effect on solar dynamics has not been evaluated.

Reference

10.1 Receiver Tilt and Aperture Offset. Rockwell International, Rocketdyne Division, EID–00805[a], Dec. 11, 1990.

[a]Space Station Freedom library at the NASA Lewis Research Center in Cleveland, OH 44135 (tel. 216–433–5367 and fax 216–433–8050).

Page intentionally left blank

Chapter 11

Summary of Development Status and Needs

11.1 Turboalternator Compressor

The solar dynamic power module development effort has been based on a solid technological heritage at both the system and component levels. The technology to build the closed Brayton cycle (CBC) power conversion unit exists. A 10.5-kW Brayton power conversion system was developed by AiResearch under the management of NASA Lewis Research Center in the 1960's and 1970's. Several sets of hardware were built and tested (ref. 11.1). These hardware sets included Brayton rotating units (BRU's), heat exchangers, controls, accumulators, etc. The BRU's are the equivalent of the turboalternator and compressor unit (TAC) in the *Freedom* solar dynamic system. These BRU's have a physical size, a turbine inlet temperature (1600 °F), and a shaft speed (36 000 rpm) that are roughly comparable to the current design of *Freedom*'s solar dynamic power system. The same type of working fluid, a mixture of helium and xenon gases, was also used. Two of the BRU's were successfully operated for 41 000 and 11 000 hr, respectively, with no failures or physical degradation. In fact, 13 600 hr of continuous operation was achieved on one of the units without any failures, maintenance, or signs of wear or excessive creep.

On a component basis the *Freedom* TAC design uses turbine, compressor, and alternator concepts that are the same as those developed previously. Aircraft auxiliary power units (APU's) having turbine and compressor designs that are similar to those intended for the TAC have endured over 200 million unit-hours with over 200 million start-stop cycles. Gas foil bearings in the *Freedom* CBC TAC machinery design are of the same type and size as those used in the DC–10 environmental control cooling turbines (over 100 million unit-hours of operation and 71 000 start-stop cycles before replacement). Because of experience in Brayton development, extensive Government and industry experience in related aircraft components, and conservative design, a high degree of confidence exists in the capability of producing a space-qualified power conversion unit.

11.2 Waste Heat Rejection Radiator

The waste heat rejection radiator is another major assembly of the solar dynamic power module for which a technology base exists. Single-phase, pumped-liquid radiators have been used aboard Apollo and Skylab and are now in use on the NSTS orbiter (ref. 11.2). The solar dynamic radiator, which uses adhesively bonded honeycomb construction techniques, takes advantage of the current state-of-the-art fabrication methods that are demonstrated by the NSTS orbiter's large single-phase, pumped-loop radiators, which are mounted on the cargo bay doors. In addition, the solar dynamic radiator uses an integrated automatic deployment mechanism of a type that has also been used on orbit. The solar arrays for the Skylab/Apollo telescope mount were successfully deployed by using the same basic concept that solar dynamics will use (i.e., a scissors arm with a cable actuator). The solar dynamic power module will incorporate all the successful radiator technologies that were demonstrated previously. Building on this technology will provide a low-risk and low-cost approach to producing a flight-qualified radiator.

11.3 Receiver and Concentrator

For the other two major assemblies, the receiver and concentrator, a strong base has been developed since 1984 with the infusion of over $20 million of NASA advanced development, contractor internal research and development, and NASA supporting development resources. For the receiver assembly an initial strong technology data base involving thermal storage materials compatibility, mechanical strength, thermal energy storage performance, and receiver thermal performance has been developed. Over 20 000 hr of exposure of the thermal storage containment materials to the $LiF\text{-}CaF_2$ salt have shown negligible corrosion. In addition, extensive testing at NASA Lewis and at contractors has shown that the thermal performance is completely verifiable by

ground testing and analysis (i.e., no flight test is required). Also, tests conducted by Allied-Signal with a single tube segment of the receiver have verified the operation of the baseline thermal energy storage configuration. Rocketdyne has completed a system demonstration test at their Santa Susanna test site. A representative receiver unit with integral thermal energy storage was mounted on a 11-m-diameter concentrator. It successfully demonstrated essentially uniform outlet gas temperature over simulated orbital Sun-shade cycles.

Finally, a full-scale, advanced-development CBC receiver for a 25-kW solar dynamic system has been designed and built at the Boeing Aerospace Corporation and was tested during the fall of 1990. Although the Boeing receiver design is different from the baseline solar dynamic receiver design by Allied-Signal, it is the first full-scale receiver for a 25-kW solar dynamic module that has been tested in both a thermal and vacuum environment. Its test results provide valuable data on design and test methods. A similar full-scale hardware build and test of the Allied-Signal design is the major remaining work needed to verify the baseline design approach. In order to enhance the design confidence of a long-life receiver for space application, material properties must be characterized after environmental exposure for periods of at least 20 000 hr (~1/10th the 30-yr design life).

Key accomplishments have been realized in concentrator reflective and protective coatings, optical characterization, and structural rigidity. The Harris Corporation, NASA Lewis, and 3M have demonstrated the reflective capability of the individual facets and the resistance of protective coatings to atomic oxygen. In addition, a full-scale concentrator (19 panels) was fabricated by Harris. A successful 19-panel assembly and repeatability test of the concentrator in normal gravity has been completed using the laser system shown in figure 11.1. The basic process of assembling the concentrator on orbit was investigated and verified by neutral buoyancy assembly testing of three full-size panels. Means to align the concentrator and to verify its optical performance have been developed at NASA Lewis' Power Systems Facility using the DIR system shown in figure 11.2 and the ceiling image system shown in figure 11.3. These means have been verified by on-Sun tests at Sandia National Laboratory in Albuquerque, New Mexico. Additional development is needed to evolve the assembly process in order to reduce the EVA time needed or to develop a deployable concentrator if EVA assembly time is seriously restricted. Because of problems encountered with fabrication of the composite reflective facets, alternative facet designs should be investigated and the most promising developed.

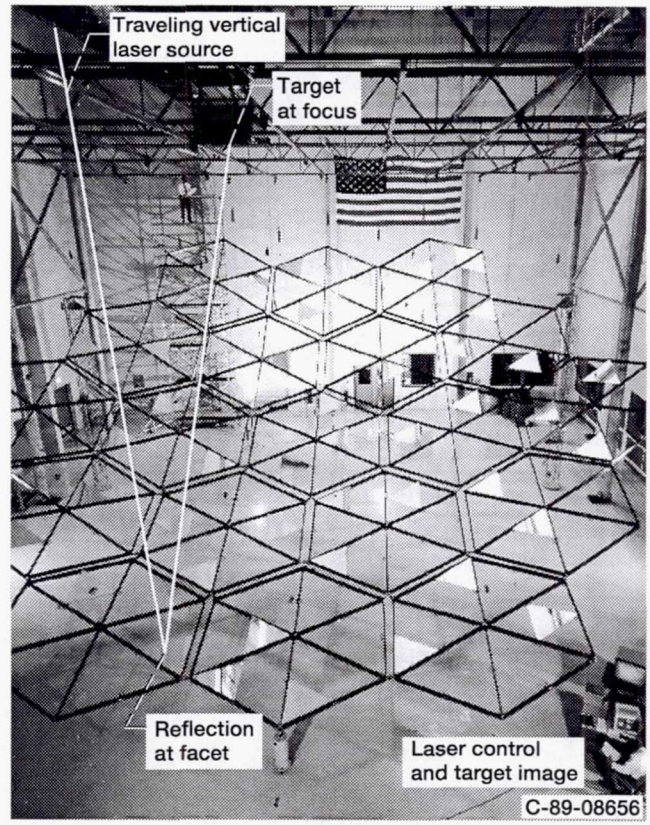

Figure 11.1.—Concentrator testing with laser system.

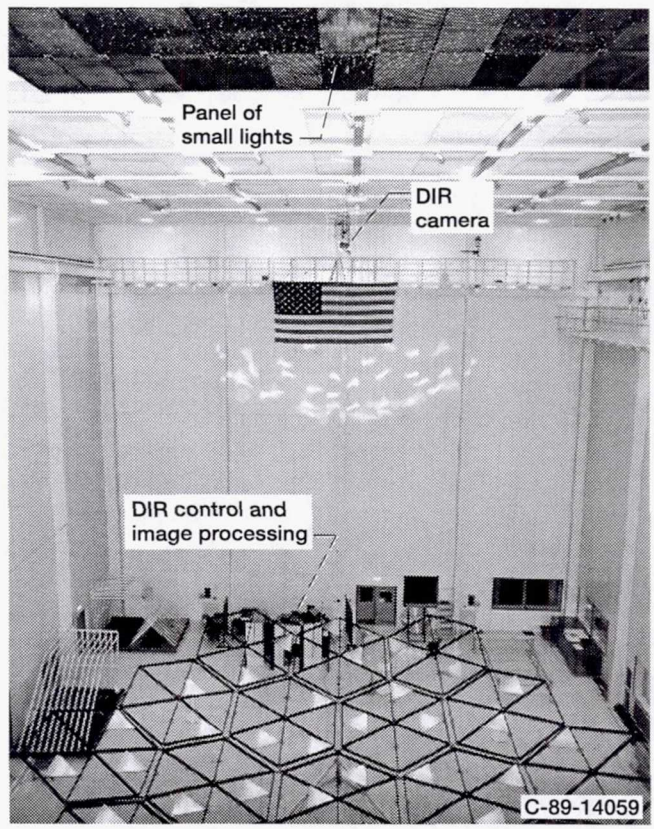

Figure 11.2.—Concentrator testing with DIR system.

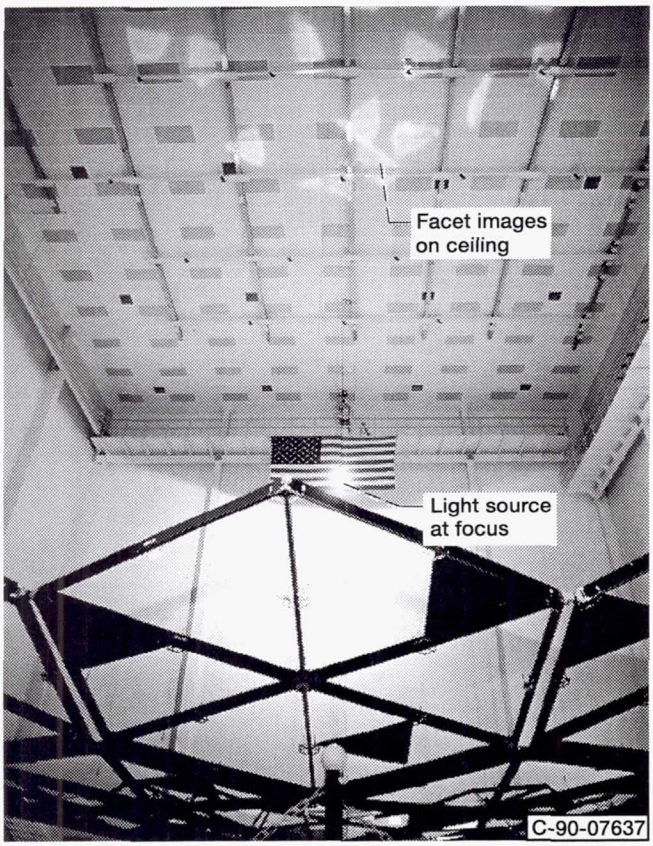

Figure 11.3.—Concentrator testing with projected ceiling image system.

11.4 Conclusions

A strong technology base exists for the development of the solar dynamic power module system, but some important additions to that base are needed to allow confident design of a long-life system for space.

References

11.1 English, R.E.: Power Generation From Nuclear Reactors in Aerospace Applications. Presented at the Symposium on Advanced Compact Reactors sponsored by the National Research Council, Washington, DC, Nov. 15–17, 1982. (Also NASA TM–83342.)

11.2 McLallin, K.L.; Fleming, M.L.; Hoehn, F.W.; and Howerton, R.: The Solar Dynamic Radiator With a Historical Perspective. Proceedings of the 23rd Intersociety Energy Conversion Engineering Conference, Vol. 3, ASME, 1988, Paper 889165.

Page intentionally left blank

Chapter 12

Hardware and Software Design Features for Power Growth

Growth in electric power capability on *Freedom* is a near certainty and the use of solar dynamic power to accomplish this growth is a strong possibility. Therefore, the design in its earliest stages should contain those software and hardware features that will allow efficient and cost-effective addition of solar dynamic power modules. These software features are known as "hooks," and the hardware features are known as "scars." Although not completed, the preliminary solar dynamic design work progressed far enough to indicate that the hooks and scars are almost entirely independent of the type of power source to be added, photovoltaic or solar dynamic. The hooks and scars were determined in a specific effort aimed at their identification. Also, the effect of not incorporating them was quantified in terms of program costs. In general, those with the greatest effect involved installation of cable boxes (trays) to hold the power and control wiring for the growth power. The net cost to defer other scars was determined to be minimal relative to overall program costs. All identified hooks and scars are described in detail in reference 12.1; reference 12.2 provides details of the cost effects.

Although desirable, no hooks need be included in *Freedom*'s software. Software can be upgraded for control and distribution of growth power during the growth, or evolutionary, phases of construction.

Obviously, some hardware scars should be included in the initial *Freedom* assembly to allow for adding hardware to distribute growth power and to dissipate the heat resulting from the use of that increased power. The solar dynamic concentrator must be pointed at the Sun more accurately than a photovoltaic array, but its fine-pointing system (described in section 5.7) will be capable of the required accuracy with the same baseline *Freedom* orientation needed for the photovoltaic power modules. The cost effect of these scars and operational procedures was not assessed.

The scars peculiar to solar dynamic power are few. During EVA maintenance of the heat rejection assembly, *n*-heptane could solidify on astronauts' space suits and then contaminate the habitation modules if the solid *n*-heptane did not sublimate during the EVA period. Sensors need to be included within the appropriate crew areas to detect and warn of the presence of *n*-heptane. *Freedom*, its payloads, and its experiments must be able to accommodate solar dynamic concentrator off-axis phenomena, such as visible, radiofrequency, and infrared flux concentrations outside of the solar dynamic receiver. The off-axis phenomena can occur during module maintenance assembly or during emergency off-pointing of the concentrator. Equipment and personnel exclusion areas on and around *Freedom* must be established to avoid damage or injury from stray flux concentrations. Initial studies (ref. 12.3) show that these exclusion areas are limited and should be readily accommodated.

References

12.1 O'Brien, D.L.: Solar Dynamic Hooks and Scars. Rockwell International, Rocketdyne Division, EID–00365, rev. D, key 33955[a], July 9, 1990.

12.2 Solar Dynamic Hooks and Scars Quantitative Impact Data. Rockwell International, Rocketdyne Division, EID–00715, Oct. 1, 1990.

12.3 Rylicki, D.S.: Flux Concentrations on Solar Dynamic Components Due to Mispointing. NASA TM–105756, 1991.

---

[a]Space Station *Freedom* library at the NASA Lewis Research Center in Cleveland, OH 44135 (tel. 216–433–5367 and fax 216–433–8050).

Page intentionally left blank

Chapter 13
Recommendations

13.1 Nontechnical Recommendations

One of the factors that inhibited the efficient use of resources in phase C/D of the SD program was the widespread attitude that the program should be constrained to a fixed dollar limit in its phase 1. This attitude, which probably accurately reflected the intentions of the top-level program decision makers, was detrimental to the process of defining the program content. This was initially evident after Rocketdyne had negotiated contracts with the subcontractors and then was compelled to formulate an integration effort out of the relatively few remaining dollars from a fixed limit. (This problem was recognized and addressed at restructuring shortly before the solar dynamic effort was terminated.) Throughout the phase 1 SD program there was little flexibility to adjust program content while at the same time changes were being imposed on the SD program. This resulted in time and dollars being spent on replanning efforts to add and delete tasks, adjusting content to match budget. (With the pressures to maintain overall WP–04 spending within guidelines, this was by no means exclusively a solar dynamic problem.)

Without resorting to budget increases it is not easy to minimize the disruptions to a program in the face of externally imposed changes. Obviously starting with a good plan for schedule and content and sticking with it throughout the program will help if the program is allowed to remain undisturbed. Perhaps it would have been best if the SD program had been treated more like a development program, where provisions are made in initial program formulation for the unplanned events that will occur naturally as a result of program progress.

13.2 Dependence on Specifications

There is a natural tendency to "nail down" as many requirements as possible early in a program in order to control changes and allow the design to progress. As a result, some requirements are not well thought through or are arbitrarily based on engineering rules of thumb that may or may not be applicable to a spaceflight program. Our experience suggests that in a large program the tenuous technical basis of these early requirements can be forgotten or buried in volumes of documentation. The result is that these same requirements can acquire an unmerited longevity and can engender an almost religious devotion.

We experienced the programmatic equivalent of "painting ourselves into a corner" in several instances owing to the early inflexibility of requirements. The problem was particularly apparent in the module integration area, where previously benign component requirements came into conflict when integrated. The problems were certainly exacerbated by the lack of integration funding.

We recommend that future program managers insist that early requirements be designated as either "hard" or "soft" to indicate design flexibility, keeping in mind that there will be natural resistance to soft designations, especially in the hardware component specifications. Preliminary design review is the appropriate time to discard these designations.

In consideration of the state of development of solar dynamic power, and the resulting "imprecision" of initial requirements, we should have done more to reevaluate requirements as the design progressed. Failure to do this in some cases may have led to the expenditure of scarce resources to provide designs that met requirements which were not well founded or had poor cost/benefit ratios. Examples of these requirements are the radiator modal frequency requirement and the power peaking requirement. The radiator frequency issue is discussed in section 9.5.6. The power peaking requirement was allowed to drive the solar dynamic design for some components. It may have been better to accept (a perhaps lower) inherent peaking resulting from a design without a peaking requirement, especially when considering that photovoltaics will be available and may be better suited to providing peaking power.

In general, during solar dynamic definition, more attention should have been given to taking advantage of natural solar dynamic strengths and to imposing only essential requirements. The design synthesis process should regularly include a requirements review to reaffirm their usefulness and accuracy.

13.3 Subcontractor Constraints on Design Changes

Throughout phase 1 of the SD program the subcontractors had specific design features and specifications, such as mass,

defined in their contracts. This situation provided a natural resistance to design changes because of the resulting contractual complexities. An example of this constraint occurred when the need arose to modify the solar dynamic module design to meet the launch packaging requirements. Because of the desire not to interfere with the subcontractor-designed assemblies, modifications of the concentrator, radiator, receiver, or PCU designs were not considered. Four options were developed that involved primarily the fine-pointing system and the interface structure. Although potential options were identified, the fact that most of the module components were off limits reduced the chance of producing the optimum solution to the launch packaging problem.

13.4 Effect of Life Cycle Costs Versus Initial Costs

Although solar dynamic life cycle cost saving is widely extolled (and either dismissed or accepted to some degree), the experience in the Space Station *Freedom* Program to date has been that life cycle costs are almost completely ignored in the decision-making process and instead there is a reliance almost entirely on initial costs. (This does not bode well for future operating costs.) With future space budgets almost certain to be equally tight, it can be expected that initial costs will weigh heavily in future decisions.

Future solar dynamic design and development programs should be reviewed with the dual aims of reducing initial costs and reducing potential cost risks. Inexpensive solutions should be sought for potentially expensive problems. For example, we might not want to achieve a costly high-reflectivity facet but instead accept an overall lower quality facet while increasing the concentrator area to maintain the specified power output. This would of course affect aerodynamic drag, mass, and life cycle cost. It is therefore essential that, up front, the relative importance of initial costs and life cycle costs are known; design options for one or the other are often conflicting.

Chapter 14
Concluding Remarks

Although development of solar dynamic power for Space Station *Freedom* has been discontinued, much progress has been made. The technology base for solar dynamic power has been expanded well beyond that which existed before this program. Preliminary design of a solar dynamic power module that meets all of the performance requirements for operating on orbit as a power source on Freedom has progressed to the point where component, as well as overall system and module, weight and performance can be realistically estimated. System and component designs are nearly optimum for this application. This module will provide 25 kW of electric power to the users under all insolation conditions. In addition, the design meets the requirements for short-term peaking power (up to 28.75 kW) and is capable of automated startup and shutdown operations. It also has been designed to provide power during the 30-year *Freedom* lifetime by periodic, as needed, replacement of orbital replacement units. Assembly of the module on orbit will incorporate methods and procedures to be developed for other *Freedom* elements. No unique equipment will be needed. The technology base for solar dynamic development and production has been shown to exist at both the system and component levels.

Component hardware development and testing have shown that the solar dynamic power module design for *Freedom* is conservative and that zero-gravity tests are not needed to verify designs. Either the basic concepts are gravity-insensitive (e.g., all-gas Brayton thermodynamic heat engine) or the components are designed to reduce the effect of gravity to a negligible level (e.g., small thermal energy storage canisters and lightweight concentrator subassemblies).

The process by which solar dynamics would become a part of *Freedom* has been described. The initial growth phase would increase the power level to 125 kW by the addition of two solar dynamic power modules, one at each end of the transverse boom. Growth power to about 300 kW will be achieved by adding more solar dynamic modules.

The reasons for adding solar dynamic power to *Freedom* have been clearly stated. The tremendous life cycle cost saving and the advantage of having a hybrid or alternative power source in case some anomaly with photovoltaics occurs are attractive reasons for pursuing development of solar dynamic power for *Freedom*.

In summary, solar dynamic power can meet the growth power requirements for Freedom, and the technology base exists. The only question now is when to resume solar dynamic development so that *Freedom* can grow beyond 75 kW in a cost-effective manner.

Page intentionally left blank

Glossary

AC	assembly complete
ANSYS	Analysis System computer code
APS	astronaut positioning system
APU	auxiliary power unit
ASME	American Society of Mechanical Engineers
BRU	Brayton rotating unit
CBC	closed Brayton cycle
CCEP	Closed Cycle Engine Program
CCTV	closed-circuit television
CDR	critical design review
CEI	contract end item
CETA	crew and equipment translation aid
CG	center of gravity
CIL	critical items list
COPAT	concentrator panel assembly tests
CRES	corrosion-resistant steel
DIR	digital image radiometer
EDD	engineering design document
EEA	electrical equipment assembly
EID	engineering information document
EMU	extravehicular mobility unit
ESH	equivalent Sun hours
EVA	extravehicular activity
EPS	electric power system
FMEA	failure modes and effects analysis
FMU	fluid management unit
FSD	Fluid Systems Division
GFRP	graphite-fiber-reinforced plastic
GN&C	guidance, navigation, and control
GTRI	Georgia Tech Research Institute
HRA	heat rejection assembly
IVA	intravehicular activity, such as manipulating robotic arm or monitoring EVA
LAMP	lift, align, move, push
LEO	low Earth orbit
M&PI	material process and improvement
MARC	Mathematical Analysis Research Corporation computer code
MFI	multifoil insulation
MSC	mobile servicing center
MTBF	mean time between failures
NASTRAN	NASA structural analysis computer code
NBS	neutral buoyancy simulation
NSTS	National Space Transportation System (also called Space Shuttle)
ORC	organic Rankine cycle
ORU	orbital replacement unit

PCM	phase-change material
PCU	power conversion unit
PDR	preliminary design review
PDRD	program design and requirements document
PGCS	power generation and control system
PLR	parasitic load radiator
PMAD	power management and distribution
PMC	permanently manned capability
POLAR	parabolic offset–linear actuator reflector
PRCS	primary reaction control system
PSF	Power Systems Facility
RADSIM	radiation simulation computer code
RADVIEW	radiation view factor computer code
RAM	reliability, availability, and maintainability
RCS	reaction control system
SCAD	solar concentrator advanced development
SD	solar dynamic
SDPM	solar dynamic power module
SDR	solar dynamic radiator
SKI	Solar Kinetics Incorporated
SOLREC–TSD	solar receiver–thermal storage device code
SPDS	stabilized payload deployment system
SPM	solar power module
SRMS	Shuttle remote manipulator system
STAR	solar thermal advanced reflector
TAC	turbine, alternator, and compressor unit
TES	thermal energy storage
TIG	tungsten inert gas
UV	ultraviolet
VFY	view factor computer code
VUV	vacuum ultraviolet
WP	work package

Bibliography

This bibliography lists significant documents that were prepared as part of the effort to develop solar dynamic power for the Space Station *Freedom* Program. Documents in this list are in addition to the references listed at the end of each chapter. Documents denoted by a superscript "a" are available only from the Space Station *Freedom* library at the NASA Lewis Research Center in Cleveland, Ohio, 44135 (tel., (216) 433–5367; fax, (216) 433–8050).

Solar Dynamic Power System

Chiaramonte, F.P.; and Taylor, J.D.: Energy Balance Simulation for Solar Dynamic Power Systems. NASA Lewis, Space Station *Freedom* Directorate, PIR 124,[a] Dec. 17, 1985.

Corrigan, R.D.: First-Order Evaluation of Reliability and Maintainability for Solar Dynamic Space Station Power Modules. NASA Lewis, Space Station *Freedom* Directorate, PIR 130,[a] Feb. 1, 1986.

Dynamic Analysis of Space Station *Freedom*: A Video Animation. NASA Lewis, key 23653,[a] 1989.

Hallinan, G.J.: Space Station WP–04 Power System Final Study Report DR-15. Rockwell International, Rocketdyne Division, NASA Contract NAS3–24666, NASA CR–179587, 1987.

Hochstein, J.I.; and Torakianitis, T.: Dynamic Modeling of Solar Dynamic Power Components and Systems. Memphis State University, Final report NASA Grant NAG3–817, Sept. 14, 1992.

Hoffman, A.C.: Conceptual Design of a Solar Dynamic High-Frequency Power System for the Space Station. NASA Lewis, Space Station *Freedom* Directorate, PIR 79,[a] Oct. 22, 1984.

Klann, J.L.: Preliminary Mass Optimization of Solar-Brayton Space Power Systems. NASA Lewis, Space Station *Freedom* Directorate, PIR 47,[a] Jan. 19, 1983.

Klann, J.L.: Tradeoffs and Revised Mass Optimizations for a Solar-Brayton Space Power System. NASA Lewis, Space Station *Freedom* Directorate, PIR 63,[a] Mar. 1984.

Klann, J.L.: Effect of Heat Storage Salt on Least Mass of a Solar Brayton Space Power System. NASA Lewis, Space Station *Freedom* Directorate, PIR 80,[a] Oct. 1984.

Klann, J.L.; and Staiger, P.J.: Design Tradeoffs for a Space Station Solar-Brayton Power System. NASA Lewis, Space Station *Freedom* Directorate, PIR 106,[a] May 1985.

Klann, J.L.; and Gallo, C.A.: Preliminary Evaluation of Design-Point Selections for the Re-Phased SD Power Module. NASA Lewis, IBR SE–287, key 24386,[a] Oct. 19, 1990.

Klann, J.L.; and Gallo, C.A.: Preliminary Performance Evaluations of the Re-Phased SD Power Module in Its Power-Rating Orbit. NASA Lewis, IBR SE–292, key 24401,[a] Nov. 19, 1990.

Kudija, C.T.: Power Flow Diagrams for Solar Dynamic Power Module. Rockwell International, Rocketdyne Division, EID–00911,[a] May 1, 1991.

Labus, T.L.; Secunde, R.R.; and Lovely, R.G.: Solar Dynamic Power for Space Station *Freedom*. Presented at International Conference on Space Power, International Astronautical Federation, Cleveland, OH, June 5–7, 1989, NASA TM–102016, 1989.

Lester, M.C.: Solar Dynamic (SD) Power Module System – Part 1 Contract End Item Specification – Change A1[a]. NASA Lewis, Space Station *Freedom* Control Board Directive, Jan. 30, 1991.

Lester, M.C.: Solar Dynamic (SD) Power Module System – Part 1 Contract End Item Specification – Change A2[a]. NASA Lewis, Space Station *Freedom* Control Board Directive, Feb. 15, 1991.

O'Brien, D.L.: SD Power Module System CEI Specification, Part 1. Rockwell International, Rocketdyne Division, CP409R0006, E–02,[a] Mar. 22, 1988.

O'Brien, D.L.: SD Power Module System CEI Specification, Part 1. Rockwell International, Rocketdyne Division, CP409R0006, rev. A., E–02,[a] Feb. 21, 1990.

Richter, C.W.: Design, Packaging, and Assembly of a 25 kW CBC Offset SD Power System and Beta Joint. NASA Lewis, Space Station *Freedom* Directorate, PIR 145,[a] Apr. 25, 1986.

Solar Dynamic (SD) Power Module System – Part 1 Contract End Item Specification. NASA Lewis, Space Station *Freedom* Directorate, Work Package 04 (WP–04), Space Station Electric Power System, LeRC–SS–003,[a] Feb. 3, 1987.

Solar Dynamic Power Module Division, Advanced Development/Supporting Development Review, Concentrator and Thermal Control. NASA Lewis, key 23735,[a] Feb. 3, 1988.

Solar Dynamic Power Supporting Development Program Review. NASA Lewis, key 23733,[a] Sept. 11–12, 1990.

Solar Dynamic Power System Presentation to Code S. NASA Lewis, Space Station *Freedom* Directorate, key 8901714,[a] June 6, 1989.

Stalnaker, D. K.: Contingency Power Capabilities for Solar Dynamic Systems. NASA Lewis, Space Station *Freedom* Directorate, PIR 139,[a] Apr. 4, 1986.

Concentrator

Bachir, M.; and Jamison, J.M.: Testing of the Advanced Development Solar Concentrator. Aerospace Design & Fabrication, Inc., key 23712,[a] June 18, 1990.

Bachir, M.; and Jamison, J.M.: Focal Point Light Source Testing of Concentrator Tilt Versus Loading. Aerospace Design & Fabrication, Inc., key 23717,[a] Jan. 29, 1991.

Campbell, J.: Summary of the Modifications to the HEXMAP Program. Harris Corp., RI–HA–0027, key 982,[a] Sept. 6, 1989.

Campbell, J.: Review of K. Jefferies Method for Determining Toroidal Facet Slope Error. Harris Corp., SDP–0084[a], June 20, 1990.

Campbell, J.: Facet Slope Error Testing at Hercules. Harris Corp., SDP–0118,[a] Sept. 7, 1990.

Campbell, J.: Facet Mold Profilometer Measurements. Harris Corp., SDP–0119,[a] Sept. 7, 1990.

Campbell, J.: Effects of Facet Radius of Curvature Error on RMS Slope Error. Harris Corp., SDP–0131,[a] Oct. 22, 1990.

Campbell, J.: Mathematical Theory and Methodology for Simulation of Scattering, Slope Error and Sunshapes for Ray Tracing Optical Analysis. Harris Corp., SDP–0138,[a] Nov. 5, 1990.

Campbell, J.: Evaluation and Validation of SOLAR18 With Comparisons With the NASA Lewis Facet On-Sun Test Results. Harris Corp., SDP–01158, key 23676,[a] Sept. 14, 1991.

Cason, R.D.: Conceptual Reflector Design. Harris Corp., RI–HA–016, key 23702,[a] June 5, 1989.

Cason, R.D.: Analysis Reflecting the Flux Tailoring and Optical Analysis Performed Since February 1989. Harris Corp., RI–HA–0018,[a] June 22, 1989.

Cason, R.D.: Review of Type II Latch Stiffness Test Data. Harris Corp., RI–HA–019,[a] June 22, 1989.

Cason, R.D.: Status of Flux Tailoring Effort. Harris Corp., RI–HA–0018, key 23697,[a] July 11, 1989.

Cason, R.D.: Closure of Action Items 6 and 15. Harris Corp., RI–HA–0020,[a] July 18, 1989.

Cason, R.D.: Preliminary 3 Panel NBT Assembly Procedures. Harris Corp, RI–HA–0035[a], Jan. 3, 1990.

Cason, R.D.: Weight Summary. Harris Corp., RI–HA–0039,[a] May 11, 1990.

Cassel, S.D.: Flux Tailoring Status and Recommendations. Harris Corp., RI–HA–0018, key 23698,[a] Apr. 17, 1989.

Cassel, S.D.: Comparison of Flux Tailoring by Facet Defocus to Flux Tailoring by Facet Repointing. Harris Corp., key 23696,[a] July 10, 1989.

Cassel, S.D.: Current Status of Flux Tailoring. Harris Corp., RI–HA–0018,[a] July 18, 1989.

Cassel, S.D.: Analysis of Granularity of Facet Nodes. Harris Corp., RI–HA–0023,[a] Aug. 23, 1989.

Cassel, S.D.: Station Flight Dynamics (Hooks and Scars Task 3). Harris Corp., RI–HA–0031,[a] Nov. 16, 1989.

Cassel, S.D.: Updated Finite Element Model for Deployed Concentrator. Harris Corp., SDP–0060, key 13286,[a] May 16, 1990.

Cassel, S.D.: Advanced Flux Tailoring (draft report). Harris Corp., key 23571,[a] Nov. 13, 1990.

Ciancone, M.L.: Fundamentals of Solar Dynamic Concentrator Sizing. NASA Lewis, Space Station *Freedom* Directorate, PIR 104,[a] Apr. 1985.

Ciancone, M.L.; and Richter, C.W.: Solar Dynamic Concentrator Optical Testing Facility (SDCOTF), NASA Lewis, Space Station *Freedom* Directorate, PIR 116,[a] Oct. 1985.

Ciancone, M.L.: An Analysis of Concentrator Specific Masses. NASA Lewis, Space Station *Freedom* Directorate, PIR 144,[a] Apr. 16, 1986.

Ciancone, M.L.; and Green, R.D.: Evaluation of Concentrator Orientations and Test Locations for Optical Testing. NASA Lewis, Space Station *Freedom* Directorate, PIR 187,[a] Feb. 3, 1987.

Cochran, C.J.; and Schumacher, K.M.: Three Panel NBF Testing Objectives Review and Implementation. Harris Corp., SDP–0077[a], June 21, 1990.

Cooke, J.P.; and Cochran, C.J.: Failure Modes and Effects Analysis. Harris Corp., SDP–0022,[a] Feb. 9, 1990.

Corrigan, R.D.; and Ehresman, D.T.: Solar Concentrator Advanced Development Project. Proceedings of the 22nd Intersociety Energy Conversion Engineering Conference, Vol. 1, AIAA, New York, 1987, pp. 156–161.

Corrigan, R.D.; Peterson, T.T.; and Ehresman, D.T.: Update of the Solar Concentrator Advanced Development Project. Proceedings of the 24th Intersociety Energy Conversion Engineering Conference, Vol. 6, 1989, pp. 2617–2622.

Dalsania, V.: Solar Concentrator Thermal Distortion Analysis—Phase I. W.L. Tanksley & Associates, Inc., key 23711,[a] Dec. 24, 1987.

Design and Demonstration of a System for the Deposition of Atomic-Oxygen Durable Coatings for Reflective Solar Dynamic Power System Concentrators. 3M Corp., NASA Contract NAS3–25075, NASA CR–4158, 1988.

Desired Locations for On-Sun Testing of Facets. Harris Corp., key 23705,[a] Sept. 1989.

Doherty, M.P.; and Dalsania, V.: Finite Element Analysis of Thermal Distortion Effects on Optical Performance of Solar Dynamic Concentrator for Space Station *Freedom*. NASA TM–102504, 1990.

Facet Capture Feature. Harris Corp., SDP–0148,[a] Jan. 23, 1991.

Fincannon, H.J.; and Jefferies, K.S.: PATRAN Maps of Incident and Reflected Receiver Flux—The Tailored Flux Case. NASA Lewis, IBR SE–185, key 23263,[a] Apr. 18, 1989.

Gallo, C.A.: Additional Plotting Added to Flux Redistribution by Reflection Within Receiver Cavity. Aerospace Design & Fabrication, Inc., key 23597,[a] June 14, 1989.

Gallo, C.A. Effect of Defocusing Facets on Flux Distribution Inside Receiver. W.L. Tanksley & Associates, Inc., key 23574,[a] Sept. 21, 1989.

Gallo, C.A.; and Jefferies, K.S.: Continued Flux Tailoring Analysis, February-May. NASA Lewis, IBR SE–189, key 23596,[a] May 16, 1989.

Gallo, C.A.; and Jefferies, K.S.: Comparison Between Two DIR Calibrations To Determine If Camera Drift Is Linear. NASA Lewis, IBR SE–235, key 23594,[a] Jan 30, 1990.

Gallo, C.A.; and Jefferies, K.S.: OFFSET Code Runs To Compare Spherical and Toroidal Facets With Different Slope Error. NASA Lewis, IBR SE–236, key 23593,[a] Feb. 2, 1990.

Gallo, C.A.; and Jefferies, K.S.: Effects of SSF SD Concentrator Facet Design Parameters on Ideal Aperture Plane Facet Images and Intercept Power Loss. NASA Lewis, IBR SE–239, key 23592,[a] Feb. 14, 1990.

Gallo, C.A.; and Jefferies, K.S.: Effects of SSF SD Power System Design Parameters on Receiver Wall Facet Images. NASA Lewis, IBR SE–240, key 23591,[a] Feb. 23, 1990.

Gallo, C.A.; and Jefferies, K.S.: Aperture Plane Flux From Single Hexagonal Panels With Different Facet Contours and Variable Slope Error—LEO Sun. NASA Lewis, IBR SE–245, key 23590,[a] Mar. 21, 1990.

Gallo, C.A.; and Jefferies, K.S.: Aperture Plane Flux From Single Hexagonal Panels With Different Facet Contours and Variable Slope Error—Terrestrial Sun. NASA Lewis, IBR SE–246, key 23589,[a] Mar. 29, 1990.

Gulino, D.A.: The Survivability of Large Space-Borne Reflectors Under Atomic Oxygen and Micrometeoroid Impact. Presented at 25th Aerospace Sciences Meeting sponsored by the American Institute of Aeronautics and Astronautics, Reno, Nevada, Jan. 12–15, 1987. NASA TM–88874, 1987.

Gulino, D.A.: Effect of Hard Particle Impacts on the Atomic Oxygen Survivability of Reflector Surfaces With Transparent Protective Overcoats. Presented at 25th Aerospace Sciences Meeting sponsored by the American Institute of Aeronautics and Astronautics, Reno, Nevada, Jan. 12–15, 1987. NASA TM–88914, 1987.

Hyland R.E.; and Morel, D.: Materials Evaluation for Advanced Solar Dynamics Concentrator. NASA Lewis, Space Station *Freedom* Directorate, PIR 134,[a] Feb. 1, 1986.

Irvine, T.B.; and Richter, C.W.: Proposed Solar Dynamic Concentrator Test Facility for NASA Lewis Research Center. NASA Lewis, Space Station *Freedom* Directorate, PIR 107,[a] May 15, 1985.

Jamison, J.M.; and Bachir, M.: Solar Concentrator Humidity Test. Aerospace Design & Fabrication, Inc., key 23713,[a] May 17, 1990.

Jamison, J.M.; and Bachir, M.: DIR Measurement of Solar Concentrator Structural Repeatability. Aerospace Design & Fabrication, Inc., key 23715,[a] Dec. 27, 1990.

Jefferies, K.S.: NASA Lewis Past Efforts on Designing, Fabrication, and Testing Solar Concentrators. Presented at JSC Solar Dynamic Power System Workshop, Part 2—Collection and Thermal Storage, key 23572,[a] Aug. 1, 1984.

Jefferies, K.S.: Optical Analysis of Parabolic Dish Concentrators for Solar Dynamic Power Systems in Space. NASA TM–87080, 1985.

Jefferies, K.S.: Optical Analysis of Parabolic Dish Concentrators for Solar Dynamic Power Systems in Space. NASA Lewis, Space Station *Freedom* Directorate, PIR 111,[a] May 21, 1985.

Jefferies, K.S.: Computer Code To Analyze Off-Axis Solar Concentration. NASA Lewis, Space Station *Freedom* Directorate, PIR 131,[a] Feb. 1, 1986.

Jefferies, K.S.: Analysis of Off-Axis Solar Concentration by Tracing Shadow Patterns. NASA Lewis, Space Station *Freedom* Directorate, PIR 136,[a] May 1, 1986.

Jefferies, K.S.: Analysis of Off-Axis Solar Concentration by Mapping Intensity Distributions. NASA Lewis, Space Station *Freedom* Directorate, PIR 153,[a] June 5, 1986.

Jefferies, K.S.: Solar Simulator for SPF (Presentation). NASA Lewis, key 23573,[a] Mar. 24, 1987.

Jefferies, K.S.: Concentrator Surface Accuracy Sensitivities. NASA Lewis, IBR SE–108, key 23588,[a] May 13, 1987.

Jefferies, K.S.: Equations for Selecting Solar Rays and Simulating Surface Slope Errors. NASA Lewis, IBR SE–110, key 23587,[a] May 22, 1987.

Jefferies, K.S.: Concentrator Code Results Match MDAC Results. NASA Lewis, IBR SE–120, key 23586,[a] July 24, 1987.

Jefferies, K.S.: Images of Offset Collector on Walls of Receiver. NASA Lewis, IBR SE–123, key 23585,[a] Oct. 2, 1987.

Jefferies, K.S.: Trip to Harris Corporation—Concentrator Analysis Techniques. NASA Lewis, IBR SE–145, key 23583[a], May 2, 1988.

Jefferies, K.S.: 1–D or 2–D Probability Functions for Approximating Facet Slope Error. NASA Lewis, IBR SE–150, key 23582,[a] May 12, 1988.

Jefferies, K.S.: Distribution of 48 Facets on Concentrator. NASA Lewis, IBR SE–162, key 23581,[a] Sept. 27, 1988.

Jefferies, K.S.: Facet and Solar Images on Receiver Wall. NASA Lewis, IBR SE–170, key 24501,[a] Dec. 13, 1988.

Jefferies, K.S.: NASA's Recent Flux Tailoring and Concentrator Analysis Efforts Presentation. NASA Lewis, IBR SE–174, key 23580,[a] Feb. 17, 1989.

Jefferies, K.S.: Concentration of Off-Axis Radiation by Solar Concentrators for Space Power. NASA Lewis, IBR SE–190, key 23578,[a] May 17, 1989.

Jefferies, K.S.: Updated Documentation of OFFSET Code for COSMIC. NASA Lewis, IBR SE–225, key 23598,[a] Jan. 5, 1990.

Jefferies, K.S.: JPL Information on Solar Intensity During Sunrise. NASA Lewis, IBR SE–342, key 23603,[a] July 29, 1990.

Jefferies, K.S.: Concentrator Testing Using Projected Images—Viewgraph Presentation for IECEC. NASA Lewis, IBR SE–343, key 23602,[a] Aug. 23, 1990.

Jefferies, K.S.: Optics Analysis Presentation for SD Supporting Development Review. NASA Lewis, IBR SE–290, key 24502,[a] Oct. 30, 1990.

Jefferies, K.S.: Ceiling Image System for Concentrator Optical Testing. NASA Lewis, IBR SE–297, key 23609,[a] Nov. 30, 1990.

Jefferies, K.S.: Concentrator Testing Using Projected Images. NASA Lewis, IBR SE–305, key 23608,[a] Jan. 17, 1991.

Jefferies, K.S.: Ceiling Image Test of STAR Facet Contours. NASA Lewis, IBR SE–331, key 23605,[a] June 14, 1991.

Jefferies, K.S.; and Buchele, D.R.: Solar Collector With Toroid Surface Segments. NASA Lewis, IBR SE–136, key 23584,[a] Feb. 11, 1988.

Jefferies, K.S.; and Fincannon, H.J.: PATRAN Maps of Incident and Reflected Receiver Flux. NASA Lewis, IBR SE–177, key 23264,[a] Mar. 14, 1989.

Jefferies, K.S.; and Gallo, C.A.: Facet Aiming Sensitivity Study. NASA Lewis, IBR SE–164, key 24503,[a] Oct. 18, 1988.

Jefferies, K.S.; and Gallo, C.A.: Offset Code Flux Tailoring Results. NASA Lewis, IBR SE–195, key 23595,[a] Feb. 28, 1989.

Jefferies, K.S.; and Gallo, C.A.: Review of Receiver Aperture Offset With Other Flux Tailoring Methods. NASA Lewis, IBR SE–215, key 23257,[a] Nov. 7, 1989.

Jefferies, K.S.; and Gallo, C.A.: Flux Tailored Results Using Various Numbers of Edge Wedges. NASA Lewis, IBR SE–217, key 23599,[a] Nov. 9, 1989.

Jefferies, K.S.; and Gallo, C.A.: Toroidal Facets for Space Station *Freedom*'s Offset Solar Dynamic Concentrator. NASA Lewis, IBR SE–318, key 23606,[a] Apr. 12, 1991.

Jefferies, K.S.; and Gallo, C.A.: Flux Distribution With Large Simulated Sun. NASA Lewis, IBR SE–352, key 23601,[a] Nov. 4, 1991.

Mancini, T.R.; and Cameron, C.P.: NASA SCAD Concentrator Terrestrial Testing Feasibility Study. Sandia National Laboratories, Final Report Contract No. C–31006–J, key 23707,[a] Sept. 1988.

Minutes of Program Management Review held on June 15, 1989. Harris Corp., RI–HA–0015, key 1151,[a] June 21, 1989.

Minutes of Technical Interchange Meeting and Program Management Review held at NASA Lewis on May 3–4, 1989. Harris Corp., RI–HA–0015, key 1169[a], June 5, 1989.

O'Brien, D.L.: Power Flux for Normally Distributed Mispointing, Solar Dynamic. Rockwell International, Rocketdyne Division, EID–00791, key 17979,[a] Apr. 15, 1991.

Preliminary On-Orbit Assembly Plan for Space Station Work Package 4. Harris Corp., RI–HA–0021,[a] July 31, 1989.

Schumacher, K.; Cochran, C.; and Cason, R.D.: Detailed Assembly Procedures for the Three Panel Neutral Buoyancy Test. Harris Corp., SDP–0021,[a] Feb. 8, 1990.

Schumacher, K.M.: Reflectivity Measurement Variations. Harris Corp., key 23704,[a] July 5, 1989.

Schumacher, K.M.: DIR Evaluation. Harris Corp., SDP–0066,[a] May 30, 1990.

Schumacher, K.M.: Evaluation of 1G & NBT Test Results. Harris Corp., SDP–0137,[a] Nov. 1, 1990.

Shadowing Effects Task in Preliminary Design. Harris Corp., RI–HA–036,[a] Jan. 2, 1990.

Smith, R.T.: Structural Analysis Criteria and Plan. Harris Corp., SDP–0039,[a] March 28, 1990.

Solar Dynamic Reflector Baseline for Space Station *Freedom* Work Package 4. Harris Corp., RI–HA–0022,[a] July 31, 1989.
Solar Dynamic Concentrator System Safety Program Plan. Harris Corp., key 23706,[a] Oct. 20, 1989.

Solar Thermal Advanced Reflector Task II Report. Harris Corp., SDP–0050,[a] Apr. 17, 1990.

Spaunburgh, D.R.: Facet Development Environmental Test Plans (1). Harris Corp., SDP–0083,[a] June 29, 1990.

Structural Analysis Criteria and Plan. Harris Corp., RI–HA–0024,[a] Aug. 31, 1989.

Talcott, R.C.: Analysis of Granularity of Facet Nodes. Harris Corp., RI–HA–0023,[a] Aug. 23, 1989.

Talcott, R.C.: Focusing of RF Energy by the Solar Concentrator. Harris Corp., SDP–0068,[a] May 31, 1990.

Talcott, R.; and Cason, R.: Desired Locations for On-Sun Testing of Facets. Harris Corp., RI–HA–0026,[a] Sept. 19, 1989.

Thermal Analysis Information. Harris Corp., RI–HA–0017, key 1144,[a] June 22, 1989.

Trudell, J.J.: Thermal Distortion Analysis of the Space Station Solar Dynamic Concentrator. NASA Lewis, IBR SE–146, key 24390,[a] May 2, 1988.

Trudell, J.J.; Dalsania, V.; Baumeister, J.F.; and Jefferies, K.S.: Thermal Distortion Analysis of the Space Station Solar Dynamic Concentrator. Presented at IECEC Conference, July 31–Aug. 5, 1988. NASA TM–100868, 1988.

Zinolabedini, R.: Effects of Specular Error on the Receiver's Flux Distribution. Aerospace Design & Fabrication, Inc., key 23600,[a] Apr. 10, 1990.

Zinolabedini, R.: Simulation of Panel and Facet Cant Error. Aerospace Design & Fabrication, Inc., key 23720,[a] May 25, 1990.

Zinolabedini, R.: Flux Concentrator on Radiator Plane Due to Changes in Alpha and Beta Mispoint Angles, Task Order 38, NAS3–25767, key 23721[a], Jan. 22, 1991.

Heat Receiver

Advanced Development Receiver Documentation From Contracts NAS3–24669 and NAS3–25716. Boeing Aerospace Co., key 23725,[a] 1989.

Beremand, D.; and Krevis, T.: Solar Receiver Test Verification Options. Interim Memo Report to Steve Johnson, key 23282,[a] Sept. 20, 1989.

Bruner, S.R.: Component Confirmation Studies Addressing the Current Design and Off-Design Performance. Allied-Signal Aerospace Co., 41–8702–19, key 23675,[a] Sept. 24, 1991.

Ciancone, M.L.; and Kerslake, T.W.: Impact of a Constant Density Orbit on Solar Dynamic Systems. NASA Lewis, PIR 135,[a] Apr. 3, 1986.

Computer Software, Advanced Development Receiver Test Data From Contract NAS3–25716, 1/2-in. Magnetic Tape. Boeing Aerospace Co., key 23727,[a] Jan. 1, 1991.

Computer Software, Backup of SDHRT and ADRT Computer and Test Data Files in VAX Format, 5 1/2-in. Floppy Disks in Standard ASCII Format. NASA Lewis, key 23730,[a] Apr. 1, 1991.

Conceptual Design of CBC/PGS Parasitic Load Radiator. Allied-Signal Aerospace Co., 41–8702–8,[a] Aug. 18, 1989.

Design and Off-Design Performance Incorporating the Latest Radiator and Thermal Environment. Allied-Signal Aerospace Co., 41–8702–18,[a] Apr. 23, 1991.

Equipment User Manuals: Receiver Fabrication and Delivery Documentation. Boeing Aerospace Co., key 23726,[a] 1989.

Errata 1 for Interim Design Review for the CBC/PGS for the NASA Space Station *Freedom*. Allied-Signal Aerospace Co., 41–9311/ER1, key 23266,[a] Nov. 29, 1989.

Experience Summary for Transition Weld of Hastelloy X to 300-Series Stainless Steel. Allied-Signal Aerospace Co., 41–8702–13,[a] Apr. 12, 1990.

Flux Distribution Requirements Meeting. Rocketdyne, NASA Lewis, Harris Corp., and Allied-Signal, Tempe, Arizona, key 23681,[a] Oct. 5, 1989.

Heat Receiver Supporting Development Splinter Session. NASA Lewis, Cleveland, OH, key 23682,[a] May 11, 1989.

High Temperature Vacuum Sublimation Testing of Candidate Space Solar Receiver Materials. Allied-Signal Aerospace Co., Final Report 41–5586A, key 23669,[a] Sept. 22, 1986.

Interim Design Review for the CBC/PGS for the NASA Space Station *Freedom*. Allied-Signal Aerospace Co., 41–9311, key 23277,[a] Nov. 16, 1989.

Interim Design Review for the CBC/PGS for the NASA Space Station *Freedom*. Allied-Signal Aerospace Co., 41–9312, key 23267,[a] Dec. 6–7, 1989.

Jefferies, K.S.: Aperture Plane Flux Intensity Maps With Mispointing of 0, 1, 2, and 3 Degrees. NASA Lewis, IBR SE–163, key 23271,[a] Sept. 28, 1988.

Jefferies, K.S.: Receiver Flux Distribution With 2 Degrees Beta Error. NASA Lewis, IBR SE–187, key 23579,[a] Apr. 18, 1989.

Kerslake, T.W.: Phase Change Boundary Motion in a Brayton Receiver PCM Containment Ring During Eclipse. NASA Lewis, PIR 132,[a] Feb. 1986.

Kerslake, T.W.: Thermal Analysis of a 25 KWe Closed Brayton Cycle Sensible Heat Storage Beryllium Receiver. NASA Lewis, PIR 165,[a] Nov. 3, 1986.

Kerslake, T.W.: LeRC Review Comments on the Reference Presentation and Recommendations for Solar Dynamic Receiver Life Estimation Activities. NASA Lewis, key 23692,[a] Oct. 30, 1990.

Kerslake, T.W.: Aperture Plate Temperature Predictions With a Boron Nitride Shield Material. NASA Lewis, key 36459,[a] Jan. 18, 1991.

Kerslake, T.W.: Receiver Thermal Energy Storage Canisters Tested and Analyzed. Research & Technology 1990, NASA TM–103759, 1991, pp. 113–115.

Kerslake, T.W.; and Ibrahim, M.B.: Analysis of Thermal Energy Storage Material With Change-of-Phase Volumetric Effects. Proceedings of the 12th Annual ASME International Solar Energy Conference, ASME, New York, 1990, pp. 315–325. (Also NASA TM–102457.)

Kerslake, T.W.; and Ibrahim, M.B.: Two-Dimensional Model of a Space Station *Freedom* Thermal Energy Storage Canister. Proceedings of the 25th Intersociety Energy Conversion Engineering Conference, vol. 2, Aug. 1990, pp. 151–159. (Also NASA TM–103124.)

Klann, J.L.: Solar Heat Receiver Transient Thermal Effects on CBC Module Orbital Performance. NASA Lewis, PIR 182,[a] Nov. 13, 1986.

Klann, J.L.: Comparison of Forced Convection Heat Transfer Correlations for the Solar Dynamic Heat Receiver. NASA Lewis, IBR SE–205, key 24396,[a] Aug. 31, 1989.

Klann, J.L.: Revised Heat-Receiver Design Tradeoffs for the SD Power Module. NASA Lewis, IBR SE–206, key 24395,[a] Sept. 13, 1989.

Kudija, C.: Thermal Energy Storage Canister Creep Analysis Evaluation. Rockwell International, Rocketdyne Division, key 23674,[a] Oct. 22, 1990.

Loeffel, D.: Solar Simulation Testing of a Heat Receiver Assembly Single Tube. Allied-Signal Aerospace Co., 41–8702–16,[a] Nov. 5, 1990.

Misra, A.K.; and Whittenberger, J.D.: Estimated Heats of Fusion of Fluoride Salt Mixtures Suitable for Thermal Energy Storage Applications. NASA TM–87320, 1986.

Monthly Performance Measurement Status Report October 1990, Volume II, Technical/Schedule Status. Rockwell International, Rocketdyne Division, DR:MA–03, key 11266,[a] Nov. 28, 1990.

Preliminary Design of the Salt/Metal Compatibility, 12,000-Hour Exposure, for Solar Receiver Thermal Energy Storage Canisters. Allied-Signal Aerospace Co., 41–8702–12,[a] Dec. 8, 1989.

Receiver Tilt and Aperture Offset. Rocketdyne Report EID–00805,[a] Dec. 1990.

Results of Melting of the Eutectic Mixture LiF-CaF_2 Under Controlled Conditions and Supporting Analysis. Allied-Signal Aerospace Co., 41–8702–14,[a] July 11, 1990.

Santarelli, K.W.: Response to NASA Comments on Allied-Signal SD Receiver TES Canister Life Briefing. Rocketdyne letter 91RC04225, key 23692,[a] Mar. 26, 1991.

Short-Term Canister Test Data (ECRL May-June 1987), ERB Test Calibration Data RDG #1–60 (Jan.-Oct. 1989), Configuration 11 – 500 cycle and 100 cycle tests. NASA Lewis, key 23695,[a] 1989.

Solar Dynamic Heat Receiver Technology Critical Design Review. Boeing Aerospace Co., NAS3–24669, key 23672,[a] May 11–12, 1988.

Solar Receiver Thermal Energy Storage Canisters Compatibility Test – Final Report. Allied-Signal Aerospace Co., 41–8702–17,[a] Jan. 21, 1991.

Space Station Solar Dynamic CBC/PGS Preliminary Start Analysis. Allied-Signal Aerospace Co., 41–8702–6,[a] Aug. 11, 1989.

Stalnaker, D.K.: Potential Variations in the Orbital Heat Balance of a Solar Dynamic System Heat Receiver. NASA Lewis, PIR 101,[a] Apr. 1985.

Stochl, R.J.: Comparison of Allied-Signal and In-House (CCEP) Solar Dynamic Power Module Design and Off-Design Performance Estimates. NASA Lewis, IBR SE–220, key 24393,[a] Dec. 15, 1989.

Strumpf, H.J.: Receiver Flux Distribution Analysis Presentation. Allied-Signal Aerospace Co., key 23680,[a] Oct. 5, 1989.

System Design and Off-Design Analysis of the Space Station Power Generation Subsystem/Solar Dynamic Power Module. Allied-Signal Aerospace Co., 41–8702–3, key 1079,[a] Aug. 11, 1989.

TES Canister Structural and Materials Assessment. Videoconference, NASA Lewis, Rocketdyne, and Allied-Signal, key 23670,[a] Feb. 8, 1989.

TES Canister Tabular and Graphical Test Data: HFTB, HFTT, and HFTS. NASA Lewis, key 23270,[a] 1989–1990.

Thermal Energy Storage Canister Manufacturing Development Status Summary Report. Allied-Signal Aerospace Co., 01860RC,[a] Feb. 20, 1991.

Viterna, Larry A.: A Finite Element Model of Conduction, Convection, and Phase Change Near a Solid/Melt Interface. NASA TM–103721, 1991.

Walzer, C.H.: Receiver Thermal Energy Storage Canister Endurance Test Facility Description. NASA Lewis, PIR 231,[a] June 1, 1989.

Whittenberger, J.D.: Mechanical Properties of Haynes Alloy 188 After Exposure to LiF-22CaF_2, Air, and Vacuum at 1093 K for Periods up to 10 000 Hours. Journal of Materials Engineering and Performance, vol. 1, no. 4, Aug. 1992, pp. 469–482.

Power Conversion Unit

Casort, L.F.: Interim Design Review #1 of Allied-Signal CBC/PGS. Rockwell International, Rocketdyne Division, DRR–00209, key 4828,[a] Jan. 3, 1990.

Design Analyses and Data Report for the CBC Power Generating Subsystem. Allied-Signal Aerospace Co., DR:SE–03, key 22825,[a] Oct. 21, 1991.

Feight, G.: Allied-Signal Closed Brayton Cycle Power Generating Subsystem Interim Design Review. Allied-Signal Aerospace Co., DRR–00264, key 20071,[a] July 9, 1991.

Gallo, C.A.: Methods Used in the Waste Heat Exchanger Performance Program (Manual for the Waste Heat Exchanger Subroutine in CCEP). NASA Lewis, IBR SE–282, key 24400,[a] Sept. 23, 1990.

Gallo, C.A.; and Klann, J.L.: Steady-State Approximation of Shaft Runaway Speed in the Phase-C Baseline SD Power Module. NASA Lewis, IBR SE–248, key 24385,[a] Apr. 9, 1990.

Hojnicki, J.S.: EASY5/W Solar Dynamic Alternator/PCU Model. NASA Lewis, IBR SE–149, key 24388,[a] May 11, 1988.

Klann, J.L.: Effect of Gas Pressure Drop in the Waste Heat Exchanger on CBC Engine Efficiency. NASA Lewis, PIR 140,[a] Apr. 11, 1986.

Klann, J.L.: Part-Power Efficiency Projections for a CBC Power Module. NASA Lewis, PIR 141,[a] Apr. 11, 1986.

Klann, J.L.: CBC Speed-Torque Variations. NASA Lewis, PIR 142,[a] Apr. 14, 1986.

Klann, J.L.: Integration of the Finite Element Pumped-Loop Radiator Program Into CCEP and Study of the Rocketdyne CBC Design Selection. NASA Lewis, PIR 143,[a] Apr. 14, 1986.

Klann, J.L.: Simulation of the Baseline SD Recuperator and Effects of Heat Transfer Correlations on Its Design. NASA Lewis, IBR SE–207, key 24394,[a] Sept. 20, 1989.

Klann, J.L.: Comparison of Calculated Heat Transport Properties for Helium/Xenon Gas Mixtures. NASA Lewis, IBR SE–280, key 24399,[a] Sept. 20, 1990.

Klann, J.L.; Gallo, C.A.; and Bitner, E.: Evaluation of an Auxiliary Heat Exchanger Computer Code for Use in CCEP. NASA Lewis, IBR SE–256, key 24397,[a] May 21, 1990.

Klann, J.L.; and Heighway, J.E.: Digital Computer Programs for Transient Analysis of a Counterflow Heat Exchanger. NASA Lewis, IBR SE–268, key 24398,[a] Aug. 1, 1990.

Lottig, R.W.: A Compilation of Brayton Cycle Power System Reports, Studies, and Contracts From 1960 Through 1975. NASA Lewis, PIR 99A,[a] Mar. 28, 1985.

Monthly Performance Measurement Status Report for November 1990, Volume II Technical/Schedule Status. Rockwell International, Rocketdyne Division, DR:MA–03, key 11830,[a] Dec. 21, 1990.

Thompson, D.M.: Containment Shield Analysis for Brayton Rotating Unit. NASA Lewis, PIR 248,[a] Dec. 10, 1990.

Heat Rejection Assembly

Benchmark/Parametric Analysis of Solar Dynamic Radiator. LTV Missiles and Electronics Group, DR:SE–03[a], July 3, 1991.

Bugiada, J.: Deployable Radiator Subassembly Specification. Rocketdyne Division, RC1894,[a] Sept. 27, 1991.

Bugiada, R.: Deployable Radiator Subassembly Specification. Rocketdyne Division, RC1894A,[a] Oct. 18, 1990.

Bunnell, K.G.: Interim Design Review #1, LTV Co. Radiator Panel. Rockwell International, Rocketdyne Division, DRR–00211,[a] Feb. 6, 1990.

Chung, D.K.: Transient Thermal Model of Solar Dynamic Radiator. Rockwell International, Rocketdyne Division, EID–00697,[a] Aug. 24, 1990.

Clark, J.D.: Preliminary Solar Dynamic Radiator Failure Modes and Effects Analysis and Critical Items List. LTV Missiles and Electronics Group, 3–44000/9DIR–030,[a] Nov. 9, 1989.

Cox, R.L.: Solar Dynamic Radiator Mass Property Data. LTV Missiles and Electronics Group, 3–12450/8DIR–3,[a] Aug. 3, 1988.

Cox, R.L.: Solar Dynamic Radiator. LTV Missiles and Electronics Group, 3–12450/8DIR–6,[a] Aug. 16, 1988.

Cox, R.L.: Solar Dynamic Radiator. LTV Missiles and Electronics Group, 3–12450/8DIR–6, rev. A,[a] Aug. 19, 1988.

Cox, R.L.: Solar Dynamic Radiator Mass Property Data. LTV Missiles and Electronics Group, 3–12450/8DIR–8,[a] Aug. 29, 1988.

Cox, R.L.: Thermal Control Coating Test Plan. LTV Missiles and Electronics Group, 3–12450/8DIR–11,[a] Sept. 17, 1988.

Cox, R.L.: Determination of Drag Area of Deployed Solar Dynamic Radiator. LTV Missiles and Electronics Group, 3–12450/8DIR–13,[a] Nov. 28, 1988.

Cox, R.L.: TRASYS Model for Environment Analysis of Solar Dynamic Radiator. LTV Missiles and Electronics Group, 3–12450/8DIR–16,[a] Dec. 19, 1988.

Cox, R.L.: Update of Solar Dynamic Radiator Baseline Performance. LTV Missiles and Electronics Group, 3–12450/8DIR–20,[a] Dec. 19, 1988.

Cox, R.L.: Solar Dynamic Radiator Design Criteria. LTV Missiles and Electronics Group, 3–46200/9DIR–021,[a] June 26, 1989.

Cox, R.L.: Solar Dynamic Radiators Interconnect Line Configuration Study. LTV Missiles and Electronics Group, 3–44000/9DIR–020,[a] July 17, 1989.

Cox, R.L.: Solar Dynamic Radiator Preliminary Support Equipment Scars Analysis. LTV Missiles and Electronics Group, 3–44000/9DIR–028,[a] Oct. 9, 1989.

Cox, R.L.: Solar Dynamic Radiator Hypervelocity Impact Test Repro Requirements. LTV Missiles and Electronics Group, 3–44000/9DIR–006,[a] Oct. 20, 1989.

Cox, R.L.: Solar Dynamic Radiator Mass Properties Quarterly Update. LTV Missiles and Electronics Group, 3–44000/9DIR–029,[a] Oct. 20, 1989.

Cox, R.L.: Solar Dynamic Radiator Enhanced Heat Transfer Literature Survey. LTV Missiles and Electronics Group, 3–44000/9DIR–031,[a] Nov. 17, 1989.

Cox, R.L.: Dynamic Response Analyses of Stowed Solar Dynamic Radiator Assembly Modal Frequency and Random Vibration Analyses. LTV Missiles and Electronics Group, 3–44000/9DIR–033,[a] Dec. 18, 1989.

Cox, R.L.: Solar Dynamic Radiator 4 and 10 SDR Growth Evaluation. LTV Missiles and Electronics Group, 3–44000/9DIR–036,[a] Dec. 21, 1989.

Cox, R.L.: Radiator Panel Design Evaluation Test Request. LTV Missiles and Electronics Group, 3–44000/9TR–003,[a] Jan. 29, 1990.

Dever, J.A.: Summary of Durability Testing of McDonnell Douglas Anodized Aluminum Samples as Candidate Radiator Materials. NASA Lewis, key 24284,[a] Nov. 19, 1990.

Evans, A.L.; and Neely, G.M.: A Finite Element Computer Program for Analysis and Optimization of Pumped Loop Space Radiator Designs. NASA Lewis, PIR 122,[a] Nov. 1985.

Fleming, M.L.: Solar Dynamic Radiator Thermal Control Coating Test Requirements. LTV Missiles and Electronics Group, 3–47300/SDR/0DIR–038,[a] May 30, 1990.

Fleming, M.L.: Solar Dynamic Radiator High Temperature Adhesive Performance Test Plan. LTV Missiles and Electronics Group, 3–47300/SDR/0DIR–044,[a] June 28, 1990.

Fleming, M.L.: Deployment/Retreat Concepts (Linkage & Cable) Failure Rate Comparison. LTV Missiles and Electronics Group, 3–47300/0DIR–055,[a] Aug. 29, 1990.

Fleming, M.L.: Optical Coating Selection Summary for the Solar Dynamic Radiator. LTV Missiles and Electronics Group, 3–47300/0DIR–062,[a] Oct. 8, 1990.

Fleming, M.L.: Estimated EOL Optical Properties of Various Materials. LTV Missiles and Electronics Group, 3–47300/1DIR–002,[a] Jan. 3, 1991.

Fleming, M.L.: Solar Dynamic Radiator Temperature Cycling Results. LTV Missiles and Electronics Group, 3–47300/1DIR–021,[a] Mar. 12, 1991.

Flores, R.R.: SINDA Thermal Model of Solar Dynamic Radiator. LTV Missiles and Electronics Group, 3–12450/8DIR–17,[a] Jan. 19, 1989.

Flores, R.R.: Comparison of Allied-Signal and LTV Radiator Model Results, Radiator Sink Temperature and Concentrator Temperature Calculations. LTV Missiles and Electronics Group, 3–12450/8DIR–18,[a] Jan. 19, 1989.

Flores, R.R.: Solar Dynamic Radiator Fluid Trade Study Results. LTV Missiles and Electronics Group, 3–12450/8DIR–19,[a] Jan. 19, 1989.

Flores, R.R.: Update of Solar Dynamic Radiator Baseline Performance. LTV Missiles and Electronics Group, 3–46200/9DIR–008,[a] Mar. 9, 1989.

Flores, R.R.: Thermal Analysis of 1-Hz Modal Frequency Design Configurations. LTV Missiles and Electronics Group, 3–46200/9DIR–009,[a] Apr. 17, 1989.

Flores, R.R.: Solar Dynamic Radiator Pressure Loss Analysis. LTV Missiles and Electronics Group, 3–46200/9DIR–010,[a] May 4, 1989.

Flores, R.R.: Solar Dynamic Radiator CBC State Point Analysis. LTV Missiles and Electronics Group, 3–44000/9DIR–023,[a] Aug. 4, 1989.

Flores, R.R.: Solar Dynamic Radiator Program Thermal Test Plan. LTV Missiles and Electronics Group, 3–44100/0R–019,[a] Mar. 8, 1990.

Gallo, C.A.: Comparison Between Design Point Radiator Results for the Rephased Solar Dynamic Power Module. NASA Lewis, IBR SE–291, key 24402,[a] Nov. 13, 1990.

Go, S.: Procurement Specification for Deployable Radiator Subassembly. Rockwell International, Rocketdyne Division, RC1894,[a] Jan. 17, 1990.

Green, R.D.: A Simplified Analysis of a Corrugated Radiator. NASA Lewis Space Station *Freedom* Directorate, PIR 69,[a] July 1984.

Green, R.D.; and Stochl, R.J.: Pumped-Loop Radiator Analysis and Effect of Segmentation. NASA Lewis Space Station Systems Directorate, PIR 93,[a] Feb. 1985.

Hoehn, F.: Procurement Specification for Panel/Deployment Subassembly, Closed Brayton Cycle Solar Dynamic Radiator. Rockwell International, Rocketdyne Division, RC1815,[a] May 31, 1988.

Hofstad, R.B.: Documentation of Design Modification to the Solar Dynamic Radiator System in Order To Accommodate a Modal Frequency of 1 Hz. LTV Missiles and Electronics Group, 3–46200/9DIR–007,[a] Mar. 2, 1989.

Hofstad, R.B.: Solar Dynamic Radiators – Panel Configuration Study. LTV Missiles and Electronics Group, 3–46200/9DIR–017,[a] May 24, 1989.

Hofstad, R.B.: Solar Dynamic Radiators – Base Support Configuration Repro Study. LTV Missiles and Electronics Group, 3–44000/9DIR–024,[a] Aug. 11, 1989.

Hofstad, R.B.; et al.: Procurement Specification for Solar Dynamic Radiator Metal Hose Assembly. LTV Missiles and Electronics Group, 304/SDR–005,[a] Sept. 27, 1990.

Howerton, R.L.: Heat Rejection System Fluid Trade Study (Solar Dynamic System), Rockwell International, Rocketdyne Division, TSR–00055, key 8901706,[a] Mar. 1, 1989.

Howerton, R.L.: Solar Dynamic Radiator Attachment Study Results. Rockwell International, Rocketdyne Division, EID–00625,[a] Apr. 5, 1990.

Klann, J.L.: Typical Radiator Area/Mass/Reliability Tradeoffs for a Solar-Brayton Space Power System. NASA Lewis, PIR 90,[a] Jan. 1985.

Klann, J.L.: A Comparison of Pumped-Loop Radiator Designs for the CBC Power Module. NASA Lewis, PIR 203,[a] Oct. 26, 1987.

Lee, S.J.: Normal Mode Analysis of Deployed Solar Dynamic Radiator Assembly and Various Modifications. LTV Missiles and Electronics Group, 3–12450/8DIR–9,[a] Sept. 12, 1988.

Lee, S.J.: Further Trade Studies for Structural Modifications to Achieve the Solar Dynamic Radiator Deployed Modal Frequency Requirement. LTV Missiles and Electronics Group, 3–46200/9DIR–011,[a] Mar. 10, 1989.

Lee, S.J.: Deployed Modal Frequency Analysis for Three Solar Dynamic Radiator Configurations Using Detailed Finite Element Models. LTV Missiles and Electronics Group, 3–46200/9DIR–015,[a] Mar. 29, 1989.

Mechanical Properties of Hexcel Honeycomb Materials. Hexcel Co., TSB120, 1984 revision.

Miao, D.: Special Characteristics of Radiator Sizing. NASA Lewis, PIR 115,[a] Sept. 24, 1985.

Micrometeoroid/Debris Parametrics. LTV Missiles and Electronics Group, 3–47300/PVR/0DIR–007,[a] June 6, 1990.

Miniatas, J.B.: Solar Dynamic Radiator Honeycomb Panels Under Vacuum Space Environment. LTV Missiles and Electronics Group, 3–12450/8DIR–5,[a] Aug. 10, 1988.

Miniatas, J.B.: Structural Studies and the Design Modifications Done To Achieve the SDR Deployed Modal Frequency Requirement of 1 Hz. LTV Missiles and Electronics Group, Missiles Division, 3–46200/9DIR–019,[a] May 8, 1989.

Miniatas, J.B.: Structural Studies and the Design Modifications Done To Achieve the Solar Dynamic Radiator Deployed Modal Frequency Requirement of 1 Hz. LTV Missiles and Electronics Group, 3–46200/9DIR–019, rev. A,[a] July 28, 1989.

Miniatas, J.B.: Results of Solar Dynamic Radiator 1-Hertz Structural Study. LTV Missiles and Electronics Group, 3–44000/9DIR–032,[a] Nov. 20, 1989.

Neely, G.M.; and McLallin, K.L.: Heat Pipe Radiator Sizing Code for a Closed Brayton Cycle. NASA Lewis Space Station *Freedom* Directorate, PIR 146,[a] May 6, 1986.

O'Young, N.; and Howell, C.: Low Frequency Solar Dynamic Radiator Thermal Environment. Rockwell International, Rocketdyne Division, EID–00741,[a] Oct. 4, 1990.

O'Young, N.; and Howell, C.: Low Frequency Solar Dynamic Radiator Thermal Effects on the PV Arrays and EPS Radiators. Rockwell International, Rocketdyne Division, EID–00757,[a] Oct. 26, 1990.

Rhatigan, J.L.: Computer Code To Perform Parametric Analyses on SD Radiator. NASA Lewis, PIR 221,[a] Dec. 15, 1988.

Rusick, J.J.: Brayton Radiator Sizing Evaluation. NASA Lewis, PIR 206[a], Dec. 14, 1987.

Solar Dynamic Radiator Mass Properties Data. LTV Missiles and Electronics Group, 3–44000/9DIR–025,[a] (Also 3–46200/9DIR–014 and 3–46200/9DIR–016), Aug. 15, 1989.

Solar Dynamic Radiator Structural Temperature. LTV Missiles and Electronics Group, 3–44000/9DIR–022[a], June 7, 1989.

Solecki, L.B.: Solar Dynamic Radiator Baseline Material Review. LTV Missiles and Electronics Group, 3–44000/8DIR–12, rev A,[a] Dec. 7, 1989.

Stoyack, J.E.: Identify the LEO Environment Simulation Test Equipment Needed. LTV Missiles and Electronics Group, 3–46200/9DIR–001, rev. A,[a] Jan. 10, 1989.

Stoyack, J.E.: Solar Dynamic Radiator High Temperature Adhesive Performance Test Requirements. LTV Missiles and Electronics Group, 3–47300/SDR/0DIR–039[a], May 31, 1990.

Viterna, L.A.: Effect of Latent Heat Thermal Energy Storage on Radiator Area and Mass. NASA Lewis, PIR 70,[a] Aug. 1984.

Webster, C.N.: Solar Dynamic Radiator System Progress Report No. 32. LTV Missiles and Electronics Group, 3–47300/OR–058,[a] Sept. 4, 1990.

Other

Atomic Oxygen Degradation of the Power Generation Subsystems in the Low Earth Environments. NASA Lewis, PIR 114,[a] Aug. 15, 1985.

Bloomfield, H.S.: An Assessment of Dynamic Conversion Systems for Space Power. NASA Lewis, PIR 21,[a] Feb. 25, 1983.

Bur, M.J.: Effective Drag Areas for Alternative SRR Space Station Power Systems. NASA Lewis, PIR 160,[a] July 1, 1986.

Fincannon, H.J.: Comparison of Life Cycle Cost for Photovoltaic, Solar Dynamic and Hybrid Options Considered at SRR. NASA Lewis, PIR 157,[a] July 21, 1986.

Irvine, T.B.: Solar Dynamic System Component Test and Verification Plan: Rotary Beta Joint, Deployment Mechanisms, Support Structure, and Concentrator. NASA Lewis, PIR 120A,[a] Oct. 1, 1985.

Motil, S.M.: Solar Dynamic vs. Photovoltaic Life Cycle Cost Analysis. NASA Lewis, IBR SE–289, key 24387,[a] Oct. 29, 1990.

Myers, J.L.; and Trudell, J.J.: Thermal Interactions of the Photovoltaic and Solar Dynamic Power Modules. NASA Lewis, IBR SE–202, key 24380,[a] Aug. 14, 1989.

Nahra, H.K.: Effects of External Contamination of Power Generation Systems Performance. NASA Lewis, PIR 133A,[a] Mar. 26, 1986.

Nall, M.M.: Space Station Solar Dynamic Module Control Structure Interaction Presentation given May 10, 1989. NASA Lewis, IBR SE–192, key 24382,[a] May 24, 1989.

Nall, M.M.; and Griffin, D.E.: Space Station Solar Dynamic Module Preliminary Controls Assessment Presentation. NASA Lewis, IBR SE–183, key 24381,[a] Apr. 14, 1989.

O'Brien, D.: Procurement Specification for Solar Dynamic Insolation Meter. Rockwell International, Rocketdyne Division, RC1820, key 4314,[a] Nov. 9, 1989.

O'Brien, D.: Procurement Specification for Solar Dynamic Sun Sensor. Rockwell International, Rocketdyne Division, RC1821, key 4315,[a] Nov. 9, 1989.

O'Brien, D.L.: SD Drag and Gravity Gradient Study Analysis. Rockwell International, Rocketdyne Division, EID–00738, key 11261,[a] Oct. 1, 1990.

O'Young, N.; and Howell, C.: Solar Dynamic Hooks and Scars Thermal Impact Studies on the PV Arrays, PV Radiators, and Central Radiators. Rockwell International, Rocketdyne Division, EID-00684, key 9890[a], Aug 1, 1990.

Sawyer, A.; Harter, D.; and Sokolowski, D.: Solar Dynamic Power and Propulsion Office Green Book Schedules, Space Station *Freedom* WP–04. NASA Lewis, key 4036,[a] Nov. 13, 1989.

Solis, B.: Sun Sensor Technology for Fine Pointing Control Schemes. NASA Lewis, PIR 208,[a] Jan. 7, 1988.

Stalnaker, D.K.: Mass Comparisons of SRR Electrical Power Systems Options at IOC. NASA Lewis, PIR 158,[a] July 21, 1986.

Transverse Boom Normal Modes Analyses for a Solar Dynamic Powered Space Station. NASA Lewis, PIR 147,[a] May 7, 1986.

Young, G.H.: Design Specification for Gimbal Assembly, Two-Axis Solar Dynamic. Rockwell International, Rocketdyne Division, RJ00164, key 987,[a] Sept. 22, 1989.

Young, G.H.: Design Specification for Plate, Utility, Solar Dynamic. Rockwell International, Rocketdyne Division, RJ00176, key 4308,[a] Nov. 10, 1989.

REPORT DOCUMENTATION PAGE

Form Approved
OMB No. 0704-0188

1. AGENCY USE ONLY (*Leave blank*)	2. REPORT DATE	3. REPORT TYPE AND DATES COVERED
	July 1993	Reference Publication

4. TITLE AND SUBTITLE

Solar Dynamic Power System Development for Space Station *Freedom*

5. FUNDING NUMBERS

WU-474-52-10

6. AUTHOR(S)

Staff of Solar Dynamic Power System Branch

7. PERFORMING ORGANIZATION NAME(S) AND ADDRESS(ES)

National Aeronautics and Space Administration
Lewis Research Center
Cleveland, Ohio 44135-3191

8. PERFORMING ORGANIZATION REPORT NUMBER

E-7059

9. SPONSORING/MONITORING AGENCY NAMES(S) AND ADDRESS(ES)

National Aeronautics and Space Administration
Washington, D.C. 20546-0001

10. SPONSORING/MONITORING AGENCY REPORT NUMBER

NASA RP-1310

11. SUPPLEMENTARY NOTES

Responsible person, Kent S. Jefferies, (216) 433-2222.

12a. DISTRIBUTION/AVAILABILITY STATEMENT

Unclassified - Unlimited
Subject Category 20

12b. DISTRIBUTION CODE

13. ABSTRACT ***(Maximum 200 words)***

This report documents the development of a solar dynamic electric power generation system as part of the Space Station *Freedom* Program. The solar dynamic power system includes a solar concentrator, which collects sunlight; a receiver, which accepts and stores the concentrated solar energy and transfers this energy to a gas; a Brayton turbine, alternator, and compressor unit, which generates electric power; and a radiator, which rejects waste heat. Solar dynamic systems have greater efficiency and lower maintenance costs than photovoltaic systems and are being considered for future growth of Space Station *Freedom*. The report covers solar dynamic development managed by the NASA Lewis Research Center from 1986 to February 1991. It summarizes technology and hardware development, describes "lessons learned," and, through an extensive bibliography, serves as a source list of documents that provide details of the design and analytic results achieved. It was prepared by the staff of the Solar Dynamic Power System Branch at the NASA Lewis Research Center in Cleveland, Ohio. The report includes results from the prime contractor as well as from in-house efforts, university grants, and other contracts. Also included are the writers' opinions on the best way to proceed technically and programmatically with solar dynamic efforts in the future, on the basis of their experiences in this program.

14. SUBJECT TERMS	15. NUMBER OF PAGES
Space stations; Solar dynamic power systems; Solar collectors; Space radiators; Energy storage; Energy conversion; Electric generators; Heat exchangers	172
	16. PRICE CODE A08

17. SECURITY CLASSIFICATION OF REPORT	18. SECURITY CLASSIFICATION OF THIS PAGE	19. SECURITY CLASSIFICATION OF ABSTRACT	20. LIMITATION OF ABSTRACT
Unclassified	Unclassified	Unclassified	